Original color illustrations will be in black and white

1992 NRL Review

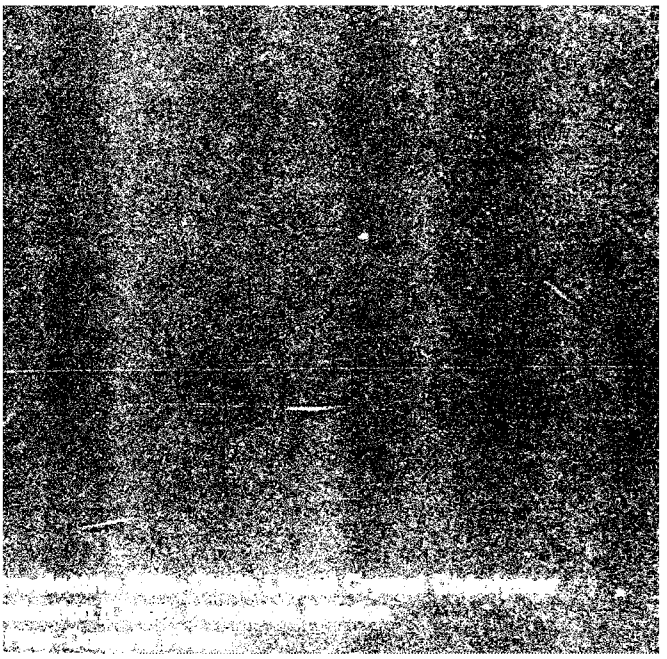

DISCLAIMER NOTICE

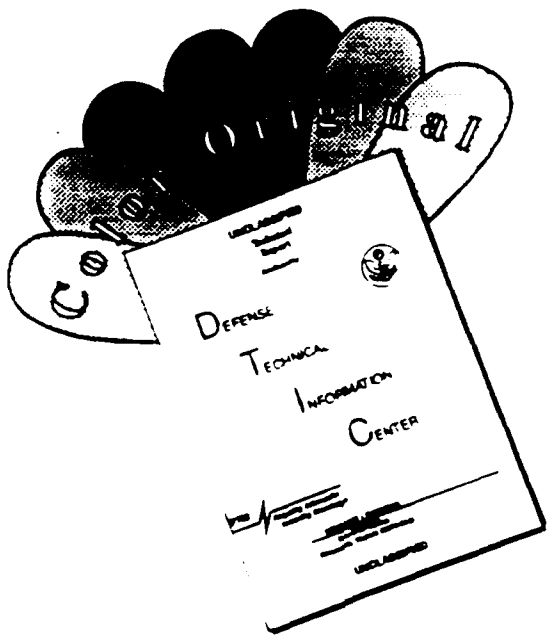

THIS DOCUMENT IS BEST QUALITY AVAILABLE. THE COPY FURNISHED TO DTIC CONTAINED A SIGNIFICANT NUMBER OF COLOR PAGES WHICH DO NOT REPRODUCE LEGIBLY ON BLACK AND WHITE MICROFICHE.

May 1992 Annual, Fiscal year 1991

1992 NRL Review N/A

See "Contents" of publication

Naval Research Laboratory
Washington, DC 20375-5001

NRL Pub. No. 202-4830

N/A

N/A

A companion video is available from DTIC or on loan from the Naval Research Laboratory, Ruth H. Hooker Technical Library and Technical Information Center, Code 4820, Washington, DC 20375-5001

Approved for public release; distribution is unlimited.

Presents highlights of several unclassified research and development programs performed at the Naval Research Laboratory during fiscal year 1991. Also presents history of NRL, highlights of NRL research in 1991, and general information.

See individual papers in publication 300 + covers

Unclassified Unclassified Unclassified SAR

CONTENTS

5 MISSION

7 INTRODUCING NRL BAY ST. LOUIS AND NRL MONTEREY

8 PREFACE—*CORPORATE LABORATORY, REAFFIRMED AND EXPANDED*
CAPT Paul G. Gaffney II, USN, Commanding Officer, and
Dr. Timothy Coffey, Director of Research

11 SCIENCE AND ART: A CONTEST AND A CELEBRATION
Herbert Gursky

19 FROM THE CHALLENGES OF WORLD WAR II TO THE FRONTIERS OF SPACE
Herbert Friedman

34 COLOR PRESENTATION

37 THE NAVAL RESEARCH LABORATORY
39 NRL—Our Heritage, NRL Today, NRL in the Future
61 Highlights of NRL Research in 1991
70 Meet the Researchers

73 FEATURED RESEARCH AT NRL
75 Understanding Superconductivity in the Cuprates: Theory and Experiment
Stuart A. Wolf, Mark E. Reeves, Joshua L. Cohn, and Vladimir Z. Kresin
85 Ion-beam-assisted Deposition Provides Control over Thin Film Properties
Fred A. Smidt
99 Low Reynolds Number Aerodynamics for Electronic Warfare
Richard J. Foch and Peggy L. Toot

111 ACOUSTICS
113 Transducer Calibration in Multipath Environments
Phillip L. Ainsleigh
115 Piezoelectric Composites for Transducer Applications
Kurt M. Rittenmyer
118 A Pictorial Analysis of Vibrating Shell Physics
Earl G. Williams

123 CHEMICAL/BIOCHEMICAL RESEARCH

125 Chemical Reaction Rates from First Principles
Maribel R. Soto

127 Fiber-optic-based Biosensor
George P. Anderson, Lisa C. Shriver-Lake, Robert A. Ogert, Joel P. Golden, and Frances S. Ligler

130 High Temperature Phthalonitrile Resins for Structural Applications
Teddy M. Keller

132 Atomistic Processes in Surface Mechanics and Adhesion
Richard J. Colton, Donald W. Brenner, Judith A. Harrison, and Nancy A. Burnham

135 Buckminsterfullerene: Building Blocks for New Materials
Mark M. Ross, John H. Callahan, Steven W. McElvany, Mark R. Pederson, Larry L. Boyer, and Warren E. Pickett

141 ELECTRONICS AND ELECTROMAGNETICS

143 Single Event Upsets in Space
Arthur B. Campbell

144 Visualization Tools for Development of Electronic Warfare Techniques
Tiziano Ricci and Robert Normoyle

147 Scale Model Analysis Facility
Stanley A. Moroz and Ernest S. Mak

149 A Programmable Antiship Infrared Guidance System
Elmer F. Williams, Robert H. Evans, and Paul L. Alles

151 Interfaces in Semiconductor Nanostructures
Daniel G. Gammon, D. Scott Katzer, and Benjamin V. Shanabrook

155 ENERGETIC PARTICLES, PLASMAS, AND BEAMS

157 Brightest X Rays Used to Probe Smallest Crystals
Earl F. Skelton, Syed B. Qadri, and Jack D. Ayers

159 Atomic Physics in Ultrastrong Fields
Jack Davis, Robert W. Clark, and John L. Giuliani, Jr.

162 Monolithic GaAs Antenna/Detector Array for 94 GHz Imaging
William M. Waters

164 Ultrawideband Radar
Grealie A. Andrews, J. Peter Hansen, and Karl Gerlach

167 INFORMATION TECHNOLOGY AND COMMUNICATION

169 A Networking Technology Demonstration for Naval Tactical Communications
Dennis N. McGregor, Dennis J. Baker, and James P. Hauser

172 A Graphical User Interface Design for Shipboard Damage Control
David L. Tate

174 Nonlinear Signal Processing for Detection in Chaotic Backgrounds
Sheldon B. Gardner

179 MARINE TECHNOLOGY

181 High Resolution Remote Sensing
Richard P. Mied, Farid Askari, George O. Marmorino, Gaspar R. Valenzuela, and Dennis B. Trizna

183 Atmospheric Aerosol Size Distribution in the Marine Boundary Layer
James W. Fitzgerald and William A. Hoppel

187 Acoustic Backscattering from the Sea Surface
Peter M. Ogden and Fred T. Erskine

191 MATERIALS SCIENCE AND TECHNOLOGY

193 Vertex Simulation of Two-dimensional Grain Growth
Steven P. Marsh, Robert A. Masumura, and Chandra S. Pande

195 Structural Mapping of Ultrathin Films
Yves U. Idzerda, Gary A. Prinz, and David E. Ramaker

196 A Process to Make Ultrafine Metal Powders
Khershed P. Cooper and Jack D. Ayers

200 Advances in the State-of-the-art Growth of InSb by Using Molecular Beam Epitaxy and Organometallic Vapor Phase Epitaxy
D. Kurt Gaskill, Phillip E. Thompson, John L. Davis, and Gregory T. Stauf

205 NUMERICAL SIMULATING, COMPUTING, AND MODELING

207 Skywave Over-the-horizon Radar Performance Model
Benjamin T. Root

209 Decision Support for Operational Logistics
James B. Hofmann

213 OPTICAL SCIENCE

215 Subpicosecond All-fiber Laser
Irl N. Duling III

216 1.06 μm All-fiber Optic Gyroscope
William K. Burns and Robert P. Moeller

218 Heavy Metal Fluoride (HMF) Glass Windows
Ishwar D. Aggarwal and John M. Jewell

221 SPACE RESEARCH AND SATELLITE TECHNOLOGY

223 Anomalous Cosmic Rays
James H. Adams, Jr. and Allan J. Tylka

226 Far Ultraviolet Cameras Experiment on STS-39: Observations of the Far UV Space Environment
George R. Carruthers

231 Probing the Magnetosphere by Using Chemical Releases from the Combined Release and Radiation Effects Satellite (CRRES)
Paul A. Bernhardt, Joseph D. Huba, and Paul Rodriguez

234 Battery Impedance Effects on Spacecraft Electrical Power System Stability
Daniel J. Shortt and William E. Baker, Jr.
236 Ground-based Laser Measurements of Vibration of the LACE Satellite
Shalom Fisher, Donald Augenstein, and Kenneth I. Schultz

243 AWARDS AND RECOGNITION
245 Special Awards and Recognition
253 Individual Honors
267 Alan Berman Research Publication and Edison Patent Awards
271 Awards for *NRL Review* Articles

273 PROFESSIONAL DEVELOPMENT
275 **Programs for NRL Employees**—University education and scholarships, continuing education, professional development, and other activities
282 **Progams for Non-NRL Employees**—Fellowships, exchange programs, and cooperative employment

283 GENERAL INFORMATION
287 Technical Output
288 Key Personnel
289 Organizational Charts
293 Contributions by Divisions and Laboratories
295 Employment Opportunities
297 Location of NRL in the Capital Area
298 Index
Inside back cover *NRL Review* Staff

VIDEO CONTENTS

Fiber Optic-based Biosensor
by George P. Anderson, Lisa C. Shriver-Lake, Robert A. Ogert, Joel P. Golden, and Frances S. Ligler
Buckminsterfullerene: Building Blocks for New Materials
by Mark M. Ross, John H. Callahan, Steven W. McElvany, Mark R. Pederson, Larry L. Boyer, and Warren E. Pickett
Scale Model Analysis Facility
by Stanley A. Moroz and Ernest S. Mak
Heavy Metal Fluoride (HMF) Glass Windows
by Ishwar D. Aggarwal and John M. Jewell
Probing the Magnetosphere by Using Chemical Releases from the Combined Release and Radiation Effects Satellite (CRRES)
by Paul A. Bernhardt, Joseph D. Huba, and Paul Rodriguez

This video is available for loan from the Naval Research Laboratory, Ruth H. Hooker Research Library and Technical Information Center, Code 4820, Washington, DC 20375-5000.

Mission

To conduct a broadly based multidisciplinary program of scientific research and advanced technological development directed toward maritime applications of new and improved materials, techniques, equipment, systems and ocean, atmospheric, and space sciences and related technologies.

THE NAVAL RESEARCH LABORATORY PROVIDES:

- Primary in-house research for the physical, engineering, space, and environmental sciences;
- Broadly based exploratory and advanced development programs in response to identified and anticipated Navy needs;
- Broad multidisciplinary support to the Naval Warfare Centers; and
- Space and space systems technology development and support.

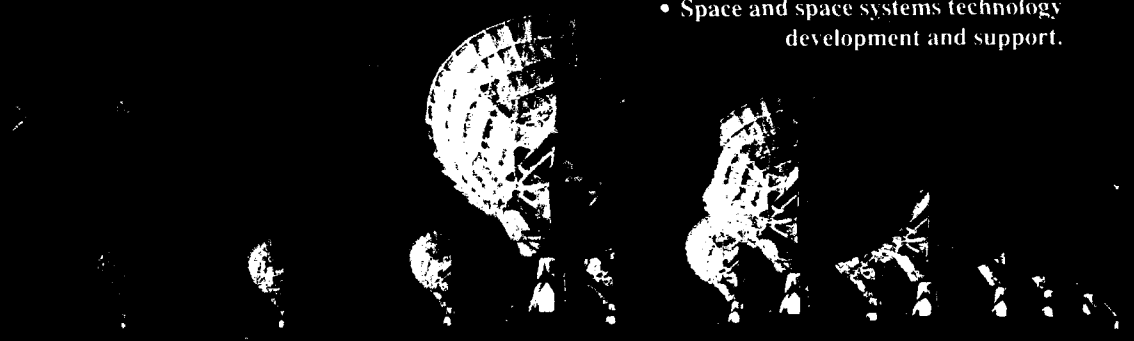

The Very Large Array
Facilities/Project Photos, *First Place*
Andrew W. Clegg

The Very Large Array (VLA) radio telescope located near Socorro, New Mexico, consists of 27 dish antennas connected in a Y-shaped configuration. Radio astronomers from NRL use the VLA to produce extremely detailed radio "photographs" that aid in the understanding of the universe.

On 14 January 1992, the Naval Oceanographic and Atmospheric Research Laboratory merged with the Naval Research Laboratory. Information about this consolidation may be found in the Preface, *Corporate Laboratory—Reaffirmed and Expanded,* on the Organization Chart, and in the listing of Key Personnel found in the General Information section of this publication.

NRL facility at
Stennis Space Center, Mississippi

Introducing NRL Bay St. Louis and NRL Monterey

NRL facility at
Monterey, California

Preface

CORPORATE REAFFIRMED

"... NRL will progressively integrate the former NOARL with NRL, joining previously discrete NOARL and NRL programs into a Laboratory directorate that focuses on the maritime environment—from space to the sea bottom."

CAPT Paul G. Gaffney II, USN
Commanding Officer

Among the myriad of scientific and management accomplishments that characterize NRL each year are a set of special highlights, which this year included significant contributions to DESERT SHIELD/STORM, important new cooperative agreements and licensing with industry, major individual recognitions, the appointment of a number of NRL employees to Navy and DoD policy-making groups, reaffirmation of NRL's corporate charter, and the merger of the Naval Oceanographic and Atmospheric Research Laboratory (NOARL) with NRL. NOARL, with campuses at the Stennis Space Center near Bay St. Louis, Mississippi, and in Monterey, California, was dedicated to expanding knowledge of the natural environment in which the Navy trains, operates, and fights. Throughout the remainder of FY 92, NRL will progressively integrate the former NOARL with NRL, joining previously discrete NOARL and NRL programs into a Laboratory directorate that focuses on the maritime environment—from space to the sea bottom. Corporate thinking will be a hallmark of the new, expanded NRL.

The most prominent characteristic of NRL's recent consolidation is seen in the ocean-atmosphere-space sciences. Yet, the consolidation is much broader than mergers within one scientific field. The Secretary of the Navy reaffirmed the need for a corporate laboratory, reaffirmed NRL's breadth and its full-spectrum nature, reaffirmed its principal but not exclusive focus on science and technology, and recognized its full spectrum lead in space systems, technology, and development, as well as in naval ocean and atmospheric related R&D. The Secretary also chartered NRL explicitly with responsibility to support the Navy's four new consolidated warfare centers.

NRL's quality has stood it in good standing through the redefinition of the Navy's technological infrastructure, and it is well positioned to contribute to the Navy of the future and to the general technological health of the nation. ★

LABORATORY—AND EXPANDED

It is an understatement to say that we are in a time of great change. The events of the past few years certainly fall into the category of "unpredictable." The consequences of these events are also unpredictable. It is assured, however, that they will have a significant impact on the national and international scene, and very specifically, upon the defense research establishment. The consolidation that Captain Gaffney has spoken about in his comments is but a first step on a long road of adjustment to a new world situation. No one knows the actual outcome of the journey we are now undertaking. I believe, however, that NRL is especially well positioned to contribute to the national effort of adjustment. The merger of NOARL into NRL restores the full breadth of the corporate laboratory. There are few organizations in the world that have the charter and the capability to engage in research and development on the scale that is possible at the new NRL. This will be especially important in the coming years. Science and technology will play an increasingly important role in the long-term defense policy of the United States. I believe the best advice to NRL is to keep technical productivity up and exploit our broad capability by engaging in cooperative programs among the various divisions and laboratory organizations. As a Laboratory, we can bring a great more to the table than we can as individual components of NRL. In the process of various adjustments, we must maintain good connectivity with the Navy and DoD planners, with the warfare centers, with academia, and with industry. We should be also looking for various teaming arrangements with activities external to NRL—there will not be adequate resources to do all that must be done by ourselves.

The Laboratory is highly regarded, it is highly productive, and it is well placed. I believe it will continue to prosper and will continue to make the type of contributions that have placed it in the position of high regard it currently occupies. ★

Dr. Timothy Coffey
Director of Research

"There are few organizations in the world that have the charter and the capability to engage in research and development on the scale that is possible at the new NRL."

Science and Art: A Contest and a Celebration

Herbert Gursky
Space Science Division

INTRODUCTION

The Naval Research Laboratory (NRL), like other contemporary research establishments, generates an enormous quantity of visual material in conjunction with its scientific and technical activities. No one keeps records, but the impression is that the quantity is increasing, not just in number, but also in variety and quality. To a great extent, this is the result of the tremendous technical advances in computer generated graphics. One hundred years ago, scientists had to engage illustrators or be artists themselves to portray their findings. Fifty years ago, photography had vastly expanded the capability of scientists to record and make representations of their findings. Today scientists have an extraordinary capability to combine data sets, create images, and produce visual products at their computer terminals.

In recognition of this body of material and its potential for visual impact, NRL held its first "Science-as-Art" contest. Fortuitously, this year also marked the 75th anniversary of the birth of Dr. Herbert Friedman, an individual who has achieved rare distinction as a scientist and who has left an indelible mark on the Laboratory during his almost 50-year career. Friedman, who received his early training as an artist, has conducted experiments

Editor's note: in May 1991, NRL sponsored the first "Science-as-Art" contest to honor Dr. Herbert Friedman, Chief Scientist Emeritus of the E.O. Hulburt Center for Space Research, on the occasion of his 75th birthday. In this first article, Dr. Herbert Gursky, superintendent of the Space Science Division, discusses the relationship between science and art. In the next article, Dr. Friedman, a space research pioneer, gives his thoughts on the frontiers of space research.

that have had a substantial scientific impact and that can be described as "beautiful." Thus it was appropriate to link the two and dedicate the contest to this remarkable individual.

In this article I will discuss the results of the contest and describe a portion of Friedman's scientific career. I will also explore the relation between science and art.

The "Science-as-Art" Contest

The contest was announced to the Laboratory in early May. Eventually 120 entries were received in five categories. The contest rules stipulated that the entry be submitted by an NRL employee and that the subject result from a scientific or technical effort supported by NRL. Since the scientific or technical merit of the work was to be used as an element in the judging, entrants were required to submit a paragraph describing the entry's significance.

"These images are attempts by professional scientists and engineers to present information ...relating to natural processes and physical phenomena or to the facilities used in the research and development processes."

The selection of winners was left to a panel of five individuals, each having an association with NRL. None was an artist or art critic by profession. All however had a substantial private interest in art. Fifty-two of the entries were displayed during a six-week period in June and July. By all accounts, the exhibit was well received. Those of us who organized and prepared for the contest were surprised at the number and quality of the entries. There is anecdotal evidence that much of the Laboratory's computational image processing capacity was tied up by entrants preparing their images during the last few days prior to the deadline of the contest.

Images as Science

Three of the winning entries are shown in this article; others appear on the cover, the Mission page, the Divider pages throughout this book, and in the Color Presentation section, which follows Dr. Friedman's article. These entries are certainly handsome, but they were not produced by individuals trained as artists or whose principal activity is producing works that are regarded as art by either the public or by art critics or art historians. These images are attempts by professional scientists and engineers to present information, accurately and economically, relating to natural processes and physical phenomena or to the facilities used in the research and development process. They are syntheses of a great body of data, physical concepts, engineering details, and theoretical speculations that comprise specific scientific and technical elements.

"A Microwave Image of the World," submitted by Glenn Sandlin, David Spangler, and James Hollinger of the Center for Advanced Space Sensing, is an example of a picture of the Earth that has only become possible with the advent of space satellites. The image was produced by recording the radio emission of the Earth by an instrument developed jointly by the

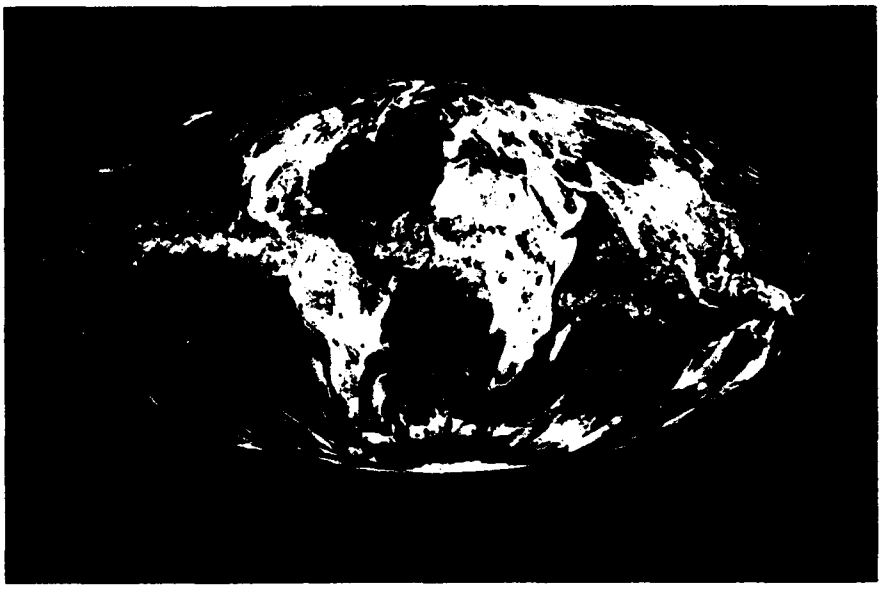

A Microwave Image of the World
Scientific Data/Visualization (Color), *First Place*
Glenn Sandlin, Center for Advanced Space Sensing

Navy and the Air Force and flown on an Air Force meteorological satellite. At any instant of time for this particular image, the radiation from a 13-km patch of the Earth was recorded; the whole Earth image was obtained by accumulating four days of data as the satellite passed over the entire globe. The Earth acts like a cool, incandescent light bulb, overlain with moist air, rain, and clouds, each of which leaves an imprint on the radiation. "A Microwave Image..." is a map of the Earth's temperature distribution, cloud cover, and moisture content with a level of detail that had never been possible before the advent of spaceborne sensors. The Earth globes produced by the mapmakers are no different today than they were 30 years ago, before space flights became routine. Yet we now look at the Earth in a different way. Whole-Earth images, such as the one shown, are an essential element in producing the change.

"A Geometric Jumble," submitted by Roger Eisinger of the Space Systems Technology Department, is an ordinary photograph taken from a construction crane above a partially completed radio telescope. The telescope will be used in a program of satellite tracking and space research. Aside from its attractiveness, this image derives importance from its uniqueness. The telescope has been captured midway through its development; thus, we can see the intricacy of its internal structure, which will completely disappear upon its completion. The telescope itself, which is 60 feet across, will be enclosed in a geodesic dome made up of triangular panels. Here the dome is only half completed, and its structure and method of assembly are clearly apparent. The telescope within resembles a large, curiously spoked wheel. It will eventually be sheathed in aluminum panels, each individually adjusted, which will comprise the

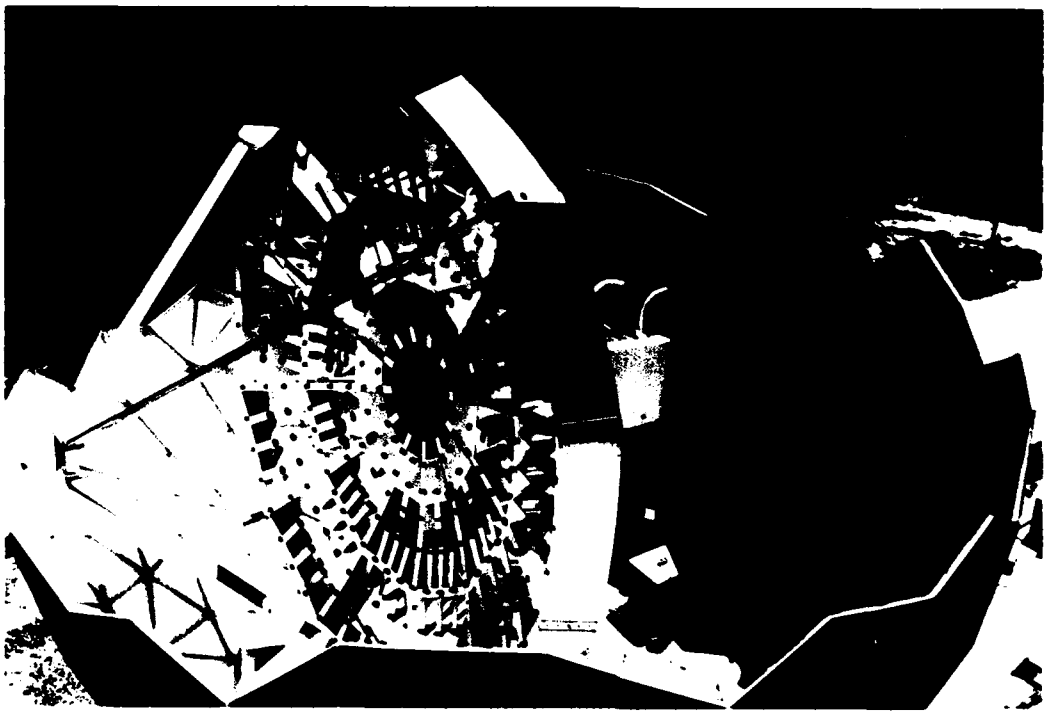

A Geometric Jumble
Facilities/Project Photos, *Third Place*
Roger Eisinger, Space Systems Technology Department

reflecting surface. This one image reveals the essence of the telescope's construction. What a pity there is no such portrayal extant of a medieval cathedral made during its construction.

"Beams in a Lens—Reflection, Refraction, Critical Phenomena," submitted by Susan Numrich of the Acoustics Division, represents a very different kind of image. This computer graphic represents the work of a theoretician in an attempt to model and understand a natural phenomena—the propagation of sound waves in the ocean. The triangle seen in the image is a prism created by arbitrarily changing the sound speed in a portion of the simulated ocean. Centered in the prism is a small region from which emanate sound waves. Their interference, reflection, and refraction as they move through the medium produce a complex pattern of waves. This image is an analog to the barely rippled ponds and heavy seas popular with traditional artists. It is also typical of a vast body of imagery emerging from the scientific community. As is frequently the case, the scientist has started with an idealized situation—a prism—to study the phenomenon. Although not apparent, the image is extraordinarily complex and required the largest computational capability available at the Laboratory to produce. It is common to think of physics as formulas and equations. More often than not, the complexity of the phenomenon under investigation does not allow representation by even the most complex formula. Its description lies in computational rules, and the results exist in huge data files that must then be translated into some sort of

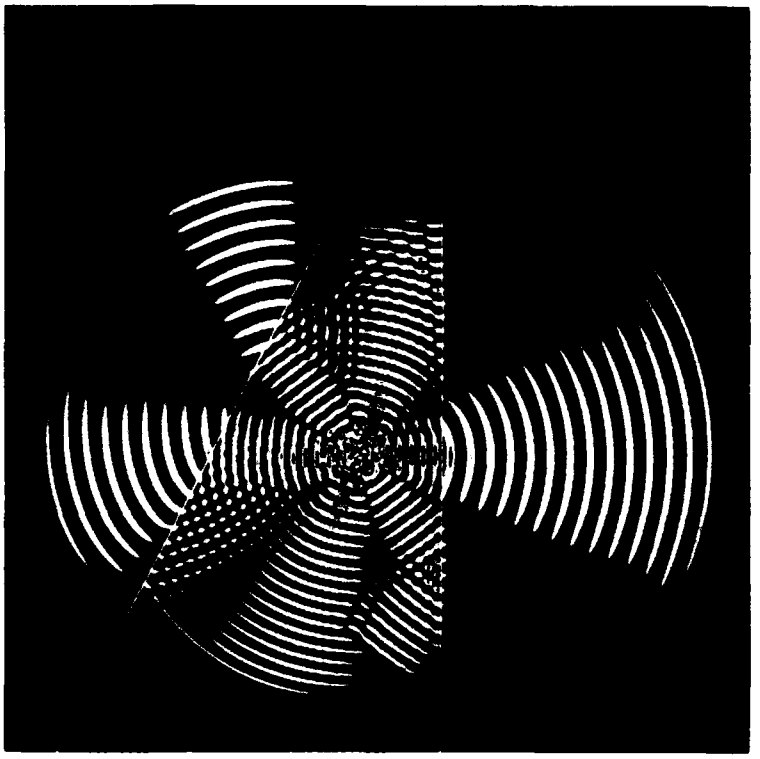

Beams in a Lens—Reflection, Refraction, Critical Phenomena
Computer Graphics, *First Place*
Susan Numrich, Acoustics Division

visualization to allow an understanding to develop.

Science as Art: Examples from a Career

In architecture, science and technology can be combined by an individual to produce a work of art. However architects produce single, relatively permanent edifices. Even scientific facilities rarely survive once their scientific goals have been met. There are examples of scientific work, however, that can be described in terms akin to architecture, where technical advances are distinct and identifiable and show the mark of a specific individual. Herbert Friedman's career contains examples of such work. Friedman was fortunate to be an active scientist at just the time that rockets began to be used for investigations from above the Earth's atmosphere. A backlog of scientific issues existed then that could only be resolved through such investigations. At its onset, science from rockets was very much an individual effort—one person could be responsible for designing and developing the instrumentation, planning the observations, organizing the field activities, and analyzing the results. Friedman did this repeatedly, and his success reflected his ability to devise the crucial observation and the technical insight needed to use the most appropriate instruments in the most effective manner. Two examples follow.

Early Rocket Research

One of the first targets for rockets was the Sun—specifically, a search for and study of the Sun's ultraviolet and X-ray emission that cannot penetrate

the atmosphere. By the late 1950s, it was apparent that the Sun was a copious source of X rays. One question that arose was "where exactly on the Sun do the X rays come from?" Was the entire atmosphere the source, or were the X rays emerging from small, discrete regions, such as sunspots? Today we can image the Sun with high quality X-ray optics; in the 1950s, no such devices were available. Friedman chose a natural occulter, the Moon, to provide the answer. He arranged to fly a series of small rockets during an eclipse of the Sun by the Moon. As the Moon gradually moved across the Sun, it would block the sources—gradually if the sources were large, suddenly if the sources were small. The series of flights was successfully carried out on 12 October 1958 from the back of a naval vessel in the South Pacific in the path of the eclipse and at the moment that the Moon began its incursion into the Sun's disk. The data, while crude by current standards, provided the answer—that the sources were small and appeared to be associated with sunspots. Furthermore, significant emission was observed even during the few moments of totality, indicating that some of the emission was emerging from high above the solar surface.

Later X-ray Research

In 1964, Friedman again turned to an eclipse by the Moon to answer a compelling scientific question, not of the Sun this time but of a celestial object, the Crab Nebula. In 1961, copious X-ray emission had been discovered from an apparently new class of celestial emitters, enormously more luminous than the Sun at these short wavelengths. One of the objects found to be a source of X rays was the Crab Nebula, known to be the thousand-year-old remains of a supernova—the explosion of an entire star. At that time, it was thought possible that a neutron star could be formed during this process. Friedman addressed the question of whether such an object existed at the center of the Crab and whether it might be responsible for the observed X rays. It has subsequently been learned that neutron stars are common. They are frequently bright X-ray sources and comprise the class of stars known as radio pulsars.

"A neutron star has since been discovered in the Crab Nebula that emits pulses in both radio and X rays. Ironically, it was Friedman himself who found the X ray pulsing during yet another rocket experiment."

Friedman devised a rocket flight to take place from the White Sands Missile Range just at the time that the Moon began to cross the nebula. This time the data showed that the X-ray emission subsided gradually, indicating that it originated from the nebula as a whole rather than being concentrated in a single point as might be expected from a neutron star. A neutron star has since been discovered in the Crab Nebula that emits pulses in both radio and X rays. Ironically, it was Friedman himself who found the X ray pulsing during yet another rocket experiment. The X-ray emission from the neutron star was simply too faint to be observed against the nebular emission during Friedman's earlier experiment.

These experiments were isolated, discrete occurrences. They involved a sequence of events—the original concept, the development of the hardware, the rocket flight, and the analysis and dissemination of the results. They were of high scientific importance at the time. The aesthetics of these experiments is very different from that associated with art or even scientific imagery. Nowhere is there the kind of visual impact associated with art; nor can one find the object or the edifice associated with the work. They are not studied as examples of how to do science; they barely get mentioned in the few books written on the history of science. The results themselves are quickly rendered obsolete and sometimes even prove to be incorrect. They exist principally as narrative descriptions of the kind that I have provided, yet scientists and engineers, at least, can look at them as things of beauty.

The various disciplines have become too complex for individuals to develop a high degree of professionalism in both science and art. One has to make a choice, as Friedman did. But there is an artistic impulse among scientists and engineers, possibly akin to what occurred when art was just developing and before it had become formalized. Individual expression and an appreciation of form and structure are human attributes that contribute to science and technology as well as they do to cathedrals and printmaking.

ABOUT THE AUTHOR

HERBERT GURSKY received a Bachelor's degree from the University of Florida in 1951, a Master's degree from Vanderbilt University in 1953, and a Ph.D. degree from Princeton University in 1959. His first professional position was at Columbia University as an instructor in the Physics Department from 1958 to 1961. In 1961, he joined American Science and Engineering, Inc. (AS&E) in Cambridge, Massachusetts, as a senior scientist and rose to the position of vice president of space research in 1967. In 1973, he joined the Smithsonian Astrophysical Observatory (SAO) as a supervisory astrophysicist. In 1974, Dr. Gursky was appointed professor in the Practice of Astronomy at Harvard University and in 1976 was named associate director of the Center for Astrophysics for the Division of Optical and Infrared Astronomy. In 1981, Dr. Gursky joined NRL as superintendent of its Space Science Division and chief scientist of the E.O. Hulburt Center for Space Research. The Space Science Division, with a professional staff of 70 scientists and engineers, conducts research in the areas of atmospheric, solar, and astronomical research, mostly from space.

Dr. Gursky is best known as a member of the group that made the discovery of cosmic X-ray sources in 1961, his work with sounding rockets that culminated in the optical identification of the bright X-ray source Scorpius X-1 in 1966, his work on clusters of galaxies and the diffuse X-ray background from the Uhuru Satellite, and the discovery of X-ray bursters on the ANS satellite. Dr. Gursky's research activities have concentrated in the area of X-ray astronomy. He has published more than 100 articles in this area and has edited two books on the subject. He was the principal investigator for NASA-sponsored programs on the ANS and HEAO-1 satellite and a co-investigator on numerous other rocket and satellite experiments. Dr. Gursky is still an active research scientist in the area of X-ray astronomy.

From the Challenges of World War II to the Frontiers of Space

Herbert Friedman
E.O. Hulburt Center for Space Research

THE "FREE ENTERPRISE" YEARS

I entered NRL's Metallurgy Division in 1940, with a brand new degree in solid state physics and a thought of pursuing fundamental studies of ferromagnetism. Instead, I discovered a world of problems that had never before penetrated my academic consciousness. My predecessors in metallurgy included Robert Mehl and Charles Barrett, who had left a legacy of X-ray diffraction research techniques and equipment to Herman Kaiser, with whom I set about designing a variety of applications to nondestructive testing, stress analyses, and studies of high-temperature phase transformations. Nondestructive testing was typically a primitive and routine operation, gamma-ray radiography of valve castings, for example. The need for electronic diagnostics was obvious, and I was led into research on all forms of radiation sensors—from diamond crystals to phosphor scintillators to gas discharge devices. These studies were pursued as basic research but with a constant eye to invention and application.

The Urgency of Wartime R&D

A gratifying opportunity to apply such techniques to an urgent military problem came immediately with our entry into World War II. B-17 bombers were grounded in Africa for lack of quartz crystal oscillator plates to fit their communication sets. The Japanese had stripped South American sources of the best-quality quartz just prior to Pearl Harbor and had left for us only poorly faced material that could not be oriented for cutting by

optical means. Because the Laboratory, through the work of Elias Klein in the Sound Division and Leo Dawson in the Optics Division, had become a center of expertise on piezoelectric crystals and their applications, it was only natural that the problem should be brought to our attention. Within a couple of days, I was able to assemble a proportional counter X-ray goniometer suitable for orienting unfaced crystals so that they could be cut to the various prescriptions for oscillator plates. This method went immediately into industrial use with commercial X-ray units, but there were no suppliers for proportional counters. An essential feature of the counter tubes was a very thin reentrant glass bubble window to transmit soft X rays. These windows were a special skill of Leland Clark, our master glassblower. We were obliged to set up manufacturing to supply hundreds of these tubes to industry on a rush basis. (Each batch included sufficient spares to satisfy the irresistible urge of the inspectors to poke a finger at the delicate glass window.) I believe this X-ray orientation device may have been the first introduction of radiation-counter techniques into an industrial-type production and control process. A citation for this invention made the generous estimate that it saved 50-million man-hours in the war production effort.

In the process of further developing the instrumentation connected with the production of crystal oscillators, interesting properties of detectors and X-ray optical systems were recognized, which stimulated new research and invention. Counters were made to be UV as well as X-ray sensitive, which offered the possibility of developing solar-blind and narrow-band UV detectors of very high sensitivity. The quartz orientation spectrometer suggested obvious extensions to diffractometry and spectrochemical analysis in its broadest aspects. About that time, I was adopted by Dr. E.O. Hulburt, who established the Electron Optics Branch. To justify this new organization, Mrs. Mae Pope, the chief clerk of the Laboratory, wrote a one-paragraph job description to the effect that I would devote my efforts to "developing applications of electrons to naval problem." (In those days Mrs. Pope could handle 90% of the administrative operations of the Laboratory.) Then, and for many years subsequently, I had no need to work up detailed budgets; money seemed to appear whenever required in response to any reasonable request to follow up a promising new avenue of research.

"I had no need to work up detailed budgets; money seemed to appear whenever required in response to any reasonable request to follow up a promising new avenue of research."

Dr. Hulburt and the Community of NRL Physical Scientists

Contact with Dr. Hulburt opened up an awareness of natural optical phenomena. We talked of ozone and the blue color of the sky, of the exosphere and particles in satellite orbits, of camouflage and haze and visibility, and solar control of the ionosphere. We produced a UV backscatter haze meter that used a solar-blind photon counter, a UV smoke detection scatterometer, and a flame detector for

use on aircraft, in hangars, and in ships' holds. The invisible UV corona around high-voltage equipment and the corona around missiles launched from aircraft were shown to be readily detectable. My chemist friends, particularly Peter King, became intrigued with the possibilities of UV detection of chemical warfare agents (like mustard and phosgene) and industrial toxic contaminants (such as mercury and tetraethyl lead). All of these were found to be detectable in extremely low concentrations with simple, nondispersive UV absorption systems.

Peter King and Alan Alexander were also attracted to the use of the X-ray diffractometer in studies of pigments. Soon I was involved in problems of bottom paints to prevent barnacle growth. The diffractometer showed very simply that the major difference in effectiveness of paints then in use depended on whether they contained cuprous or cupric oxides. From the diffractometer to an X-ray fluorescence elemental analyzer was a short step, and our metallurgists were enthralled with the new capability for rapid analyses of alloys that ordinarily required hours of wet chemistry. These early diffractometer and fluorescence analyzers have since grown to great sophistication and are basic to any modern analytical laboratory. At the time of their development, however, most physicists were still using slow thyratron counting circuits. Claude Cleeton and his electronics group at NRL had developed hard vacuum tube circuits for fast counting, which were immediately adapted to our X-ray systems. The first visibility of such hard vacuum tube, fast-counting instruments in industrial applications came from these NRL inventions.

"From the diffractometer to an X-ray fluorescence elemental analyzer was a short step, and our metallurgists were enthralled with the new capability for rapid analyses of alloys that ordinarily required hours of wet chemistry."

Development of Improved Sensors and Their Applications

We never lost touch with a host of nondestructive testing applications of X rays and gamma rays coupled with specially devised detectors. The requirements of uniformity in production of detectors of long life and ruggedness were solved with the knowledge gained from fundamental studies of electronegative quenching gases in electrical discharges. First, halogenated hydrocarbons and then halogens themselves came to be used as quenching agents in relatively stable and permanent gas counters. These were applied to the recovery of radium-tagged test torpedoes at Piney Point, Maryland, to a backscatter gamma-ray device for checking the corrosion of tanker bulkheads at the Norfolk Navy Yard, to measuring the lead coating thickness on condenser tubing aboard the USS *New Jersey* in the Boston Navy Yard. A publication describing many such potential uses came to the attention of Commander Lester Wolfe at the Navy Bureau of Aeronautics and brought him quickly to talk with us about applications to

aircraft instruments. Fuel quantity gauges on aircraft were a particularly sore problem. On the SBD dive bomber, the tendency during takeoff was for the float gauges in the wing tanks to bounce against the tacky self-sealing liner and then stick to that surface for the rest of the flight, leaving the pilot to guess about his fuel reserves. Commander Wolfe wanted a radiation gauge. We placed radium buttons on four corners of the SBD wing tank and a Geiger counter on the underside. The system worked well and was contracted to Bendix for further development. Later the basic principle was applied to fuel flow gauges on rockets.

With the end of the war in Japan, the Navy Medical Research Center was assigned the responsibility for assessing radiation damage on the islands of Hiroshima and Nagasaki. Shields Warren, then a Navy Captain, came to NRL to discuss the problem of measuring residual radioactivity. No simple portable radiac devices were available. The Manhattan Project had done a magnificent job in building the bomb, but it had not developed any of the now-common types of portable radiation monitoring devices. Within a week, we prepared a set of portable radiacs for the Navy team, which permitted them to contour map the entire radiation pattern.

This contact with medical people led to many new ideas for research and instrumentation. Captain R. H. Draeger, then Executive Officer at the Naval Medical Research Institute, became a regular visitor to NRL. We worked on an evaluation of anoxia by flicker fusion tests and developed an instrument intended for use aboard military aircraft. Studies of blood hemoglobin were accomplished by X-ray fluorescence of the iron constituent, and detectors were developed for use with radioactive iodine tracers in studies of thyroid malignancy. The possibilities for physical instrumentation in medicine seemed endless.

Atomic Weapon Effects

In the immediate aftermath of the war, we became concerned with atomic weapons effects. Ed Hulburt, John Sanderson, and Ernst Krause organized a program of tests for the Bikini Island test site. Simple, rugged, high-dose dosimeters were required. From experience in the frequency adjustment of quartz crystal oscillator plates by X-ray irradiation, we had become aware of radiation-induced color centers in crystals and glasses. Silica glass dosimeters were placed near bomb zero and gave direct measures of dose and spectrum. Next came the challenge of how to guarantee detection of a Soviet bomb test if and when the Russians succeeded in producing a nuclear device. NRL's expertise included filter technology for chemical warfare under Gene Ramskill in the Chemistry Division. With his help, Irving Blifford and Joe Nemecek designed a variety of collectors, ranging from small portable units to hugh, hundred-thousand-cubic-feet-per minute installations. As we began to observe the collection of

"Next came the challenge of how to guarantee detection of a Soviet bomb test if and when the Russians succeeded in producing a nuclear device."

atmospheric radon decay products with such equipment, we became aware of the scrubbing action of rainfall. We went back to Peter King with the question of how could we concentrate particulate radioactivity from rainfall. He proposed the standard flocculation treatment of our municipal reservoirs. From Dalecarlia reservoir in Washington, D.C., we scooped some flocced sludge, and at NRL, Sverre Gulbrandesen and Luther Lockhart teamed to extract cerium and yttrium. Our beta-ray counter went wild when their concentrate was placed under it. We were detecting fission products from the Bikini Island test. Lockhart made similar analyses of rainwater from catchments in the Virgin Islands and Kodiak, Alaska, with positive results. We then equipped Navy air weather centrals with catchments made of Sears, Roebuck and Company's plastic roofing and arranged to routinely floc the collected rainwater and ship the residues back to NRL. At each site, we placed large banks of Geiger counters covered by water trays to directly and immediately indicate any large precipitation of radioactivity. The first Soviet test triggered the Rain Barrel system with a bang. Lockhart analyzed the floc from Kodiak for plutonium without access to the secret procedures developed in the Manhattan Project. Maurice Shapiro, in the Nucleonics Division, confirmed the plutonium analysis with measures of the alpha tracks in photographic emulsions.

THE EARLY ROCKET YEARS

In 1936, Peenemunde had been established by the German military as the center for rocket development. By 1939, Wernher von Braun and his team had perfected the V-1 rocket, and by the end of World War II, the V-2 was also hitting England. When American forces entered Germany in 1945, the huge underground factory for V-2 production at Nordhausen was high on their priority list to capture. In a race to beat the Russians to Nordhausen, the Americans won and confiscated about a hundred rockets. The rockets were shipped to the White Sands Missile Range in New Mexico, where the

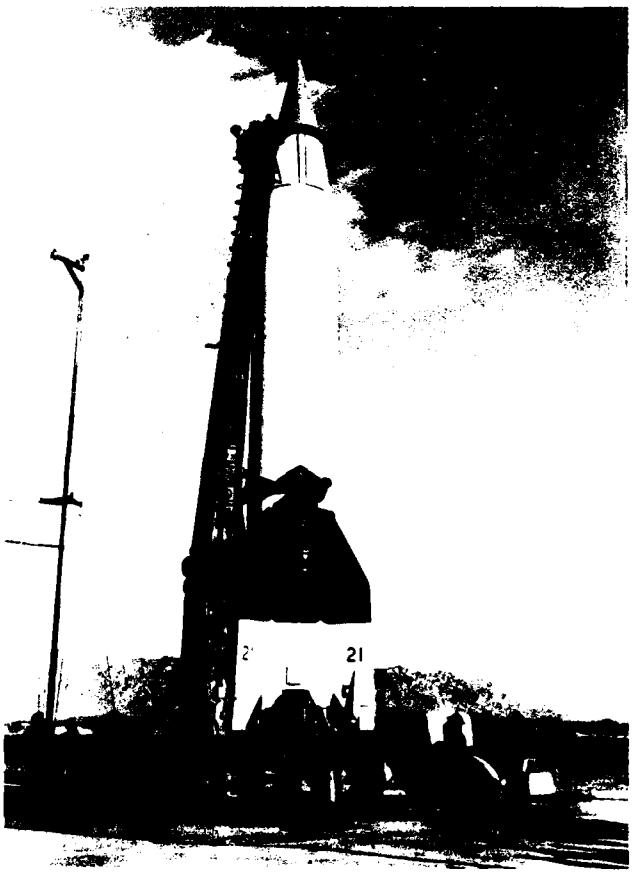

Early V-2 preparatory to launch at the White Sands Missile Range

Army set about studying the propulsion system. The first American-launched V-2 flew from White Sands on 16 April 1946. Some 60 launches were carried out—up to the fall of 1952.

With the arrival of V-2 rockets in the United States, NRL scientists immediately grasped the new opportunities for upper atmosphere research and solar astronomy. My sights focused on the prospects of solar-terrestrial physics, and in a few years, I was totally committed to the project. Solar astronomy became the pathway to study of the entire universe in every realm of the electromagnetic spectrum. No matter how many times you witnessed it, the launch of these rockets was always inspiring. After the short-lived bursts and rapid acceleration that characterized the firing of small rockets, the slow, majestic rise of the V-2 and the sudden vanishing of the roar of the rocket in the eerie quiet of burnout was a breathtaking experience. Silent, snaking vapor trails marked the passage of the rocket through the stratosphere, and sound returned only near landing when shock waves reverberated from the mountains.

Solar Astronomy with the V-2s

We expected the V-2 to become a great asset for solar astronomy, but it came with a variety of handicaps. It was 45 feet tall and 5 feet in diameter, and the motor was so large that a man could crawl through the nozzle. It had been designed as a weapon, not as a tool for high-altitude research, but the Army offered the space of the 2000-pound warhead to the scientific community for instrumentation. In the early days at White Sands, one had to be something of an acrobat to mount an experiment in the nose of the V-2. To get to the top of the rocket meant climbing a long extension fire ladder. A little later a gantry was built, and from then on, access to the rocket was much simpler and safer.

The first five of the huge rockets all returned nose down in streamlined flight and buried their pulverized remains in craters about 30 feet deep and 80 feet in diameter. Not a trace could be found of the first spectrograph flown by NRL in June 1946. In the few buckets of debris that were sifted from tons of overlying sand, there was no trace of the film cassettes. Subsequently, to reduce the impact speed, streamlining was destroyed by blowing off the warhead at 50 kilometers on the down-leg. The rocket then broke up, scattering parts over a large area of the desert. Smaller and lighter parts decelerated to landing speeds below 0.1 kilometer/second. The separated warheads tumbled down erratically with only minor impact damage.

Rarely did the V-2 fly like an arrow, straight into the sky. As often as not, the rockets tumbled and faltered. Some burned up furiously upon ignition. One rocket reversed direction from north to south and headed for El Paso, Texas. It crossed the Mexican border and struck next to Tepeyac Cemetery, about a mile and a half from Juarez. The impact barely missed a warehouse full of commercial blasting powder and dynamite. This event may be recorded as the first U.S. ballistic missile strike on foreign soil. On the day after the incident, street urchins were hawking souvenir parts (total weight about ten times the

rocket!) in the markets of the city. On another occasion, a rocket fell near wandering tourists on the pristine sands of White Sands National Park, which borders the rocket range.

The first NRL success in rocket astronomy came on 10 October 1946, when a team led by Richard Tousey flew a small, grating spectrograph only a foot-and-a-half long and captured the solar UV spectrum below the ozone cut-off at 3000 Å down to a short wavelength limit at about 2200 Å. When compared to modern instruments for spectroscopy, the rocket was flea-weight and toylike, but it worked.

Ionospheric Studies with X-Ray and UV Sensors

From studies of electro-negative gas mixtures in discharge counters, I discovered interesting possibilities for combining long wavelength filters and selected gas mixtures to produce narrow bandwidth response characteristics in photon counters for the extreme UV. At the time, the NRL solar spectroscopy team in the V-2 program was experiencing many frustrations in their efforts to achieve simultaneously high altitude, good pointing control, and successful recovery of instrumentation and film cassettes. It occurred to me then that photometric measurements could be carried out over the entire range of the UV and X-ray spectra with our newly developed, very sensitive, narrow bandwidth detectors in combination with radio telemetry. This procedure avoided pointing controls and film recovery after impact.

"The first NRL success in rocket astronomy came on 10 October 1946.... When compared to modern instruments for spectroscopy, the rocket was flea-weight and toylike. but it worked."

The earliest opportunity to fly a set of photon counters came in 1949 and was entirely successful. Solar X rays were measured for the first time as a function of altitude of penetration of the upper atmosphere; they revealed the direct connection with production of the E region of the ionosphere. The principal resonance radiation of the hydrogen atom is known as Lyman alpha at 1216 Å. It penetrated to D region where it could ionize the trace constituent, nitric oxide. In the broad span of the Schumann region (1450 to 1750 Å), the flux of radiation was sufficient to dissociate molecular oxygen in a way that explained the height dependence of electron loss processes in the F-region ionosphere. Observations made with rockets over the next decade by the NRL team traced the full solar cycle control of the ionosphere and made it possible to model ionospheric processes in sophisticated detail.

From V-2s to Aerobees

In the micromanaged environment of today's big rocketry, it is hard to recall the casual coordination between shared experiments in the early V-2s and Vikings and the emphasis on individual initiative. For the first few years of the V-2 program, experimental preparations were rushed, and glitches in the operations were common. There was sometimes great dismay and

embarrassment—for example, when a sophisticated cloud chamber instrument for cosmic ray studies was flown with the lens cap left on the camera. Because there was so much space aboard the V-2, it was parceled out on each flight to experimenters and last-minute bidders. Instruments were often placed in less-than-ideal juxtaposition. Packets of frogs' eggs or seedlings could be thrust upon the launch crews late in the preparations with pleas to tape them into any free space.

I was both guilty and innocent of ruining a colleague's experiment on my first V-2 flight. Unbeknownst to me, Herman Yagoda, a cosmic ray physicist from the Air Force's Cambridge Research Laboratory, had sent a photographic emulsion package to White Sands with instructions to mount it in any available V-2 space. It was the practice of my group to do a final checkout of our Geiger counters and telemetry after the payload was buttoned up by exciting them from outside with a 5-milligram radium source. Unwittingly, we were also exposing Yagoda's emulsion. To his subsequent consternation, his developed film exhibited an incredibly large number of electron tracks for the few minutes of exposure during the rocket flight. Yagoda was baffled, while we were totally unaware of the damage we had wrought. It was some time before the connection was made, and we all suddenly understood what had gone wrong with Yagoda's experiment.

To simplify conducting research with rockets, it was clearly desirable to trade the heavy payload lift capability of the larger rockets for more modest payloads aboard smaller, less expensive rockets dedicated to a single experiment. The Navy supported the development of the Aerobee, a two-stage research rocket consisting of an acid-aniline sustainer atop a solid propellant booster. The combination was fired out of a tiltable tower, which was 140-feet tall.

The sealing-wax-and-string approach to instrumenting the Aerobee typified much of our effort in the 1950s. We often went into the field with three rockets to attempt a single experimental objective because the rockets were relatively inexpensive. Mistakes experienced on the first attempt could be adjusted at the launch site by quickly preparing new detectors, for example, on a

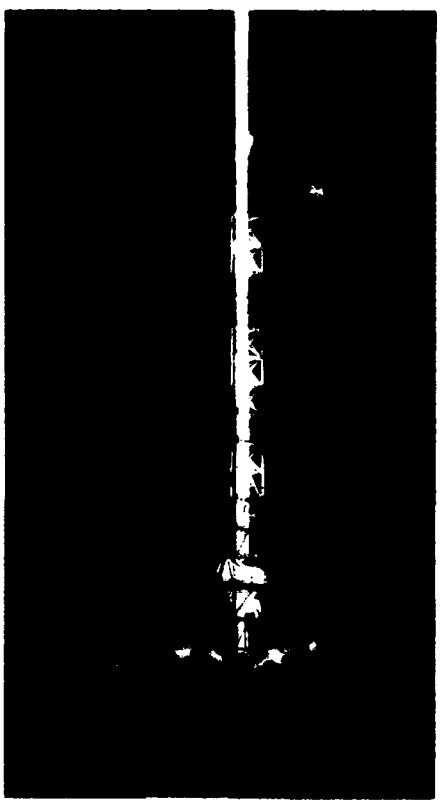

Night launch of Aerobee at White Sands Missile Range

rudimentary vacuum system—often with liberal use of wax and Glyptal resin paint to cement new windows, seal leaks, and insulate the electronics against corona discharge. The first Aerobee barely reached 80 to 90 kilometers, but simple modifications soon doubled its height performance, and the rocket became the workhorse of the research community. A cartoon drawn by Gilbert Moore (after Walt Kelly's Pogo) characterizes the team during the time of the Aerobee operations at the White Sands Missile Range.

Rockets at Sea

Of all the forms of solar activity, flares are the most spectacular and create the strongest impact on the terrestrial environment. A large solar flare produces prompt shortwave radio blackout that may last for two to three hours; this is followed by great auroral displays and ionospheric and geomagnetic storms for one to two days that seriously degrade radio communications.

The Aerobee was ill-suited to the study of solar-flare radiation because there is little capability for predicting the onset of a flare even within minutes of its outburst. It was impractical to tie up the launching tower for days with a rocket in place while awaiting a solar flare. Furthermore, the fuel system had to be pressurized with helium and, once ready, the launch could not be delayed for more than an hour.

In the early 1950s, Lieutenant Lee Lewis, assigned to the Office of Naval Research (ONR), conceived of launching a rocket suspended from a

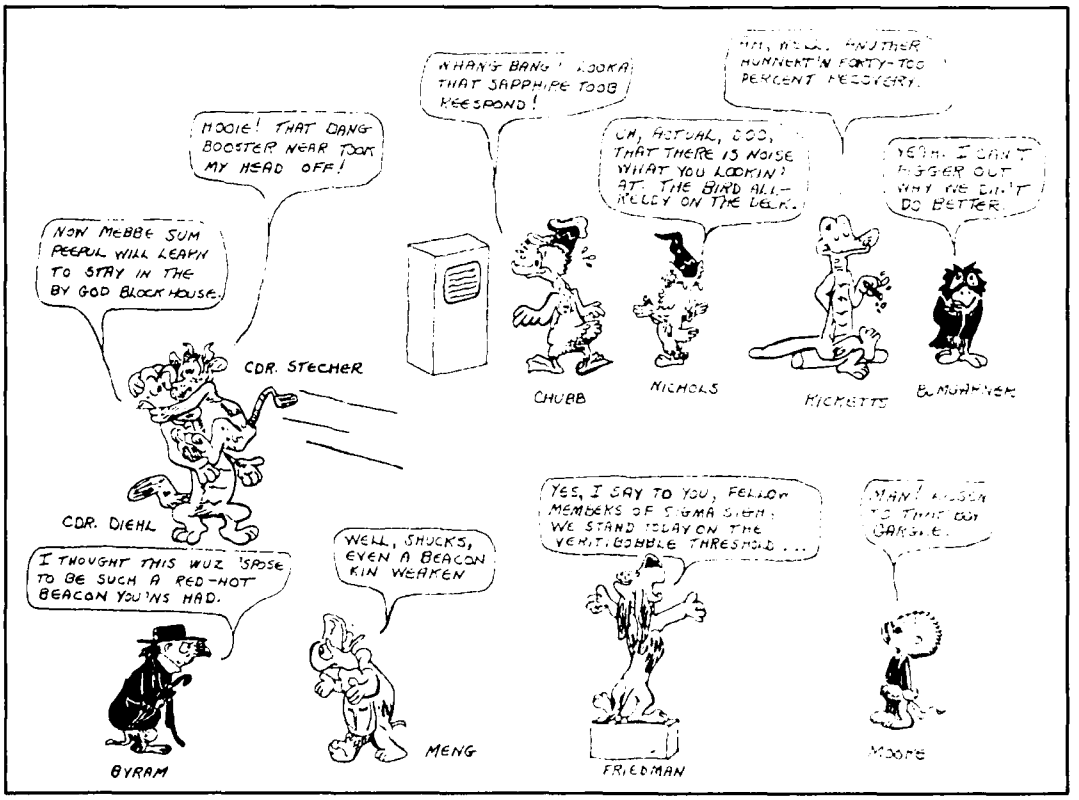

Aerobee operations at White Sands. Cartoon by Gilbert Moore after Walt Kelly's Pogo.

Deacon rocket and firing box dangling behind radar corner reflectors on skyhook balloon

balloon at stratospheric altitude. Experiments began with the "Rockoon," a solid-propellant Deacon rocket hung on a Skyhook balloon and floated at 25 kilometers from where it could be fired by radio command. Here was an inexpensive system (about $1,350) that could be kept in the air all day and fired at the moment that evidence of the onset of a flare was obtained.

Without recourse to a sophisticated orientation system on the balloon, the rocket's impact point could not be predicted within a circular area of about 100 miles radius, and winds contributed further uncertainty. Launch from shipboard far at sea offered range safety and facilitated the balloon launching operation. When the Skyhook balloon was being inflated, surface winds had to be less than 5 to 10 knots. By sailing downwind, the ship could achieve nearly zero relative wind conditions for inflation and release of the balloon with its suspended payload.

Solar Flares

The Rockoon seemed to be ideal for studying solar flares. An NRL proposal for a naval expedition as part of the International Geophysical Year (IGY) was strongly endorsed by the National Academy of Sciences, and ONR obtained the use of the USS *Colonial*, an LSD, and the USS *Perkins*, a destroyer, to support the experiment. However, in working with Rockoons, there was precious little experience to guide us. Igniters, for example, that had been designed for the ground-launched Deacon were unreliable at 80,000 feet. It must have appeared very amateurish for one of the NRL scientists, Jim Kupperian, to be playing the part of an explosives expert under the watchful eyes of the gunner's mate and to fiddle with new formulations of the igniter on the deck of the ship.

In 1956, the USS *Colonial* embarked on Project San Diego-Hi. We sailed to a launch area about 400 miles southwest of San Diego and released a Rockoon each morning on successive days. While the ships chased the drifting balloon, communications were monitored for information about flare occurrence. One flare finally gave convincing

Arriving at San Nicholas Island to initiate IGY solar flare program in 1957

evidence that X rays were responsible for the ionospheric disturbance.

A year later Rockoons were out of style. In place of the balloon, a Nike solid rocket booster lifted the Deacon to the stratosphere. The two-stage rocket was fired from a simple rail launcher that the NRL team set up on San Nicholas Island off Point Mugu, California. In 1958 and 1959, a series of these rockets were launched at times of solar flares, giving quantitative confirmation of the dependence of sudden ionospheric disturbances (SIDs) on the intensity and wavelength of flare X-ray emission.

NRL's marriage of rocketry with naval vessels in those years also involved launchings of the Aerobee and the Viking from the deck of the USS *Norton Sound*, but certainly the most exciting and glamorous outing was the IGY eclipse expedition to the Danger Islands in the South Pacific Ocean aboard the LSD USS *Point Defiance*.

The X-Ray Sun

Before the direct measurements of X rays from the Sun, theorists had surmised that the corona would be a source of thermal X rays at a temperature of millions of degrees. They argued that the great extent of the

Herbert Friedman, John Lindsey, and William Nichols with instrument sections of Nike-Deacon rockets launched from San Nicholas Island

corona required this high temperature to overcome the very strong pull of gravity at the surface of the Sun. This simple reasoning assumed that the corona was a great bag of gas—almost without structure. But the corona as seen at solar eclipses showed a great variety of structure that connected with sunspot regions. Although no X-ray images of the Sun had been obtained up to the time of the IGY, the evidence from NRL rocket measurements over a decade indicated a close link of X-ray emission to active sunspot regions on the face of the Sun. In 1958, a true X-ray-reflecting telescope had not yet been built and used successfully, but the eclipse of October 10 offered an opportunity to observe the X-ray distribution by making a series of measurements as the Sun was being occulted by the passage of the Moon across its face. In its path across the Pacific Ocean, the eclipse crossed only one piece of land, a group of coral atolls, the Danger Islands, about 400 miles southwest of Samoa. Following our experience with Project San Diego-Hi, I proposed to the IGY Satellite Committee of the National Academy of Sciences that support be provided to NRL to carry out a series of rocket firings from shipboard at the time of the 1958 eclipse in the vicinity of the Danger Islands. The proposal

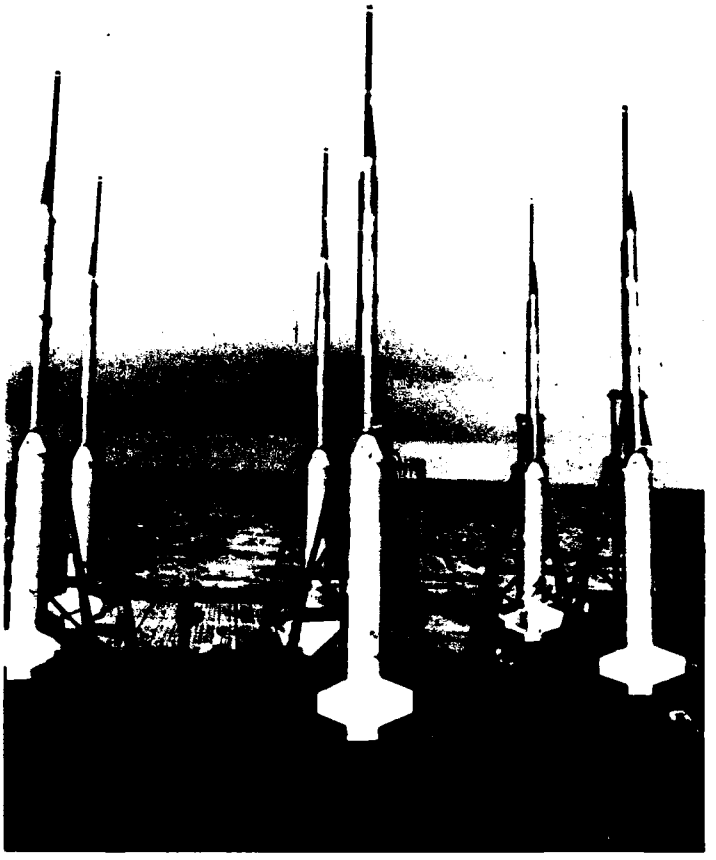

Six Nike-Asp rockets on the deck of the USS *Point Defiance*, poised for the IGY eclipse shoot of October 10, 1958

was given high marks for scientific interest but was rejected because the committee thought the technical requirements were too risky. In 1957, Sputnik began to play its tune overhead and suddenly research money became much easier to find. I approached Admiral Rawson Bennett, Chief of Naval Research, directly and obtained his promise of $70,000 and the use of a Navy vessel for an eclipse expedition to the South Seas.

The NRL rocket team was joined by a group of optical astronomers to conduct the traditional types of ground-based eclipse observations under the leadership of Jack Evans, Director of the Sacramento Peak Observatory. Our base of operations was the LSD USS *Point Defiance*. The plan was for Jack Evans to set up his instruments on the island of Puka Puka and my group to erect six Nike-Asp rockets on the ship's helicopter deck on simple rail launchers. For this complex operation, the Navy provided a marine demolition team that had to work for weeks to blast a channel through the coral reef to the island in order to get the heavy astronomical instruments ashore. Aboard ship we had to jury-rig arrangements to keep our instrumentation dry and functional. Never before had a barrage of six high-altitude rockets been fired from such close spacing aboard ship in the course of an hour.

On eclipse day, it rained precisely at totality, and the astronomers on Puka Puka were washed out. Just 20 nautical miles away, we had clear skies and a perfect view of the eclipse from the deck of the USS *Point Defiance*, although it was immaterial to the rockets that rode high above the weather. The rocket observations were excellent and revealed clearly that X-ray emission came from localized condensations of the corona that were tightly bound to sunspot groups by magnetic fields.

Herbert Friedman and Talbot Chubb sailing the South Seas to rendezvous with 1958 solar eclipse at Puka Puka

An astronomy lesson is given to the children of Puka Puka

First X-ray photograph of the Sun obtained with pinhole camera flown on Aerobee rocket

In 1960, we flew the simplest kind of X-ray pinhole camera on an Aerobee rocket from White Sands and obtained the first X-ray photograph of the Sun. It showed all the detail we had deduced from the eclipse experiment with almost trivial effort but without the high adventure of a Polynesian trip. Within a few years, reflecting X-ray telescopes were perfected, and an entirely new invisible universe of high-energy celestial sources was discovered.

SEQUEL

In the modern era of space science via robotic satellites and manned orbital laboratories, NRL has held a prominent role. In 1960, NRL's SOLRAD was the first space astronomical observatory; NRL's Oriented Scintillation Spectrometer Experiment (OSSE) for gamma-ray measurements now shares the spotlight on the 1991-launched NASA Compton Observatory. In every category—from small science to big science, NRL can be proud of its many accomplishments.

ABOUT THE AUTHOR

HERBERT FRIEDMAN, Chief Scientist Emeritus of the E.O. Hulburt Center for Space Research, received his B.S. degree from Brooklyn College in 1936. He received his Ph.D. degree from The Johns Hopkins University in 1940. He holds two honorary D.Sc. degrees presented by the University of Tubingen in 1977 and the University of Michigan in 1979.

In 1940, Dr. Friedman came to NRL as a physicist in the Metallurgy Division. Shortly thereafter he became active in rocket astronomy, and over the subsequent decades, Dr. Friedman's efforts to map the sky for celestial X-ray sources have discovered many X-ray stars, X-ray galaxies, and the X-ray pulsar in the Crab Nebula. By observing the lunar occultation of the Crab in 1964, he obtained the first identification of a discrete X-ray source with a known celestial object. In 1968, he obtained the first evidence of X-ray pulsations from the neutron star in the Crab Nebula. He was a principal investigator on NASA's HEAO-1 mission for the NRL experiment that produced a catalog of nearly one thousand sources and showed their classification into a variety of objects.

Dr. Friedman holds 50 patents, has published 300 articles in professional journals, and has written three books. He has served on the staffs of academic institutions such as the Naval Medical School, Yale University, University of Pennsylvania, and University of Maryland. He has served as a member, officer, chairperson, or councilor of many organizations, committees, and boards—among them the General Advisory Committee to the U.S. Atomic Energy Commission, the President's Science Advisory Committee, and NASA's Space Program Advisory Council. He is currently Vice President of COSPAR, the International Committee for Space Research. He has served on the editorial boards of 11 scientific journals and has been on boards and planning committees for three others.

Among the awards Dr. Friedman has received are the President's Distinguished Federal Civilian Service Award in 1964 and the National Medal of Science in 1968. He has received numerous prestigious national and international awards, including the Eddington Medal of the Royal Astronomical Society, the Wolf Foundation Prize in Physics and most recently, the Janssen Medal from the French Astronomical Society in 1990. His memberships include the National Academy of Sciences, the International Academy of Astronautics, the American Philosophical Society, and the American Academy of Arts and Sciences.

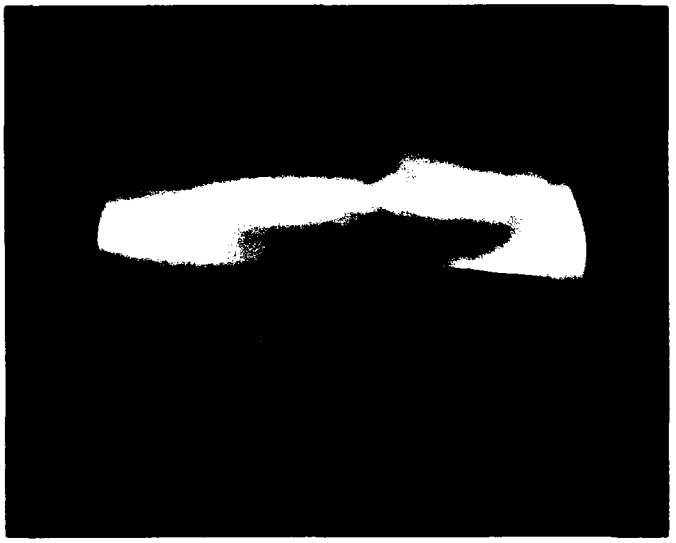

Mars Rising Over the Horizon
Scientific Data/Visualization (Color),
Honorable Mention
Nancy Garland, Chemistry Division

"Mars" is actually the laboratory seen through the exit window of a vacuum chamber that contains a 10 Torr methane/oxygen flame above a flat-flame burner. The blue and purple light comes from the flame front. Because the pressure in the chamber is low, the flame front spreads out and rises from the surface of the burner. This allows better spatial resolution for laser diagnostics of molecules in the flame. The blue light is emission from electronically excited C_2 radicals near 500 nm and the purple halo is emission from electronically excited CH radicals near 400 nm.

Concept for Tactical Support
Artist's Concepts/Illustrations,
Honorable Mention
Vincent E. Nobel, Center for Advanced Space Sensing

This rendering demonstrates the concept of tactical support of naval missions with satellite remote sensing and communications systems. Space sensors look over the horizon and describe limiting environmental (wind, seas, rain, ice, clouds, fog, shoals) conditions and enemy threats and targets. Measured environmental parameters can be sent to central processing facilities to support forecasts of changing conditions.

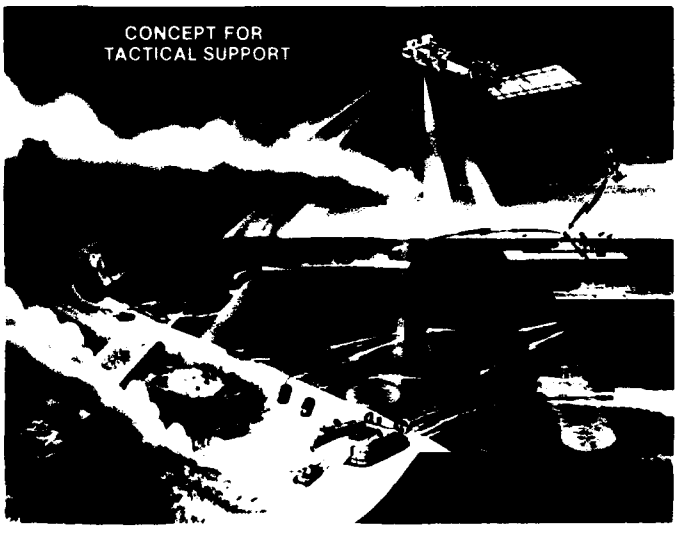

Active Infrared Countermeasures
Artist's Concepts/Illustrations,
Honorable Mention
Melvin R. Kruer, Optical Sciences Division

An F-4 aircraft with a countermeasure pod that contains a developmental active infrared system to counter attacking antiaircraft missiles is shown. In the proposed system, a passive missile warning system based on staring infrared sensors detects and tracks the attacking missile; it then passes location information to a pointer-tracker system, which directs a laser beam onto the missile to defeat its guidance system.

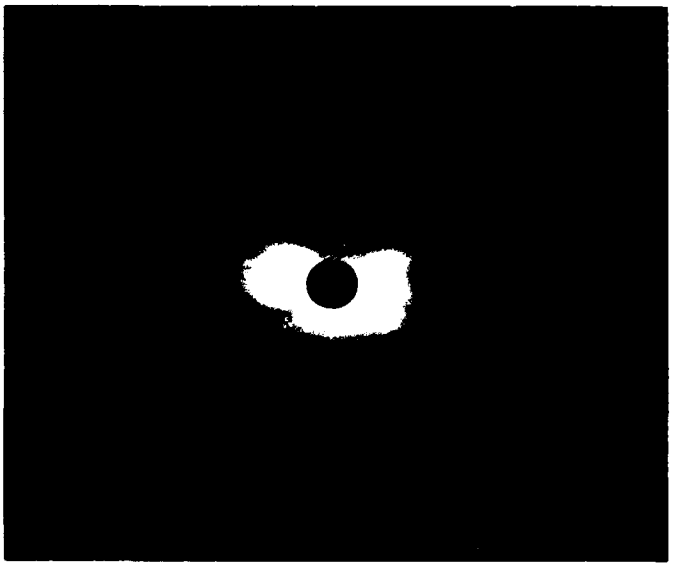

The Solar Corona
Scientific Data/Visualization (Color),
Honorable Mention
Herbert Gursky, Space Science Division

The Sun's atmosphere, which can only be seen during solar eclipses or with specialized instruments, is shown here as it would appear in December during its yearly transit of the Milky Way in the vicinity of the galactic center. The image was created on an image processing computer by combining the solar eclipse images with a numerical model for sunlight scattered by dust particles in the principal plane of the solar system. A low resolution photograph of the Milky Way was superimposed on this panorama and individual stars were added from a compilation of several astronomical star catalogs. The actual brightness range in the scene covers a ratio of 100,000 to 1.

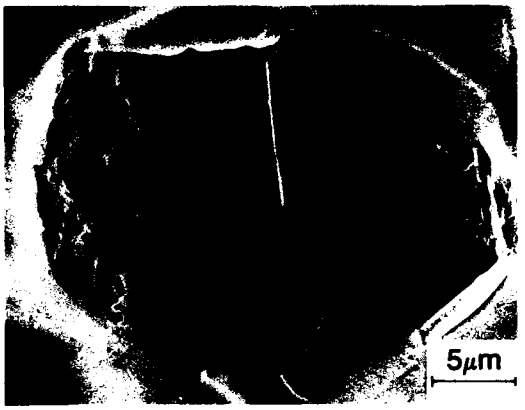

A Corrosion Pit on Aluminum Ion Implanted with Niobium
Scientific Data/Visualization (B&W),
Honorable Mention
P.F. Slebodnick, E. McCafferty, and P.M. Natishan
Materials Science and Technology Division

This micrograph shows the fourth stage of the blister formation and rupture mechanism of pitting corrosion. Such micrographs, along with determinations of hydrogen pressure using both thermodynamic and Griffith-type calculations, were used to develop the mechanism of blister formation and rupture.

Ther's Gold in Them Thar Holes
Scientific Data/Visualization (Color),
Honorable Mention
Ronald T. Holm, Electronics Science and Technology Division

A scanning electron microscope (SEM) picture of one cell in the first silicon field emitter array (FEA) used to make the world's first vacuum transistor is shown. The sharp gold spike in the center of the picture is a single crystal silicon field emitter whose tip has a radius of curvature of about 300 Å (e.g., 100 atoms). The purple layer is the vacuum transistor's metal gate, about 0.5 micrometers thick.

Lattice Image of Intergrowths in a Titanium-Doped $MgAl_2O_4$ Ceramic
Scientific Data/Visualization (B&W),
Honorable Mention
Roy J. Rayne, Materials Science and Technology Division

A bright field transmission electron microscope (TEM) image using lattice fringe imaging of the intergrowths that developed in a titanium-doped MgO-AlO ceramic is shown. Small amounts of titanium were added to the ceramic as part of a research effort to improve its mechanical properties.

Micro-Stonehenge
Scientific Data/Visualization (B&W), *First Place*
Bruce D. Sartwell, James A. Sprague, and
George P. Chambers

Micro-Stonehenge
Scientific Data/Visualization (B&W), *First Place*
Bruce D. Sartwell, James A. Sprague, and George P. Chambers
Condensed Matter and Radiation Sciences Division

Silver was sputter-deposited to a thickness of 10 nm onto a single crystal silicon substrate maintained at 420°C. To observe how the silver was distributed on the surface, the sample was mounted in a high-resolution Hitachi scanning electron microscope (SEM). A surprising phenomenon occurred during the examination; the electron beam in the SEM induced the growth of exotic-looking silver structures. This was a very dynamic occurrence, with the vertical growth rate being about 100 nm in a few minutes. Studies are ongoing in an attempt to explain the mechanism responsible for this previously unobserved phenomenon.

THE NAVAL RESEARCH LABORATORY

39 **NRL—Our Heritage, NRL Today, NRL in the Future**

61 **Highlights of NRL Research in 1991**

70 **Meet the Researchers**

THE NAVAL RESEARCH LABORATORY

Our Heritage

Today, when government and science seem inextricably linked, when virtually no one questions the dependence of national defense on the excellence of national technical capabilities, it is noteworthy that in-house defense research is relatively new in our Nation's history. The Naval Research Laboratory (NRL), the first modern research institution created within the United States Navy, began operations in 1923.

Thomas Edison's Vision—The first step came in May 1915, a time when Americans were deeply worried about the great European war. Thomas Edison, when asked by a *New York Times* correspondent to comment on the conflict, argued that the Nation should look to science. "The Government," he proposed in a published interview, "should maintain a great research laboratory.... In this could be developed...all the technique of military and naval progression without any vast expense." Secretary of the Navy Josephus Daniels seized the opportunity created by Edison's public comments to enlist Edison's support. He agreed to serve as the head of a new body of civilian experts—the Naval Consulting Board—to advise the Navy on science and technology. The Board's most ambitious plan was the creation of a modern research facility for the Navy. Congress allocated $1.5 million for the institution in 1916, but wartime delays and disagreements within the Naval Consulting Board postponed construction until 1920.

The Laboratory's two original divisions, Radio and Sound, pioneered in the fields of high-frequency radio and underwater sound propagation. They produced communications equipment, direction-finding devices, sonar sets, and, perhaps most significant of all, the first practical radar equipment built in this country. They also performed basic research, participating, for example, in the discovery and early exploration of the ionosphere. Moreover, the Laboratory was able to work gradually toward its goal of becoming a broadly based research facility. By the beginning of World War II, five new divisions had been added: Physical Optics, Chemistry, Metallurgy, Mechanics and Electricity, and Internal Communications.

The War Years and Growth—Total employment at the Laboratory jumped from 396 in 1941 to 4400 in 1946, expenditures from $1.7 million to $13.7 million, the number of buildings from 23 to 67, and the number of projects from 200 to about 900. During WWII, scientific activities necessarily were concentrated almost entirely on applied research. New electronics equipment—radio, radar, sonar—was developed. Countermeasures were devised. New lubricants were produced, as were antifouling paints, luminous identification tapes, and a sea marker to help save survivors of disasters at sea. A thermal diffusion process was conceived and used to supply some of the ^{235}U isotope needed for one of the first atomic bombs. Also, many new devices that developed

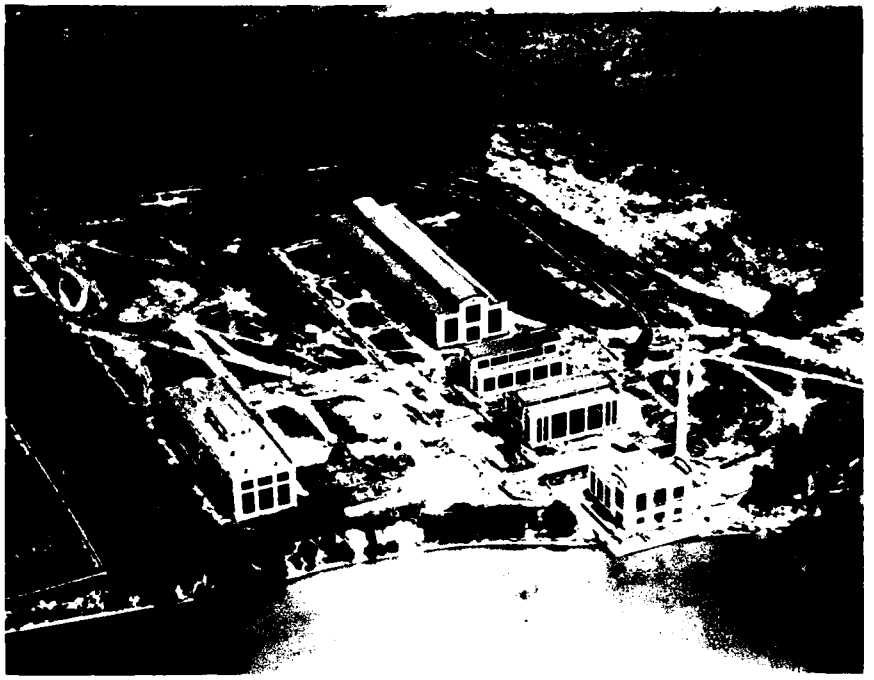

The original Naval Research Laboratory in 1923 among the farmlands of Blue Plains as viewed from the Potomac River

from booming wartime industry were type tested and then certified as reliable for the Fleet.

NRL Reorganizes for Peace—Because of the major scientific accomplishments of the war years, the United States emerged into the postwar era determined to consolidate its wartime gains in science and technology and to preserve the working relationship between its armed forces and the scientific community. While the Navy was establishing its Office of Naval Research (ONR) as a liaison with and supporter of basic and applied scientific research, it was also encouraging NRL to broaden its scope and become, in effect, its corporate research laboratory. There was a transfer of NRL to the administrative oversight of ONR and a parallel shift of the Laboratory's research emphasis to one of long-range basic and applied investigation in a broad range of the physical sciences.

However, rapid expansion during the war had left NRL improperly structured to address long-term Navy requirements. One major task—neither easily nor rapidly accomplished—was that of reshaping and coordinating research. This was achieved by transforming a group of largely autonomous scientific divisions into a unified institution with a clear mission and a fully coordinated research program. The first attempt at reorganization vested power in an executive committee composed of all the division superintendents. This committee was impracticably large, so in 1949 a civilian director of research was named and given full authority over the program. Positions for associate directors were added in 1954.

The Breadth of NRL—During the years since the war, the areas of study at the Laboratory have included basic research concerning the Navy's environments of Earth, sea, sky, and space. Investigations have ranged widely from monitoring the Sun's behavior, to analyzing marine atmospheric conditions, to measuring parameters of the deep oceans. Detection and communication capabilities have benefited by research that has exploited new portions of the electromagnetic spectrum, extended ranges to outer space, and

provided means of transferring information reliably and securely, even through massive jamming. Submarine habitability, lubricants, shipbuilding materials, fire fighting, and the study of sound in the sea, have also been steadfast concerns.

The Laboratory has pioneered naval research into space, from atmospheric probes with captured V-2 rockets, through direction of the Vanguard project—America's first satellite program—to involvement in such projects as the Navy's Global Positioning System. As part of the SDI Program, the Low-Power Atmospheric Compensation Experiment (LACE) satellite was designed and built by NRL. Today, NRL is the Navy's lead laboratory in space systems research, fire research, tactical electronic warfare, microelectronic devices, and artificial intelligence. NRL has also evaluated new issues, such as the effects of intense radiation and various forms of shock and vibration on aircraft, ships, and satellites.

NRL scientists and engineers made important advances in several research fields during FY 91. In on-going research in the Optical Sciences Division, scientists discovered a new high-temperature epitaxy process for growing millimeter-sized, transparent diamond crystals by using an oxygen-acetylene flame. This was an important breakthrough in the field of low-pressure diamond synthesis. Investigators in the Information Technology Division developed mathematical means for improving the performance of multiple target tracking and correlation systems. The method uses a gating algorithm to reduce the complexity of computations by identifying sensor reports that correlate with targets. NRL scientists from the Navy Technology Center for Safety and Survivability have produced a method for improving the operation of water-cooled, very low frequency transmitters by greatly reducing the corrosion in their cooling systems. The new processes reduce corrosion in transmitters to one-hundredth of previous levels.

In other work, scientists from the E.O. Hulburt Center for Space Research implemented an important system to reconstruct images from the Hubble Space Telescope by using NRL's Connection Machine, a massively parallel computer. Researchers in the Condensed Matter and Radiation Sciences Division discovered traces of the rare isotope Beryllium-7 by using an NRL-developed array of high-resolution detectors on the NASA Long Duration Exposure Facility launched by the Space Shuttle Challenger on April 7, 1984. An analytical model for ionospheric plasma clouds was developed by a research team in the Plasma Physics Division. The aim of the research is to allow scientists to predict the behavior of the ionized gas environments that surround the Earth.

The Laboratory's Oriented Scintillation Spectrometer Experiment (OSSE) on board NASA's Gamma Ray Observatory (GRO) produced several important observations in the last year. OSSE was launched as part of the GRO on April 5, 1991, on the Space Shuttle Atlantis. Under the scientific and technical management of scientists within NRL's Space Science Division, OSSE is designed to measure the spectra and time

On February 22, 1991, CAPT Paul G. Gaffney II (left) replaced RADM (Sel) John J. Donegan, Jr. (right) as the Naval Research Commanding Officer

variability of gamma rays from sources as near the Sun to active galaxies a billion or more light years away. Detailed data from a series of solar flares beginning in June were collected by the instrument. The flares are among the most intense ever to be detected by gamma-ray detectors. OSSE also carried out observations to study a high-energy variable point source of galactic radiation at or near the galactic center and to determine the origin of diffuse high-energy emission from the central portions of the Milky Way.

In other work in NRL's active space and satellite research programs, two NRL experiments were flown as part of Space Shuttle Mission STS-39, the DoD's first unclassified shuttle mission. The experiments included the Ultraviolet (UV) Limb Imaging experiment and the Far UV Cameras experiment. Both experiments were developed by the Space Sciences Division to measure far-UV radiation caused by natural and artificial sources in near-Earth space. An advanced version of the Laboratory's Solar Ultraviolet Spectral Irradiance Monitor (SUSIM) was launched as part of NASA's Upper Atmosphere Research Satellite on September 12, 1991. SUSIM is a high-precision instrument that will measure the Sun's UV radiation output in the wavelength region of 120 to 400 nanometers. Finally, laser measurements of vibrations in the Low-power Atmospheric Compensation Experiment (LACE) satellite were conducted by MIT/Lincoln Laboratory and NRL. The successful tests were the first time that ground-based lasers have measured vibrations of an orbiting spacecraft.

In other NRL highlights during FY 91, several cooperative research and development agreements (CRDAs) with private industry were signed. Signees include Johnson Controls, Inc. (to achieve first spaceflight of a common pressure vessel (CPV) nickel hydrogen battery); CER Corporation (to examine the feasibility of a fiber-optic-based borehole gravimeter for the purpose of locating oil and gas deposits); and Man Labs, Inc. (to develop corrosion-resistant zirconia thermal barrier coatings for turbine engines.)

Additionally, NRL provided important research and development support for Desert Shield/Desert Storm operations. Assistance was provided in electronic countermeasures, in the development of an Identification Friend or Foe (IFF) system for surface combat vehicles, and in the development of a biological warfare sensor for use in combat operations. Other NRL research was used in UHF and EHF communications. Voice processing algorithms for secure tactical and office communications were also developed at NRL. One of the big successes of the war was the Global Positioning System (GPS) NAVSTAR satellite system. The GPS provided extremely accurate navigation and positioning information to all elements of the American and Allied Forces during the conflict. The GPS is a joint Navy/Air Force project with roots in NRL's TIMATION research program of the 1960s.

NRL participated in the Nation's Victory Celebration saluting our troops who served in the Persian Gulf War. The display was held on the Mall in downtown Washington, D.C., in June.

NRL Today

ORGANIZATION AND ADMINISTRATION

The position of NRL within the Navy is that of a field command under the Chief of Naval Research.

Heading the Laboratory with joint responsibilities are the naval commanding officer, Capt. Paul G. Gaffney II, USN, and the civilian director of research, Dr. Timothy Coffey. Line authority passes from the commanding officer and the director of research to four associate directors of research and the director of one technology center. Research is performed in the following areas:

- General Science and Technology
- Warfare Systems and Sensors Research
- Materials Science and Component Technology
- Naval Center for Space Technology.

Further details of the Laboratory's organization are given on the organizational chart appearing in the "General Information" section.

Through FY 91, NRL operated as a Navy Industrial Fund (NIF) activity. As a NIF activity, all costs, including overhead, were charged to various research projects. Funding in FY 91 came from the Chief of Naval Research, the Naval Systems Commands, and other government agencies, such as the Defense Advanced Research Projects Agency, the Department of Energy, and the National Aeronautics and Space Administration as well as several nongovernment activities. NRL's relationship with its sponsoring agencies, both inside and outside DoD, is defined by a comprehensive policy on interagency support agreements.

Besides funding for scientific work, NRL receives Navy monies for general construction, maintenance, and operations.

PERSONNEL DEVELOPMENT

At the end of FY 91, NRL employed 3590 personnel—34 military officers, 68 enlisted men and women, and 3488 civilians. In the research staff, there are 788 employees with doctorate degrees, 404 with masters degrees, and 642 with bachelors degrees. The support staff assists the research staff by providing administrative,

NRL today as viewed from the east

computer-aided designing, machining, fabrication, electronic construction, publication, personnel development, information retrieval, large mainframe computer support, and contracting and supply management services.

Opportunities for higher education and other professional training for NRL employees are available through several programs offered by the Employee Development Branch. These programs provide for graduate work leading to advanced degrees, advanced training, college course work, short courses, continuing education, and career counseling. Graduate students, in certain cases, may use their NRL research for thesis material.

For non-NRL employees, several postdoctoral research programs exist. There are also cooperative education agreements with several universities, summer and part-time employment programs, and various summer and interchange programs for college faculty members, professional consultants, and employees of other government agencies.

NRL has active chapters of Women In Science and Engineering, Sigma Xi, Toastmaster's International, and the Federal Executive and Professional Association. Four computer clubs meet regularly—NRL IBM-PC, Mac, NeXT, and Sun NRL Users Groups. An amateur radio club, a drama group—the Showboaters, and several sports clubs are also active. NRL has a recreation club that provides swimming, saunas, whirlpool bath, gymnasium, and weight-room facilities. The recreation club also offers classes in martial arts, aerobics, swimming, water-walking, and cardiopulmonary resuscitation.

A community outreach program at NRL provides tutoring for local students, science fair judging, participation in high school and college career day programs, an art and essay contest during Black History Month, student tours of NRL, and a Christmas party for disadvantaged children, with gifts donated by Laboratory employees.

NRL has an active, growing Credit Union with assets of almost $135 million and a membership numbering over 17,000. Public transportation to NRL is provided by Metrobus.

For more information, see the *NRL Review* chapter entitled "Programs for Professional Development."

SCIENTIFIC FACILITIES

In addition to its main campus of about 130 acres and 152 buildings, NRL maintains 12 other research sites including a vessel for fire research and a Flight Support Detachment. The many diverse scientific and technological research and support facilities are described in the following paragraphs.

Research Facilities

- Space Science

NRL is the Navy's main laboratory for conducting basic research and development in the space sciences. The Space Science Division has a number of commitments for space experiments in the areas of upper atmospheric, solar, and astronomical research aboard NASA, DoD, and other space projects. Division scientists are involved in major research thrusts that include remote sensing of the upper atmosphere by using ultraviolet sensing, studies of the solar atmosphere by using spectrographic techniques, and studies of astronomical radiation ranging from the ultraviolet through the cosmic rays. This includes the mission operations and data analysis facilities for NRL's OSSE experiment on NASA's Compton Observatory. The division maintains facilities to design, construct, assemble, and calibrate space experiments. A network of VAX computers, super minicomputers, image processing hardware, a PDS microdensitometer, and Cray and Connection Machine accesses are used to analyze and interpret space data. The division also operates the SDIO Backgrounds Data Center, which is a repository and analysis center for experimental data pertaining to natural backgrounds.

Two NRL experiments were flown during Mission STS-39, the first unclassified DoD-dedicated space shuttle mission. The experiments, the Ultraviolet (UV) Limb Imaging (UVLIM) experiment and the Far UV Cameras experiment, which were developed by scientists in NRL's Space Science Division, measured far-UV radiation caused by natural and artificial sources in near-Earth space. Here the Space Payload-1 (STP-1) is being lifted into position in the Vertical Processing Facility at Kennedy Space Center. UVLIM is the top left cannister. Its celestial camera is bottom left.

• Advanced Space Sensing

The Center for Advanced Space Sensing conducts a program of basic research, science, and applications to develop new concepts for sensors and imaging systems for objects and targets on the Earth and in the near-Earth environment, as well as in deep space. The research, both theoretical and experimental, leads to discovering and understanding the basic physical principles and mechanisms that give rise to the background environmental emissions and targets of interest and to absorption and emission mechanisms of the intervening medium. Accomplishing this research requires the development of sensor systems technology. The development effort includes active and passive sensor systems used for the study and analysis of the physical characteristics of phenomena that evolve from naturally occurring background radiation, such as that caused by the Earth's atmosphere and oceans and man-made or induced phenomena, such as ship/submarine hydrodynamic effects. The research includes theory, laboratory, and field experiments leading to ground-based, airborne, or space systems for use in remote sensing, astrometry, astrophysics, surveillance, nonacoustic ASW, and improved meteorological/oceanographic support systems for the operational Navy. Special emphasis is given to developing space-based platforms and exploiting existing space systems.

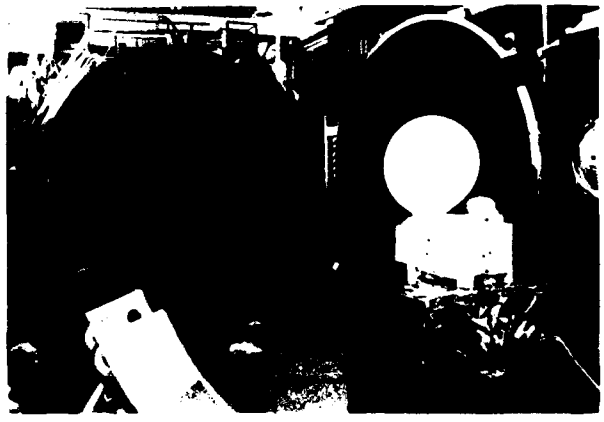

The MAS flight instrument is shown here entering a large thermal vacuum chamber and being readied for a space flight. The instrument spectrometer was designed and fabricated in NRL's Center for Advanced Space Sensing.

• Computational Physics and Fluid Dynamics

The Laboratory for Computational Physics and Fluid Dynamics (LCP&FD) is a participant in the DARPA Touchstone Scalable Parallel Processing Project. An Intel IPSC/860 Touchstone Gamma supercomputer provides the environment necessary to develop, debug, and benchmark parallel simulations. With multi-MFLOP processors as building blocks, the computer is configured as a hypercube and is a MIMD local memory machine. The installed 24-node (planned expansion to 32 nodes) machine is expected to attain a computational speed of several hundred MFLOPS. Access to the 528-node Touchstone Delta machine at Cal Tech is also available. The Delta machine currently holds the world record of 11.9 GFLOPS for the LINPACK benchmark.

LCP&FD has also developed a Graphical and Array Processing System (GAPS), which is a MIMD shared memory system. This system provides a significant computational engine for parallel computations, with real time, high resolution visualization and simulation steering capabilities.

A 64-million word Convex C210 currently provides LCP&FD with medium performance scalar and vector capability for jobs that require large amounts of memory.

Work is underway to create a high quality video studio that uses digital recording techniques; this will provide the capability to create graphical representations of simulation data for analysis and presentation.

A wide range of graphical workstations are used, including an IRIS 4D vector display, Sun Microsystems, Tektronics, Metheus, and Macintosh.

• Condensed Matter and Radiation Sciences

The Condensed Matter and Radiation Sciences Division is the primary Navy center studying the effects of radiation on material items including electronic equipment, satellites, etc., and the condensation of materials (thin films) on other objects through the use of charged and neutral particles. The division approaches these activities with both theoretical and experimental methods, with applications to medical, environmental, and military situations. These are the facilities that are available to the division:

Ion Implantation Facility—The facility consists of a 200-keV ion implanter with specialized ultrahigh vacuum chambers and associated in situ specimen analysis instrumentation. The facility is used to develop advanced surface treatments of materials to modify their properties and improve corrosion and wear resistance.

3-MeV Tandem Van de Graaff—This facility is used to study charged particle radiation damage effects such as occur in space, to perform Rutherford backscattering spectroscopy and nuclear reaction analysis, to provide high-sensitivity composition depth profiles, and to perform MeV energy implants in materials.

60-MeV Electron Linear Accelerator (LINAC)—The LINAC produces intense electron beams that are used to study radiation effects on

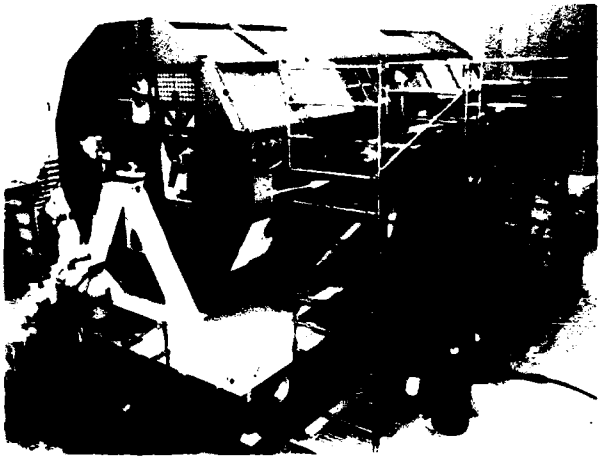

Scientists from the Condensed Matter and Radiation Sciences Division report that traces of the rare isotope Beryllium (BE-7) were found on NASA's Long Duration Exposure Facility (LDEF) unmanned spacecraft, which was retrieved after nearly six years in space. The arrow shows the array setup for the radiation survey of LDEF.

microelectronics and materials for DoD satellite and missile programs. It is also used to study radiation effects on the new, high-critical-temperature superconductors.

Hypervelocity Impact Facilities—Three facilities are used for ballistics research at speeds exceeding 6 km/s with toxic and explosive targets, while measuring projectile velocity, orientation, and dynamic projectile-target interaction.

Synchrotron Radiation Facility—An intense monochromatic X-ray photon source, tunable from 10 eV to 12 keV, is available on the NRL-developed beam lines at the National Synchrotron Light Source at the Brookhaven National Laboratory. Environmental target chambers can span a pressure range from ambient to several hundred kbar and temperatures from 10 to 1500 K.

• Plasma Physics

The Plasma Physics Division is the major center for in-house Navy and DoD plasma physics research. The division conducts a broad experimental and theoretical program in basic and applied research in plasma physics, which includes laboratory and space plasmas, pulsed-power sources, intense electron and ion beams, atomic physics, laser physics, and numerical simulations. The facilities include an extremely high-power laser, Pharos III, for the laboratory simulation of space plasmas and high-latitude nuclear explosion effects studies. The division has developed a variety of pulsed power sources to generate electron and ion beams, powerful discharges, and various types of radiation. The largest of these pulsers, GAMBLE II, is used to study the production of megampere electron beams and for producing very hot, high-density plasmas. Other generators are used to produce particle beams that are injected into magnetic fields and/or cavities to generate intense microwave pulses. A charged-particle-beam (CPB) propagation facility exists for testing advanced CPB propagation (both endo- and exoatmospheric) concepts. A 5-MW generator injects pulses of electron current into pre-heated ionization channels to study the effectiveness of propagation under various conditions. This division also operates a modified betatron facility for studying methods to accelerate high-current electron beams to energies in the 25- to 50-MeV range.

• Acoustics

NRL's facilities in support of acoustical investigations are located at the main Laboratory site and in Orlando, Florida, at the Underwater Sound Reference Detachment (USRD). At the main Laboratory site, there are three research tanks instrumented to study echo characteristics of targets and to develop devices. There is also an underwater acoustic holography facility for research in acoustic fields and a water tunnel having a large blow-down channel with a 15-m test section used for acoustic and flow-induced vibration studies of towed line arrays and flexible cables. NRL is investigating dynamic GPS interferometric navigation to extend the capabilities of their fixed-wing airborne gravity measurement system, which is accurate to better than 3 mGal (3×10^{-5} m/s^2), to operation over land. In addition to providing the accurate positioning necessary for airborne gravimetry, GPS interferometric altimetry, in conjunction with radar altimeters, may be used in the future to study oceanographic phenomena and to obtain accurate ice profiles in glaciated parts of the world. The division also has several acoustic receiver array systems used to collect data for coherent signal processing. The primary system consists of a 64-element, towed, seismic-type receiver array with the associated tow cable, winch, and electrical components. The towed array component can be replaced with a 64-element, fixed bottomed array or 64-element vertical array. There are also two radio-telemetered, buoyed, acoustic receiver array systems with 20-element arrays capable of being vertically or horizontally deployed. All receiver arrays are interfaced into the At-sea Data Acquisition, Recording, and Real-time Processing System.

• Radar

NRL has gained worldwide renown as the "birthplace of radar" and has maintained its reputation as a leading center for radar-related research and development for a half century. An impressive array of facilities managed by NRL's Radar Division continues to contribute to this reputation. These include airborne and laboratory radar cross section measurement systems, an airborne APS-137 radar with ISAR image processing, and an airborne adaptive array laboratory. Also, the division manages and maintains a radar display test bed, an IFF ground station, a digital signal processing facility, and a radar cross section prediction facility. A radar research and development activity is located at the Chesapeake Bay Detachment (CBD), Randle Cliffs, Maryland. It has separate facilities for specific types of systems that range from high-frequency, over-the-horizon systems to millimeter wave radars. The SENRAD radar test bed, a flexible and versatile system for demonstrating new developments in radar, and a point defense radar test bed are also located at CBD.

• Information Technology

The Information Technology Division, which includes the Navy Center for Applied Research in Artificial Intelligence, is at the forefront of DoD research and development in telecommunication, computer science, and artificial intelligence.

The division maintains a local area computer network to support its research. The network comprises a Symbolics, LISP machines, Sun 35 and 45 and Apollo workstations, Macintosh laser printers, network gateways, and terminal servers. Other computer resources include a Butterfly 128-node parallel processor, Silicon Graphics 4D/35, MASSCOMPS, IBMs, DTC-2, IBM 6000 RISC with 128MB RAM, and a Connection Machine with 16K processors for exploiting the natural computational parallelism in data-intensive research. The network is connected to NRL's Central Computing Facility and to the MILNET, ARPANET, and other university networks.

The Radar Division's new shipboard radar facility located at the Chesapeake Bay Detachment

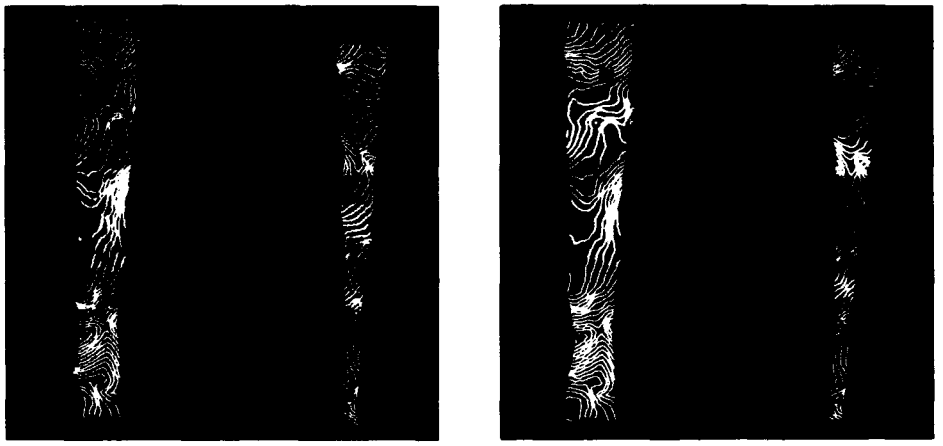

(a) (b)

Researchers at NRL's Navy Center for Applied Research in Artificial Intelligence have developed algorithms for use in an automated system to obtain correctly registered bathymetric charts. Four bathymetric data swaths are shown: (a) a picture of the misregistered originals, and (b) picture taken after applying the registering algorithms.

• Electronic Warfare

The scope of research and development at NRL in the field of electronic warfare covers the entire electromagnetic spectrum, from basic technology research, component and subsystem development, to system design and effectiveness evaluation. Major emphasis is placed on providing the methods and means to counter enemy hostile actions in all battle phases, from the beginning—when enemy forces are mobilized for an attack—through the final engagement stages. For this purpose, NRL has constructed special research and development laboratories, anechoic chambers, and facilities for modeling and simulation. NRL has also added extensive new facilities where scientists can focus on the coordinated use of all organic defensive and offensive resources now present in the Fleet.

• Structure of Matter

The Laboratory investigates the atomic arrangement of matter to improve old materials or to invent new materials. Various diffraction methodologies are used to make these investigations. Subjects of interest include the structural and functional aspects of energy conversion, ion transport, device materials, and physiologically active substances such as drugs, antibiotics, and antiviral agents. Theoretical chemistry calculations are used to complement the structural research. A real-time graphics system aids in modeling and molecular dynamics studies.

• Bio/Molecular Science and Engineering

The Center for Bio/Molecular Science and Engineering conducts research in biotechnology aimed at solutions of Navy and DoD problems. Long-term research directions focus on complex bio/molecular systems and are aimed at gaining a fundamental understanding of the structures and functions of biologically derived systems. The staff of the center is an interdisciplinary team performing basic and applied research in a number of diverse areas including biochemistry, biophysics, synthesis, and thin-film fabrication. Because of the interdisciplinary nature of this work, most of the research being performed in the center is of a collaborative nature. The center's associate concept is a key way of establishing this collaboration. Center associates come from other research areas within NRL as well as universities, industry, and other government laboratories.

The Tactical Electronic Warfare's Scale Model Analysis Facility (SMAF) allows precision scale models, such as the ship mounted on the six degrees-of-freedom positioner, to be raster scanned through a narrow beam submillimeter wavelength monostates radar analog to identify and characterize radar scattering centers

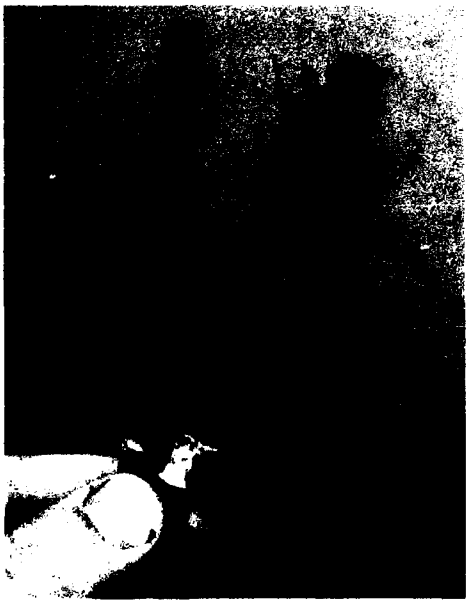

Fiberglass rods treated with antifouling coatings are shown. The rod on the left has tubules in the coating and the rod on the right does not. The antifouling tubules were developed by the Center for Bio/Molecular Science and Engineering.

• Chemistry

NRL has been a major center for chemical research in support of naval operational requirements since the late 1920s. The Chemistry Division continues its tradition with a broad spectrum of basic and applied research programs concerned with controlled energy release (fuels, fire, combustion, countermeasure decoys, explosives), surface chemistry (corrosion, adhesion, tribology, adsorbents, film growth/etch), advanced polymeric materials (high strength/low weight structures, drag reduction, damping, special function), and advanced detection techniques (environment, chemical/biological, surveillance). Facilities for research include a wide range of the modern photon electron, magnetic and ion-based spectroscopic/microscopic techniques for bulk and surface analysis; multiple facilities for materials synthesis and physical/chemical characterization; a 325-M^3 (11,400 ft^3) fire research chamber (Fire I), and a 475-ft ex-USS *Shadwell* (LSD-15) advanced fire research ship.

NRL scientists have developed a method to improve the operation of water-cooled, low frequency transmitters by greatly reducing the corrosion in their cooling systems. Here researchers investigate the corrosion of a copper test panel.

• Materials

NRL has capabilities for X-ray and electron diffraction analyses and for electron and Auger spectroscopy. It has a secondary ion mass spectrometer for surface analysis that significantly extends the diagnostic capability of the technique. A high-resolution, reverse-geometry mass spectrometer is used to probe reactions between ions and molecules. The Laboratory has a fully equipped fatigue and fracture laboratory, a modern vacuum arc melting furnace for reactive metals, an ultrasonic gas atomization system for making metal powders, and hot isostatic press facilities. The Laboratory's cryogenic facilities include dilution refrigerators and superconducting magnetic sensors for measuring ultrasmall magnetic fields. Also available are two molecular beam epitaxy devices for growing thin films.

This state-of-the-art high-resolution electron microscope was recently installed by the Materials Science and Technology Division. The Phillips Model CM-30 instrument can be used to image planes of atoms that are 1.4 Å apart and to resolve features in a crystal as small as 2.4 Å. This instrument will be the centerpiece of an analytical facility that will combine microscopy at atomic resolution levels with determination of chemical composition by computer processing X-ray emission of metallurgical, ceramic, and electronic materials samples.

• Optics

Ultralow-Loss, Fiber-Optic Waveguides— NRL has developed record-setting ultrahigh transparency infrared waveguides. These fluoride glass materials offer the promise of long-distance communications without the need of signal amplification or repeaters.

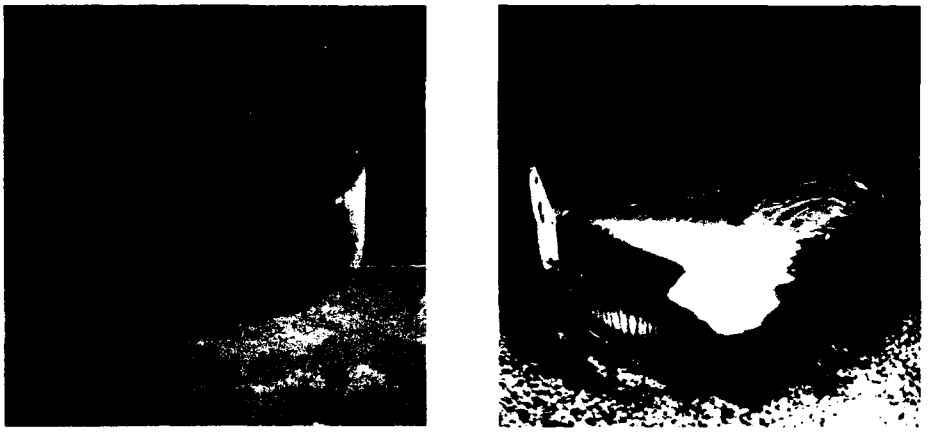

(a) (b)

A team of scientists from the Optical Sciences Division reports the discovery of a new high-temperature epitaxy process for growing millimeter-sized, transparent diamond crystals by using an oxygen-acetylene flame. Shown are electron and optical micrographs of laser cut, cylindrically shaped natural diamond seed crystal before and after a one-hour deposition at 1250 ± 30°C: (a) electron micrograph before deposition; (b) electron micrograph after deposition showing faceted diamond crystal with distinct octagonal shape.

Focal Plane Evaluation Facility—This facility has extensive capabilities to measure the optical and electrical characteristics of infrared focal plane arrays being developed for advanced Navy sensors.

IR Missile-Seeker Evaluation Facility—This facility performs open-loop measurements of the susceptibilities of infrared tracking sensors to optical countermeasures.

Large Optic, High-Precision Tracker—NRL has developed a tracker system with an 80-cm primary mirror for atmospheric transmission and target signature measurements. By using a quadrant detector, the servo system has demonstrated a 12-mrad tracking accuracy. An optical correlation tracker system tracks objects without a beacon.

High-Energy Pulsed Hydrogen Fluoride, Deuterium Fluoride Laser—NRL has constructed a pair of pulsed chemical lasers each capable of producing up to 30 J of laser energy at 2.7 to 3.2 mm and 3.8 to 4.5 mm in a 2-ms pulse. This facility is used to investigate a variety of research areas including stimulated Brillouin scattering, optical phase conjugation, pulsed laser amplification, propagation, and beam combining.

Fiber-Optics Sensors—The development and fabrication of fiber-optic sensor concepts, including acoustic, magnetic, and rate-of-rotation sensors, are conducted in several facilities within the Laboratory's Optical Sciences and Acoustics Divisions. Equipment includes facilities for evaluating optical fiber coatings, fiber splicers, an acoustic test cell, a three-axis magnetic sensor test cell, a rate table, and various computers for concept analysis.

Digital Processing Facility—This facility is used to collect, process, analyze, and manipulate infrared data and imagery from several sources.

Emittance Measurements Facility—NRL routinely performs measurements of directional hemispherical reflectance from 2 to 16 mm in the infrared by using a diffuse gold integrating sphere and a Fourier Transform Spectrophotometer (FTS). Sample temperatures can be varied from room temperature to 250°C and incidence angles from 0° to 60°.

• Electronics Science

In addition to specific equipment and facilities to support individual scientific and technology programs in electronics and electronic-materials growth and analysis, NRL operates the Nanoelectronics Processing Facility. The facility provides services to electronics programs throughout the Laboratory and to external organizations. This facility provides support for NRL programs that require microelectronics processing skills and equipment. The facility includes a nanowriter that can be used to fabricate nanoscale (80 Å) structures and, in general, supplies NRL programs with a range of items from discrete structures and devices to complete integrated circuits with very large scale integration (VLSI) complexity based on silicon metal oxide semiconductors (MOS) submicrometer technology.

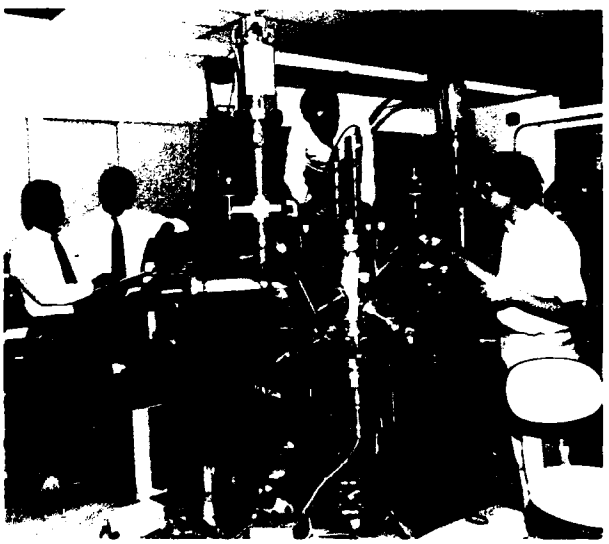

Scientists from the Electronics Science and Technology Division have developed a technique to fabricate silicon-on-insulator (SOI) materials. Here the research team attends the Silicon Molecular Beam Epitaxy Facility, where this technique takes place.

• Space Technology

In its role as a center of excellence for space systems research, the Naval Center for Space Technology (NCST) designs, builds, analyzes, tests, and operates spacecraft, as well as identifies and conducts promising research to improve spacecraft and their support systems. NCST facilities that support this work include large and small anechoic radio frequency chambers, clean rooms, shock and vibration facilities, an acoustic reverberation chamber, large and small thermal/vacuum test chambers, and modal analysis test facilities. NCST has a facility for long-term testing of satellite clock time/frequency standards under thermal/vacuum conditions linked to the Naval Observatory; a 5-m optical bench laser laboratory; and a hologram research laboratory to conduct research in support of the development of space systems.

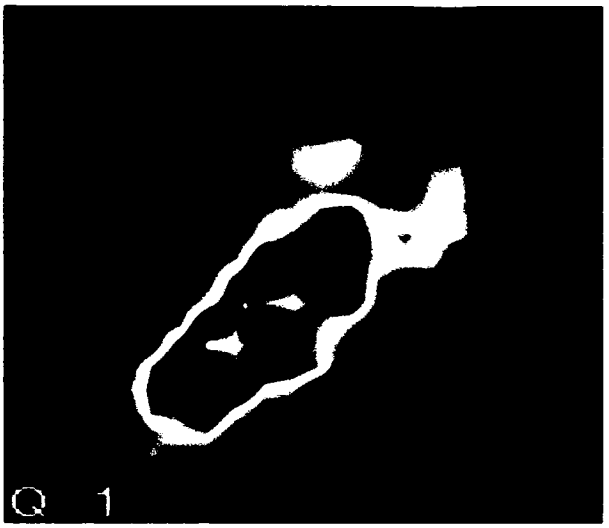

On February 14, 1991, NRL researchers and Strategic Defense Initiative Organization (SDIO) sponsors observed the one-year anniversary of the launch of the Low-power Atmospheric Compensation Experiment (LACE) Satellite. This image shows the ultraviolet emission in the 260- to the 280-nanometer band from the core of a rocket plume, as observed by the Ultraviolet Plume Instrument aboard the LACE satellite.

Research Support Facilities

• Technical Information Services

The Ruth H. Hooker Research Library and Technical Information Center contains more than one million items, including current journals. Its collections can be searched by computer-based

The Technical Information Division's Video Services Facility was officially opened on October 31, 1990. The new editing suite for 3/4" video tape is shown.

catalogs. The Library also provides interlibrary loans, on-line literature searches, access to CD ROM databases, loans of microcomputer software and laptops, and a full range of reference services, including assistance in selecting and using microcomputer software.

Publication services include writing, editing, composition, phototypesetting, and publications consultation. The primary focus is on using computer-assisted publishing technology to produce scientific and technical information containing complex artwork, equations, and tabular material.

The diversity of the research conducted at NRL requires a corresponding diversity of graphic support, such as technical and scientific illustrations, computer graphics, design services, photographic montages/composites, airbrushing/photographic retouching, calligraphy, display panels, sign making, and framing.

Photography services include motion picture, video, and still-camera coverage for data documentation both at NRL and in the field. A photographic laboratory offers custom processing and printing of black and white and color films. Video services include producing video reports of scientific and technical programs. A new video studio and editing facility with 3/4 in. and VHS editing equipment support video production.

Public affairs specialists prepare written and visual materials for dissemination to the public and the news media, traveling exhibits, the biweekly NRL newspaper (*Labstracts*), and the weekly publication (*Billboard*); process Freedom of Information Act requests; and schedule and manage the maintenance of three major TID auditoriums, the exhibit room, and the science lounge.

The DICOMED computer graphics system produces high-resolution, high-quality color images on 35-mm slides, 8 in. × 10 in. viewgraphs, 16-mm movies, or microfiche. It is driven by tapes generated on many different computer systems. It also accepts Macintosh files in PICT or Scrapbook format.

• Central Computing Facility

The Central Computing Facility (CCF) consists of a Cray X-MP/216 supercomputer with an 8.5 nanosecond clock supported by five DEC/VAX 700/8000 front-end systems. The peak processing speed of the two-processor Cray supercomputer is 470 million floating point operations per second (MFLOPS). This supercomputer is a balanced vector and high-speed scalar processor with hardware that allows simultaneous memory fetches, arithmetic, and memory store operations in a series of related vector operations. The Cray has 16 million (64-bit) words of static MOS memory in 32 interleaved banks and three interconnected I/O processors with four million words of shared buffer memory.

A separate Cray I/O subsystem offers parallel streaming and striping of disk drives, I/O buffering for disk resident and buffer memory resident datasets, online tape handling, and communications to front-end systems. Approximately 24 gigabytes of disk storage are available. The Cray disks are capable of reading and writing at four megabytes per second. The CCF is scheduled to be integrated with the NRL Central File Server/Archiving System (CFS/AS) that arrived last Fall. The CFS/AS provides online storage in the form of Control Data 5830 Disk Array Subsystems and nearline storage featuring advanced robotics in an automated tape cartridge system.

The system is accessed by a VAXcluster at the central computing site, by local area networks at NRL, by the INTERNET (MILnet/DDN), and by SURAnet/NSFnet at remote sites. The CCF front-end system provides terminal access by direct line, dial-up, local area networks, or the INTERNET. It also provides database management, document processing, electronic mail, and graphics support. FORTRAN, PASCAL, and C are the primary programming languages for the Cray system. A wide range of scientific, statistical, and mathematical software is also available. MSC NASTRAN, NAG, IMSL, and ABAQUS are available on the Cray.

A complete range of graphics output devices is available including graphics terminals, laser printers, and plotters. Graphics software can also generate tapes for the DICOMED film processing system located in TID. The RCD Visualization Lab has available two IRIS graphics workstations, a Sun SPARCstation, a Macintosh II cx, an IBM R6000 320, and a Stardent GS1000 workstation.

FIELD STATIONS

NRL has acquired or made arrangements over the years to use a number of field sites or auxiliary facilities for research that cannot be conducted in Washington, D.C. They are located in Maryland, Virginia, California, Alabama, and Florida. The two largest facilities are the Chesapeake Bay Detachment (CBD) and the Underwater Sound Reference Detachment (USRD).

- Chesapeake Bay Detachment (CBD)

CBD occupies a 168-acre site near Chesapeake Beach, Maryland, and provides facilities and support services for research in radar, electronic warfare, optical devices, materials, communications, and other subjects. Because of its location high above the Chesapeake Bay on the western shore, unique experiments can be performed in conjunction with the Tilghman Island site 16 km across the bay from CBD. Some of these experiments include low clutter and generally low background radar measurements.

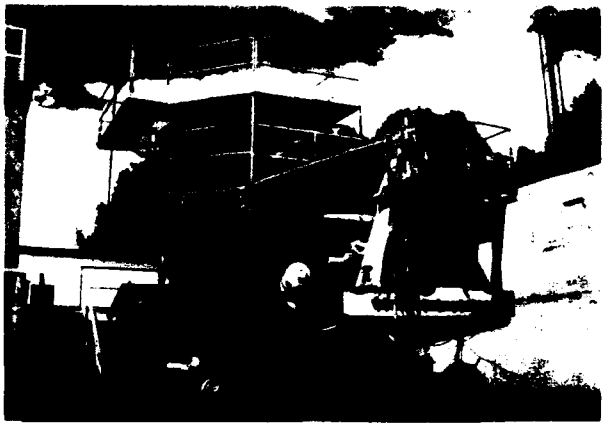

A ship motion simulator, located on the shoreline of the Chesapeake Bay at NRL's Chesapeake Bay Detachment, can be used to test and evaluate radar, satcom, and line-of-site RF communications systems under dynamic conditions (various sea states)

By using CBD's support vessels, experiments are performed involving dispensing chaff over water and radar target characterizations of aircraft and ships. Basic research is also conducted in radar antenna properties, testing of radar remote sensing concepts, use of radar to sensor ocean waves, and laser propagation. CBD also hosts facilities of the Navy Technology Center for Safety and Survivability, which conducts fire research on simulated carrier, surface, and submarine platforms.

- Underwater Sound Reference Detachment (USRD)

Located at Orlando, Florida, USRD functions as a link in the traceability of underwater sound measurements to the National Institute of Standards and Technology and also performs R&D for sonar transducers and related acoustic materials. Its semitropical climate and two clear, quiet lakes (the larger 11-m deep and nearly circular) are distinct assets to its research and development on sonar transducers and underwater reference standards and to its improvement of techniques to calibrate, test, and evaluate underwater acoustic devices. USRD has two large, high-pressure tanks for simulating ocean depths to approximately 700 m and 2100 m. Smaller pressure tanks simulate depths to approximately 7000 m. A spring-fed lake, located in a remote

Scientists at NRL's Underwater Sound Reference Detachment (USRD) in Orlando, Florida, have developed an inexpensive closed-chamber test facility for shock testing naval sonar tranducers

area about 40 miles north of USRD (the Leesburg Facility), provides a natural tank for water depths to 52 m with an ambient noise level 10 dB below that for sea state zero; larger objects can be calibrated here. A 15-cm shock tube simulates 60 pounds of high explosive at a range of 20 ft for shock testing small sonar transducers. The detachment provides acoustic equipment and calibration services not only to hundreds of Navy activities and their contractors but also to private firms and universities not engaged in DoD contracts.

• Marine Corrosion Test Facility

Located on Fleming Key at Key West, Florida, this facility offers an ocean-air environment and clear, unpolluted, flowing seawater for studies of environmental effects on materials. Equipment is available for experiments involving weathering, general corrosion, fouling, and electrochemical phenomena, as well as coatings, cathodic protection devices, and other means to combat environmental degradation.

• Flight Support Detachment (NRL FSD)

Located on the Patuxent River Naval Air Station at Lexington Park, Maryland, NRL's FSD provides maintenance and ground support for the uniquely modified P-3 Orion turboprop aircraft operated by NRL and Detachment personnel. In 1991, the Detachment received the NAVAIR Safety Award in recognition of their outstanding safety record. These four aircraft, which annually log over 2000 flight hours worldwide are the sole airborne research platforms for a variety of projects ranging from bathymetry and electronic countermeasure research to studies of radar signal reflections.

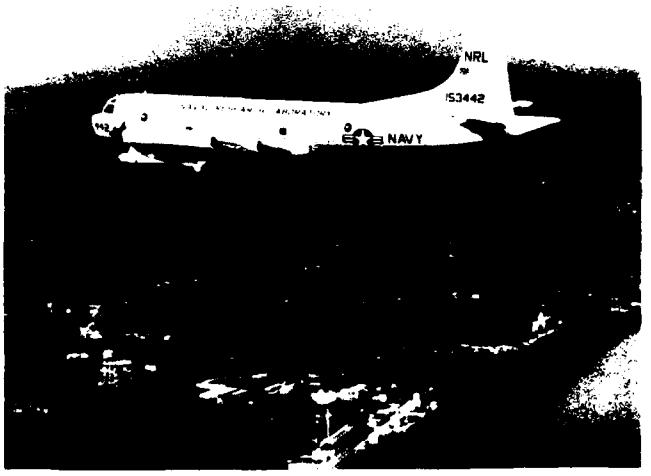

One of NRL's specially configured P-3 aircraft

• Other Sites

Some field sites have been chosen primarily because they provide favorable conditions to operate specific antennas and electronic subsystems and are close to NRL's main site. Maryland Point, south of NRL, operates two radio telescopes (25.6 and 26 m in diameter) for radio astronomy research. NRL's Waldorf Facility, south of NRL, operates 18.3-m, X-band, and S-band antennas for space and communications research. Pomonkey, a field site south of NRL, has a free-space antenna range to develop and test a variety of antennas. The antenna model measurement range in Brandywine, Maryland, has a 4.6-m diameter turntable in the center of a 305-m diameter ground plane for conducting measurements on scale-model shipboard and other antenna designs.

• Advanced Space Sensing

The Midway Research Center (MRC), located in Virginia, is now an operational facility dedicated solely to space-related applications in Naval communications, navigation, and basic research.

• Research Platforms

NRL uses ships and aircraft to conduct some of its research. Ocean-going research ships are obtained from a pool of vessels maintained by the Naval Oceanographic Office, Bay St. Louis, Mississippi.

NRL in the Future

To continue its growth and provide preeminent research for tomorrow's Navy, NRL must maintain and upgrade its scientific and technological facilities at the forefront. Its physical plant to house these facilities must also be adequate. NRL has embarked on a Corporate Facilities Investment Plan (CFIP) to renew its physical plant. This plan and future facility plans are described below.

THE CORPORATE FACILITIES INVESTMENT PLAN (CFIP)

The CFIP is a financial spending plan to provide modern research facilities at NRL by the year 2000. The plan calls for both Congressional and Laboratory investment and is updated and altered as changes occur in scientific emphasis and Congressional attitude. Over the past several years, Congressionally approved military construction (MILCON) funds were used to construct the new Electro-Optics Laboratory and to complete the final phase of the Tactical Electronic Warfare Facility. At this time, funds have been provided to build a second wing to the Electro-Optics Building, and funds have been requested for a facility to house the Naval Center for Space Technology.

In the past years, NRL's general and administrative (G&A) funds were used to renovate Buildings 16, 32, 34, 35, 46, 47, 56, 58, 72, 101, A11, and A13 and major portions of several other buildings. Approximately $4 million of Laboratory funding is budgeted for modernization each year.

• Center for Bio/Molecular Science and Engineering

Planning has begun for the renovation of Building 30 as a new home for the Center for Bio/Molecular Science and Engineering. When completed, the center will have over 36,000 ft^2 of modern laboratory and office space. Facilities will include laboratories for biochemistry, organic synthesis, surface chemistry, and spectroscopy. Specialized facilities include controlled environment rooms, a computer graphics laboratory, and electron and scanning microprobe laboratories.

Ample space is planned in which the center's highly interdisciplinary staff can meet and discuss joint projects.

• Vacuum Ultraviolet Space Instrument Test Facility

The Space Science Division will soon install a new vacuum ultraviolet space instrument test facility. This facility will be capable of housing space instrumentation up to 2 m in diameter and 5 m in length. While exposed to high vacuum (10^{-7} torr), instruments can be illuminated by a simulated solar spectrum for alignment and verification tests. The facility will also include a 13-m evacuated extension containing sources to simulate the solar corona. An externally mounted 1-m diameter heliostat will be employed to project a beam from the Sun directly into the vacuum chamber. In the near future, the facility will be used to test space instruments that are presently under development for flight on NASA's Orbiting Solar Laboratory spacecraft and the European Space Agency's Solar and Heliospheric Observatory spacecraft.

• Optical Sciences

In FY 91, NRL began construction of the second phase of the Electro-Optics Research Laboratory (MILCON Project P-115). This will be a 50,000 ft^2 addition to the existing Bldg. 215 and will accommodate approximately 120 scientists and engineers and their research facilities. Completion and occupancy should occur in the last quarter of FY 93 or the first quarter of FY 94. This facility will allow consolidation of the fiber optics and glass materials activities into one location and will replace obsolete and inadequate silica glass facilities in Bldg. 12 with new, state-of-the-art facilities. It will allow closer coordination between the infrared detector development activity and sensor system activities. Many computational sensor testing and modeling facilities will be contained in the new structure.

• Plasma Physics Facilities

A major 2-kJ KrF-laser facility will be established in the Plasma Physics Division by the end of FY 93. This facility is being initiated to provide intense radiation for studying inertial confinement fusion target heating at short wavelengths. A large-volume (2-m diameter by 5-m long) space chamber facility will be completed in FY 92 to do space plasma physics research in the laboratory. A uniform axial magnetic field up to 1 kG and adjustable plasma density and temperature allow great flexibility to study laboratory simulation of space phenomena under controlled conditions.

• Center for Materials Research

The Department of the Navy is in the process of programming construction of a special-purpose laboratory. This special facility will provide stringently clean laboratories with carefully controllable temperature, humidity, vibration isolation, ambient dust, and power for investigations in the rapidly evolving fields of electronic technology and nanometrics.

• Midway Research Center

NRL's newest field site, the Midway Research Center (MRC), is located on a 158-acre site in Stafford County, Virginia. Located adjacent to the Quantico Marine Corp Base's Combat Development Command, the MRC will have approximately 10,000 ft^2 of operations and administration area and three precision 18.5-m diameter parabolic antennas housed in 100-ft radomes. When completed, the MRC, under the auspices of the Naval Center for Space Technology, will provide NRL with additional state-of-the-art facilities dedicated solely to space communications and research.

• Electronics Science and Technology

In collaboration with the Materials Science and Technology Division, the epitaxial materials center, the "Epi-Center," is being improved. At the heart of the Epi-Center is an MBE system that

consists of two linked chambers, one dedicated to narrow energy gap semiconductors and the other dedicated to large energy gap semiconductors. In addition, the division recently acquired a high resolution transmission microscope (HRTEM) for use in structural analysis associated with its many materials' growth programs. Other important division emphases are the continual upgrading of the Nanoelectronics Processing Facility and expanding activities in the nanoelectronics physics program.

• Radar

The Radar Division and the Naval Center for Space Technology are jointly establishing a new microwave test facility located in Building A-59. This compact range facility will allow test and evaluation of antennas and radar targets over a frequency range of 1 to 100 GHz. The indoor range and supporting laboratories will occupy approximately 6000 ft^2 of space. Test objects up to 8-ft diameter will be accommodated. This facility obviates the need for an outdoor test range several thousand feet in length, achieving far-field radiation conditions from a large, prime focus, parabolic reflector.

• Shock Test Facility

A new facility for shock testing small transducers has been introduced at the Underwater Sound Reference Detachment. The present capability of the shock tube duplicates the MILSTD open-water shock tests but with a size limitation that the test object fit inside a 6-in. diameter cylinder. An extension of the shock tube to 10-in. diameter is under construction and should become operational sometime in FY 92.

REHABILITATION OF SCIENTIFIC FACILITIES

Specialized facilities are being installed or upgraded in several of the research and support divisions.

• Information Technology

An expanded computer/communication network is being implemented that will provide each researcher in the division with an office workstation (Sun, Apollo, or equivalent) connected to all the major scientific networks. Special test facilities are also being planned in support of specific R&D tasks. Facilities to support human-computer interaction research include an eye-monitoring system, touch screens and tablets, speech I/O hardware, high-resolution graphic displays, a 6-D tracker, a wall-sized display, and time-stamped video and audio recording equipment for monitoring experiments. An information security testbed is being planned to enable the interconnection of communication security and computer security devices to address network and system security problems.

• Plasma Physics

A state-of-the-art short-pulse (< 1 ps) high-intensity (> 1 TW) Table-Top Terawatt (T^3) laser has been procured for a variety of physics studies. The T^3 laser will be integrated into the Pharos III Nd-laser facility to boost its power into the 10 to 100 TW range. This will provide a facility to do fundamental physics experiments in intense laser-plasma interactions and intense laser-electron beam interactions.

A low-frequency (300 MHz to 10 GHz), high-power microwave facility, which uses a relativistic klystron concept, is being upgraded to produce multigigawatt coherent radiation pulses. A new laser facility is also planned. It will use a powerful KrF laser and a target chamber to conduct inertial confinement fusion research.

• Radar

The Radar Division has installed a computer-aided engineering (CAE) facility to aid in digital system design. The system has seven full-color graphics workstations to provide capabilities for circuit design and simulation and printed circuit board layout. The facility has been used to design systems based on commercially available com-

ponents as well as advanced systems incorporating VHSIC and gate array technologies. It has proven to be a valuable tool in evaluating new technologies for radar signal-processing requirements. The facility is currently being expanded to include Sun workstations and ADAS software, which will allow designs to be modeled and simulated at the system level. Future plans call for acquiring VHDL (VHSIC Hardware Description Language) software for the workstations, which is supported by ADAS. This would provide designers with an integrated toolset to model and simulate their designs from the system level down to the device level.

• Acoustics-Target Research Tank

Tank facilities for acoustic target research in the Acoustics Division will be significantly expanded to extend the range of target sizes. The expanded model tank is planned to contain a water volume of approximately 30,000 m^3.

• Underwater Sound Reference

A new, precision measurement system (PMS) is being installed in each of four facilities—at the Lake Facility, the Leesburg Facility, and the two large high-pressure tank facilities. PMS is a sophisticated, computer-controlled, signal-generation and data-acquisition system that provides significantly increased accuracy, dynamic range, and signal to noise than was previously available. It allows the use of new, sophisticated signal-processing techniques being developed for making lower frequency measurements on sonar transducers and related acoustical coating materials under reverberation-limited conditions, such as in the large, high-pressure tank facilities. PMS will also process acquired data very rapidly so that most results can be presented to customers at the time of the measurements.

• Materials Science and Technology

Renovation is proposed for Building 3, which is now made up of two of the original five buildings at NRL, to contain modern laboratories for studies of thin-film deposition and characterization, superconducting materials, magnetic materials, and other materials science projects. The new space will feature the most modern molecular beam epitaxy and other materials synthesis and processing equipment, an up-to-date fatigue and fracture laboratory and state-of-the-art diagnostic equipment, including electron microscopes, spectrometers, and electron and X-ray diffraction equipment. The renovated building will also contain office and laboratory space for approximately 70 technical personnel.

• Electronics Science and Technology

In a move to meet existing safety standards, the Electronics Science and Technology Division has moved its most hazardous materials' growth effort to a newly refurbished laboratory in Building A11.

• Flight Support

In 1992, NRL's Flight Support Detachment's aircraft Bureau number 154589 will undergo an extensive year-long modification and service life extension. This will expand NRL's capabilities for airborne research projects well into the next decade.

HIGHLIGHTS OF NRL RESEARCH IN 1991

The Far Ultraviolet Cameras Experiment on AFP-675/STS-39

Cameras on a Space Shuttle Discovery flight obtained the first far-UV imagery of shuttle surface glow. These results should aid in the determination of mechanisms and chemical species responsible for the glow, imagery of the ionospheric airglow attributable to 0^+ recombination, a lower altitude airglow layer caused by NO band emission, and imagery of several celestial targets. This experiment, performed by the Space Science Division, demonstrated a number of remote-sensing techniques for measuring and monitoring the ionosphere and neutral atmosphere on a global basis.

***

Oriented Scintillation Spectrometer Experiment (OSSE)

The Space Science Division is conducting a space program of gamma-ray observations in the 50 keV to 10 MeV energy range where high-energy nuclear processes occurring in very energetic sources can be studied. Four large scintillation detectors installed aboard the Compton Gamma Ray Observatory will provide a much improved capability for detecting gamma-ray line and continuum radiation from sources such as solar flares and massive black holes and for detecting atmospheric nuclear weapons tests.

***

The High-Resolution Remote Sensing Accelerated Research Initiative

The Center for Advanced Space Sensing is conducting experiments designed to understand the physics responsible for complicated submesoscale (< 10 km) features appearing in the radar backscatter images of the ocean surface. These features may be associated with changes in atmospheric stratification across ocean surface temperature fronts, surface current gradients, surface slicks, Langmuir cells, and with turbulence in the surface-layer wind field. This work has relevance and application to ASW and surface ship wake detection.

***

Sea Slicks Formation in the Presence of Upwelling

The Center for Advanced Space Sensing is conducting experiments in the western Atlantic to determine the physical and chemical hydrodynamic processes involved in the formation of sea slicks that are surface phenomena causing unusually low backscatter in radar imagery. Data show that upwelling, weak mixing, and strong current gradients were present in regions of sea slicks and that the water was colder and more saline than in adjacent areas outside of the slick area. This finding sheds new light on the physical processes involved in the formation of sea slicks and will impact Navy programs in ocean surveillance and ASW.

***

Exothermicity and Three-dimensionality in Reactive Turbulent Shear Flows

An objective of research on turbulent shear flows is to determine the basic physical mechanisms controlling their initiation and subsequent evolution. By using a shear-flow model, the Laboratory for Computational Physics and Fluid Dynamics is investigating the effects of chemical energy release and spanwise exitation on the development of the planar mixing layer and the nature of axis-switching phenomena in square jets. Understanding the evolution and structure of these reactive shear flows has many important applications in the area of combustion, such as the optimal design of jet engines with emphasis on combustion efficiency and noise reduction.

***

Radiation-Resistant, Space Qualifiable InP Solar Cells

To maximize the efficiency and radiation resistance of solar cells, the starting material has to be considered, and InP is currently the most radiation-resistant material available for this application. By using metalorganic chemical vapor deposition, the Condensed Matter and Radiation Sciences Division has fabricated InP solar cells with high beginning life efficiency and high radiation resistance for space applications with metal-organic chemical vapor deposition. These InP cells offer a solar power source with significantly improved performance in high radiation environments and open up satellite orbits not previously achievable.

***

Brightest X-rays Probe Smallest Crystals

The Condensed Matter and Radiation Sciences Division and the Materials Science and Technology Division have obtained X-ray diffraction data from single crystal samples as small as 28 attoliters by using energy-dispersive diffraction techniques and polychromatic radiation available at the Brookhaven National Laboratory. These samples came from extremely thin filaments of materials a few hundred angstroms in diameter. An apparently new phase of bismuth was observed during this work that demonstrates the possibility of obtaining X-ray diffraction data from submicron-size crystals.

***

Instability of Taylor-Sedov Blast Waves Propagating Through a Uniform Gas

In a laser-laboratory facility used to simulate space and high-altitude nuclear explosion effects, the Plasma Physics Division performed the first measurement of an instability in Taylor-Sedov blast waves propagating through a uniform gas. In that facility, blast waves comparable to those attained in a nuclear explosion are produced by the expansion of ablation plasma from the hot surface of laser-irradiated foils into the ambient gas. These measurements show that Taylor-Sedov blast waves propagating through a uniform gas are unstable when the adiabatic index of the gas is sufficiently low. These results will impact future blast wave theory as it applies to supernovae, the formation of stars and galaxies, and in calculating the environment existing after a nuclear engagement.

***

Greenland Aerogeophysical Project: Airborne Gravity, Topographic, and Magnetic Mapping of an Entire Continent

Obtaining geodetic and geophysical data in a remote and harsh environment, such as Greenland, has been a long-standing problem. By using new techniques and technology, the Acoustics Division, in collaboration with the Naval Oceanographic Office and the National Oceanic and Atmospheric Administration, has addressed this problem by performing an aerial survey of Greenland to collect gravity, topography, and magnetic data. The primary goal of mapping the gravity field over the entire island was achieved with sufficient resolution to produce half-degree mean anomalies to rms accuracy of 2 to 3 mGals. A combination of radar and laser sensing provided ice topography accurate to less than a meter. The collected data will be used to support many DoD and science requirements from gravity information for the Defense Mapping Agency to satellite orbit determinations and global climate studies.

***

FLEX: A Programmable, Real-time Radar Signal Processing Architecture

The Radar Division has successfully developed a programmable, real-time radar signal processor that supports up to a 10 MHz sample rate and allows algorithmic changes with software modifications. The system consists of a high-speed front-end to perform all the signal processing functions through detection and a lower-speed back-end to perform the postdetection processing. These programmable, real-time processors allow the modification of processing algorithms without costly hardware changes; this type of technology should lead to reduced development and life-cycle costs for these systems.

***

Machine Learning Software for Learning Tactical Rules

The Information Technology Division conducts research in machine learning focused on the development of SAMUEL, a general software shell for adaptive learning. SAMUEL interacts with a simulator to produce rule sets that are able to perform at an expert level in a tactical domain. More complex simulations have been developed to demonstrate SAMUEL's ability to learn control rules for realistic tactical scenarios. These include a mission evasion task for an automonous aircraft, a two-player surveillance task for an automonous underwater vehicle, a two-plane dogfight scenario, and a mine-field navigation task for an automonous underwater vehicle. Also, the learning operators in SAMUEL have been extended and improved, and a beta test version of SAMUEL has been packaged for external use. Machine learning techniques offer the potential to reduce doctrine development time by at least a factor of 10.

***

Tripod Operators for Rapid Recognition of Objects in Range Images

Scientists in the Information Technology Division have developed the tripod operator, a new class of feature extraction operators for range images, which facilitate the recognition and localization of objects. Tripod operators are applicable to all 3D shapes and reduce the need for specialized feature detectors. They can be moved on the surface of an object in only three degrees of freedom, so only a 3D manifold of feature space points can be generated for any number of test curves. This work shows

promise as a practical way to recognize landmarks for automonous system navigation by matching current measurements to a known topographic map in an air vehicle or by locating known fixtures in a terrestrial or ship deck environment.

***

InterFIS: A Natural Language Interface to the Fault Isolation Shell (FIS)

FIS, an expert system shell designed with menu-oriented and mouse-oriented interfaces, both interacting with an electrician's troubleshooting interface to an expert system, has been developed by the Information Technology Division. To the troubleshooting interface of FIS has been incorporated a natural language interface—now speech-activated—called InterFIS. This natural language interface provides a robust, flexible, friendly mechanism by which the user can interact with an expert system shell by using natural language commands with both speech and keyboard entry. Such systems can reduce training time because the user can react with the computer systems at a relatively high level.

***

A Software Tool for the Specification and Analysis of Cryptographic Protocols

Cryptographic protocols use encryptation to achieve secure communication between computer systems, and these protcols can have subtle security flaws, independent of the strengths and weaknesses of the cryptographic algorithms used. The Information Technology Division has developed a software tool that can be used to prove statements about security properties of cryptographic protocols and assist in the discovery of existing security flaws in these protocols. This software tool has been used successfully to analyze several protocols and has uncovered some previously unknown security flaws in two of them. It represents one of the first successful applications of formal methods to the analysis of cryptographic protocols.

***

Transition of the Technology from the Tactical ASW Battle Management System (TABS) into the Spotlight Advance Technology Demonstration

TABS is a tactical decision aid implemented as an object-oriented computer program in the expert system Knowledge-Engineering-Environment shell and integrates techniques from the operations research and artificial intelligence communities. TABS contains a nonlinear discrete submarine-tracking algorithm, NODESTAR, which will support any motion model that can be described by a Markov process. NODESTAR can also process negative information and line-of-bearing contacts in convergence zones. NODESTAR technology has been extended in SPOTLIGHT to include nonlinear correlation and static dynamics likelihood functions for the purpose of land avoidance, adherence to traditional patrol patterns, and sensor avoidance. SPOTLIGHT is a superior ASW tracking and search system. This program is conducted by the Information Technology Division.

***

Multinational Infrared (IR) Decoy and Ship Signature Measurement

The Tactical Electronic Warfare Division was tasked to evaluate two foreign-made IR decoys designed for naval surface ship protection. This led to a multinational program (United Kingdom, United States, Germany, and Canada) to make a comprehensive evaluation of the decoy hardware. Concomitantly, detailed radar cross section (RCS) and IR signature measurements were made on the Canadian ship, HMCS *Halifax*. This program has allowed DoD activities and foreign nationals to evaluate the technical performance of the two IR countermeasures devices—devices deemed potentially applicable for U.S. naval surface combatants. The RCS and IR data from the Canadian ship will provide significant, new information to U.S. ship designers with regard to EW issues.

***

Method for Electrostatic Transducer Transient Suppression

The Underwater Sound Reference Detachment has devised a new method of driving an electro-acoustic transducer so that it instantaneously radiates a steady, sinusoidal waveform that exhibits no turn-on and turn-off transient radiation to prevent transducer calibration at low frequencies. In this frequency range, transient radiation produces interfering reflections from the test vessel walls. By eliminating these reflections, this method can be used to improve low-frequency transducer calibration and improve low-frequency scattering and reflection measurements conducted in test facilities of limited size.

***

Detection System for Biological Warfare Agents

DNA-based and antibody-based detection systems for detecting biological warfare agents have been developed by the Center for Bio/Molecular Science and Engineering. DNA probes were fabricated that recognize toxins and some pathogenic organisms. The generic, ultrasensitive antibody-based system has an immunoassay response time of < 1 min and sensitivities in the ng/ml range. A fiber optic-based sensor was developed to support both detection systems. In addition to biological warfare defense, rapid, automated sensors employing antibodies and DNA as the as the detection elements, can be used for environmental control, process monitoring, detection of environmental hazards, drug detection, and clinical diagnoses.

***

Microsensors and Materials for Vapor Detection

Scientists in the Chemistry Division have developed small, chemical microsensors for detecting chemical vapors. These sensors consist of a physical transducer and a chemically selective material deposited as a thin film on the sensor's surface. Chemical interactions governing the sorption of vapors into thin polymeric films on a surface-acoustic-wave device have been determined. The primary method of vapor sorption involves the reduction in modulus of the polymer that occurs as it swells to accommodate the sorbed vapor. New, chemically selective polymers have been synthesized for use as sensor thin-film material. When used in smart sensor systems, these sensors can detect chemical warfare agents with high sensitivity and selectivity and provide improved fire detection.

***

Shock Simulation

Chemistry Division researchers have developed new computer simulation methods that will enhance the atomic-scale understanding of detonating materials. Processes leading to detonations must start at this scale, and molecular dynamic simulations can provide explicit information concerning the atomic- and molecular-scale behavior over very short time and distance. Specifically, this research requires the development of potentials capable of realistically modeling shock-induced chemical reactions in detonating solids. These potentials can be tailored to incorporate strong intramolecular forces that bind atoms into molecules and weak intermolecular forces that bind molecules into molecular solids. These simulation techniques will aid in the design of safer explosives and find wide use in the study of cluster, adhesion, friction, and surface sputtering.

***

Phthalonitrile Resins

The Chemistry Division has developed phthalonitrile resins for use as matrices materials for fiber-reinforced composites that are required to withstand temperatures in excess of 300°C. Chemical principles used in the design of these phthalonitriles have produced resins superior to conventional composite materials. These resins are easy to process into void-free components, have high thermal and oxidative stability in air, low equilibrium moisture uptake, and with proper processing can exhibit controlled electrical conductivity. The prepolymers show indefinite stability at room temperature. Thus, these resins should be excellent candidates for use in advanced structural composites needed for aerospace and marine applications, particularly when high operating temperature is a factor.

***

Invention and Implementation of Low Cost Hydrophone Ceramics for Large Scale Towed Arrays

Research on the effect of the Poisson's ratio on the hydrostatic response of lead-zirconate-titanate (PZT) has lead to a ceramic structure with ordered voids and high hydrostatic gain. While PZT ceramic has a high charge sensitivity to uniaxial pressure, low temperature sensitivity, inertness, and good mechanical strength, its sensitivity to hydrostatic pressure is quite low. This was countered by the optimization of the effects of Poisson's ratio and Z-axis compressibility through the introduction of photolytographically defined void layers. The cost of hydrophones with ordered voids is predicted to be about 2% of the cost of conventionally towed array hydrophones. This research is conducted by researchers in the Materials Science and Technology Division.

***

Parallel Computer Simulation of Ultrasonic Wave Propagation in Materials

By taking advantage of the communication and parallel-processing features of the Connection Machine, the Materials Science and Technology Division has developed an efficient simulation procedure for studying ultrasonic wave propagation in a material specimen of arbitrary complexity. A detailed understanding of the propagation of ultrasonic waves in materials is essential for the development of quantitative nondestructive evaluation techniques; this simulation procedure paves the way for the development of acoustic, tomographic, nondestructive evaluation methods.

***

Microstructural Evolution During Solid-Solid Phase Transformations

The Materials Science and Technology Division has conducted a systematic study of microstructural evolution in a model Fe(0.12%)-C(3.28%)-Ni steel. This required the design, construction, and implementation of a state-of-the-art isothermal heat treatment facility whose inert/reducing environment is necessary to prevent complete decarburization of the specimen at high temperatures. During this work, the interphase boundary mechanism of precipitaion was observed for cementite formation in the model alloy. This was the first detailed transmission electron microscopy evaluation of interphase boundry carbide precipitation in a steel containing only "noncarbide forming" substitutional alloying elements. This accomplishment demonstrates the generality of the interphase boundry mechanism of precipitation in steels.

***

A Numerical Model for Deep-penatration Laser Welding

The nature of fluid convection and heat transfer during a welding process can have a significant effect on the microstructure—and hence, strength—of the weld. Unlike conventional welding where energy deposition occurs on the surface of the workpiece, during laser welding, energy deposition occurs at the boundry of a vapor-liquid interface that moved through the workpiece at constant speed. The Materials Science and Technology Division has developed state-of-the-art models for simulating welding in a three-dimensional workpiece by the deep penetration laser process. This modeling will be used for the analysis and prediction of welding properties of laser weldments between metals and alloys.

***

Flashpumped, 2.1 μm Cr;Tm;Ho:YAG Laser

The Optical Sciences Division has developed a novel, high-efficiency, flash-pumped, solid-state laser that operates at room temperature and produces optical pulses at a nominal wavelength of 2.1 μm. The laser material is composed of yttrium aluminum garnet sensitized with trivalet chromium and thulium and activated with trivalent holmium. $Y_3Al_5O_{12}$ (YAG) was the optimum host material. Laser output efficiency exceeds 5%, and output energies of approximately 3 J-per-pulse were measured. This work provides the Navy with a flash-pumped, mid-IR solid-state laser that has potential use as an IR countermeasures source and for laser radar for remote sensing applications. The medical community is also interested in this laser for various surgical operations.

***

Low-light-level Imaging Through Scattering Media

Researchers in the Optical Sciences Division have demonstrated imaging through dense scattering media by using a quantum limited amplifier based on stimulated Raman amplification. Imput images at the level of one photon-per-pixel have been amplified to easily detectable levels. By using the natural time gating that occurs in such amplifiers, scattered light can be discriminated against. The results demonstrate amplified Raman imaging using a single photon-per-pixel level and time-gated imaging through a dense scattering material; they are applicable to underwater imaging and communication, the analysis of translucent materials, in medical imaging for techniques to see through scattering media, and in imaging through fog or other aerosols.

***

Optical Processor for Enhanced Sonar Signal Processing

A hybrid digital-optical correlator for broadband sonar signal processing has been designed and built by the Optical Sciences Division. This correlator is designed to be integrated into existing signal processing systems where it acts as a special purpose processor that enhances the computational capability of these systems. This is the first time that an optical correlator has been integrated into an existing Navy signal processing system and applied to real data. This capability will allow the Navy to use techniques in ASW and other areas that were formerly not feasible because of inadequate computational resources.

***

High-temperature Epitaxy (HTE) of Diamond

The Optical Sciences Division has succeeded in growing macroscopic, facetted diamond crystals epitaxially at 1200° to 1500°C in a thermal plasma reactor and in an atmospheric pressure combustion flame. Measured growth rates of 100 to 220 μm/h were the highest ever reported for the epitaxial synthesis of diamond at low pressure. This HTE process has been demonstrated with atmospheric pressure oxygen-acetylene flames and with DC plasma torches. With this process, it may be possible to grow boules and/or large single crystals of diamond at low pressure. Because of its thermal conductivity, large diamond crystals would be useful as heat sinks for ultralarge-scale integrated circuits, high temperature electronic devices, and certain laser diode arrays.

***

Comparison of the Time-dependent Interface-trap Buildup in Oxides Annealed in H_2 or D_2

Much research has been performed on the time-dependent build-up of interface traps in metal-oxide semiconductor (MOS) devices following pulsed irradiation. It was argued that the rate-limiting step in this build-up was a drift of a radiation-induced, positively-charged species—most likely H^+—through the oxide to the $Si-SiO_2$ interface. The Electronic Science and Technology Division fabricated oxides incorporating either hydrogen or deuteriun and showed that the interface trap growth rate after irradiation was retarded by factors of 3.2 to 4.5 in the deuterated samples. This led to the conclusion that the drift of H^+ ion was the rate-limiting process in the formation of these postirradiative traps. This work represents a major advance toward resolving long-standing questions in the field of radiation effects in MOS devices.

***

Opto-electronic Technique for On-ship Measurement of Millimeter-wave Device and Circuit Characteristics

The development of monolithic integrated circuits at millimeter-wave frequencies has been severely hampered, the main impasse being the difficulty in establishing removable, high-frequency connections between test equipment and chip in a reliable and reproducible manner. The Electronics Science and Technology Division has developed a new opto-electronic technique for measuring scattering parameters of semiconductor devices and monolithic integrated circuits at millimeter wavelengths. This technique solves the accuracy problem associated with unreproducible, high-frequency chip connections. The solution comprises the chip-level integration of miniature

reflectometer circuits. These rely on photoconductive on-chip pulse generation and multiposition sampling and involve special pulse-conditioning networks.

***

Monte Carlo Simulation of High Electron Mobility Transistor (HEMT) Failure Mechanisms

The HEMT is a relatively new device developed for low noise applications. Life testing of this device often caused failure, defined as a 20% decrease in the current drain; concomitantly, the peak transconductance was reduced and shifted to a lower gate bias. A systematic Monte Carlo particle model study was made of the deterioration of transconductance, threshold bias, and drain current of these HEMTs as a result of RF reliability life testing. The Electronics Science and Technology Division has determined that the failure of these heterojunction transistors following life testing was caused by partial alloying of the gate metal into the AlGaAr layer. Now that the failure mechanisms have been identified, improved HEMTs can be designed and fabricated. With these improvements, low noise devices will be available for missions out to 20 years.

***

Pt/SiC Interface Structure and the Roles of Oxygen and Carbon

The Electronics Science and Technology Division has shown that Pt/SiC interfaces undergo rapid evolution with increasing annealing temperature. Oxygen contamination can be prevented by depositing the metal onto SiC heated above 900° C, and free graphitic carbon can be avoided by codepositing Si to form additional SiC. There is a complicated reaction sequence in the annealing of thin Pt layers, including the possible appearance of ordered PtSi. The results of this study are relevant to the problem of high operational temperature contacts in SiC electronic devices.

***

Scanning Tunneling Microscope (STM) Lithography: A Solution to Electron Scattering

The STM is demonstrated by the Electronics Science and Technology Division to be a valuable tool for very high-resolution lithography as well as a useful probe of resist materials. The vacuum STM, operated in a field emission mode, provides a small probe of low voltage electrons. The proximity effects caused by electron scattering—the predominant resolution limiting mechanism in conventional high energy lithographic systems—is eliminated through the use of these low energy electron beams. The high voltage resolution can be improved by a factor of four in both feature size and line-to-line resolution.

***

Rocket-Plume Observations from the LACE Satellite

By using the Low-power Atmospheric Compensation (LACE) satellite as a platform and the Ultraviolet Plume Instrument, the Space Systems Development Department has collected high quality ultraviolet emission images from rocket plumes, as well as from natural and man-made UV background data. This UV emission data is not obtainable from the ground because of the absorption of UV by the ozone layer. Images of the UV emission from rocket plumes are required to develop valid computer models that can accurately predict the emission characteristics of any rocket plume and for evaluating the feasibility of using the ultraviolet emission from rocket plumes to detect the presence of missiles.

MEET THE RESEARCHERS

Dr. William A. Kuperman of NRL's Acoustics Division says, "Research in ocean acoustics involves a challenging blend of physics, geophysics, oceanography, seagoing expeditions, remote sensing, and signal processing; NRL, as a leader in all of these fields, provides the ideal research environment.

"My research has two main goals. The first is to use the complexity of the ocean to enhance our ability to extract acoustics signals, either sonar related or environmental, from a noisy background. The second is the inverse problem: to use acoustics to extract information about the ocean. By doing this, we hope to both increase the Navy's science base with reference to emerging sonar system concepts and, at the same time, increase our knowledge of the ocean environment. A recent spinoff of this latter research has been the successful modeling of transoceanic acoustic propagation for research into using the ocean as a global thermometer for global warming studies."

Dr. Kuperman is a Fellow of the Acoustical Society of America, an associate editor for the *Journal of the Acoustical Society of America*, and is the NRL senior scientist for Underwater Acoustics.

Dr. Stuart A. Wolf, head of the Material Physics Branch of the Materials Science and Technology Division, leads an outstanding effort in the science and technology of collective phenomena. Branch scientists have made pioneering contributions to magnetism, superconductivity, and nonlinear phenomena. Dr. Wolf's own research has recently focused on understanding the behavior of a new class of high-temperature superconducting materials both theoretically and experimentally—work for which he won the 1991 NRL Sigma Xi Pure Science Award.

"I find NRL a great place to work because it provides the proper environment for individual creativity both in pursuing fundamental science as well as solving real Navy problems."

Dr. Wolf is a Fellow of the American Physical Society and has been elected to serve on its Executive Council as a representative of the Division of Condensed Matter Physics. He has been awarded five Alan Berman Research Publication Awards and the Navy Meritorious Civilian Service Award.

Dr. Richard H. Rein came to NRL in 1990 to head the Office of Technology Transfer. The office is responsible for the implementation of the Stevenson–Wydler Act and the 1986 Technology Transfer Act, which established the principle of royalty sharing for federal inventors and allowed federal laboratories to enter into Cooperative Research and Development Agreements with private industry. Dr. Rein states, "The exciting thing about technology transfer is that it provides American industry with access to completed research that has been paid for and is ready to be commercialized. I am convinced that transfer technology from federal laboratories to industry represents the lowest cost means for most companies to develop high technology products covered by patents." The means of accessing this technology is by licensing patents and through participation in the Cooperative Research and Development Agreements, which Dr. Rein administers.

The Technology Transfer Office also oversees the Navy's Science Assistance Program, which establishes an information loop between the Fleet and the R&D shore establishments to expedite technology transfer to the user. In addition, the Technology Transfer Office administers the Navy's Scientist–to–Sea Program, which offers the Navy's researchers and R&D managers the opportunity to learn firsthand about factors that affect shipboard system design and operation.

Mr. Gerald (Jerry) Hoskins, acting superintendent of the Space Systems Technology Department, heads activities leading to the development of broad–based technology for future space activities. Department scientist and engineers support remote sensing, precise timing and navigation, advanced processing, and system performance evaluation testing.

"I consider my biggest challenge to be how to meet the Navy's and the Nation's space needs by continuing a strong, highly technological and innovative environment in a period of requirements change and declining budgets."

Near-Earth Magnetic Structure and Plasma Regions
Artist's Concepts/Illustrations, *First Place*
David N. Walker

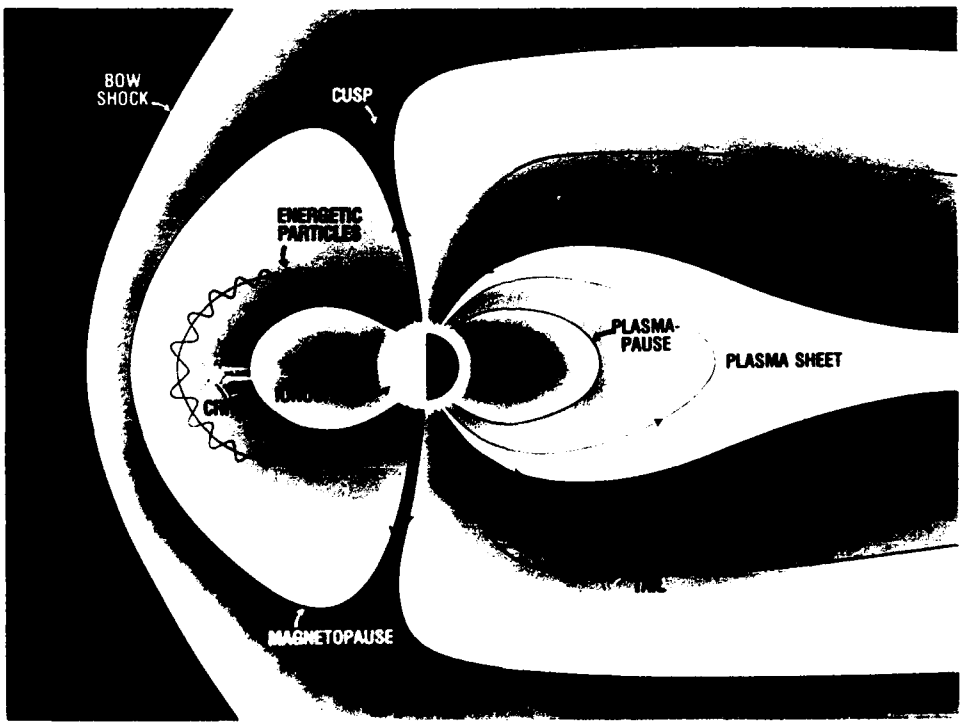

Near-Earth Magnetic Structure and Plasma Regions
Artist's Concepts/Illustrations, *First Place*
David N. Walker
Plasma Physics Division

This artist's concept shows the different near-Earth plasma regions and the gross magnetic structure of the Earth's magnetosphere as encountered by the Combined Release and Radiation Effects Satellite (CRRES). The bow shock region is one in which the solar wind particles (impinging from the left—not shown) begin to flow differently as they encounter the stronger magnetic field of the Earth. For reference, the bow shock can be taken as near 15 Earth radii from the Earth's center. The plasma regions are characterized by charged particle populations, which differ in physical characteristics among the different regions. The CRRES Satellite is designed to study these characteristics in the ionosphere, plasmasphere, and magnetopause regions. In addition, measurement of the more energetic particles will yield valuable information to designers of future spacecraft in relation to degradation of satellite electronics caused by the energetic particle fluxes.

FEATURED RESEARCH AT NRL

75 **Understanding Superconductivity in the Cuprates: Theory and Experiment**
Stuart A. Wolf, Mark E. Reeves, Joshua L. Cohn, and Vladimir X. Kresin

85 **Ion-beam-assisted Deposition Provides Control over Thin Film Properties**
Fred A. Smidt

99 **Low Reynolds Number Aerodynamics for Electronic Warfare**
Richard J. Foch and Peggy L. Toot

Understanding Superconductivity in the Cuprates: Theory and Experiment

Stuart A. Wolf, Mark E. Reeves,* and Joshua L. Cohn†
Materials Science and Technology Division
**NRC Post Doc*
†*ONT Post Doc*

and

Vladimir Z. Kresin
Lawrence Berkeley Laboratory

In 1986, a new class of compounds was found to be superconducting at remarkably high temperatures [1]. This initial discovery by two Swiss scientists, Alex Mueller and Georg Bednorz, was rapidly followed by discoveries that have raised the transition temperature to the unprecedented value of 129 K in a compound containing thallium, barium, calcium, copper, and oxygen. Scientists at NRL have made major contributions toward developing a fundamental framework for understanding these materials. These compounds all have some common features: perovskitelike crystal structures, copper-oxygen "quasi-two-dimensional" planar structures that form the principal conducting subsystem within the crystal, highly anisotropic behavior, and unusual, low-energy optical modes of the crystal lattice vibrations (phonons).

Understanding these materials has been a major challenge for condensed-matter physicists and solid-state chemists for the last five years. The work described here combines theoretical development with experimental measurements and forms a unified framework for describing and understanding the normal-state properties, the superconducting properties, and the underlying microscopic mechanism for the superconductivity. In addition, other scientists at NRL have performed electronic structure and lattice dynamics calculations [2] that have contributed substantially to our understanding of the normal-state properties. The results of these calculations have guided some of our analyses.

Here we focus on two of the more than fifty cuprate superconductors. The treatment, however, is general and applies to all members of the cuprate family. Figure 1 shows the structures of these two compounds, $La_{1.85}Sr_{0.15}CuO_4$ (LSCO), with a superconducting transition temperature T_c of 38 K and $YBa_2Cu_3O_7$ (YBCO), with a T_c of 93 K. Notice the planar Cu-O structures in both of these compounds; these are common to *all* the cuprate superconductors. Also notice that $YBa_2Cu_3O_7$ has Cu-O linear structures (chains) that form an additional conducting subsystem, which complicates the experimental interpretation and the theoretical development. Our work has concentrated on $YBa_2Cu_3O_7$ because of the availability of excellent samples and extensive experimental data.

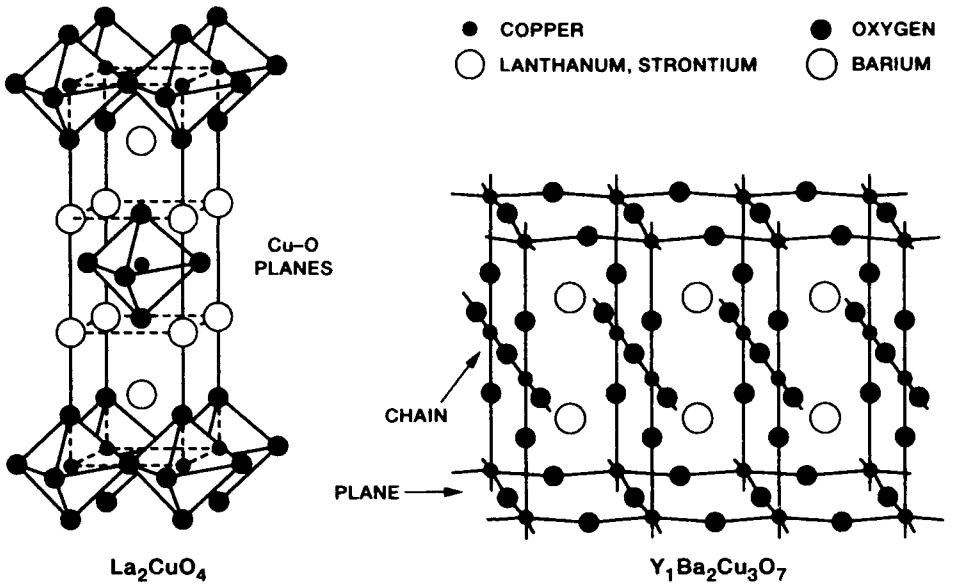

Fig. 1 — The crystal structures of $La_{1.85}Sr_{0.15}CuO_4$ and $YBa_2Cu_3O_7$. Notice the Cu-O planes in both compounds and the Cu-O chains in $YBa_2Cu_3O_7$.

Normal State Properties

We model the Cu-O planes as quasi-two-dimensional (2D) metals. (This model has now been verified by many different experiments.) The locus of energies for the most energetic carriers (electrons or holes) in a metal defines the Fermi surface. For the quasi-2D Cu-O layers, this surface is represented by a simple cylinder as shown in Fig. 2(a). The important parameters that describe this surface are the Fermi energy E_F, the Fermi velocity v_F, and the effective mass m^* (m^* includes the effect of the surrounding atoms on the mass of the carriers, so it can be quite different from the free electron mass). We derive appropriate quasi-2D expressions that relate these parameters to measured properties, and by using literature values for the electronic specific heat and Hall coefficient, we determine the Fermi-surface parameters for LSCO (Table 1).

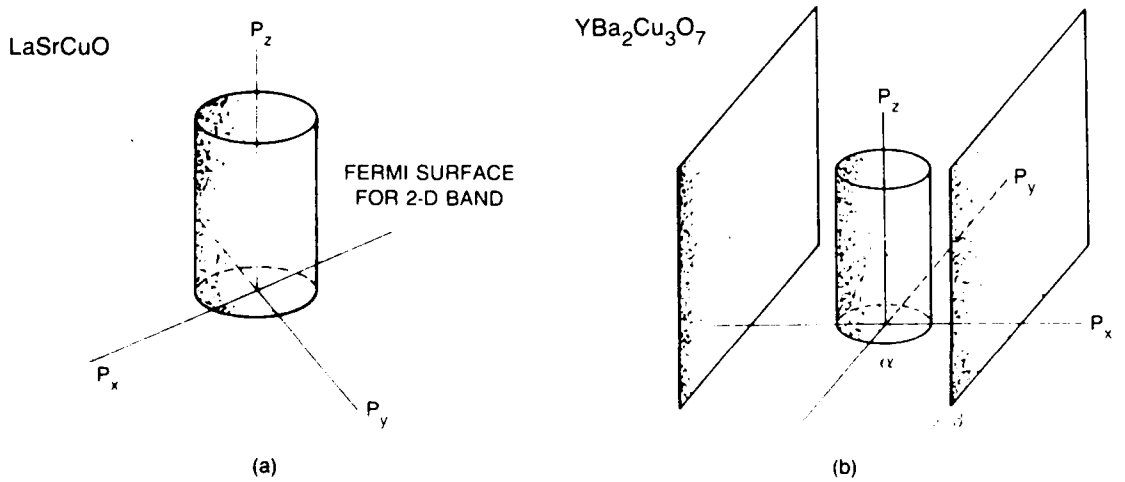

Fig. 2 — (a) The Fermi surface for a layered, quasi-2D metal. This cylindrical Fermi surface is how we model $La_{1.85}Sr_{0.15}CuO_4$; (b) the Fermi surface expected for a system consisting of quasi-1D and quasi-2D electronic subsystems. This is how we model $YBa_2Cu_3O_7$.

Table 1 — Normal and Superconducting Parameters for the Cuprates and for Conventional Superconductors

	CONVENTIONAL	LaSrCuO	YBaCuO
m^* (me)	1-15	5	5
E_F (eV)	5-10	(0.1)	(0.3)
v_F (cm/sec)	10^8	10^7	10^7
ξ_o (Å)	10^3- 10^4	20	15

UNUSUAL TRANSPORT AND SPECTROSCOPY BECAUSE OF SMALL FERMI ENERGY

For YBCO, the situation is more complicated, since the chains also have a Fermi surface. Figure 2(b) shows that the Fermi surface of quasi-one dimensional (1D) chains is a planar sheet. We derive appropriate expressions that relate both the 1D and 2D Fermi surfaces to experimentally determined properties. From our measurements of the temperature-dependent specific heat and neutron-scattering data from the literature, we determine the Fermi surface parameters. The high-temperature specific heat C_v of YBCO is the sum of lattice C_{vl} (calculated from the neutron scattering results) and electronic contributions C_{ve}. Figure 3 illustrates the experimental data for the specific heat showing these individual contributions. The Sommerfeld constant, $\lambda = C_{ve}/T$, which is related to m^*, is determined for both planes and chains. Finally, we calculate the Fermi parameters for the YBCO planes, which are also included in Table 1.

It is important to note that the Fermi energy for both these compounds is extremely small in comparison to that of a conventional metal. It is this anomalously small Fermi energy that is responsible for many of the unusual properties of this class of materials. For example, in a conventional metal, heat conduction due to the lattice of ions (phonons) is usually much smaller than that associated with the carriers. The electronic part of the thermal conductivity is proportional to the Fermi energy, and thus, in YBCO, the phonons provide most of the heat conduction. Figure 4 shows our thermal conductivity measurements for a single crystal of YBCO. The upturn in the thermal conductivity evident at temperatures just below the transition to the superconducting state is widely observed in the cuprates. This feature clearly indicates that phonons dominate the heat conduction process and that their ability to transport heat is substantially impeded by scattering from the carriers.

Thus a simple model for the Fermiology along with some important transport and thermodynamic measurements have enabled us to understand much about the normal state of two of the most important cuprate superconductors.

Superconducting Properties Independent of the Mechanism

Superconductivity, according to Bardeen, Cooper, and Schrieffer (BCS) [3] results when carriers near the Fermi surface form a new state of lower energy by combining into pairs (Cooper pairs), which have mass 2 m_e and charge 2 e. There are several important parameters describing the superconducting state that can be determined from

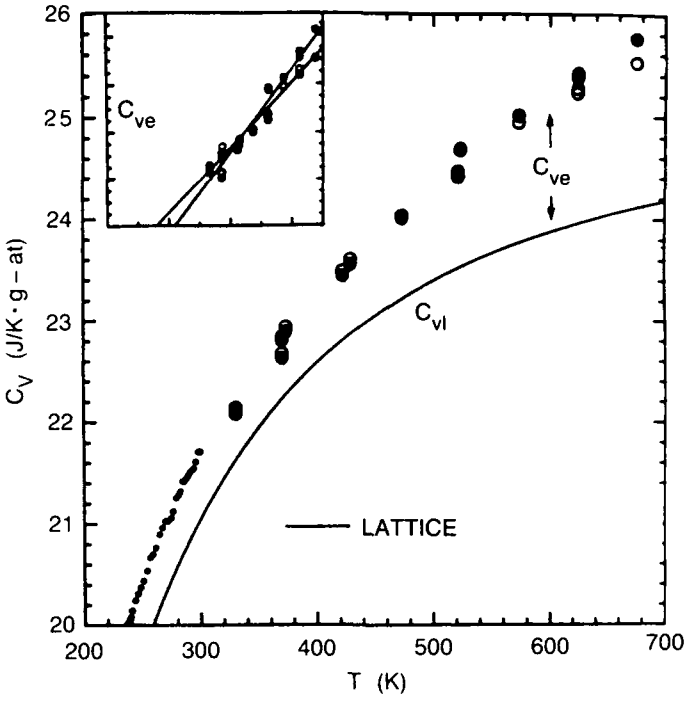

Fig. 3 — The specific heat C_v vs temperature for a high-quality powdered sample of YBCO. The points are the experimental data and the solid curve is the calculated lattice (phonon) contribution. The inset shows the electronic specific heat, which is the difference between the data and the calculated lattice contribution. We determine γ from the slope of the curve in the inset.

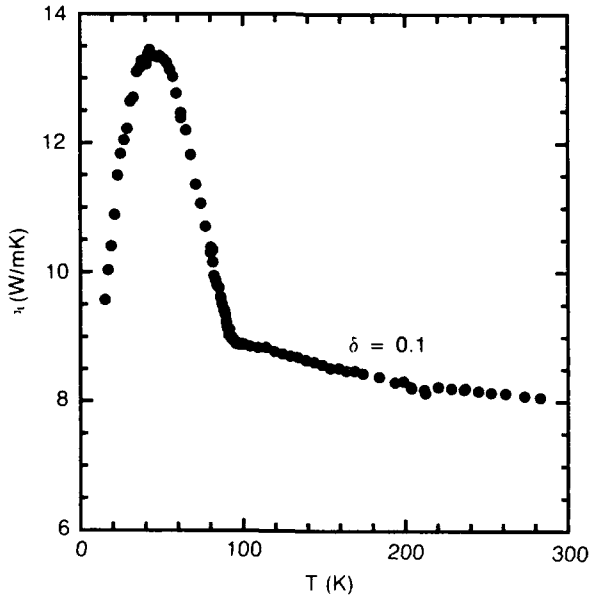

Fig. 4 — The thermal conductivity vs temperature for a high-quality single crystal of YBCO. Notice the large change in slope at the transition temperature.

the normal state properties discussed above. The most important of these are the superconducting coherence length, the magnetic penetration depth, and the energy gap.

At the microscopic level, the spatial variation of the superconducting properties is described by the coherence length ξ: the size of a superconducting pair. This length is proportional to the ratio of the Fermi velocity to the transition temperature and because the Fermi velocity is uniquely small and the transition temperature uniquely large, ξ is very small (ranging from about 20 Å in LSCO to less than 15 Å in YBCO). The quoted values are for carriers moving along the Cu-O planes. For carriers moving perpendicular to the planes, the coherence length is much smaller, reflecting the basic anisotropy of the electronic structure. The uniquely small values of the coherence lengths make these materials particularly sensitive to the presence of defects. Consequently, several experiments that confirm theoretical models of the superconducting state (e.g., electron and pair tunneling) in conventional materials, yield ambiguous results for the cuprates.

Other important superconducting properties are directly related to the coherence length. For example, the magnetic field at which superconductivity is destroyed (the upper critical field H_{c2}) is inversely proportional to the square of the coherence length; thus these materials have uniquely large values for H_{c2}. On the other hand, the usefulness of these materials to produce large magnetic fields is frustrated by the small value of the coherence length. Dissipation is prevented when the magnetic field lines that thread a superconductor are trapped by coherence-length-sized crystallographic defects. The small size and anisotropy of the coherence length make such trapping difficult to achieve in the cuprates.

A superconductor responds to the presence of an external electromagnetic field by generating currents that shield its interior. These currents penetrate the superconductor to a depth Λ, the magnetic penetration depth; Λ is proportional to the ratio of m^* and the carrier concentration. We use the parameters in Table 1 to estimate Λ = 2000 Å for LSCO and 1500 Å for YBCO (for screening currents in the Cu-O planes). Measurements of high-frequency surface impedance and dc mag- netization confirm these theoretical values.

Both the coherence length and penetration depth that we estimate from our simple model are completely consistent with the values that have been obtained from magnetic and electromagnetic measurements and confirm the power of our simple model.

Another prediction that we make based on our estimation of the coherence length is the appearance of two energy gaps in the electronic excitation spectrum of YBCO. A typical BCS superconductor has one gap that forms as the carriers condense into the lower energy superconducting state. The presence of this gap is a hallmark of superconductivity. The two necessary conditions for the observation of multiple gaps are (1) the existence of more than one distinct electronic subsystem or Fermi surface, and (2) an electronic mean-free path longer than the superconducting coherence length. YBCO satisfies the first condition because the Cu-O chains and the Cu-O planes give rise to distinct Fermi surfaces. The cuprates are nearly unique among superconductors in satisfying the second condition. The prediction of two distinct gaps in YBCO has been confirmed by the NMR relaxation time measurements of Barrett et al [4].

The Mechanism of Superconductivity

Many theories have been proposed to explain superconductivity in the cuprates. Central to all theories is the interaction that leads to pairing. A plethora of new interactions have been postulated for the cuprates, however nearly all of the superconductors discovered prior to 1986 have been explained by the generalized Eliashberg formulation [5] of the BCS theory. This theory allows one to calculate T_c and the energy gap provided the details of the pairing interaction are known. For the 6000 or so *conventional*

superconductors, the pairing is due to interactions between carriers and phonons.

Our theoretical development was initially guided by the adage "entia non sunt multiplicare praeter necessitatem," attributed to William of Ockham, A.D. 1238—1320—in other words, don't add complexity until the simple explanation fails (Ockham's razor). To demonstrate that a particular interaction is responsible for superconductivity, the interaction must exist and be of sufficient magnitude so that the high T_c can be obtained. The interaction between electrons and phonons certainly exists (e.g., the thermal conductivity). We set out to show conclusively that this interaction is sufficient to explain high T_c. The traditional method to determine the interaction between phonons and the carriers is electron tunneling spectroscopy. Unfortunately, as mentioned above, the small value of the coherence length renders this method unreliable, and only very recently have preliminary results been obtained. We use another method based on the fact that the Sommerfeld constant γ is not really a constant but is enhanced at low temperatures by this same interaction between carriers and phonons. In fact, the low-temperature Sommerfeld constant γ^L is related to the high-temperature value γ^H by:

$$\gamma^L = \gamma^H (1 + \lambda),$$

where λ is the electron-phonon coupling constant (interaction strength) at $T = 0$. The most important parameter for calculating the superconducting properties in the Eliashberg theory is λ. By employing literature values for the specific heat of LSCO and using the above analysis, we find that λ is about 2.5. This makes the electron-phonon interaction quite strong (most superconductors have values of $\lambda < 1$). The other important parameter needed to determine T_c from the Eliashberg theory is the value of the average phonon energy Ω. We determine this from neutron scattering measurements for LSCO, which were performed in a collaborative experiment between NRL and the National Institute of Standards and Technology. One of us (Kresin) solved the Eliashberg equations at T_c for any value of λ and Ω; by using this solution, we estimate $T_c = 30$ K for LSCO, quite close to the measured value of 38 K. Thus, for the lower T_c cuprates, we believe that Ockam's razor has cut true.

For YBCO, the situation is more complicated. There are planes and chains in the structure, and both these electronic subsystems are important for understanding the details of the normal and superconducting properties. One of the most important questions is whether these two subsystems can be treated separately, since they really are part of the same structural unit. Insight into this question has been gained from our thermopower measurements on high-quality crystals of YBCO. Removing oxygen from the chains yields a dramatic change in the thermopower (Fig. 5), while T_c and many other superconducting properties remain largely unchanged. These measurements clearly show that the planes are important in determining the superconducting properties, while the chains are more important in determining the normal-state properties.

As mentioned above, measurements have indicated the presence of two energy gaps in the excitation spectrum of YBCO. To establish the theoretical framework for these observations, we extend the Eliashberg theory to include the two electronic subsystems (planes and chains) and all of the charge transfer mechanisms that couple them. We consider two charge transfer processes. The first is a pure tunneling process, in which a pair from one band tunnels into the other band. A second process involves tunneling of single carriers between the electronic subsystems. The phonons that induce these tunneling events give rise to pairing. Figure 6 schematically illustrates these processes. Our treatment represents the first time that all of these complications have been incorporated into the Eliashberg theory at the same time. We have solved these equations numerically for T_c and for the smaller of the two energy gaps. The solution is more complicated than the simple one-band Eliashberg theory, which has only two

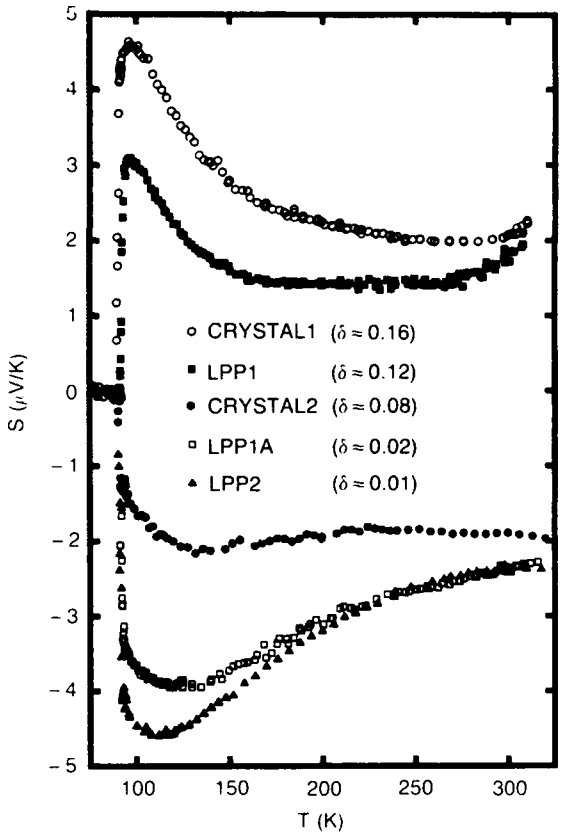

Fig. 5 — The thermopower vs temperature for several crystals of YBCO with differing amounts of oxygen along the chains. Notice the large change in the thermopower (even the sign changes) as oxygen is depleted from the chains. This illustrates the dramatic effect that these oxygen defects have on the transport. All these samples have T_c's greater than 90 K.

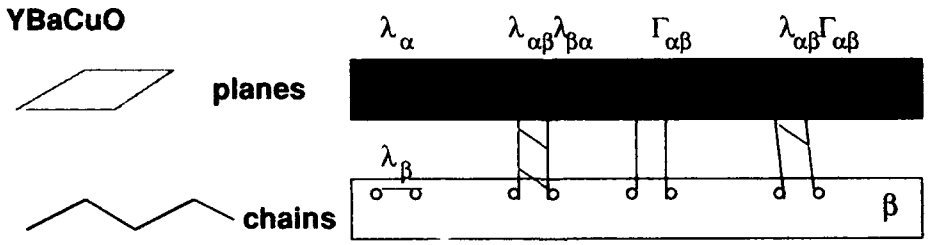

Fig. 6 — Illustration of the various charge transfer terms in our two-band model. The terms involving λ_α and λ_β are the ordinary one-band terms that are described by the usual Eliashberg equations. The term in $\lambda_{\alpha\beta}\lambda_{\beta\alpha}$ is the phonon mediated charge transfer term, or the ordinary two-band term. The term involving Γ is the proximity-effect term, and the term involving $\lambda_{\alpha\beta}\Gamma$ the interference or cross term.

parameters: the average phonon energy Ω and the electron phonon coupling strength λ.The multigap extension of Eliashberg's theory has five independent parameters, Ω, λ_α and λ_β (the coupling constants for each band), $\lambda_{\alpha\beta}$ (the coupling constant for the interband transitions), and Γ (the strength of the pair tunneling or proximity effect process).

We rely on many experiments to determine these parameters independently. The average phonon energy Ω is determined from inelastic neutron scattering measurements to be 30 meV. (Typical values for conventional superconductors are substantially smaller.) The electron-phonon coupling constant for the plane band, λ_α, determined to be about three from the ratio of the

high- and low-temperature values of the electronic specific heat. Other experiments show that λ_{ij} is very small. Using various transport and high-frequency measurements in the literature, $\lambda_{\alpha\beta}$ is estimated to be about 0.5 and Γ about 1. These choices of parameters are not arbitrary—they are based on independent experimental measurements. We use these parameters in the modified Eliashberg theory to calculate T_c = 83 K. This close agreement with the experimental value of 93 K shows that the conventional electron-phonon theory of superconductivity can account for the high T_c in these cuprate compounds.

One can improve the agreement between the experimental and theoretical values of T_c by considering the electrostatic (Coulomb) repulsion that exists between carriers. This effect is accounted for explicitly in the Eliashberg theory (via the parameter μ^*) and tends to suppress pairing in an isotropic material. For carriers constrained to move in two dimensions (the Cu-O planes), unique electronic excitations (acoustic plasmons) tend to enhance pairing. This effect, which has been calculated by one of the authors (Kresin), raises the calculated T_c to 91 K.

Another important result of our model is the prediction of an induced energy gap for the chains. This second gap is smaller than the plane gap and is quite sensitive to the properties of the chains. By adjusting the chain parameters in our theory, we find that T_c remains essentially unchanged, even as the induced chain gap is substantially suppressed. This is exactly what the experiments show! It is a strong confirmation of the validity of our two-band model and of the parameters chosen to represent superconductivity in the YBCO compound.

Summary

Over the past few years, we have developed a theoretical description of the normal and superconducting states of the cuprate superconductors. We performed crucial experiments that have allowed us to test the validity of our description of these materials. Our theory is evolutionary rather than revolutionary: it is an extension of the Eliashberg formalism for describing the electron-phonon interaction in superconductivity. The cuprates are unusual, highly anisotropic metals with small Fermi energies and large effective masses. These normal-state properties lead us to predict a superconducting state that is characterized by very small coherence lengths, large penetration depths, and in some cases, a multigap structure. By incorporating this multigap behavior in the Eliashberg theory, we can account for many of the unusual superconducting properties observed in YBCO. *Thus the conventional electron-phonon interaction can account for the high T_c's characteristic of the cuprates.*

References

1. J.G. Bednorz and K.A. Mueller, "Possible High T_c Superconductivity in the Ba-La-Cu-O System," *Z. Phys.* **B64**, 189 (1986).

2. W.E. Pickett, "Electronic Structure of the High-Temperature Oxide Superconductors," *Rev. Mod. Phys.* **61**, 433 (1989).

3. J. Bardeen, L.N. Cooper, and J.R. Schrieffer, "Theory of Superconductivity," *Phys. Rev.* **108**, 1175 (1957).

4. S.E. Barrett, D.J. Durand, C.H. Pennington, C.P. Slichter, T.A. Friedman, J.P. Rice, and D. M. Ginsberg, "^{63}Cu Knight Shifts in the Superconducting State of $YBa_2Cu_3O_{7-\delta}$ (T_c = 90 K)," *Phys. Rev.* **B41**, 6283 (1990).

5. G.M. Eliashberg, "Interactions Between Electrons and Lattice Vibrations in a Superconductor," *Sov. Phys. JETP* **11**, 696 (1960).

STUART A. WOLF received an A. B. degree in physics from Columbia College in 1964, and M. S. and Ph.D. degrees in experimental superconductivity from Rutgers University in 1966 and 1969, respectively. He was a research associate at Case Western Reserve University from 1969 to 1972, where he continued his work on transport properties of superconducting materials. He joined the Applied Superconductivity Section of the Crystal Physics Branch of NRL in 1972, where he was responsible for the fabrication, optimization, and application of superconducting *qu*antum *i*nterference *de*vice (SQUID) magnetometers. In the ensuing years, he branched out into other aspects of the science of superconductivity and, in particular, pioneered the field of inhomogeneous superconductivity. In the process, he authored over 150 articles in refereed journals. During the 1981–1982 academic year, he was a visiting scholar at UCLA and on his return to NRL, he became head of the Superconducting Materials Section of the Metal Physics Branch. In 1984, he received the Navy's Meritorious Civilian Service Award and in 1986 was elected a fellow of the American Physical Society for his pioneering work on granular superconductors. In 1987, he was appointed head of the Materials Physics Branch and started his effort to understand the unusual superconductivity in the newly discovered cuprate compounds. In 1990, he coauthored a book entitled *Fundamentals of Superconductivity* published by Plenum Press and in 1991, he received the NRL Sigma Xi Pure Science award for his work in understanding the properties of the cuprate superconductors.

JOSHUA L. COHN received a B.A. degree from Wesleyan University in 1983 and a Ph.D. degree in physics from the University of Michigan in 1989. His doctoral thesis involved low temperature electronic transport measurements and the study of weak localization and Coulomb interaction effects in disordered thin bismuth films. He joined NRL's Materials Physics Branch in April 1989 as an Office of Naval Technology postdoctoral fellow. His research at NRL has focused on measurements of normal state transport in single crystals of $YBa_2Cu_3O_{7-\delta}$, with particular emphasis on developing a conventional metallic description of the thermopower and thermal conductivity. Dr. Cohn has co-authored more than 20 publications in the fields of superconductivity and disordered materials.

MARK E. REEVES graduated from the Catholic University of America in 1982 with B.S. and M.S. degrees in physics. He received a Ph.D. degree in experimental solid-state physics from the University of Illinois in 1989, where his thesis involved measurements of the low temperature specific heat of the high T_c superconductors. Since 1989, he has worked in NRL's Materials Physics Branch as a National Research Council postdoctoral fellow. His research has included measurements of the high temperature specific heat of $YBa_2Cu_3O_{7-\delta}$ and studies of the effect of radiation damage on the transition temperature and critical current density in high T_c thin films. Dr. Reeves has co-authored more than 20 publications in superconductivity.

VLADIMIR Z. KRESIN received his Ph.D. degree in 1959 and D. Sci. in 1968, both from Moscow University for his work on the theory of superconductivity. During this time, Dr. Kresin was also a student in the Landau School for Theoretical Physics. He has published 150 articles and authored two monographs and one textbook on the physics of superconductivity. His major research interests are the mechanism of superconductivity, transport properties, exotic superconductivity, and thin film superconductivity. From 1960 to 1978, Dr. Kresin was a professor of theoretical physics at Moscow University. In 1978, he applied for permission to emigrate to the United States, and he left the Soviet Union in 1979. For the past 12 years, Dr. Kresin has been a staff scientist in the Molecular and Chemical Sciences Division at Lawrence Berkeley Laboratory of the University of California.

Ion-beam-assisted Deposition Provides Control over Thin Film Properties

Fred A. Smidt
Condensed Matter and Radiation Sciences Division

A recent study by the National Research Council clearly documented the importance of materials in pacing the advance of modern technology and particularly underscored the need for expanded research in synthesis and fabrication of advanced materials to sustain the rate of progress. The Department of Defense (DoD) is likewise dependent on advances in materials and materials processing to achieve the increases in performance needed for the platforms and weapons of the future. Indeed, no less than 11 of the 20 areas targeted as critical technologies in 1990 were advanced materials technologies.

Thin films and coatings and the ability to produce them are an important element in the advanced materials revolution. Figure 1 shows the issues and elements of the science of thin film deposition. Four technologies representative of the end products of the science are tribological coatings for cutting tools and wear surfaces, environmental protection coatings (such as those for aircraft engine turbine blades), optical coatings and filters, and thin films for microelectronics and opto-electronic devices. The key to improved properties in these coatings and thin films is the control of the processing variables that in turn control the composition and microstructure of the films, as seen graphically in the center of Fig. 1. Reports in the scientific literature and experiments at NRL in the early 1980s [1] indicated that bombardment of a growing film with energetic ions could lower the temperature at which films could be deposited with a dense equiaxed grain structure, thus altering the relationship between grain size and shape and deposition temperature. Other benefits attributed to the impingement of an energetic flux on the growing film are improved adhesion, alteration of the nucleation and growth process, texture development, and control of stress. Many of these effects were noted in plasma deposition processes but could not be quantified because of the complexity of the plasma processes. An Accelerated Research Initiative (ARI) entitled "Ion-beam-activated D( )osition" was initiated in 1987 to study these processes in detail and apply them to the deposition of high-technology coatings for Navy and DoD applications. Findings from this program, completed in 1991, are described.

The Ion-beam-assisted-deposition (IBAD) Process

The IBAD process is a modification of conventional physical vapor deposition (pvd) (vacuum evaporation or sputtering) in which an energetic flux of ions bombards the film as it is deposited. Figure 2 shows a typical IBAD apparatus. An electron beam is used to evaporate a metal onto a substrate positioned above the vapor source. A Kaufman ion source ionizes a gas and accelerates the ions through a potential of 500 to 2000 eV to bombard the film as it deposits. The deposition rate of the film is measured by a quartz

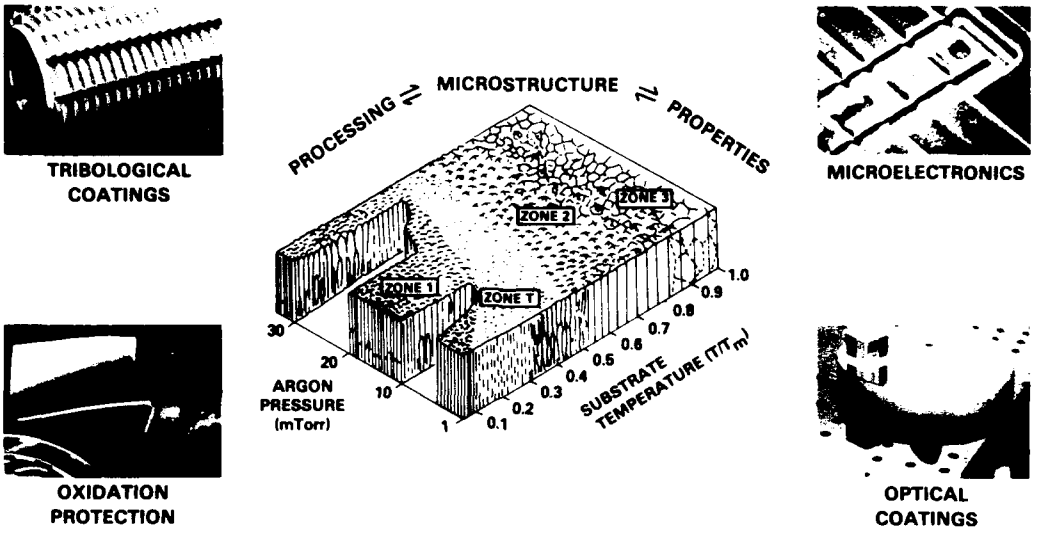

Fig. 1 — Thin film deposition science makes possible the coatings used in modern technology through knowledge of how the processing variables control the microstructure (shown schematically for the change in grain size and morphology) that, in turn, controls the coating properties

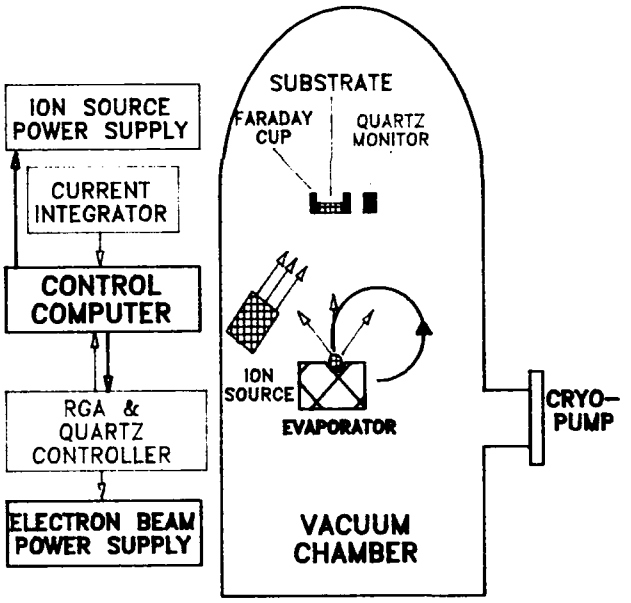

Fig. 2 — Ion-beam-assisted deposition apparatus with electron beam evaporation of vapor species, ion bombardment of the film deposited on the substrate, sensors for the atom and ion fluxes, and the control logic

crystal monitor that changes frequency of vibration as material is deposited. The flux of ions is monitored by a Faraday cup, which measures the ion current. The deposition rate and ion flux data are monitored by a computer that, in turn, controls the current in the ion source and the power to the evaporator, thus providing precise control of the depositing films. Important parameters in the process are the energy of the impacting ion, the arrival rate ratio of ions to vapor atoms, and the temperature of the substrate.

Several variants on the IBAD process were investigated and found to be beneficial. A high-energy (25 to 200 kV) system using the beam from an ion implanter was built and evaluated, but most effects were found to be produced just as

effectively by the low energy (500 to 2000 eV) beam, and the apparatus was much more compact, less expensive, and produced higher beam currents. Bombardment of a growing film with the inert gas argon (Ar) produces refinements in grain structure, with minimal incorporation of Ar. Introduction of an active gas, such as nitrogen, into the beam allows precise control of the stoichiometry of the film and the synthesis of compound films, such as Si_3N_4, BN, and Al_2O_3. Another approach to compound synthesis was the introduction of the active gas into the chamber at low partial pressures so that compound formation occurred by reaction with the gas. Ion bombardment was found to influence the mechanism of gas adsorption.

Fundamental Research

The issue in this research was to understand the mechanisms by which the energetic ions altered the properties of the deposited film so that the process could be controlled. The interaction of an energetic ion with a solid produces a number of effects. The Coulomb interaction with the outer-shell electrons produces electronic excitation; elastic collisions of the nuclei displace atoms from their lattice positions and produce interstial and vacancy defects; the deposition of energy in a localized region creates a thermal spike lasting on the order of 10^{-13} s. Atoms are also sputtered from the surface as a result of the ion impact. The depth of the region affected by the ion impact is a function of the energy of the ion and the inverse of the square of the mass of the bombarding ion. For example, a 100 keV Ni ion in a Ni substrate penetrates to a depth of about 50 nm, while a 1 keV ion penetrates only a few atom layers. The sputtering yield, the number of atoms ejected from the surface-per-incoming-ion, is also a function of energy and typically exceeds 1.0 at an energy of approximately 1 keV. Thus, for practical considerations, it is desirable to operate at or below 1 keV and with a low ratio of ions to evaporated atoms.

Modeling of Film Deposition

The effects of energy on the structure of films was investigated by molecular dynamics modeling of the deposition process [2]. Ag atoms, with energies ranging from 0.1 to 40 eV, were deposited on an Ag substrate at 300 K by using an embedded-atom method to treat the atomic interactions. Th Ag atoms were deposited at 0.5- or 1.0-ps intervals by using a random number generator to determine the deposition position. The substrate consisted of a 12-atom × 14-atom × 6-atom section of crystal (1008 atoms), with periodic boundary conditions in the film plane. Three monolayers (500 atoms) were deposited in each run, and the positions and velocities were recorded immediately before each atom release.

Several significant effects were noted in the modeling of deposition. Epitaxial growth was observed at all energies from 0.1 to 40 eV. At 0.1 eV (thermal deposition), the film grew as three-dimensional islands and redistributed by collapse of unstable configurations. At 10 eV, the film grew as essentially monolayers as a result of redistribution of the surface atoms by ballistic collisions. Figure 3 illustrates that these effects result in the difference in surface coverage after deposition of 1.2 monolayers.

Another important effect is percolation mixing. As the energy of the deposited atoms increased to 10 eV, mixing between the substrate layer and the deposited layers began to appear. Figure 4 shows that at 20 eV, approximately 20% intermixing between the substrate and deposited layers occurred. This intermixing of layers takes place not by displacement collisions but by an exchange interaction in which the deposited atom becomes embedded in the substrate layer, and a substrate atom at another site is ejected into the film layer. Thus, mixing occurs as the atoms percolate from layer to layer. This phenomena would appear to have implications for improving adhesion and for roughening of the interface.

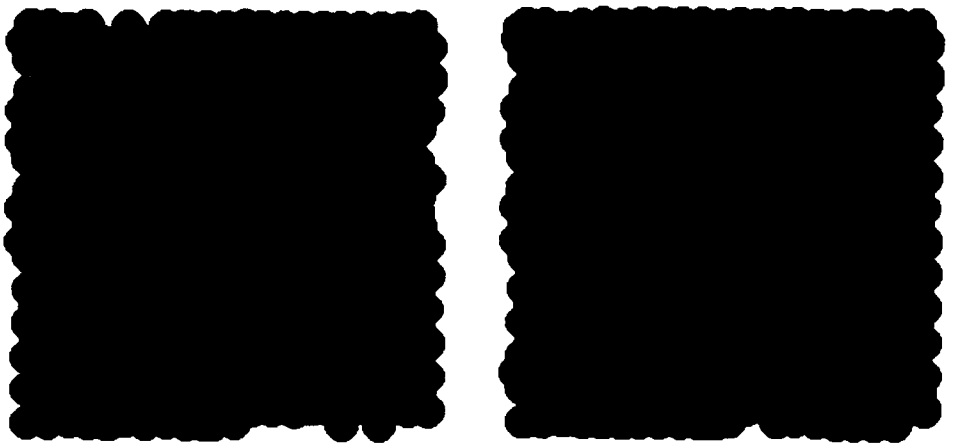

Fig. 3 — The degree of surface coverage shown by molecular dynamics simulation of the deposition of 1.2 monolayers of Ag (red) on an Ag (111) substrate (green)

Fig. 4 — The effects of percolation mixing after deposition of 500 atoms (3.0 monolayers) at 20 eV energy. Deposited film atoms (red) are embedded into the substrate layer (green), which causes substrate atoms to be ejected into the first film layer with some additional mixing into the second layer.

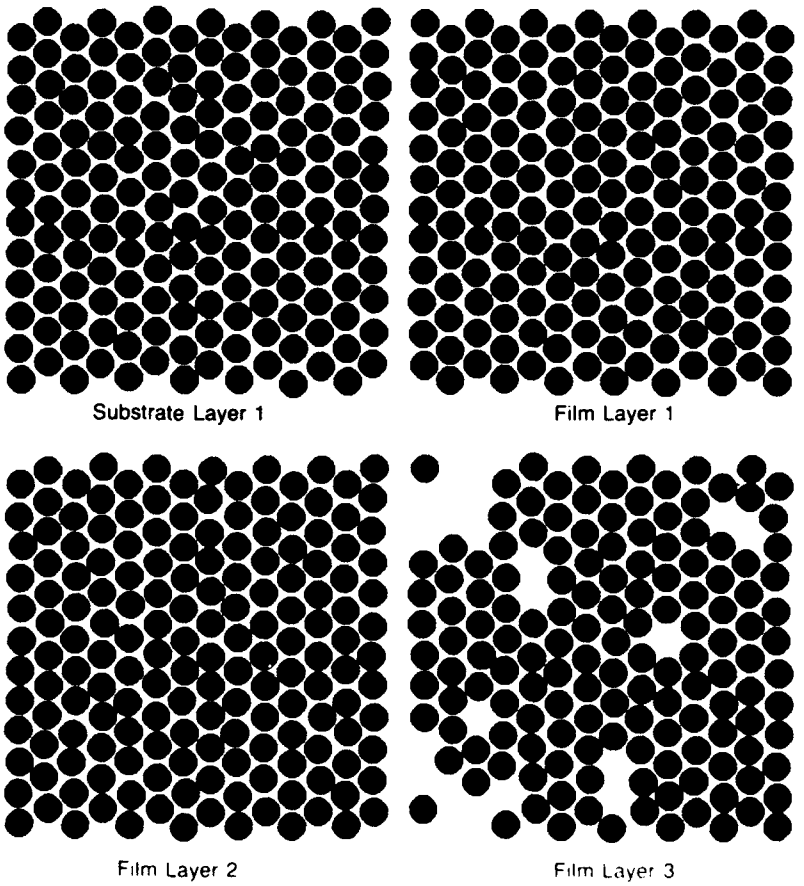

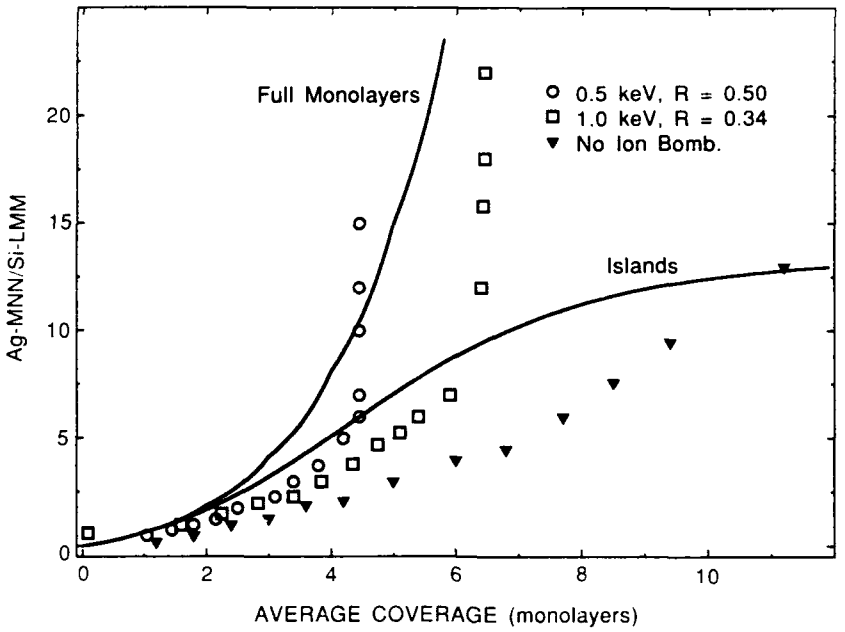

Fig. 5 — The effect of ion bombardment on surface coverage of Ag deposited on Si. The extent of surface coverage was measured by the ratio of Auger line intensities as a function of the number of monolayers deposited. A model was used to predict the trend lines for a layer-by-layer growth mode and an island growth mode. Ion bombardment of the film during deposition caused a shift from island growth to more complete coverage with a sputter-limited thickness dependent on the ion energy and *R* value (ion/atom arrival rate ratio).

Nucleation and Growth Experiments

Several experiments were performed to study the early stages of nucleation and film growth for IBAD conditions as compared to film growth for conventional pvd. Sartwell and Chambers [3] studied the film growth mode of Ag deposited on Si by monitoring the change in strength of the Auger signal as Ag covered the Si substrate. Figure 5 shows the results for the case of no ion bombardment and bombardment with 500 eV and 1000 eV Ar^+ ions with arrival rate ratios of 0.50 and 0.34, respectively. The change in the ratio of Auger line intensities as a function of the Ag deposited can be predicted for film growth models in which either Ag islands form on the Si, or the film grows layer by layer. Films grown by pvd with no ion-beam assist are seen to follow the island growth mode, while ion bombardment during the deposition leads to a more uniform coverage and saturation at a certain thickness. This saturation occurs because the sputtering yield from bulk Ag is high enough to remove Ag atoms as fast as they are deposited. At thicknesses less than the limiting thickness, the bombarding ion penetrates the film and dissipates most of its energy in the Si substrate so that less Ag is lost and the film builds up. Some of the Ag atoms sputtered from the islands redeposit in the open channels so that the surface becomes uniformly covered. Figure 5 also shows that the sputter-limited thickness is energy dependent.

Another approach to study nucleation and growth of films used high-resolution transmission electron microscopy (TEM) to follow film growth. The experiments were conducted at higher growth rates than the Auger studies described and under a wider range of *R* values. Under *R* values less than those required for sputter-limited film growth ($R = 0.2$), there appears to be a decrease in the number of islands nucleated and an increase in size followed by additional nucleation with a more uniform coverage between the large islands. At

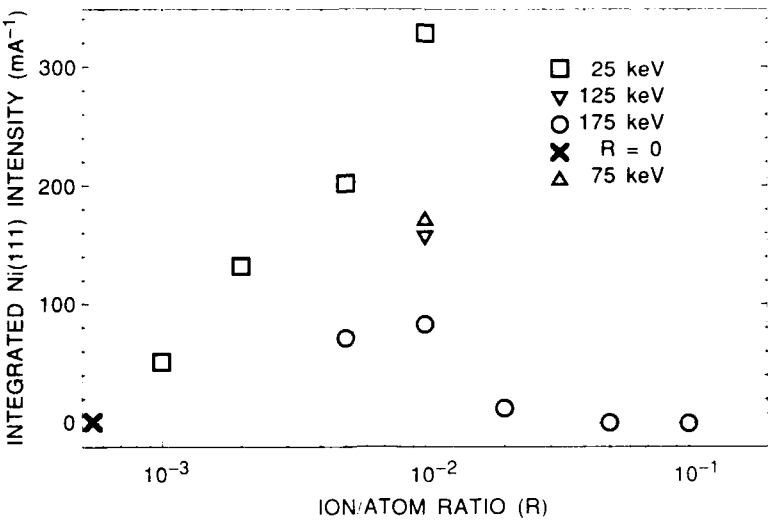

Fig. 6 — The effect of ion beam energy and R on the degree of epitaxy of Ni films deposited on <111> Si

high R values ($R = 0.8$), a film deposited as islands remains in the island morphology. Thus, ion bombardment during film deposition can modify the film growth characteristics in a variety of ways that depend on the process variables.

Ni Films Grown by IBAD

A parametric study of the effect of IBAD on the properties of thin films of Ni examined the effect of ion energy (100 eV to 50 keV), arrival rate ratio (0 to 0.1), and substrate temperature (75°C, 280°C) on various properties of Ni, such as density, resistivity, TEM microstructure, Ar incorporation, and epitaxy [4]. One of the more obvious effects of IBAD was a decrease in grain size to 5- to 10-nm diameters. Other effects noted were a decrease in Ar incorporation at R values >0.05 at 1500 eV energy and an increase in lattice strain up to damage levels of about 10 displacements-per-atom (dpa) with a decrease to zero strain at 100 dpa. In summary, there is a parameter space in which thermal processes dominate (280°C) and the ion flux has little effect, and a parameter space in which ballistic processes dominate (75°C) and bombardment produces damage and an accumulation of defects. In the intermediate region, the additional energy and ballistic collisions may induce beneficial effects, such as densification of the film by shifting it from a metastable state to a more stable state nearer to equilibrium.

Growth of Oriented Films

One of the more striking effects of ion bombardment on the growing film is the enhancement of preferred orientation or texture in the film. A film grown by IBAD has all its grains oriented along the same crystallographic axes rather than being randomly oriented as is the case for thermal deposition. While some preferred orientation effects were observed for Ni with low energy IBAD (1500 eV at $R = 0.02$) [4], the effect was much more pronounced at high energies. Epitaxial Ni films were grown on <111> Si at Ni^+ ion energies ranging from 25 to 175 keV [5]. Figure 6 shows the effect-of-arrival-rate ratio on the degree of preferred orientation as measured by the intensity of the Ni(111) X-ray reflection. The reference with no ion-beam assist is indicated by the "x." The greatest degree of alignment was produced by a 25 keV beam and was still increasing at the maximum R attainable with the ion beam (0.01). Higher energy beams produced more damage at the highest energy (175 keV), and the degree of alignment is seen to decrease above

an R of 0.01. The preferred growth direction is found to correspond with the passage of the ion beam along the preferred channeling direction in the crystal that is the direction in which the ion beam sees the largest spacing between crystal planes. Passage of the ion beam down the open channels produces less damage than for other directions where the beam collides with atoms and produces damage. The promotion of hetero-epitaxial growth is a very promising application of IBAD that requires further investigation.

Synthesis of Compounds by Ion-beam-assisted Deposition

The synthesis of compounds, where one component is provided by the evaporant flux and the other is provided by the ion beam, requires a thorough understanding of all factors involved in the deposition process and the measurement process if the stoichiometry of the films is to be controlled and reproduced. The Si-N system was selected for a detailed study of compound synthesis by IBAD by using electron-beam evaporation of Si and ion bombardment with a 500 eV ion beam from a Kaufman source [6] in the geometry shown in Fig. 2. The growth rate of the Si-N film is determined by the deposition rate of Si atoms and the implantation rate of N less the removal of film atoms by sputtering. As noted previously, the Si deposition rate is measured by a quartz-crystal monitor, and the N ion current is measured by a Faraday cup. However, for quantitative control of the process, there are a number of additional phenomena that must be understood. The beam current measured by the Faraday cup measures only current and must be corrected to determine the true N flux to the surface. First, several charge states of N are produced in the Kaufman source. Calibration of the source in a test stand with a magnetic spectrometer gave a charge state distribution of 89% N_2^+ and 11% N^+. Second, charge exchange neutralization of the beam through collisions with gas atoms in the chamber produces uncharged particles that are not measured in the Faraday cup but add N to the film and produce sputtering. Charge exchange neutralization was determined by measuring the decrease in ion current as a function of partial pressure of the chamber gases. Finally, the reflection coefficient of ions from the surface was calculated to be 0.1. Sputtering removes atoms from the film, so the sputtering yield must be known accurately as a function of energy. There are also tooling factors to correct for differences between the flux at the sensors and the actual flux on the sample. The calculated composition of the films was compared to the true composition by Rutherford back-scattering spectroscopy (RBS).

The result of this research was that the composition of SiN_x films could be accurately controlled through the process parameters. Figure 7 shows data from a number of runs for the N/Si ratio in films deposited at a rate of 1.0 nm s^{-1} with a 500 eV nitrogen beam as a function of ion current density. The scale on the top of the graph shows the arrival-rate ratio of ions/atoms. Error bars represent a relative error in composition of <3 atom percent. The attainment of this degree of control over the process permitted the fabrication of multilayer optical filters, which required precise control of the index of refraction through control of the composition of SiN_x film. We will describe this later in the paper.

The Si-N system described represents a situation in which all of the N is introduced into the film by implantation. There are many other systems where a reaction occurs between gas adsorbed on the surface of the growing film and the deposited material. Several of these systems have been studied, and the work on TiN is particularly interesting. Experiments similar to those performed on Si-N [7] showed that with no ion beam in a partial pressure of 2×10^{-5} Torr N_2 gas, a film with N/Ti ratio of 0.4 formed. The addition of a 500 eV N ion beam with an arrival rate ratio of 0.2 increased the N/Ti ratio in the film to 1.0, stoichiometric TiN. Since not enough N was being added to the film through the N beam to reach this

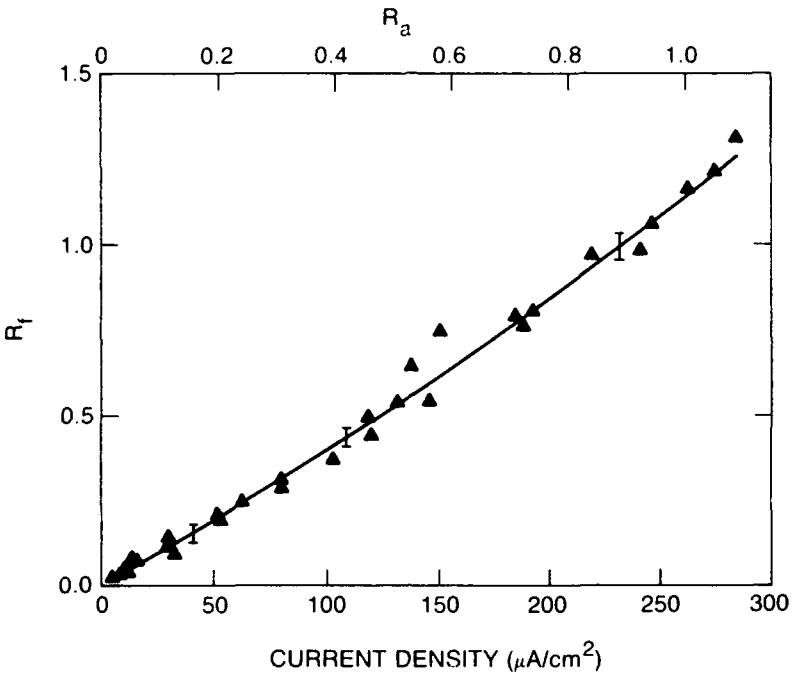

Fig. 7 — The composition of Si–N films, expressed as the ratio of N/Si, as a function of current density for 500 eV N ions and a deposition rate of 1.0 nm Si s^{-1}. The arrival rate ratio R_A is superimposed on the top scale. Results illustrate the degree of control over ion-beam synthesis by using IBAD.

composition, the balance was obviously coming from the absorbed gas, and the ion beam was promoting or activating the incorporation. Subsequent experiments [8] showed that the process of nitrogen incorporation into the film could be described by a set of kinetic equations with additional factors for impingement of N_2 gas onto the surface from the chamber atmosphere, physisorption of the N_2, removal of N_2 by sputtering, and conversion of physisorbed N to a chemisorbed N by the ion beam. As a consequence of these insights, a modification of the IBAD process—termed reactive IBAD—was developed in which TiN films were grown by using the N partial pressure as the source of N for the film and an Ar ion beam to activate the chemisorption of N. A further advantage of this process is that the oxygen content of the films is lower than in films deposited by pvd. This is believed to be a consequence of sputter removal of O_2 and H_2O adsorbed on the surface.

Tribological Properties of TiN IBAD Films

Ceramic coatings have many potential applications for reducing wear, however, the brittleness of the coating and poor adhesion to metals are problems. IBAD has the ability to control microstructure, has inherently good adhesion because of the intermixing of the interface, and has a low deposition temperature, so the microstructure produced by heat treatment of steel components would not be degraded during the deposition; thus superior films should result. TiN films produced by several IBAD techniques have been evaluated for tribological applications and found to realize this promise.

The adhesion of TiN coatings deposited on AISI 52100 steel was evaluated by using a scratch adhesion test in which a diamond indenter is moved across the surface of the sample at progressively increasing loads [9]. Failure of the coating is monitored by acoustic emission if it is

brittle or by changes in the coefficient of friction if the coating is soft. Figure 8 shows an SEM micrograph comparing a scratch test on a high-quality TiN coating deposited by reactive sputtering and an IBAD TiN coating. The conventional coating failed by decohesion and spalling of the coating at a load of 40 N. The IBAD film deformed under the indenter and failed by plowing through the coating at loads of 50 to 60 N rather than failing by decohesion. Debris resembling metal machining chips can be seen near the edge of the track, a further indication of the ductility of these films. TEM examination of these films revealed the origin of the ductility as a very fine-grain structure (7-nm grain diameter). This is very similar behavior to ceramic materials fabricated from nanocrystalline material by powder consolidation.

Further studies of the IBAD TiN revealed that the microhardness of the coatings could be controlled by the ion-to- atom arrival rate ratio R [9]. Films produced at R values of 0.1 were soft with a Knoop hardness value near 1000, while coatings produced with an R value of 0.4 had a hardness value of 2700. Microscopy indicated the major difference between the soft and hard materials was the connectivity across the grain boundary. The soft material had porosity—either gas bubbles or voids—at the grain boundaries. Wear tests of IBAD TiN prepared at different R values showed material prepared with an R value of 0.3 (H = 1700) had better wear life than the hardest (R = 0.4) specimen. IBAD coatings of TiN have also been evaluated in rolling contact fatigue tests done cooperatively with National Aeronautics and Space Administration-Marshall Space Flight Center and with the Army Materials Technology Laboratory. Coatings were applied to cylindrical rolling contact fatigue specimens of 440C and M50 steel and were tested at loads up to 5420 MPa (786 ksi) with no coating failure on either material. The rolling contact fatigue life of the 440C was improved by a factor of five.

Rugate Optical Filters

Optical filters are used to protect sensors and eyes from laser radiation at specific wavelengths. Conventional quarter-wave dielectric stacks consist of optical materials of different refractive index n and 1/4 wavelength in thickness glued together in a stack with alternating high n and low n material. The resulting filter absorbs light in a narrow bandwidth and transmits other frequencies but tends to be rather fragile and subject to

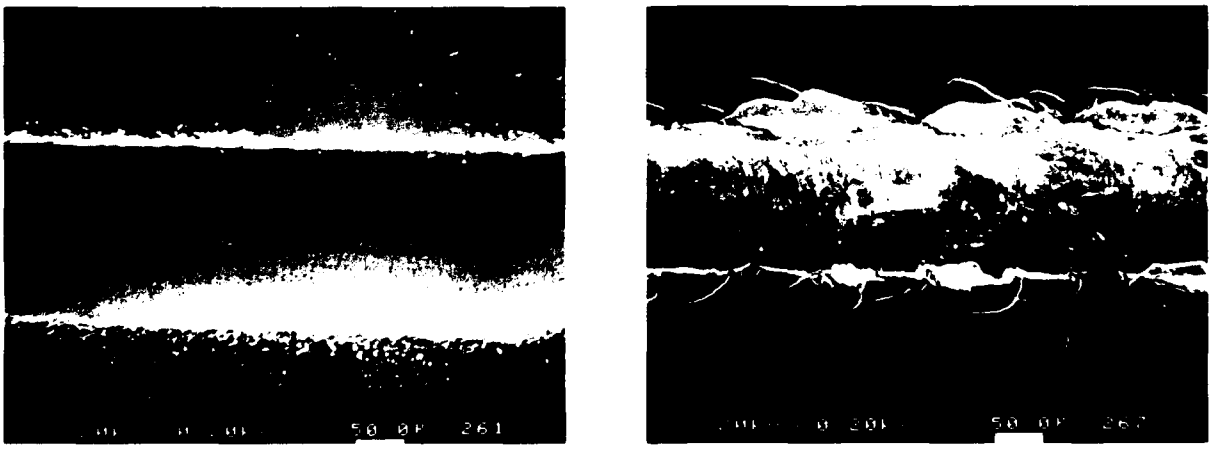

Fig. 8 — Scanning electron micrographs of a diamond scratch adhesion test track in TiN coatings deposited by IBAD and by sputtering. The sputtered coating is brittle and fails by decohesion, while the IBAD coating fails by plowing through the coating. Both coatings had similar hardness values.

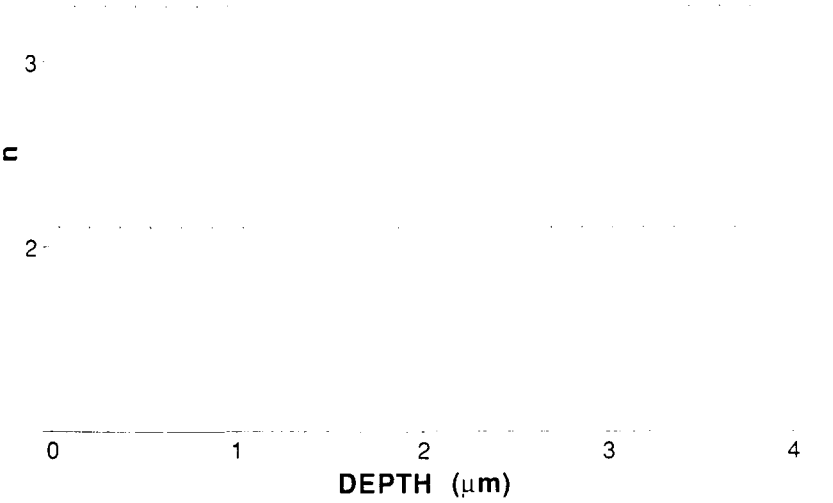

(a)

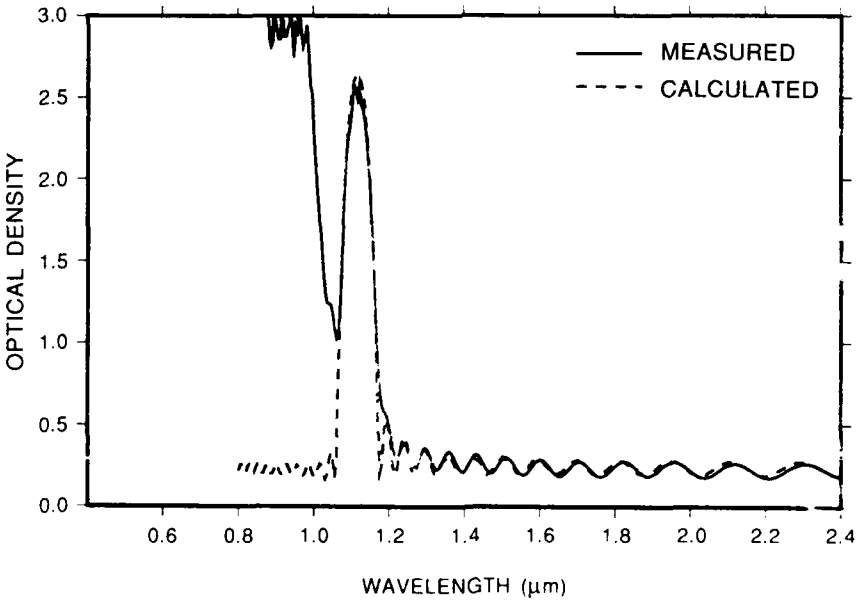

(b)

Fig. 9 — A 23-cycle Rugate optical filter deposited by IBAD. The N content of the film was varied to produce the refractive index profile shown in (a), which produces the band reflection spectrum shown in (b). Agreement between measured and calculated response is excellent (except for the Si-absorption region not included in the filter calculation).

delamination under high heat loads or thermal cycling. A new concept for a filter termed a "Rugate" (as in "corrugated") uses a periodically varying index of refraction with 1/4 wave periodicity to produce the same interference effects.

The refractive index of amorphous silicon-nitride films varies with the nitrogen content of the film. Since IBAD provides excellent control of N content in Si-N films, it provided a possible means to fabricate Rugate filters that would have no discrete interfaces. The feasibility of the concept was proven at NRL after considerable effort [10]. Figure 9(a) shows the refractive index profile for a Si-N Rugate filter and Fig. 9(b) shows the optical density spectrum for a 23-cycle filter of Si-N designed to block radiation at the 1.1 μm wavelength. The performance of the filter is in excellent agreement with that predicted (except for the band above the Si absorption edge, which is not included in the calculation). Rugate filters have been fabricated from Si-N and B-N materials, and filters have been fabricated for several wavelengths including the 3 to 5 μm IR band. The incorporation of more than one periodicity in the filter can broaden the blocking band or produce multiple line filters.

X-ray Mirrors

Multilayer IBAD films have a variety of applications. Another interesting demonstration of the technique is the fabrication of an X-ray mirror by using Si and Si_3N_4 as the layer materials. X-ray mirrors commonly use high-atomic-mass (Z)/low-atomic-mass material combinations to reflect X rays. Some theoretical work in the literature indicated that low Z/low-Z combinations might produce narrower linewidth because of the deeper penetration of X rays in low-Z materials and, hence, an increase in the number of multilayers that would be active. Figure 10 shows a TEM micrograph of a multilayer Si/Si_3N_4 film (with four different layer spacings) to illustrate the planarity and uniformity of multilayers that can be produced by the IBAD technique.

Six X-ray mirrors were fabricated with 28 nm/3.5 nm Si_3N_4/Si layer spacings with the total number of layers varying from 100 to 400 [11]. The ion-beam energy was lowered to 100 eV to minimize surface roughening caused by ion mixing, and the films were deposited on a low thermal expansion glass. The best mirror showed an absolute peak reflectivity of 1% with a

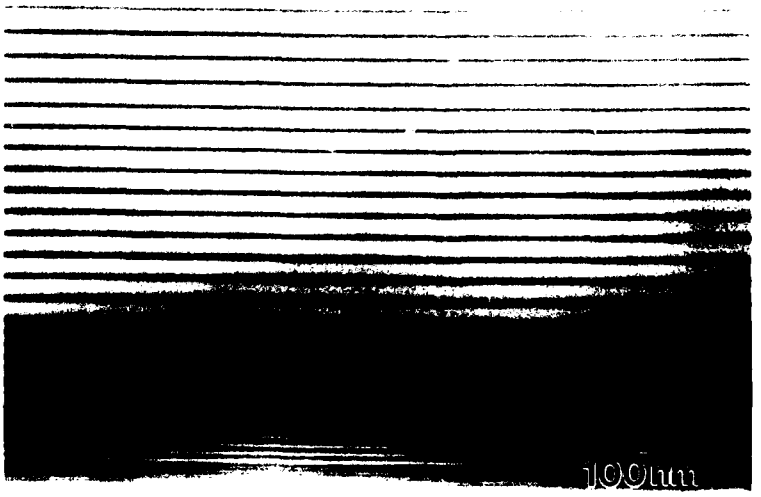

Fig. 10 — Transmission electron micrograph of multilayer film with alternating Si and Si_3N_4 layers deposited by IBAD at four different periodicties illustrating the excellent planarity and reproducibility of layer spacings

full-width/half-maximum peak width of 0.24° (2Θ) for Al Kα X rays, values comparable to commercially available mirrors and a clearly successful demonstration of the IBAD technique.

Spin-offs and Opportunities for Future Research

The ARI on IBAD has enabled NRL to document the purported benefits of IBAD and gain insight into the mechanisms that produce the phenomena. A comprehensive review of the world's literature on IBAD was published in 1990 [1] and clearly shows the impact of the NRL work on the development of this powerful processing technique. The ability to produce a fine-grained microstructure, to reduce the deposition temperature, to achieve good adherence, to control stress in the film, to produce oriented films, and to independently control the energy of the bombarding particle, the flux of depositing species, and the chamber pressure make this a powerful technique.

Several applications have been described here, and others are under development. Tribological coatings—particularly of ceramic coatings—show high promise. MoS_2 solid lubricants show unique properties when prepared by IBAD. Environmentally safe coatings prepared by IBAD are under study to replace Cr and Cd electroplating. Several applications in microelectronics packaging, such as high current density contacts to GaAs and diamond and the deposition of masks for X-ray lithography, are under study. Ion-beam-activated etching shows promise for certain materials, such as HgCdTe. Finally, the new understanding of the effects of ion-beam-activated processes can be incorporated into plasma processing systems that are less amenable to accurate process control but are more cost effective for large-scale production facilities and for coating components with complex geometries.

Acknowledgments

The work described was performed by C.A. Carosella, G.P. Chambers, S.A. Dillich, E.P. Donovan, C.M. Gilmore, K.S. Grabowski, G.K. Hubler, R.A. Kant, B.D. Sartwell, J.A. Sprague, and D. VanVechten of the Surface Modification Branch and I. Singer of the Surface Chemistry Branch.

References

1. F.A. Smidt, "Use of Ion Beam Assisted Deposition to Modify the Microstructure and Properties of Thin Films," *Int. Mater. Rev.* **35**, 61-128 (1990).
2. C.M. Gilmore and J.A. Sprague, "Molecular-Dynamics Simulation of the Energetic Deposition of Ag Thin Films," *Phys. Rev.* **B44**, 8950 (1991).
3. G.P. Chambers and B.D. Sartwell, "Growth Modes of Ag Deposited on Si(111) with Simultaneous Low Energy Ion Bombardment," *Surf. Sci.* **218**, 55 (1989).
4. R.A. Kant, G.P. Chambers, and B.D. Sartwell, "The Structure and Properties of Ni Films Grown by Ion Beam Assisted Deposition," in *Beam-Solid Interactions: Physical Phenomena, Vol. 151*, J.A. Knapp, P. Bergesen, and R.A. Zuhr, eds. (Materials Research Society, Pittsburgh, 1990), p. 67.
5. K.S. Grabowski and R.A. Kant, "Epitaxial Growth of Ni on Si by Ion Assisted Deposition," in *Thin Film Structures and Phase Stability, Vol. 187*, B.M. Clemens and W.L. Johnson, eds. (Materials Research Society, Pittsburgh, 1990), p. 237.
6. D. VanVechten, G.K. Hubler, E.P. Donovan, and F.D. Correll, "Fundamentals of Ion Beam Assisted Deposition I. Model of Process and Reproducibility of Film Composition;" and G.K. Hubler, D. VanVechten, E.P. Donovan and C.A. Carosella, "Fundamentals of Ion Beam Assisted Depositions II. Absolute Calibration of Ion and Evaporant Fluxes," *J. Vac. Sci. Technol.* **A8**, 821-830 and 831-8 (1990).
7. G.K. Hubler, D. VanVechten, E.P. Donovan, and R.A. Kant, "Ion Beam

Assisted Deposition of Titanium Nitride," in *Processing and Characterization of Materials Using Ion Beams, Vol. 128*, L.E. Rehn, J. Greene, and F.A. Smidt, eds. (Materials Research Society, Pittsburgh, 1989), p. 55.

8. R.A. Kant and B.D. Sartwell, "The Influence of Ion Bombardment on Reactions between Ti and Gaseous N_2," *J. Vac. Sci. Technol.* **A8**, 861 (1990).
9. S.A. Dillich, R.A. Kant, B.D. Sartwell, J.A. Sprague, and F.A. Smidt, "The Tribological Behavior of TiN Coatings Prepared by IBAD," *Trans. ASME, J. Tribology* **113**, 214 (1991).
10. E.P. Donovan, D. VanVechten, A.D.F. Kahn, C.A. Carosella and G.K. Hubler, "Near Infrared Rugate Filter Fabrication by Ion Beam Assisted Deposition of $Si_{(1-x)}N_x$ Films," *Appl. Opt.* **55**, 2940 (1989).
11. G.K. Hubler, C.A. Carosella, P.G. Burkhalter, R.K. Freitag, C.M. Cotell and W.D. Coleman, "Fabrication of Low Z X-Ray Mirrors by Ion Beam Assisted Deposition," *Nucl. Instrum. Meth. Phys. Res.* **B59/60**, 268 (1991).

THE AUTHOR

FRED A. SMIDT received a B.S. degree from the University of Nebraska in 1954 and a Ph.D. degree in Physical Chemistry from Iowa State University in 1962. He served in the U.S. Air Force from 1954 to 1956. Prior to joining the technical staff at NRL in 1969, he held positions as senior scientist at the Atomic Energy Commission's Hanford Laboratory in Richland, Washington, which was operated by the General Electric Company, and Battelle Northwest. Dr. Smidt held positions as research metallurgist, section head, and served on the staff of the associate director of research before being named head of the Surface Modification Branch in 1982. He has had one-year special assignments as a program administrator in the Department of Energy and on the staff of the Deputy Director of Research and Engineering, Office of the Secretary of Defense. Dr. Smidt's research contributions include radiation damage in materials, reactor and thermostructural materials performance, and more recently, ion implantation and ion-beam-assisted deposition for surface modification. He has authored or coauthored over 150 technical papers and articles and is a Fellow of ASM International.

Low Reynolds Number Aerodynamics for Electronic Warfare

Richard J. Foch and Peggy L. Toot
Tactical Electronic Warfare Division

INTRODUCTION

The Naval Research Laboratory is a technology leader for low Reynolds number (LNR) aerodynamics research that focuses on significantly enhancing the flight performance of small, unmanned aircraft. These small, unmanned aerial vehicles (UAVs) are demonstrating their superiority for efficiently performing many high-value Navy and other military missions.

Unique to the ships' electronic warfare (EW) community is the need for very low-speed, low-altitude, small UAVs for use as ship decoys. UAVs that are launched from a container on the ship's deck and that carry electronic payloads away from the ship's location can provide highly effective offboard countermeasures against hostile radars and radar-guided weapons. By creating realistic-appearing radar images, these UAVs can decoy incoming missiles. A decoy's effectiveness increases when its flight speed is reduced to match the speed of a ship and when its flight endurance is maximized. Achieving long-endurance flight performance by using a small vehicle in combination with low flight speed is technologically challenging, especially with respect to the demands it places on the aerodynamics. Additional technology drivers include the constraining combinations of efficient packaging and compatibility with shipboard storage/launch/recovery requirements, as well as low production cost.

The Vehicle Research Section in the Tactical Electronic Warfare Division's Offboard Countermeasures Branch began developing deployment vehicles for EW offboard countermeasures in the mid-1970s. Although these early unmanned aircraft flew successfully, they did not meet the desired low flight speeds or long flight duration. The goal of developing a useful decoy that could meet mission-critical requirements made it necessary to conduct extensive studies into LRN aerodynamics.

Recognizing that the performance shortfalls of these early EW UAVs were a direct result of the lack of technologies, the Office of Naval Research supported an extensive basic research program on LRN aerodynamics for Navy unmanned aircraft applications. From 1980 to 1985, these LRN aerodynamics research efforts involved extensive participation by NRL and other government facilities, major universities, and industry. It was apparent by 1985 that these advances in LRN aerodynamics, if combined with advanced composite structures and miniaturized digital-electronics technologies, would allow the desired performance goals for a practical EW UAV to be met. Subsequently, the Office of Naval Technology tasked NRL to develop a remotely piloted, instrumented research aircraft under the Low Altitude/Airspeed Unmanned Research Aircraft (LAURA) exploratory development program, from 1985 through 1990. LAURA's goals were (1) to validate the laboratory and computational results from the LRN research efforts under actual flight conditions, and (2) to demonstrate the flight performance needed for an effective EW UAV. LAURA's eleven test flights successfully demonstrated the practicality of flying

long endurance missions at shiplike speeds with a ship-compatible package. The LAURA program also validated the numerous design tools and techniques developed specifically for aerodynamically efficient UAVs during the decade of LRN research at NRL.

Following the LAURA effort, the Flying Radar Target (FLYRT) Advanced Technology Demonstration (ATD) program was initiated. By using truly state-of-the-art LRN, structural, and electronic technologies, the FLYRT is being developed to perform actual EW mission demonstrations.

THEORY

The fundamental difference between normal and LRN aerodynamics is the importance and complexity of the behavior of the airflow close to the surfaces of the aircraft, especially its wings. The viscosity of real fluids does not allow them to slip over surfaces without friction, so a thin "boundary layer" having a high velocity gradient and shear stresses forms between the free air flow and the surface of the wing. For large and/or fast aircraft, the boundary layer is extremely thin in comparison to the dimensions of the wing's airfoil and does not greatly affect the aerodynamic performance of the airfoil. However, for small and/or slow aircraft, the boundary layer is sufficiently thick to make it more difficult for the airfoil to efficiently generate and maintain a strong pressure differential between its upper and lower surfaces. As a result, more friction (drag) is created to produce less aerodynamic lift.

The ability to characterize the boundary layer and predict when the effects of fluid viscosity become dominant is crucial for studying small-scale aerodynamics and improving the aerodynamic qualities of small airfoils. While studying the flow of water in pipes, nineteenth-century British physicist, Osborne Reynolds, discovered the fundamental, non-dimensional parameter needed for boundary-layer analysis. When this parameter, the Reynolds number (RN), is below a critical value, viscous effects dominate the characteristics of the boundary layer and the condition is known as low Reynolds number (LRN) aerodynamics. The critical RN for most airfoils is approximately 500,000. The RN equals the ratio between the momentum of a moving fluid to its bulk viscosity multiplied by the fundamental dimension of the object:

$$\mathrm{RN} = \frac{(\text{density}) \times (\text{velocity})}{\text{bulk viscosity}} \times (\text{reference dimension})$$

For the standard sea-level condition of air, density divided by bulk viscosity is approximately 68,460 s/m^2. The RN for a wing based on the length of the airfoil (wing chord) is, therefore:

$$\mathrm{RN} = 68460\ s/m^2 \times (\text{velocity [m/s]}) \times (\text{wind chord [m]}).$$

Until recently, most research in aircraft aerodynamics involved man-carrying aircraft whose wings have RNs between 3 and 50 million, well above the critical RN for airfoils (approximately 500,000). The aerodynamics of these flight conditions have been well studied and are relatively well understood. Figure 1 shows how the boundary layer flow over the wing transitions from laminar to turbulent conditions and remains attached to near the trailing edge of the airfoil for cruise flight angles of attack.

For small, low-speed aircraft (such as EW UAVs), the RN can be significantly below the critical value of 500,000. Here the boundary layer is more sensitive to the development of a laminar separation bubble, an area of adverse pressure gradient within the laminar boundary layer. For many airfoils forced to operate outside their design envelope, the laminar separation bubble can burst, causing a catastrophic loss of lift and a significant increase in drag. Recent research conducted in LRN aerodynamics broadens our understanding of the physics involved within the boundary layer, laminar separation bubbles, and airfoil design that is optimized for operating under LRN conditions.

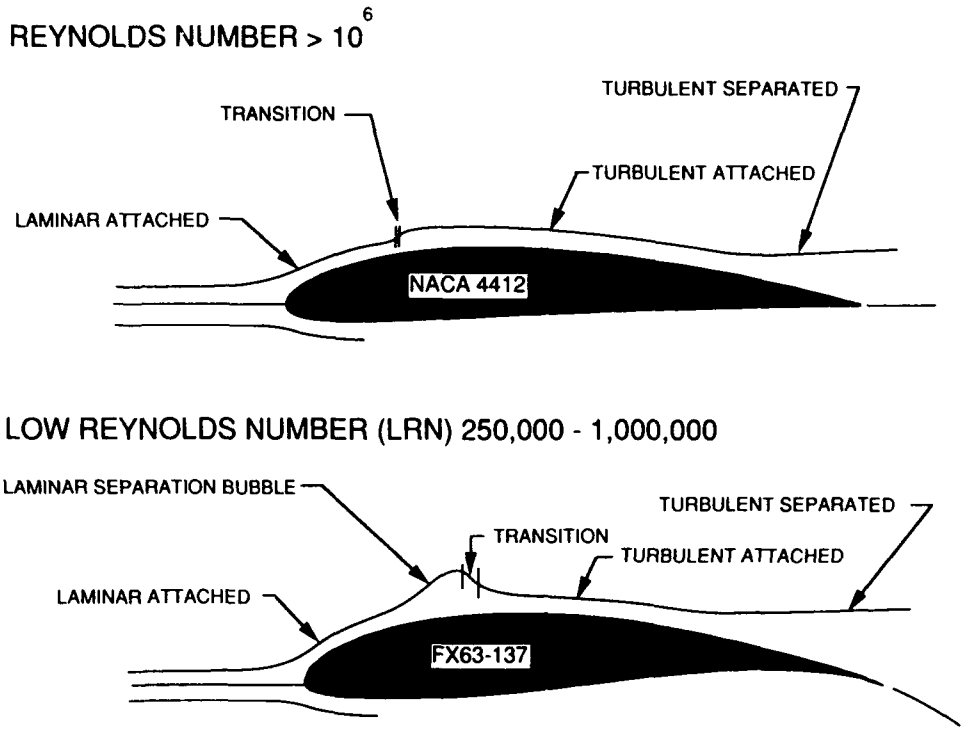

Fig. 1 — Boundary layer characteristics, a Reynolds number comparison

A typical UAV for EW applications may fly at a speed of 13 m/s and have a wing chord measuring 25 cm. Its RN value would therefore be 222,950. Since this value is well below critical, the boundary layer on the wings is definitely influenced by viscosity. Special precautions must be taken in the airfoil design and selection to achieve high, aerodynamic efficiency. Additionally, transforming these efficient airfoil shapes into producible wings and then developing practical aircraft involves careful system engineering, since tails, propellers, and wing/tail/fuselage junctures also experience LRN effects.

RESEARCH METHODS

Three primary research methods are used for studying LRN aerodynamics of aircraft: computational fluid dynamics (CFD), wind-tunnel testing, and flight testing. All three are essential, since each alone cannot provide the required information. CFD is a digital simulation of an ideal reality and requires a database for validation. Wind-tunnel testing provides realistic data taken in an atmospheric environment containing small-scale turbulence and acoustic noise. Flight testing is true reality, but provides less than ideal conditions for data collection.

Computational Fluid Dynamics

CFD computer codes provide a digitally approximated solution of the Navier-Stokes equation of fluid motion. The Navier-Stokes equation, developed in the first part of the nineteenth century could, theoretically, precisely predict the motion of every single, falling leaf. Unfortunately, there is no known closed-form solution for the complete equation; however, the availability of powerful digital computers has allowed many solutions to be closely approximated. The full, Navier-Stokes equations are the nonlinear conservation of momentum equations that include the second-order viscous flow terms. These equations are computationally solved by making assumptions for the behavior of

the boundary layer. Since viscous effects dominate LRN flow, modeling the boundary layer is critical to realistic computational predictions. To date, the only accurate predictions for LRN flight have been for two-dimensional (2D) airfoils rather than for whole wings or the entire aircraft. This CFD limitation is due to reaching the limits of computer speed and memory.

LRN airfoil design codes must capture the complex nature of the boundary layer, including its laminar, transition, separation bubble, turbulent, and separated regions, as well as the strong and nonlinear coupling between viscous, transition, and inviscid flow at the separation bubble. This is still as much an art as a science, since the fundamental mechanism of turbulence generation in the transitional region of the boundary layer is not yet fully understood. ISES is one code for LRN airfoil design and analysis that has been successful in routinely predicting the flow field about LRN airfoils. ISES has been used to design and analyze airfoils for use on human-powered planes and for other applications; however, it can be very demanding on computer time. The XFOIL code was designed to retain the ability of ISES to predict LRN flows while significantly reducing the computational requirements. Another design and analysis code, developed by Richard Eppler, uses an empirical criterion to warn the user of a possible drag increase of unknown magnitude caused by the laminar separation bubble. If not properly computed, drag predictions will be significantly less than indicated by experimental data, resulting in unrealistic performance predictions.

Some of the LRN airfoil designs that perform well in computational analyses prove to be difficult to fabricate and are very sensitive to off-design conditions. As an example, many computationally designed LRN airfoils require smooth surfaces. In application on an aircraft, a minor accumulation of salt spray or a few spattered insects on these airfoils will cause loss of lift, greatly increase drag, and possibly cause complete separation in the boundary layer. Some airfoils are insensitive to surface roughness and environmental conditions. One such airfoil, the Wortmann FX63-137, has excellent aerodynamic performance at RNs as low as 150,000.

Wind-Tunnel Testing

Wind-tunnel testing plays a significant role in LRN airfoil development for validating computational predictions and designing LRN aircraft. Wind-tunnel tests of airfoils are used to validate the Navier Stokes codes that attempt to predict boundary-layer transition and laminar separation bubble location and size. Tests of a model of the entire aircraft verify the design predictions for the actual three-dimensional (3D) wing that was based on the 2D airfoil design. Aerodynamic forces and moments on the model are measured for a range of flight conditions to determine the aircraft's performance, stability, and control characteristics. Tests of the entire aircraft are essential, since the tail surfaces are typically smaller than the wing and, therefore, operate at even lower RNs than the wing and encounter their own performance problems. As might be expected, achieving satisfactory stability and control can be even more challenging than attaining efficient flight performance.

At LRNs, the laminar and transitional portion of the boundary layer is extremely sensitive to external disturbances. Poor flow quality in the tunnel can cause the boundary layer to prematurely transition to turbulent flow as if the RN were higher, thereby giving a false indication of the airfoil's performance. In flight, the airfoil would respond to the flow quality of the atmosphere. The boundary layer, now no longer artificially transitioned by the turbulence of the flow in the wind tunnel, would tend to remain laminar over a larger portion of the airfoil and could develop a larger separation bubble. As a result, a large, unacceptable increase in drag and loss of lift could occur. LRN airfoils can only be reliably tested in a low-turbulence, wind-tunnel environment.

The NRL Offboard Test Platform (OBTP) is a 0- to 200-knot low-turbulence wind tunnel designed specifically for testing small-scale

vehicles at low flight speeds within its 4-ft by 4-ft test section. Three-dimensional models are mounted on a sting that contains a six-component strain gauge balance. When the tunnel is running with a model in place, the air loads on the model are measured by the deflection of strain gauge balances on the sting. These measurements are converted to aerodynamic force and moment coefficients. Since many EW UAVs have full-scale wing spans of about 100 in. or less and flight speed goals of less than 60 knots, one-third-size models can be tested at three times the flight speed. The resulting data will be taken at the same value of RN as that of the full scale UAV, thereby eliminating critical data corrections.

Flight Testing

Two methods of flight testing have been successfully used by NRL: flying by radio-control powered research UAVs carrying flight test sensors and instrumentation or by dropping gliding radio-controlled test models from either manned aircraft or large UAVs.

Based in part on the rapid increase in sophistication and reliability of radio-controlled model airplane electronics and engines, research flight testing of advanced technology UAVs has become routine, timely, and cost effective. The simplest data-collection systems use real-time ground-based video to record flight maneuvers of a test airplane painted with markings that facilitate determining its flight attitude. This type of test involves the smallest and least expensive UAV—basically a specially constructed, advanced model airplane. The most sophisticated data collection rivals the flight-test instrumentation of manned aircraft. Typically, the test UAV is equipped with several dozen sensors, including pressure transducers, rate gyros, position gyros, accelerometers, and thermocouples. These sensors provide real-time data on the aircraft's attitude, velocity, accelerations, control settings, engine performance, and other parameters needed to accurately determine the performance and characteristics necessary for comparison to wind-tunnel predictions. Figure 2 shows data-acquisition and flight-control system components, as installed in a LAURA. During such flight tests, data are both telemetered to the ground and stored in an onboard digital microcomputer memory. The data stored onboard are a backup should the telemetry system encounter problems; they also provide a second reference. These fully instrumented test UAVs are not only relatively expensive to build and operate, but they provide the best method of truly validating the results of the LRN research.

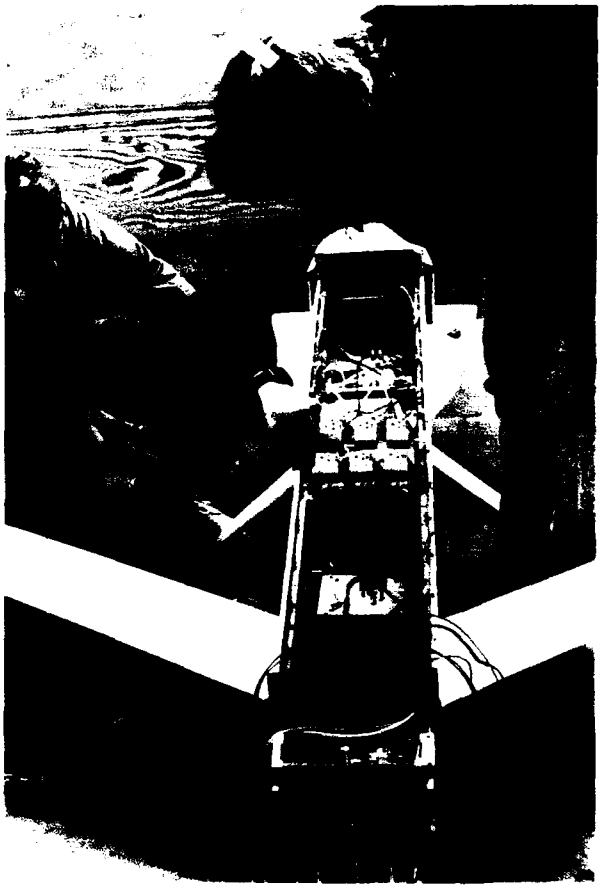

Fig. 2 — Preflight checkout of LAURA flight test sensor components

Drop-testing is an inexpensive technique to evaluate aircraft handling qualities. The aircraft to be tested is constructed in a reduced scale as a lightweight, radio-controlled glider. A series of drop tests are made to verify flying qualities. For

UAVs that unfold wings, tails, or antennas in flight, these features may also be incorporated. Figure 3 shows how a large powered, radio-controlled UAV is configured with a mounting bracket to carry the glider. The carrier UAV is flown to a desired altitude where the drop model is released. During the glide, preselected control inputs are commanded to evaluate response and handling characteristics of the drop model. Prior to these tests, computational six degree-of-freedom flight-motion codes were used to predict the flying and handling qualities of the drop model. The qualitative drop tests validate these predictions. Thus, computer codes can now be used to predict the flight characteristics of the full-scale vehicle with a high degree of confidence.

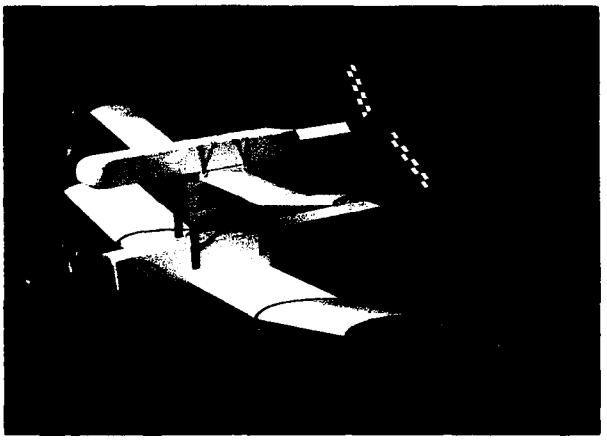

Fig. 3 — FLYRT drop test model mounted on carrier UAV

RESEARCH RESULTS

Figure 4 shows examples of some of the best LRN airfoils for Navy EW UAV applications. Notice the variation in shapes. The Wortmann FX63-137 is perhaps the highest-lift LRN airfoil that has a low sensitivity to surface finish while maintaining good stalling characteristics at RNs as low as 100,000. However, originally it was nearly impossible to fabricate into a practical wing because of an extremely thin trailing edge. Computational tools used in the basic LRN research efforts allowed the FX63-137 to be redesigned to the shape shown; this makes it difficult but feasible to manufacture. The Liebeck LA2573A was designed for flying-wing-type LRN aircraft designs. Reflexing the trailing edge upward is necessary to give the airfoil itself sufficient longitudinal stability to eliminate the need for a tail on any aircraft on which it may be used. Although this reflex reduces the maximum lift, the LA2573A still features excellent performance and is especially useful when the best system engineering solution is a tailless UAV design. The Foch RF-1165FB has maximum lift capabilities that place it between the very high value of the FX63-137 and the acceptably high LA2573A. The RF-1165FB and LA2573A are more well suited for slightly higher RNs than the FX63-137. They are also somewhat insensitive to surface roughness that affects their overall

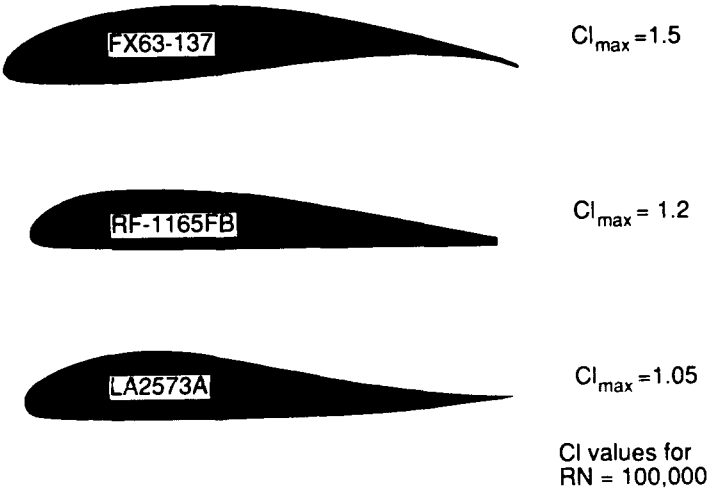

Fig. 4 — Low Reynolds number airfoils flown by NRL

performance, which is crucial for UAVs operating in salt-spray environments.

In opposition to the critical preciseness of shape required for high-performance LRN airfoils is the reality of building an actual wing. Special fabrication methods can be implemented; however, cost is a limiting factor in exotic techniques. The primary concern is to maintain the features of the 2D airfoil used to predict the performance of the aircraft. Ease of manufacturing is the special quality of the NRL-developed RF-1165FB because of its straight lower surface that allows a wing to be constructed on an inexpensive, flat jig surface.

LRN AIRCRAFT DESIGN

All LRN aircraft designed by NRL for Fleet EW applications are characterized by having the highest aerodynamic efficiency attainable in conjunction with their mission requirements. They must carry microwave RF antennas, fold into very tightly packed containers, be catapulted or rocket-propelled away from the launching ship, deploy some or all of their aerodynamic surfaces after launch (i.e., while in flight), and be relatively inexpensive to produce. Two distinct EW missions drive LRN technology. One mission permits time for unpackaging and checkout on the deck and requires an endurance of several hours at very low, shiplike flight speeds. The other requires that the UAV be powered-up, launched, and ready to perform a several minute, low-speed mission in a matter of seconds.

The LAURA program, conducted from 1985 through 1990, addressed the technology for the long-endurance, very low-speed mission. Since the LAURA was a research platform rather than just a mission demonstrator, it featured a unique, modular fuselage capable of being reconfigured to accommodate various wing and tail platforms, as well as LRN airfoils. Ultimately four different UAV designs were test flown: a joined-wing, variable-span, tandem-wing, and three-surface configuration. Figure 5 shows these designs.

LAURA research included detailed wind-tunnel testing of one-half-scale models of each configuration to provide a database for design and verification of computer codes. The flight dynamics, as well as structural properties of each, were extensively analyzed with state-of-the-art computational and experimental methods. Two of

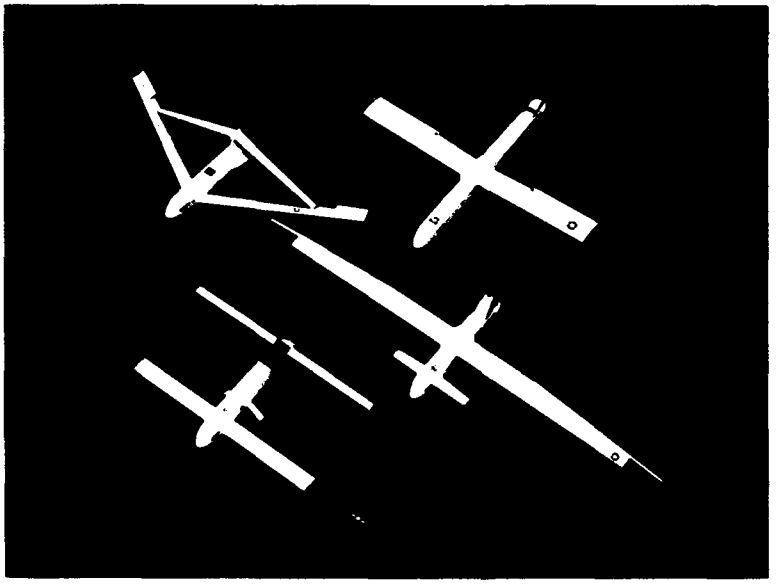

Fig. 5 — LAURA aircraft: (clockwise from upper right) variable span, three surface, tandem wing, joined wing

these methods included the development of a real-time digital flight simulator and a truck-mounted "captive carry test rig" (Fig. 6) to which the final aircraft were mounted and checked out under simulated flight conditions prior to actual free flight. The identical fuselages of each of the four designs carried a complete set of flight test sensors, an autopilot, an 18-channel digital data acquisition system with a real-time telemetry down-link, a dual-redundancy radio-command control system, landing gear, and a two-cylinder, four-cycle power plant. Flight testing was conducted on each LAURA. Although highly limited by time and money, eleven test flights, each lasting 20 to 60 minutes, were flown. The results of these test flights were sufficient to prove that the latest LRN technology in conjunction with today's advanced composite structures and micro-computerized, digital electronic control systems make the desired EW mission feasible. Moreover, lessons learned and technologies developed as a result of LAURA research have found additional Navy, military, and civilian applications. High-altitude, long-endurance aircraft, and battery or solar-powered electrically propelled aircraft are ideal for atmospheric research, long-range communications, and surveillance.

Fig. 6 — Captive carry test fixture with variable span LAURA installed

The reactive-type maritime mission requires a cleverly unfolding type of design. At first appearances, the mission flight performance requirements may not seem to severely task LRN technology, since an endurance of only several minutes at speeds much higher than that of the LAURA are mission-acceptable. However, the tight packaging constraints require the wings to generate high lift. Because of advances in battery technology, the requirements for quick reaction, high reliability, and extended flight duration of several minutes are met by using an electric motor-driven propeller as the propulsion system. A battery-powered electrically propelled airplane must be aerodynamically efficient because of the low power density of the batteries, and its propeller blades must be good LRN airfoils for acceptable performance. Additionally, allowances must be made for hinge brackets or slight gaps created between aerodynamic surfaces that add drag and reduce lift.

The FLYRT ATD program began in 1991 to demonstrate the reactive mission with an actual EW payload under realistic conditions by the end of FY 93. Figures 7 and 8 show the finalized design and method of deployment for the FLYRT. Air vehicle specifications required that a minimum lift- to-drag ratio (L/D) of 10 be achieved for the overall aircraft. For an aerodynamically clean design, an L/D of 10 is readily achievable despite LRN effects. However, the realistic, practical design is not "clean;" it has hinges, external antennas, battery, and motor air-cooling ducts that create so much drag that the "clean" airframe must have an L/D significantly greater than 10. Based on lessons learned and technology attained from previous LRN research, the NRL-designed FLYRT develops an L/D of 20.5 for the clean airframe as tested in the NRL OBTP wind tunnel. Based on these measurements, there is now high confidence that the FLYRT vehicle will meet its performance goals.

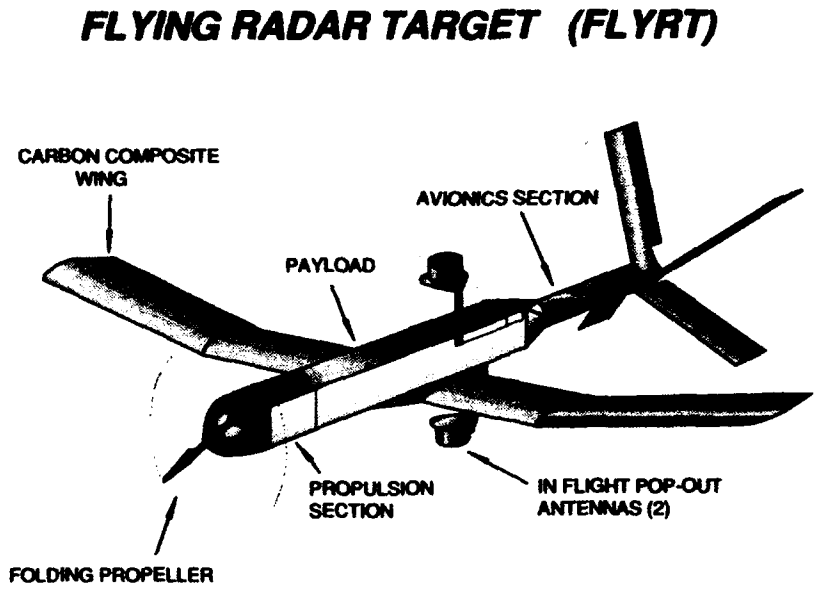

Fig. 7 — FLYRT final design configuration

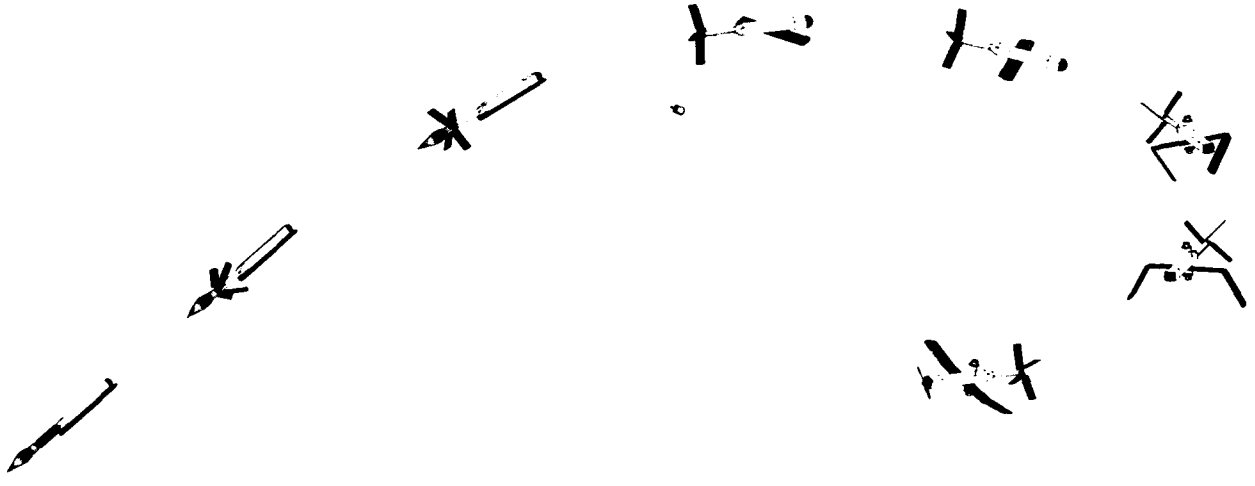

Fig. 8 — FLYRT launch and deployment sequence

SUMMARY

The performance limits of designs for unmanned aircraft for EW and the reliability of predicting their performance are limited by the state of LRN technology. To date, much of the experimental research work has been in 2D airfoil analysis and boundary layer investigation. Even though LRN boundary layers are now fairly well understood, reliable aerodynamic performance data are limited to those airfoils that have been wind-tunnel tested. Computational analysis codes that predict airfoil performance are limited at LRNs because viscous effects are still difficult to model. LRN wind-tunnel testing is very sensitive to the turbulence intensity of the tunnel facility. The flow quality of a wind tunnel can greatly affect the boundary layer over the airfoil. Even using wind-tunnel test results as input to the available analyses capabilities, LRN airplanes can have unpredicted flying qualities. Therefore, captive carry testing and flight testing are necessary, albeit high risk, research techniques for advanced development. Fortunately, flight testing with unmanned, radio-controlled aircraft is highly affordable.

CONCLUSION

Major strides and breakthroughs in LRN aerodynamics for unmanned aircraft have been made during the past decade of NRL research. The success of small, unmanned aircraft being developed and demonstrated today is directly related to recent advances in LRN aerodynamics and other key technologies. Today's technological resources will undoubtedly make tomorrow's systems smaller, less expensive, and better performing for EW applications and beyond.

BIBLIOGRAPHY

M. Drela, "XFOIL: An Analysis and Design System for Low Reynolds Number Airfoils," Lecture Notes in Engineering, Low Reynolds Number Aerodynamics, Proceeding of the Conference (Springer-Verlag, Berlin, 1989).

R. Foch and P. Toot, "Flight Testing Navy Low Reynolds Number (LRN) Unmanned Aircraft," Lecture Notes in Engineering, Low Reynolds Number Aerodynamics, Proceeding of the Conference (Springer-Verlag, Berlin, 1989).

R. Eppler, *Airfoil Design and Data*, (Springer-Verlag, Berlin, 1990).

THE AUTHORS

RICHARD J. FOCH graduated from the Florida Institute of Technology (FIT) with a B.S. degree in mechanical engineering in 1979. While at FIT, he obtained his private pilot's license and assisted with a local airport's operations. Following his graduation in 1979, Mr. Foch joined NRL as an aerospace engineer. While working for the Tactical Electronic Warfare Division's Offboard Countermeasures (OCM) Branch, Mr. Foch attended the University of Maryland from1980 to 1985, and received an M.S. degree in aerospace engineering. His thesis work focused on low Reynolds number aerodynamics at transonic speeds. Since 1985, Mr. Foch has been the head of the OCM Branch's Vehicle Research Section. During this period, the Vehicle Research Section has developed numerous unmanned aircraft for EW applications, including the Low Altitude/Airspeed Unmanned Research Aircraft (LAURA). Currently, he is the project manager and chief designer for the air vehicle portion of the Flying Radar Target (FLYRT) Advanced Technology Demonstration (ATD). An avid enthusiast of radio controlled (RC) model airplanes for the past 19 years, Mr. Foch currently serves as the chief RC test pilot for the Vehicle Research Section. Mr. Foch has led several quick reaction EW efforts to support Fleet activities, prior to and during Desert Storm, for which he received Meritorious Civilian Service Award in 1989 and an NRL Special Act Award in 1991.

PEGGY L. TOOT graduated from Texas A&M University with a B.S. degree in aerospace engineering in 1986. She worked as a summer hire at NRL prior to her senior year at A&M. Following graduation in 1986, she joined NRL full time. Ms. Toot is currently pursuing an M.S. degree in aerospace engineering at the University of Maryland. Ms. Toot participated in the full duration of the Low Altitude/Airspeed Unmanned Research Aircraft (LAURA) program, where she held the key role of flight test director, and during the last two years acted as liaison between the NRL engineers and the program sponsor at the Office of Naval Research. Currently, she is the principal engineer monitoring the development of the rocket booster motor for the $12M Flying Radar Target (FLYRT) Advanced Technology Demonstration (ATD) program. Ms. Toot has authored several papers on the LAURA program. She routinely presents briefings covering the LAURA and FLYRT programs and other work performed by the Vehicle Research Section. An active member of the American Institute of Aeronautics and Astronautics (AIAA), Ms. Toot serves on the Flight Test Technical Committee (FTTC) and currently holds the position of General Chairperson for the 1992 FTTC Conference. Previously, she chaired the Unmanned Vehicle Session at the 1990 FTTC Conference. Ms. Toot was presented an NRL Special Act Award for her part in the efforts on the Crystal Vortex project, a quick response decoy system developed for Desert Shield/Desert Storm.

The ACRO Attractor
Computer Graphics, *Second Place*
Paul A. Bernhardt

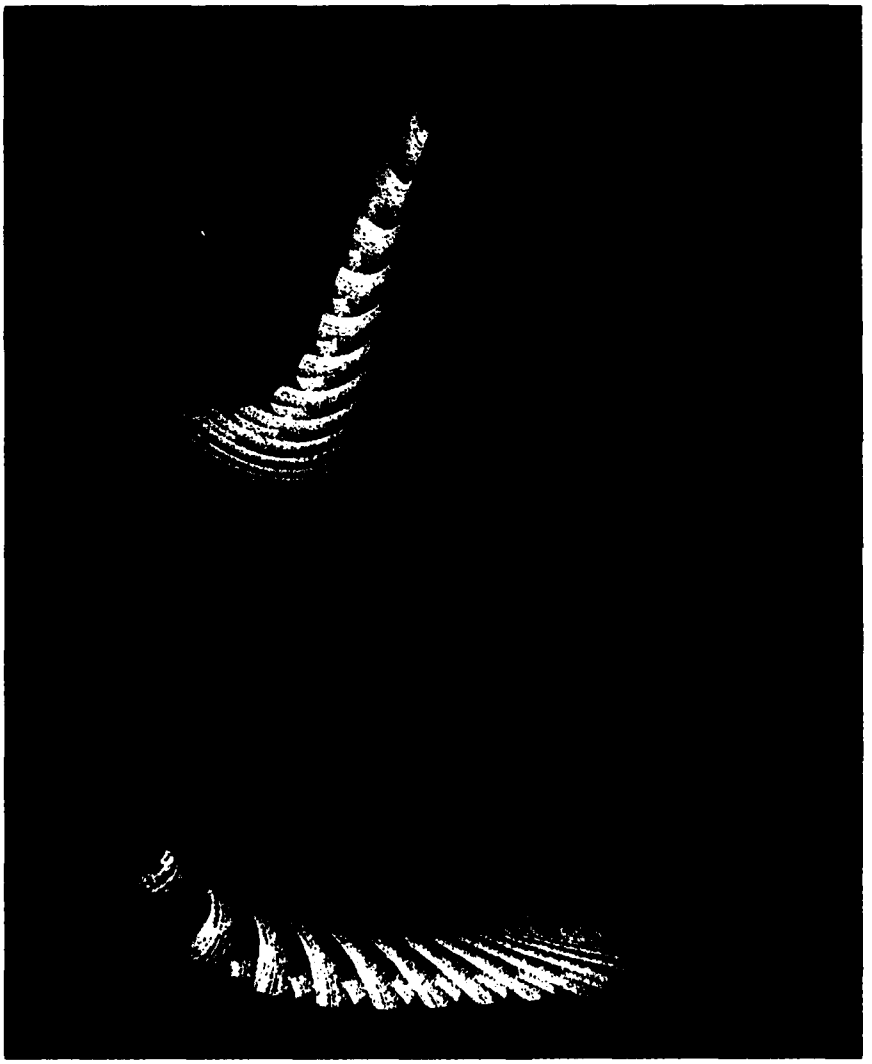

The ACRO Attractor
Computer Graphics, *Second Place*
Paul A. Bernhardt
Plasma Physics Division

Discrete strange attractor (top) and surface-of-section (bottom) for the autonomous chaotic relaxation oscillator (ACRO) is shown for an aperiodic mode. The ACRO is a simple analog to a number of physical processes including the dripping faucet, magnetospheric substorms, firing of neurons in the nervous system, and interaction of high-power radio waves in the ionsophere.

ACOUSTICS

113 **Transducer Calibration in Multipath Environments**
Phillip L. Ainsleigh

115 **Piezoelectric Composites for Transducer Applications**
Kurt M. Rittenmyer

118 **A Pictorial Analysis of Vibrating Shell Physics**
Earl G. Williams

Transducer Calibration in Multipath Environments

P.L. Ainsleigh
Underwater Sound Reference Detachment

Problem Context: The ability to accurately calibrate underwater electro-acoustic transducers in controlled temperature and pressure environments (i.e., pressurized vessels that simulate ocean environments) is vital for the reliability of naval operations. As the Navy continues to develop lower frequency, high-power transducers, however, calibration accuracy in these confined regions is degraded because reflections from boundaries, or echoes, corrupt the measured data before the desired information can be acquired.

The usual method for characterizing a transducer's transfer function or beam pattern is to measure the steady-state response when the transducer is excited by a stepped sinusoid at discrete frequencies across the desired range of frequencies, or at a prescribed frequency for the desired set of directions. Currently, the steady-state amplitude and phase are measured directly during the portion of the transducer's response signal occurring after the transient response dies out but before the arrival of echoes at the hydrophone. Clearly, if the transient response does not die out before the echoes arrive, then accurate measurements cannot be made by using this technique.

Transient Modeling: Previous research partially resolved this issue by using signal modeling techniques in which a weighted sum of exponential functions models the transient response data collected before the arrival of echoes [1]. By modeling the transient data, estimates are obtained for the signal arrival time and the frequency, amplitude, and phase parameters characterizing each of the exponential signal components. Estimates for the desired steady-state response parameters then equal the amplitude and phase estimated for the undamped exponential component whose frequency equals the excitation frequency.

As still lower frequency resonant transducers are excited at the resonant frequency, however, the estimation process becomes inherently problematic. Because the excitation frequency is at or near the transducer resonance, the transient signal contains resonant and steady-state signal components whose frequencies are very closely spaced, making it difficult for an estimation algorithm to separate the signal characteristics attributable to the different components. With enough resonant cycles of data, the estimation algorithm can distinguish these components based on differences in their decay properties. In the present case, however, because of the low frequencies (and hence the long wavelengths) involved, very few resonant cycles are available prior to the arrival of echoes. Consequently, a lower limit develops for the resonant frequency of transducers that can be calibrated in a facility of given size. Below this threshold, the estimation accuracy deteriorates rapidly as the number of available cycles decreases.

Multipath Modeling: To increase the amount of the useful data from which the model parameters are estimated, a multipath modeling technique was devised to simultaneously estimate the parameters in the direct and the reflected signals. This model contains multiple arrivals of exponential signals, which correspond to the arrivals of the acoustic signal at the hydrophone via the various propagation paths available between the projector and hydrophone (Figs. 1 and 2). The algorithm estimates the arrival times for the direct and each of the reflected signals. It also estimates the frequencies, amplitudes, and phases for the exponential components in each of the arriving signals. Since the first signal arrival in the multipath model corresponds to the direct signal, the parameters of interest are the amplitude and phase of the steady-state signal component with the earliest arrival time.

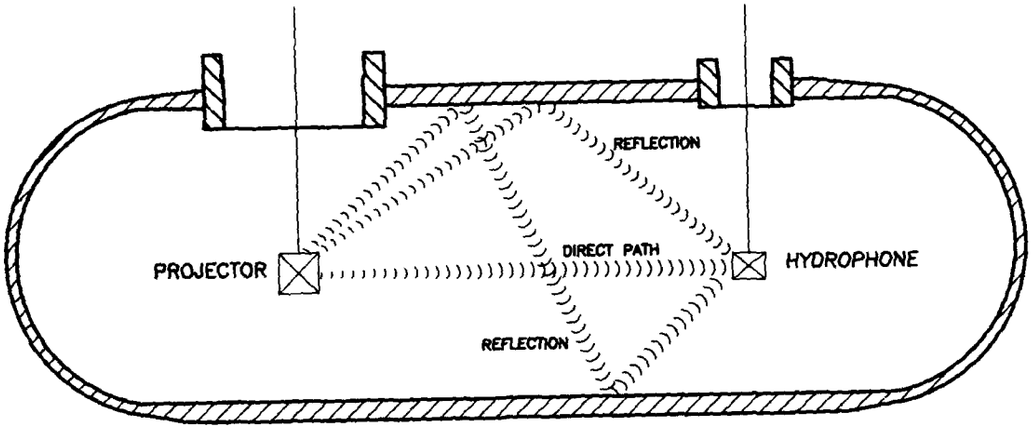

Fig. 1 — Example measurement vessel showing the direct sound propagation path and two likely propagation paths for echoes

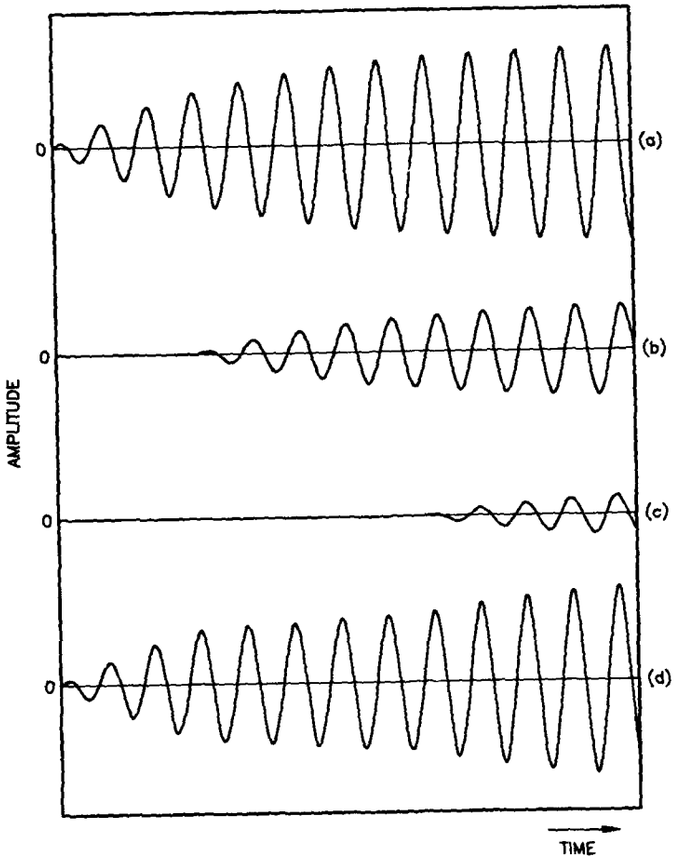

Fig. 2 — Hypothetical response signal showing (a) direct signal, (b) the first echo to reach the hydrophone, (c) the second echo to reach the hydrophone, and (d) the composite response signal containing the sum of the direct and the reflected signals

A key feature of this multipath modeling technique is the ability to simulate frequency sensitive attenuation in the different acoustic propagation channels. In other words, while the signal frequencies usually remain constant from one signal arrival to another, the amplitude proportionalities tend to change with each signal arrival. Although the technical literature contains a number of strategies for modeling multipath signals composed of delayed scaled replicas of the direct signal, no previous algorithm was found for the scenario in which the amplitude relationships vary from one signal arrival to another.

Conclusions: We performed tests in which the transfer function for a low frequency flexural disc transducer was (1) estimated by using the multipath technique in an enclosed tank, and (2) measured by using current methods in a large lake where steady state is reached before the onset of echoes. Close agreement between the two curves demonstrates that the multipath modeling technique extends the low frequency limit on the resonance of transducers that can be calibrated in vessels simulating ocean conditions. Future work will include investigating the use of the multipath technique for modeling more complex devices that cannot be represented by lumped element circuit analogs.

Acknowledgment: This work is the result of a collaboration between the author at NRL/USRD and J.D. George of Signalmetrics, Inc.

[Sponsored by ONT]

Reference

1. J.D. George, R.R. Muise, and J. Abel, "Simultaneous Estimation of Time-of-Arrival, Damping, Frequency, and Amplitude for Signals Described by Rational Function Laplace Transforms," *IEEE Trans. Signal Processing*, submitted for publication; and P.L. Ainsleigh and J.D. George, "Variable Projection Methods with Applications to Sums of Exponentials in White Noise," NRL Memorandum Report 6643, Dec. 1990 ■

Piezoelectric Composites for Transducer Applications

K.M. Rittenmyer
Underwater Sound Reference Detachment

New piezoelectric materials that combine the advantageous mechanical properties of polymers and piezoelectric ceramic materials in various geometries are useful for a number of acoustic applications. These include large-area hydrophones, actuators, and "smart" structures that combine materials and electronic feedback to produce materials that can alter their properties under a particular environmental influence, such as temperature, pressure, or motion. Composite materials can be optimized with respect to certain properties important to the application [1]. They are particularly useful for large area, low-frequency hydrophones because of their flexibility and capability of being manufactured in large sheets.

Unfortunately, the elastic properties of the softer polymer tend to exhibit a strong relaxational character, particularly in the region where the material becomes glasslike. This has been a major objection to their application in submarine transducers, where a 40°C temperature range is encountered. Because of its viscoelastic nature, a soft, flexible polymer becomes rigid at lower temperatures, thus changing the characteristics of any transducer in which it is used. A first step in addressing this problem is to characterize the important properties as functions of temperature. Questions that need to be answered include the following:

- What techniques can be used to determine the elastic, dielectric, and piezoelectric properties of piezoelectric, viscoelastic polymers?
- How can values of these parameters be obtained over the ranges of frequency and temperature encountered in the ocean?
- What are the limitations of these materials with respect to transduction parameters,

such as voltage sensitivity, resonant frequencies, and flatness of response?

- Can the properties and their temperature dependence be described simply?

Resonance Measurements: The elastic, dielectric, and piezoelectric properties specific to several modes of vibration can be determined by electrically driving a piezoelectric sample near frequencies where the sample will vibrate in resonance. Different shapes of samples relate to different elastic and piezolectric constants. By measuring the properties at different temperatures, the relaxational behavior of the material can be studied. At low temperature, the vibrational modes are slightly damped, and conventional calculations of mode parameters are possible. At higher temperatures, the material becomes rubbery, and the mechanical damping peaks at the transition temperature. New calculation techniques were applied in this temperature region to estimate the property coefficients and the dielectric, mechanical, and electromechanical losses.

Time-temperature Superposition: The resonance technique provides information only near the resonance frequency. To extend resonance measurements to lower frequencies, time-temperature superposition can be applied. Two relationships are commonly used to describe the relationship between frequency and temperature and are derived from the theory of viscoelectric solids, including the Williams-Landau-Ferry equation

$$\log a_T(T) = ln\left(\frac{\tau}{\tau_0}\right) = \frac{-c_1(T - T_0)}{c_2 + T - T_0}, \quad (1)$$

where c_1 and c_2 are constants characteristic to a particular material, and E^* is a constant related to the energy of activation for the thermally activated process. The other common equation is a modified form of the Arrhenius equation

$$\log a(T) = \left(\frac{E^*}{K}\right)\left(\frac{1}{T} - \frac{1}{T_0}\right), \quad (2)$$

which is equivalent to Eq. (1) for temperatures far away from the glass transition region. This latter equation was found to fit both dielectric and elastic data and can be used to extend measurements over several decades of frequency. Figures 3 and 4 show the dielectric data, and Fig. 5 shows the elastic data.

Direct Optical Measurements: Laser Doppler vibrometry (LDV) can be used to directly measure the strain induced in the sample as a function of electric field. LDV determines the velocity of a moving surface from which the strain is calculated by measuring the Doppler shift of coherent laser light reflected from the surface. The piezoelectric constants are calculated from the ratio of strain to field. Measurements can be made over extended ranges of temperature and frequency, but some complications occur. Flexural waves are introduced by boundaries that are not completely free because these materials are flexible compared with ceramics. Also, unlike conventional ceramics, body resonances of the particular geometries are highly damped and, therefore, influence the response of the material over wide ranges of frequency. Dielectric relaxations occur at low frequency because of the heterogeneous structure of the material. LDV was used to analyze and separate various effects from the pure piezoelectrically induced strain. Their presence indicates that these effects must be considered when designing transducers with flexible composite materials.

[Sponsored by ONR]

Reference

1. R.E. Newnham, L.J. Bowen, K.A. Klicker, and L.E. Cross, "*Composite Piezoelectric* Transducers," *Mater. Eng.* **2**, 93-106 (1980).

■

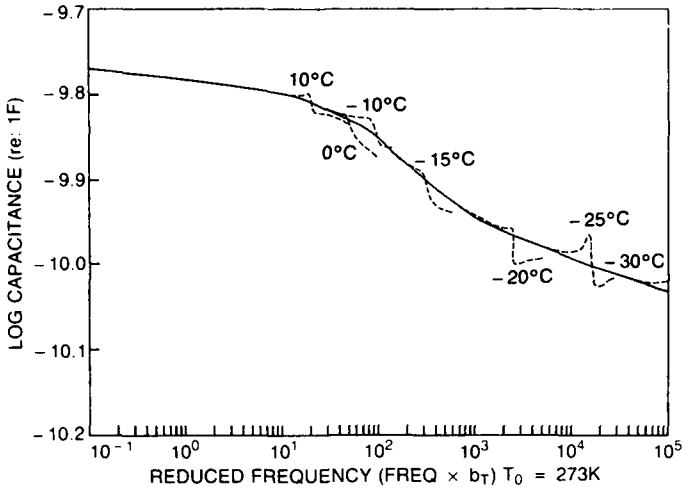

Fig. 3 — Real part of capacitance as extended by the Arrhenius form of the time–temperature superposition principle with E^*/k = 7400 (Eq. 2)

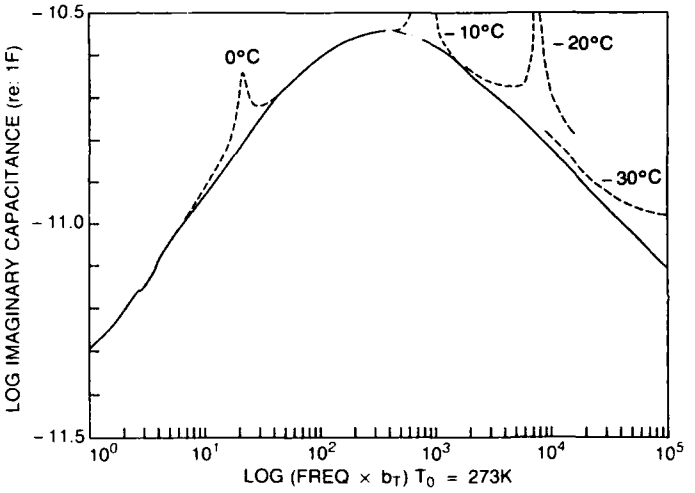

Fig. 4 — Imaginary part of capacitance as extended by using time–temperature superposition via the Arrhenius equation with E^*/k = 7400 (Eq. 2)

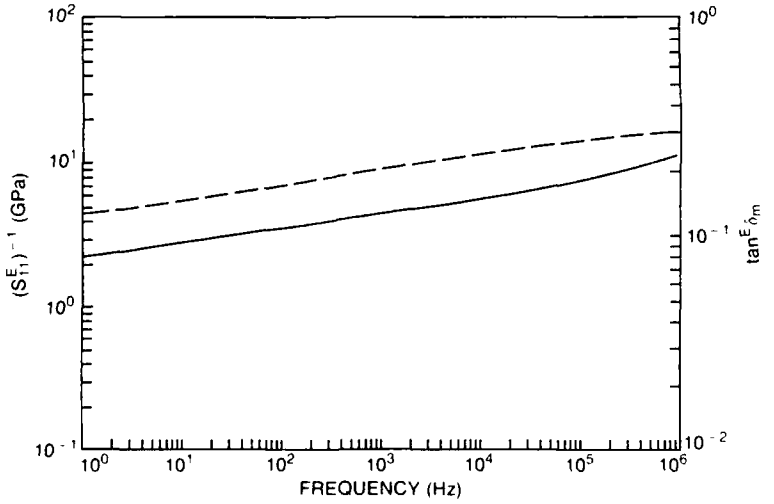

Fig. 5 — Young's modulus of piezoelectric composite material as extended by using time–temperature superposition (E^*/k = 9420)

A Pictorial Analysis of Vibrating Shell Physics

E.G. Williams
Acoustics Division

The quieting of submarines is a subject of major interest to the U.S. Navy. To uncover basic mechanisms of vibration that lead to radiation from submarine hulls, it is important to have a thorough understanding of simple shell structures. The simplest of all is a cylindrical shell with spherical-like endcaps driven into vibration by a point force inside. Although simple in structure, this vibrator is rich in basic physics, as we will see. To study this simple structure, the Physical Acoustics Branch at NRL has several advanced research large pool facilities. Robotic scanners measure the pressure fields generated from the vibrator over cylindrical or conformal surfaces positioned very close to the shell. By using a technique developed by the author [1] (nearfield acoustical holography), these data are used to predict the complete pressure and vector velocity fields from the surface of the shell to the farfield. Unique to this technique is its ability to provide an experimental dispersion analysis (free waves of propagation) of the shell. The graphics that follow provide a journey through the process and analysis steps of this technique and point out the interesting and important physics along the way.

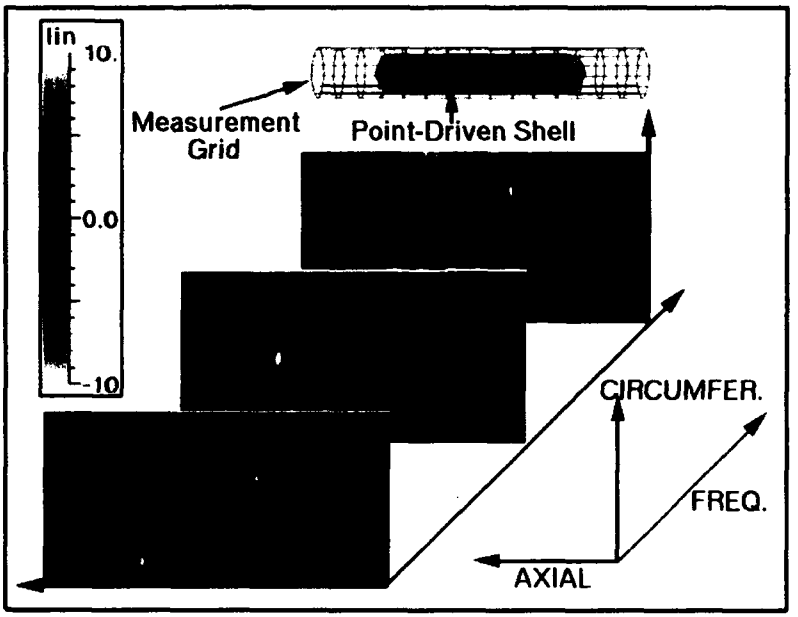

Graphic 1 — At the top is a typical shell, impulsively point-driven and enclosed by a wire grid that represents the measurement contour (typically 128 axial by 64 circumferential points) of pressure followed by the robotic scanner. This measurement provides a cube of data, with axes as indicated. Three two-dimensional (2D) cuts along the frequency axis (selected from one thousand 2D displays, a 3D cube of data) show the pressure fields unwrapped from around the cylinder and laid flat. The color bar shows the linear color-amplitude relationship. One can see the spatially oscillating (modelike) nature of the pressure fields, as well as the dramatic change in character as one moves away from the ends. Each color picture (mosaic) consists of 128 by 64 pixels each representing a measurement location.

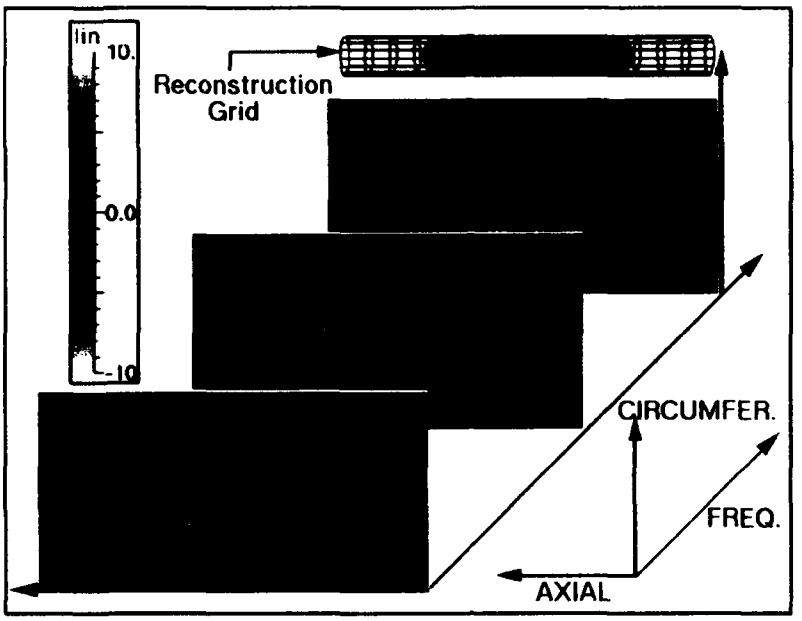

Graphic 2 — The data in Graphic 1 is processed by using nearfield acoustical holography to provide the normal velocity on the wire grid (128 by 64 points) coincident with the shell surface as shown. Clearly the spatial variation of the velocity field is much more rapid than the pressure field in Graphic 1. The regions (in the fluid) to the left and right of the shell have very low velocity levels.

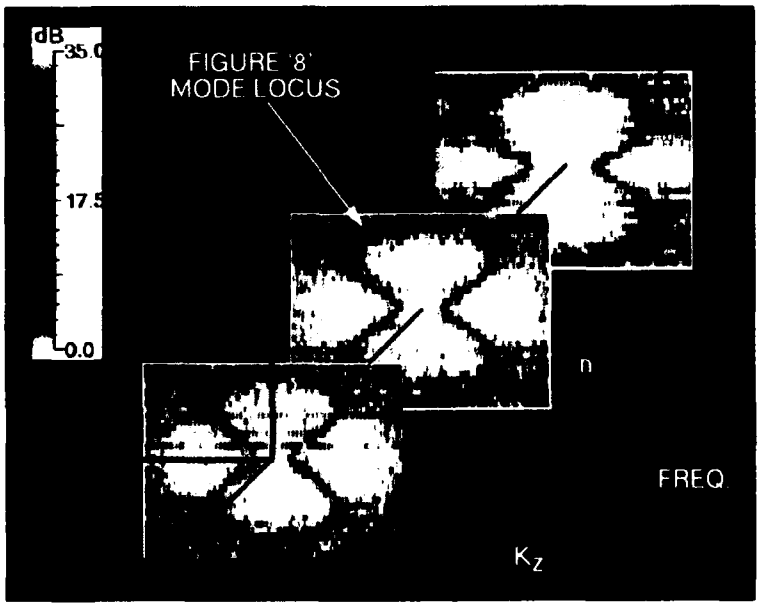

Graphic 3 — The results of a 2D Fourier transform of the mosaics shown in Graphics 1 and 2 (dB scale) are displayed. Thus the spatial data along the axial and circumferential directions become spatial frequencies k_z and n respectively. A great deal more of the physics becomes apparent. Nature's love of symmetry produces figure "8" patterns (surrounded by noise). These figure "8's" show the loci of modes that are excited at a single frequency and indicate how rich the modal content is. The spatial variation shown in Graphic 1 corresponds to a low (spatial) frequency mode near the origin of the figure "8" and Graphic 2 to a high circumferential frequency mode near the n-axis intercepts.

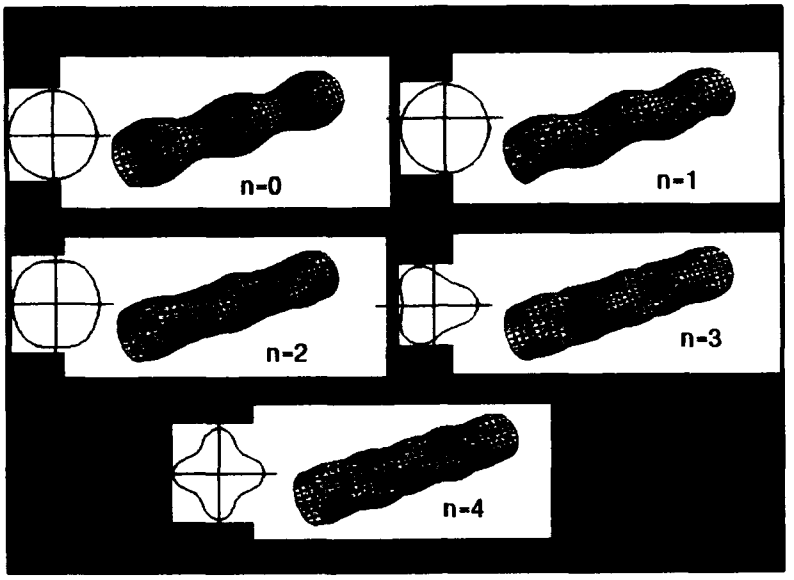

Graphic 4 — We see typical mode shapes represented by the figure "8." We show modes with five axial half-wavelengths for five different circumferential harmonics. In this case $k_z = \pm 5\pi/L$, where L is the length of the cylinder. The inserts to the left show the cross-sectional displacement. (Note: the displacements are grossly exaggerated for display purposes.)

Graphic 5 — Here we see the result after rotation of the 3D data box in Graphic 3 about the k_z axis. Dispersion curves result (shown in red). They indicate several different kinds of waves traveling on the shell at different group speeds (given by the slope of the different curves) as a function of circumferential order n. This representation is probably the richest of all for display of physical phenomena. Comparisons with theory have identified these waves as shear, bending, longitudinal, and acoustic.

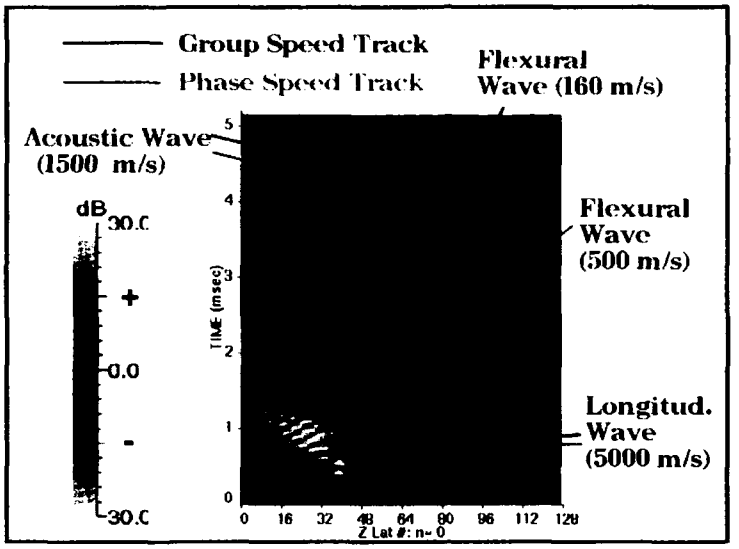

Graphic 6 — The inverse Fourier transform of the first mosaic in Graphic 5 ($n = 0$) of both the vertical (frequency) and horizontal (k_z) axes yielding time and axial position, respectively, are shown. Because the force driving the shell was an impulse in time (located at z lattice number 38), this display shows the tracks of the magnitude and phase of this impulse as it travels down the shell, reflecting off the ends. With the phase information (red vs green), one can measure both the phase and group speeds of waves (the speed is the inverse of the slope). Several important phenomena appear here. The phase and group velocities differ for the flexural wave track as they should for a dispersive wave, but they do not differ for the acoustic wave (nondispersive) launched at the ends of the shell. Weak traces of a fast longitudinal wave can be seen. Important is the excitation of acoustic waves resulting from the reflection of flexural and longitudinal waves off the ends of the shell. This kind of display adds information not seen in any of the figures above—the cause and effect relationships between the different wave types.

[Sponsored by ONR]

Reference

1. E.G. Williams, B.H. Houston, and J.A. Bucaro, "Experimental Investigation of the Wave Propagation on a Point-driven, Submerged Capped Cylinder using K-space Analysis," *J. Acoustic. Soc. Am.* **87**, 513-522 (1990). ■

Growth of Si_3N_4 Whiskers on the Surface of a Heat-Treated Polymer-Derived SiC Fiber

Scientific Data/Visualization (B&W), *Second Place*

Barry A. Bender

Growth of Si_3N_4 Whiskers on the Surface of a Heat-Treated Polymer-Derived SiC Fiber
Scientific Data/Visualization (B&W), *Second Place*
Barry A. Bender
Materials Science and Technology Division

A scanning electron micrograph of a polymer-derived SiC fiber that has been heat treated in nitrogen at 1300°C. During the heat treatment, Si_3N_4 whiskers form and grow on the SiC fiber.

CHEMICAL/BIOCHEMICAL RESEARCH

125 **Chemical Reaction Rates from First Principles**
Maribel R. Soto

127 **Fiber-optic-based Biosensor**
George P. Anderson, Lisa C. Shriver-Lake, Robert A. Ogert, Joel P. Golden, and Frances S. Ligler

130 **High Temperature Phthalonitrile Resins for Structural Applications**
Teddy M. Keller

132 **Atomistic Processes in Surface Mechanics and Adhesion**
Richard J. Colton, Donald W. Brenner, Judith A. Harrison, and Nancy A. Burnham

135 **Buckminsterfullerene: Building Blocks for New Materials**
Mark M. Ross, John H. Callahan, Steven W. McElvany, Mark R. Pederson, Larry L. Boyer, and Warren E. Pickett

Chemical Reaction Rates from First Principles

M. Soto
Laboratory for Computational Physics and Fluid Dynamics

To develop future propellants and explosives, it is fundamental to understand the detailed sequence of chemical reactions that take place during combustion. However, many of the elementary chemical reactions relevant to combustion are difficult to monitor experimentally because they involve species that are transient and short-lived. For this reason, theoretical predictions of reaction rates play a key role in determining the reaction mechanism of a combustion process. The types of theoretical calculations that are done to predict reaction rates encompass a very broad range. For some calculations, the kinetic rate parameters are obtained by fitting limited experimental data within the framework of a theoretical model. In other theoretical calculations, the kinetic rate parameters are obtained by starting with chemical information about the atoms and solving the quantum mechanical equations of motion. These are so-called calculations from first principles.

The Navy is particularly interested in understanding the decomposition of nitramines (nitrogen-containing hydrocarbon compounds), which are used as solid propellants. One of the reactions that has been identified as an elementary step in nitramine decomposition in general is the following:

$$H + HNO \rightarrow H_2 + NO.$$

Two important questions about this reaction remain unanswered: what is the rate of this reaction and how does the rate of the reaction change with temperature? The answer to these questions relies heavily on the temperature-dependent rate constant. This parameter is a direct measure of the rate of the reaction. Experimental studies have ascertained that the rate constant is high, i.e., that the reaction is fast, but the results disagree markedly on the value of the rate constant. Furthermore, because the experiments have been done over small temperature ranges, they have been inconclusive about the effect of the temperature on the rate of the reaction. This lack of understanding and the persistent discrepancy in the experimental determinations of the rate constant are factors that make a theoretical study of this reaction necessary. We have used ab initio quantum chemical methods and transition state theory methods to calculate the temperature-dependent rate constant for this reaction. Our approach is strictly from first principles, i.e., there are no experimental parameters used throughout the calculation.

Potential Energy Profile: The basic premise of how a reaction proceeds is that the reactants exist in some medium where they collide, form some intermediate complex, and become products. The energy needed to form the intermediate complex, called the activation energy or barrier, is one of the factors that determines the rate of this process. In our reaction, the reactants are $H + HNO$, the products are $H_2 + NO$, and the intermediate is a nonlinear complex of $HHNO$. We used configuration interaction and multireference configuration interaction methods [1] to determine the activation energy and other potential energy changes of this reaction. Figure 1 shows the potential energy profile for this reaction. Here the activation energy (the difference in potential energy between the reactants and the intermediate) is very small, or negligible. More specifically, it is < 1 kcal/mol. By proceeding to products, the energy of the complex is lowered dramatically, by 54 kcal/mol. Our theoretical calculations of the energy changes coincide very well with the experimental findings.

Rate Constant: To calculate the rate constant over a wide range of temperatures, we used variational transition state theory methods [2], which are especially well-suited for reactions with negligible barriers. Figure 2 shows our results for the logarithm of the rate constant plotted against

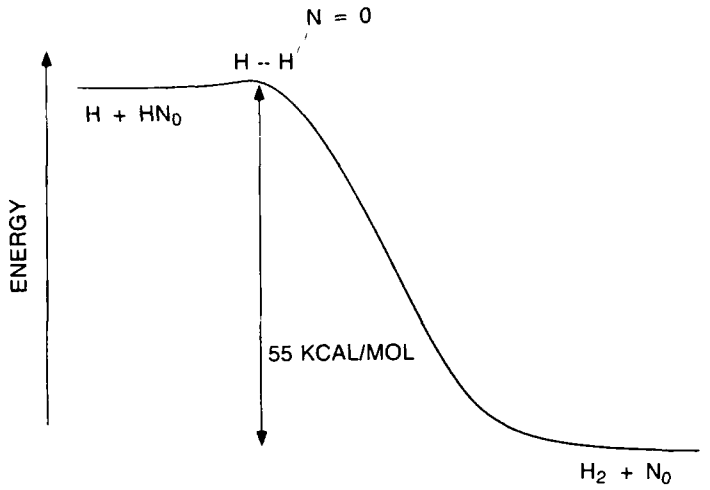

Fig. 1 — The potential energy profile of *H + HNO → H_2 + NO*

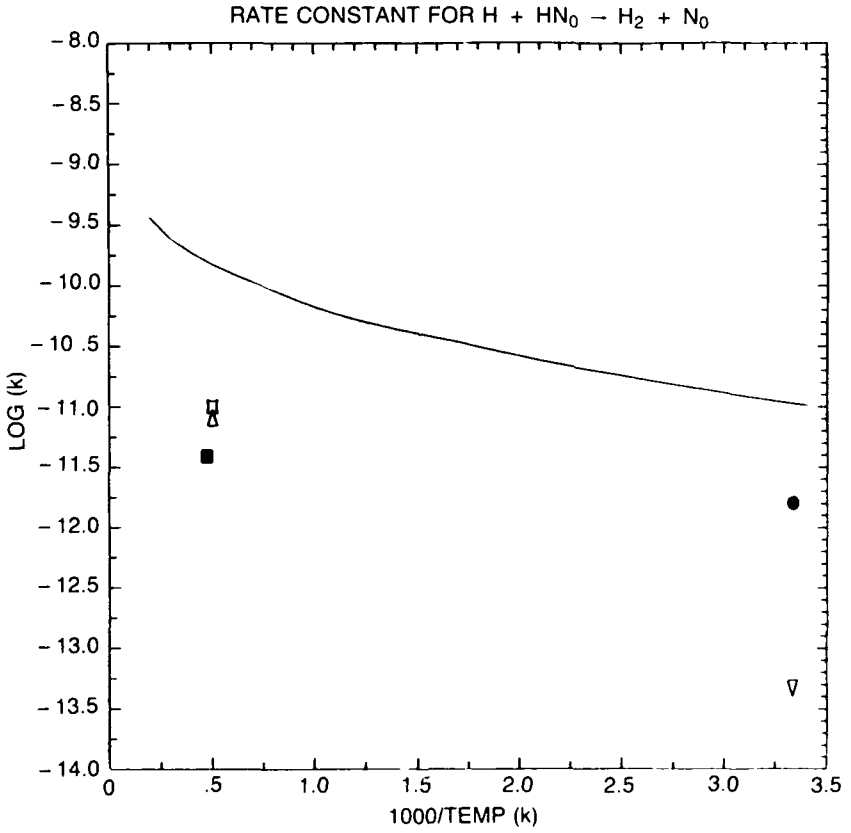

Fig. 2 — Plot demonstrating the temperature dependence of the rate constant. The curve is the result of our theoretical study; the other symbols represent different experimental results.

the reciprocal of the temperature. This is the typical format in which we analyze the temperature dependence of the rate constant. This graph also shows the experimental values. As mentioned previously, there is a large disparity in these values despite the fact that the experiments and data analysis were very similar.

Overall, our theoretical rate constants are higher than the highest experimental values by an order of magnitude. This discrepancy could arise from a deficiency in the theoretical model or from inaccurate input to the model from our electronic structure calculations. We have examined carefully both of these factors. First, the theoretical model has been successfully used before [2] to predict rates for reactions without potential energy barriers similar to reaction 1. Second, the input to the model agrees closely with comparable experimental results. Based on this, we conclude that the high temperature rate constants obtained experimentally are too low by an order of magnitude.

More recent experiments done on the reverse reaction, $H_2 + NO \rightarrow H + HNO$, indicate that the high-temperature experimental values are questionable. This recent analysis suggests that the experimental high-temperature rate constants are too low by an order of magnitude. This recent experimental work provides further confirmation that our theoretical findings are correct.

[Sponsored by ONR]

References

1. W.J. Hehre, L. Radom, P. v.R. Schleyer, and J.A. Pople, *Ab Initio Molecular Orbital Theory* (John Wiley & Sons, Inc., New York, 1985), p. 37.

2. D.G. Truhlar, A.D. Isaacson, and B.C. Garrett in *Theory of Chemical Reaction Dynamics*, Vol. IV, M. Baer, ed. (Chemical Rubber, Boca Raton, 1985), Ch. 2.

Fiber-optic-based Biosensor

G.P. Anderson, L.C. Shriver-Lake, R.A. Ogert, J.P. Golden, and F.S. Ligler
Center for Bio/Molecular Science and Engineering

Recently, our military forces came under the direct threat of biological warfare. To help counter that threat, NRL is developing a fiber-optic biosensor that permits the rapid detection and identification of biological agents while keeping our personnel safe at remote locations. A fiber-optic biosensor is a detection system that exploits the sensitivity and selectivity of biomolecules, such as antibodies or deoxyribonucleic acid (DNA) binding proteins, for analyte recognition and incorporates them into an opto-electronic device for signal transduction. In addition to the detection of biological warfare agents, the biosensor can be used to identify explosives, pathogens, and toxic materials.

Biosensor Design: The laboratory version of our fiber-optic biosensor (Fig. 3) has many novel features. One innovation, depicted in Fig. 4, is the positioning of the chopper between the focusing lens and the fiber. This modulates the signal coming back from the fiber probe, thus allowing a lock-in amplifier to exclude noise from the excitation light scattered by the optical components. A laser light source was selected for its stability and narrow excitation bandwidth. The rhodamine-based fluorescent labels used with this sensor are excited by the 514 nm laser line and emit in the 600 $\pm$ 50 nm range where there is little intrinsic fluorescence in most clinical and environmental samples.

The optical fiber is the most critical component of the biosensor. For convenience, fibers of 1 m are normally used; however, lengths of up to 20 m have been tested. The distal or "business" end of the fiber, which is immersed into the sample, receives intensive preparation. The cladding (5 to 10 cm) is stripped from the distal end to access the fiber core. Additionally, this core

Fig. 3 — NRL's fiber-optic biosensor

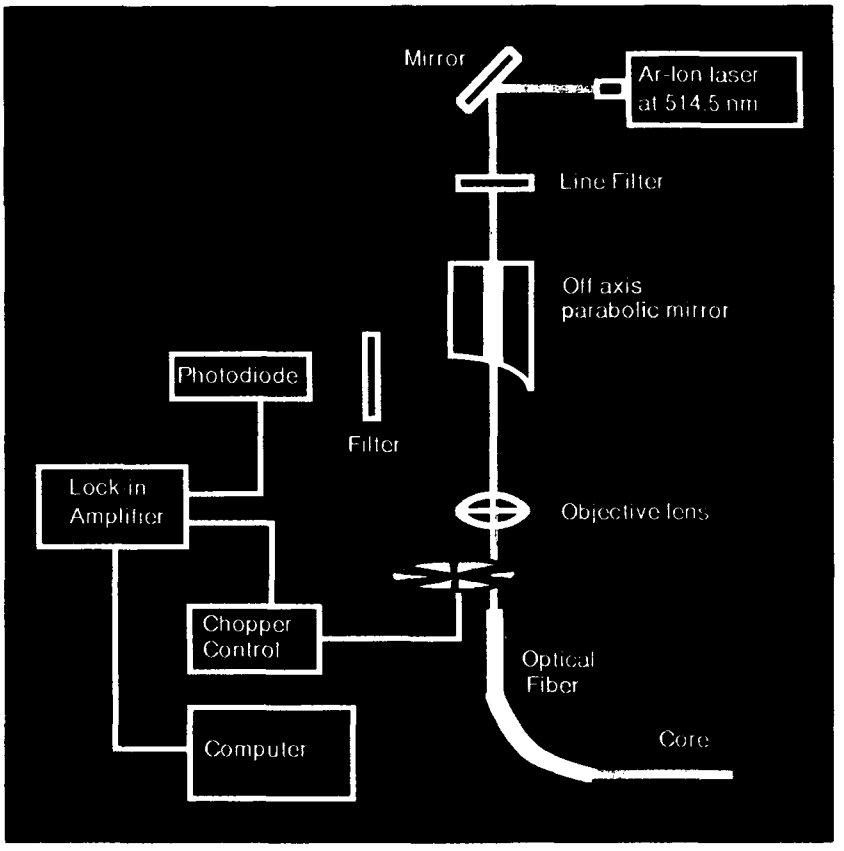

Fig. 4 — The biosensor

section is tapered by slowly dipping into hydrofluoric acid. Tapering was found to greatly improve sensitivity. Presumably, tapering allows the signal to propagate closer to the center of the fiber in lower order modes, thereby avoiding the loss of returning fluorescent light at the interface between the solution and the cladding [1].

Chemistry: In a procedure developed at NRL, the binding proteins are immobilized onto the core [2]. First, the fiber is cleaned and coated with a thiol-terminal silane. This thiol group is reacted with a heterobifunctional crosslinker, whose other reactive group covalently attaches the antibodies or DNA binding proteins through terminal amino groups. This yields fibers with a high density (2 ng/mm^2) of functional molecules that retain activity at room temperature for almost two years.

Assays: The capacity to discriminate between bound fluorescent compounds and those free in solution is fundamental to all the following assays. To achieve this goal, the fiber is configured to measure signals generated in the evanescent wave region (Fig. 5). The evanescent wave extends approximately 100 nm beyond the fiber core into the surrounding aqueous medium. Fluorescent molecules that are bound by antibodies in this region are excited; a portion of the fluorescent light that they emit reenters the fiber. Excitation light does not reach the fluorophores in the bulk solution and, thus, they generate no fluorescence. Therefore, no physical separation procedure (i.e., washing or filtering) is required.

Many types of immunoassays are being developed for use with fiber-optic-based biosensor. To demonstrate the biosensor's ability to detect biological warfare threats, affinity-purified polyclonal antibodies that bind botulinum toxin are immobilized on the fiber. After the anchored antibody binds toxin, it is placed in a solution containing fluorescently labeled antitoxin antibodies. When these antibodies bind to the toxin on the fiber, they immediately generate a signal. Figure 6 shows the signal produced by 50 ng/ml of toxin, however as little as 5 ng/ml can be detected.

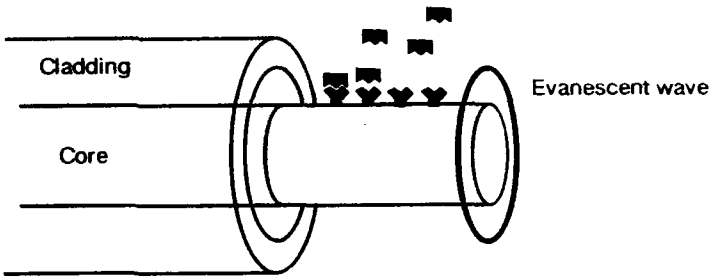

Fig. 5 — Evanescent wave sensing by using a fiber-optic probe

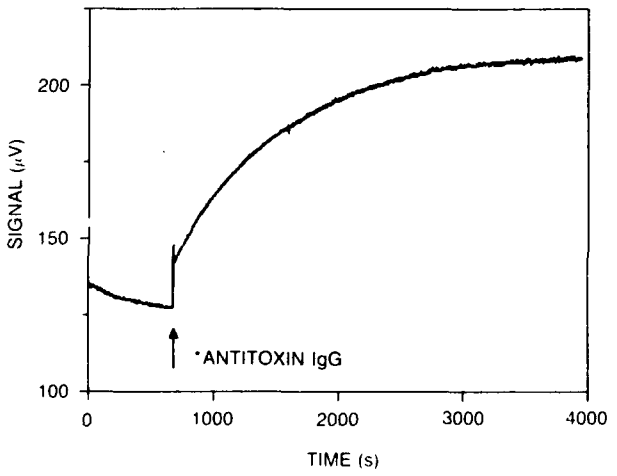

Fig. 6 — Affinity purified antibotulinum toxin A IgG was immobilized on the distal section of a tapered optical fiber. This portion was first incubated with 50 ng/ml botulinum toxin A. At the arrow, the fiber was placed in 5 μg/ml fluorescently labelled polylonal antitoxin IgG. The immediate rise is indicative of bulk fluorescence, while the slower rise is due to specific binding of antibody.

Other immunoassays include those specific for small molecules, bacteria, and DNA. An interesting example of a small molecule assay is the use of antibodies that bind trinitrotoluene (TNT). By incorporating these antibodies, the biosensor can be used to detect explosives. To illustrate the detection of pathogenic bacteria, antisalmonella antibodies are immobilized and the probe exposed to a preparation of nonspecifically stained cells. The cells specifically bound to the fiber by the antibody generate a signal. To achieve the ultimate sensitivity, DNA-binding proteins are immobilized on the fiber. This probe, used in conjunction with the ability of the polymerase chain reaction (PCR) technology to amplify a single DNA molecule a million-fold, offers the potential for rapid identification of a single pathogenic organism.

Conclusion: Operation Desert Storm graphically illustrated the need for an effective system to detect biological warfare agents. The NRL fiber-optic biosensor progressed from a design concept to a deployable model during the course of the conflict. Since then, the prototype of a truly portable sensor has been developed and is now being tested.

Acknowledgments: The DNA binding assay was envisioned by J.R. Campbell, Cdr., U.S.N., S.E. Walz, Cdr., U.S.N., and M.E. Young, Lt., U.S.N., who are pursuing its development.

[Sponsored by ONT and USMC]

References

1. R. Thompson and C. Villaruel, "Waveguide-binding Sensor for Use with Assays," U.S. Patent Application #07/6610895 (Allowed 5/20/91).

2. F.S. Ligler, J. Calvert, J. Georger, L. Shriver-Lake, S. Bhatia, "A Method for Attaching Functional Proteins to Silica Surfaces," U.S. Patent Application #07/297,088 (Allowed 5/91). ■

High Temperature Phthalonitrile Resins for Structural Applications

T.M. Keller
Chemistry Division

High temperature composite materials that are easily processed and exhibit high thermal and oxidative stability are in increasing demand for advanced aerospace and marine applications. The search for high temperature matrix materials that could bridge the gap between currently used high temperature polymers and metals/ceramics is extremely important. When considering strength-to-weight ratios, polymeric organic materials are being sought due to the low density, ease of processibility, and enhanced mechanical properties of the corresponding polymeric composites relative to metals/ceramics.

The key to synthesizing high temperature organic-based polymers is to incorporate highly stable molecular units, such as aromatic and/or heterocyclic rings, within the molecular "backbone" structure. Unfortunately, polymeric materials composed entirely of these units tend to be inherently insoluble and intractable. Thus, flexible linkages must be introduced into the polymeric system at a sacrifice in the thermal stability to enhance the processibility. The real problem has been to devise synthetic methods for linking these groups through flexible units with sufficient versatility and freedom from side reactions while retaining excellent thermal and oxidative properties.

To meet the future need for advanced composites for high temperature applications, phthalonitrile-based polymers with exceptional thermal, oxidative, and mechanical properties have been under development at NRL. These resins are showing superior properties to current state-of-the-art (SOA) high temperature thermosetting polymers.

Synthesis and Polymerization: Phthalonitrile polymers (Fig. 7) prepared from polymerization of 4,4'-bis(3,4-dicyanophenoxy) biphenyl *1A* or 2,2-bis[4-(3,4-dicyanophenoxy)

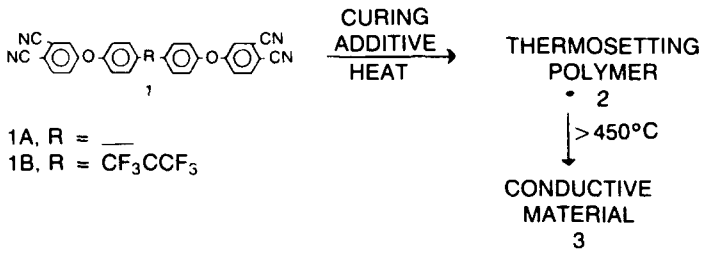

Fig. 7 — Synthesis and pyrolysis of phthalonitrile polymers

phenyl]hexafluoropropane *1B* show excellent thermal and oxidative stability at temperatures approaching 372°C (700°F) [1]. The phthalonitrile monomers are readily converted to highly crosslinked thermosetting polymers in the presence of thermally stable organic amines, phenols, or strong acids. Polymerization occurs by an addition reaction through the terminal phthalonitrile units to afford void-free polymeric materials. The properties of the polymer are controlled as a function of the amount of curing additive used and the curing temperature, more than 200°C.

Processibility: These thermosetting polymers are easily processed in a controlled manner into shaped components or films. After the addition of the curing additive, the reaction mixture is rapidly converted from a crystalline into an amorphous phase. At this stage, the curing temperature can be lowered to a point above the glass transition temperature T_g of the prepolymer. The polymerization reaction can be performed in one step by heating the melt of the curing mixture above T_g until gelation occurs. When postcured at 375°C, the resulting polymers do not show any evidence of glass/rubber transition upon thermal analysis up to 375°C. Alternatively, low molecular weight prepolymers, which can be stored indefinitely under ambient conditions, can be formed by quenching the reaction before gelation occurs. The amorphous prepolymers are soluble in common solvents, such as methylene chloride, chloroform, and dipolar aprotic solvents. Because of the solubility properties and indefinite stability at ambient temperatures, the prepolymers formed from these monomers are potential candidates for the preparation of stable prepregs and their application as laminates for advanced fiber-reinforced composites.

Thermal Stability: The thermal and oxidative stabilities of these phthalonitrile-based polymers have been assessed under isothermal and dynamic conditions. Isothermal measurements in an air flow at 100 cc/min indicate that these polymers can be expected to perform well for relatively long exposures at moderate temperatures between 300° and 375°C (572° and 675°F). The thermal and oxidative properties were found to be enhanced as the polymers were postcured at elevated temperatures. Catastrophic failure in air occurred consistently between 525° and 600°C (980° and 1110°F).

Mechanical Properties: The pthalonitrile-based polymers exhibit excellent mechanical properties. Compared with other SOA thermosetting polymers, these phthalonitrile polymers display superior tensile strength values and retain these values when aged at 315°C (600°F) for extended periods in an oxidizing environment (see Table 1). The phthalonitrile polymers have also been found to exhibit fracture toughness values similar to those of unmodified epoxy resins.

Electrical Conductivity: The excellent thermal stability displayed by the phthalonitrile polymers contributed to further pyrolytic studies [2]. These studies were performed on the resin prepared by polymerization of 4,4'-bis (3, 4-dicyanophenoxy)biphenyl *1A*. The electrical

Table 1 — Effect of Cure Conditions on the Room Temperature Tensile Strength of Phthalonitrile Polymer *1A*

(°C)	Cure/Postcure* Conditions (Hrs)	Atmosphere	Tensile Strength at Break (MPa)
315	24	air	94 + 17
350	12	argon	94 + 21
375	12	argon	80 + 7
315	100	air	72 + 5

*All materials were initially cured at 240°C for 6 h and at 280°C for 16 h. Tabulated conditions are successive thermal and oxidative treatments.

behavior can be systematically changed from an insulator to a semiconductor and made to approach metallic regions by controlling the thermal processing temperature. For pyrolytic temperatures up to 500°C, the conductive nature changes from an insulator and approaches the semiconductive region. At 900°C, the conductivity of *3* (Fig. 7) approaches the metallic regions. Although some shrinkage and a weight loss of 28% at 900°C occurred, the pyrolytic material retained its structural integrity with minimum formation of microvoids.

Summary: The phthalonitrile polymers are potential high temperature materials for structural composite applications. The synthesis is short and potentially low cost. The resin is easily processed into void-free components. The polymers exhibit high thermal and oxidative stability, low flammability, high char yields, good mechanical properties, and can be made to exhibit electrical conductivity at elevated temperatures. Prepolymer formation is readily achievable in a controlled manner. The payoff could be especially high in space and military applications, where the low weight and corrosion resistance of plastics are important. The phthalonitrile technology has been licensed by Cardolite Corporation of Newark, New Jersey.

[Sponsored by ONR]

References

1. T.M. Keller, "Phthalonitrile Matrix Resins and Composites," *International Encyclopedia of Composites*, Vol. 4, 111 (VCH Publishers, New York, 1991).

2. T.M. Keller, "High Performance Electrically Conductive Polymers," *Chemtech* **18**, 635 (1988). ■

Atomistic Processes in Surface Mechanics and Adhesion

R.J. Colton, D.W. Brenner,
J.A. Harrison, and N.A. Burnham
Chemistry Division

Mechanics is a branch of physical science that deals with the effects of energy and forces on solid, liquid, or gaseous materials. Materials scientists and chemists often try to make new materials that have specific mechanical properties, e.g., hardness or strength. In this context, there is growing evidence for a revolution in materials centered around nanometer-scale structures. For example, some nanocrystalline materials and multilayered films show enhanced properties when compared to the bulk properties of individual constituents. The properties of these

nanostructured materials are governed by the large number of interfaces within the material. Because the interfacial regions between two crystallites or thin films vary in width from a monolayer to tens of nanometers, their chemical, structural, and mechanical properties cannot be measured directly (nor deduced from bulk properties)—until now.

Recent progress in experimental and computational methods are providing new insight into the atomic-scale processes at surfaces and interfaces. Experimentally, the revolution in nanometer-scale science and technology is being fueled by the success of scanning tunneling microscopy (STM) and related techniques such as atomic force microscopy (AFM), which are capable of imaging solid surfaces (in air and in real time) with atomic resolution. Computationally, the advent of fast computers with extended memory permits the modeling of larger arrays of atoms that approach the size of the experimental measurement.

At NRL, we pioneered the use of AFM to study the mechanical properties of materials [1-3]. Our instrument can image surface topography with atomic resolution, measure surface forces and adhesion with nanonewton sensitivity, and determine modulus and hardness of films as thin as a monolayer.

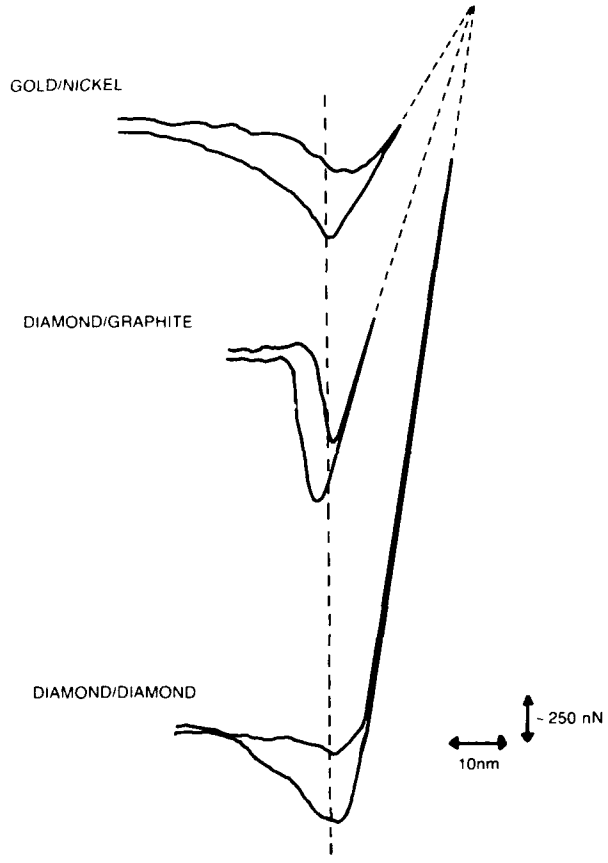

Fig. 8 — Measurement of surface force vs distance curves for different tip/sample materials. The vertical axis is cantilever deflection, or force in nanonewtons. The horizontal axis is sample displacement in nanometers. The dashed line depicts the approximate point of tip/sample contact.

Force Microscopy: A force microscope consists of a sensor that responds to a force and a detector that measures the sensor's response. The sensor—a cantilever beam with an effective spring constant k—moves in response to the forces acting on its tip. The detector measures the cantilever's position, which can be converted to force by using Hooke's Law, $F = -kz$, where z is the cantilever displacement. (The displacement can be measured by tunneling, capacitive, or optical instruments.) If the cantilever beam is either microfabricated or a fine wire, then small spring constants (0.1 to 100 N/m) are possible. For 0.01-nm displacement sensitivity, 10^{-8} — 10^{-12} N forces are measurable. These forces are comparable to the forces associated with chemical bonding, e.g., $\sim 10^{-7}$ N for an ionic bond and $\sim 10^{-11}$ N for a hydrogen bond.

Both attractive and repulsive forces can be measured, as well as the adhesive force needed to separate the cantilever tip and sample surface once in contact. Figure 8 illustrates the force measurement among several different materials. The curves depict the net forces acting between the tip and sample as a function of separation. The cycle starts (at the left) with the sample far away and the cantilever in its rest position. As the separation decreases, the cantilever bends towards the sample responding to an attractive force. In Fig. 8, the attractive force between the diamond tip and graphite is much higher than the other two systems due predominately to the higher surface

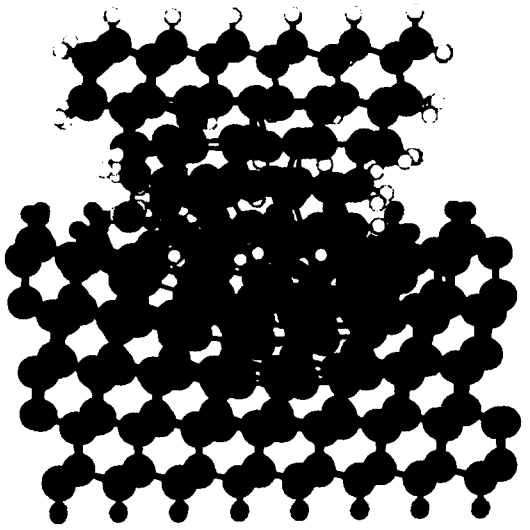

Fig. 9 — Molecular dynamics simulation of a diamond tip indenting a diamond (111) surface

energy of the graphite. Continuing to push the sample in the direction of the cantilever after contact causes the cantilever to back up through its original rest position until a predetermined load is applied. The slope of the curve in this repulsive force region is a function of the nanomechanical properties and local geometry of the tip and sample. The steeper the slope, the higher the modulus of the material as seen for the diamond data. When the load is removed, the curve shows hysteresis due in part to adhesion between the tip and sample.

Molecular Dynamics: Molecular dynamics simulations are used to visualize the atomistic processes. For example, Fig. 9 illustrates the interaction of a diamond tip indenting a diamond surface [4]. Both elastic and plastic interactions have been observed depending on the maximum value of the applied load and the surface chemistry of the materials. Furthermore, the deformation mechanism can be studied by examining the distribution of tensile and compressive forces during indentation. Calculated force curves are used to interpret the experimental data and to predict the modulus and hardness of materials.

Until now, the contact deformation mechanism has been traditionally modeled by using continuum mechanics, which does not necessarily provide an accurate description of atomic-scale processes. In fact, our understanding of many materials processes—such as friction, wear, fracture, and adhesion—are based on phenomenological principles. Therefore, measuring these properties with atomic resolution will help to develop a fundamental understanding of these processes.

[Sponsored by ONR]

References

1. N.A. Burnham and R.J. Colton, "Measuring the Nanomechanical Properties and Surface Forces of Materials Using an Atomic Force Microscope," *J. Vac. Sci. Technol.* **A7**, 2906 (1989).
2. N.A. Burnham, D.D. Dominguez, R.L. Mowery, and R.J. Colton, "Probing the Surface Forces of Monolayer Films with an Atomic Force Microscope," *Phys. Rev. Lett.* **64**, 1931 (1990).
3. U. Landman, W.D. Luedtke, N.A. Burnham, and R.J. Colton, "Atomistic Mechanisms and Dynamics of Adhesion, Nanoindentation, and Fracture," *Science* **248**, 454 (1990).
4. J. A. Harrison, C.T. White, R.J. Colton, and D.W. Brenner, "Nanoscale Investigation of Indentation, Adhesion, and Fracture of Diamond (111) Surfaces," *Surf. Sci. Lett.*, in press. ■

Buckminsterfullerene: Building Blocks for New Materials

M.M. Ross, J.H. Callahan,
and S.W. McElvany
Chemistry Division

and

M.R. Pederson, L.L. Boyer,
and W.E. Pickett
Condensed Matter and Radiation Sciences Division

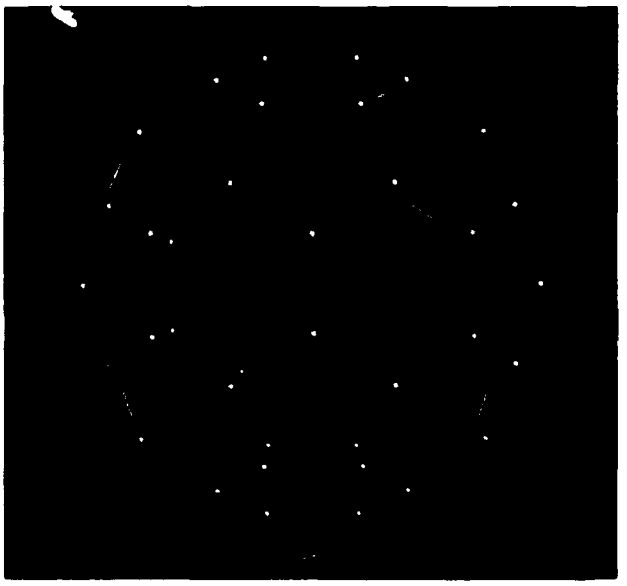

Fig. 10— The buckministerfullerene molecule. Although the atoms are all equivalent, the icosahedral symmetry allows for two different bond lengths. In good agreement with experiment, our calculations predict hexagonal and pentagonal bond lengths of 2.64 and 2.74 Bohr.

Background: Detailed mass spectrometry studies of gas-phase carbon clusters, which in 1985 were performed by groups at Exxon, Bell Labs, Rice University, and NRL, have led directly to a third form of carbon (diamond and graphite being the first two) [1]. The discovery [2] of a simple method by which large quantities of C_{60} (Fig. 10) and other all-carbon molecules (C_n, with n = 60, 70, 76, 78, and 84) can be produced has resulted in an explosion of research activity focused on complete characterization of these new materials. While mass spectrometry played the key role in providing the evidence for the controversial postulation by Kroto and Smalley that the fullerenes were spheroidal species, this method continues to provide new insights into properties of fullerene-based materials. In addition to laboratory studies, computer-based theoretical investigations have played a significant role in understanding several complex questions about this new molecule. We start by discussing two mass-spectrometry-based experimental investigations [3, 4], which constitute a small part of the ongoing cluster chemistry program in the Chemistry Division at NRL, and then turn to several complementary theoretical investigations that have been performed by members of the Complex Systems Theory Branch of the Condensed Matter and Radiation Sciences Division [5-8].

Experimental Work: Many properties of pure fullerenes are now known, and some of these, including ionization potentials, proton affinities, gas-phase stability, and reactivity, were measured by this group. However, the most exciting potential for new materials may be associated with doped fullerenes. There are three types of doped fullerenes: (1) externally doped, such as alkali metal/C_{60} films that exhibit superconductivity, (2) intrinsically doped by substituting a different atom for one or more carbon atoms in the cage, e.g., $C_{60-x}B_x$, and (3) internally doped by inserting an atom or molecule inside of the cage. We are investigating two approaches to formation and characterization of internally-doped, or endohedral complexes of fullerenes.

Fullerene/Rare Gas Atom Collisions: In an investigation of the dissociations of fullerene cations, H. Schwarz in Berlin found that kilovolt collisions of C_{60}^+ with helium in a tandem sector mass spectrometer resulted in formation of not only fullerene fragment ions, resulting from C_2 losses, but also these same fragments with a helium atom attached. Shortly after the report of this unexpected observation, we used our hybrid, three-sector mass spectrometer to provide the first

unambiguous evidence that $C_{60}He^+$ is formed. The novel configuration of this instrument allows measurement of the kinetic energy *and* mass of the unusual product. More importantly, we were able to probe the structure of $C_{60}He^+$ by inducing its dissociation through gas-phase collisions. Many of the resulting fragment ions retained the helium atom, which provided strong evidence for the helium being located inside of the C_{60} cage ($He@C_{60}^+$, according to Smalley's nomenclature). Other fullerenes, C_{70} and C_{84}, behave similarly. This type of reaction is unprecedented in mass spectrometric studies of ion collision phenomena and is illustrative of the unique nature of fullerenes. Recent molecular dynamics simulations of these collisions by R. Mowrey (in the Chemistry Division) have provided further insights, and Fig. 11 shows the $He@C_{60}$ species calculated to result from one He/C_{60} collision trajectory. This work has opened up a new area of endohedral complex formation and characterization by using a variety of cage molecules and hetero-atomic and molecular species.

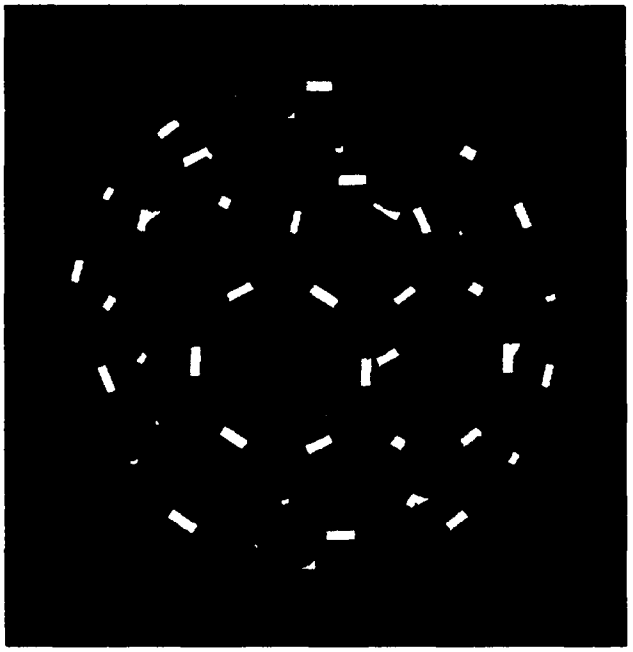

Fig. 11 — The helium/buckminsterfullerene endohedral complex ($He@C_{60}$) formed by a collision of the two species from molecular dynamics calculations (R. Mowrey, Chemistry Division)

Laser Vaporization of Fullerene/Metal Mixtures: The second approach to produce and study internally doped fullerenes follows early work by the Rice group in which laser vaporization of metal (M)-impregnated graphite yielded $M_xC_n^+$ species in the gas phase, which photodissociation studies indicated to be endohedral complexes. Our recent work consists of laser vaporization of samples consisting of graphite, yttrim oxide (Y_2O_3), *and* C_{60} and C_{70}, which were extracted from arc-generated graphitic soot. In a Fourier transform mass spectrometer, this novel addition of the bulk fullerenes allowed production of abundant YC_n^+ (n = 56 to 96) and $Y_2C_n^+$ (n = 68 to 90) species (Fig. 12), which are subsequently characterized by their reactivity. Specifically, the $Y_xC_n^+$ species formed as described above are stable towards oxidation, unlike externally bound adducts formed by gas-phase association. These studies provide convincing evidence that the latter species are externally bound metal/fullerene species, while those formed by laser vaporization are endohedral complexes. In addition, the $Y_x@C_n$ species depend on the laser fluence and time in a way that suggests that these complexes are formed by coalescence reactions induced by laser irradiation, deposited on the surface of the pellet and desorbed in subsequent laser pulses. These results are similar to recent observations by Smalley and coworkers with lanthanum/fullerene complexes and may form the basis for a new synthetic method for doped fullerenes.

Theoretical Investigations: It is an interesting and fortunate coincidence that the breakthrough in snythesis of the large fullerene molecules occurred at a time when several different quantum-mechanical computational methods have matured and the computational resources are readily available. The simultaneity of these three technological advances has provided condensed matter physicists and physical chemists with a rare opportunity to solve a myriad of challenging problems either prior to, or in concert

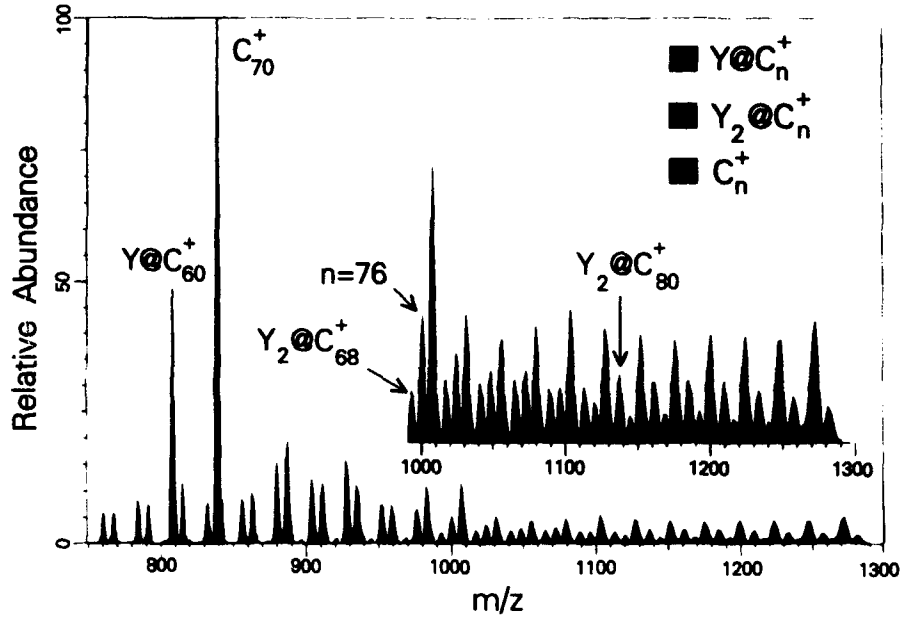

Fig. 12 — Fourier transform mass spectrum resulting from laser vaporization of a mixture of Y_2O_3, graphite and bulk fullerenes (C_{60}/C_{70}), which shows C_n^+, $Y@C_n^+$, and $Y_2@C_n^+$

with, experimental confirmation. We provide an overview of several results obtained by using methods developed in the Complex Systems Theory Branch at NRL within the last five years [5].

Energetic Stability of Fullerenes: One of the most fundamental questions is the observed extreme stability of the fullerene molecule (Fig. 10). To evaluate the energetic stability, we employed the recent generalized-gradient improvements to density functional theory to calculate the cohesive energy of the isolated molecule. We find the fullerene molecule to be only 0.3 eV/atom less stable than diamond [6], which itself is extremely stable. For comparison, a simple carbon molecule is less stable than diamond by approximately 4.4 eV/atom. While energetic stability is a requisite attribute for a molecular building block, the fullerenes will retain their molecular integrity only if they are also relatively unreactive. The observed (theory and experiment) noble-gaslike (closed shell) character of their electronic structure is in accord with a reasonably unreactive system (bond formation with closed shell systems is relatively unlikely). However, the fullerene molecule differs from ideal gas atoms in that the electron affinity is relatively large. Our calculated electron affinity of 2.88 eV is in excellent agreement with the experiment (2.74 eV) and is similar to that of the halogen and oxygen atoms that readily form ionic insulators. Based on this analogy, it is not surprising that fullerene molecules and alkali metals have been observed to form ionically bonded crystals. We now turn to these systems.

Alkali-Doped Fullerene Crystals: Figure 13 shows the unit cell for the K_6C_{60} crystal. While it is useful to visualize a "cage" of twenty-four potassium atoms surrounding each fullerene molecule, the atoms that form nearest-neighbor pairs with the potassium atoms are actually carbon atoms (pictured in green). In accord with experimental observation, our calculations predict the K_6C_{60} crystal is a small, band-gap ionic insulator [7]. The fullerene molecule in the K_6C_{60} crystal exists in an extremely high-charge state, accepting nearly all of the 4s valence electrons from the six K atoms. The arrangement of the potassium atoms on the unit cell faces is unusual in that a classical point charge model predicts the opposite distortion

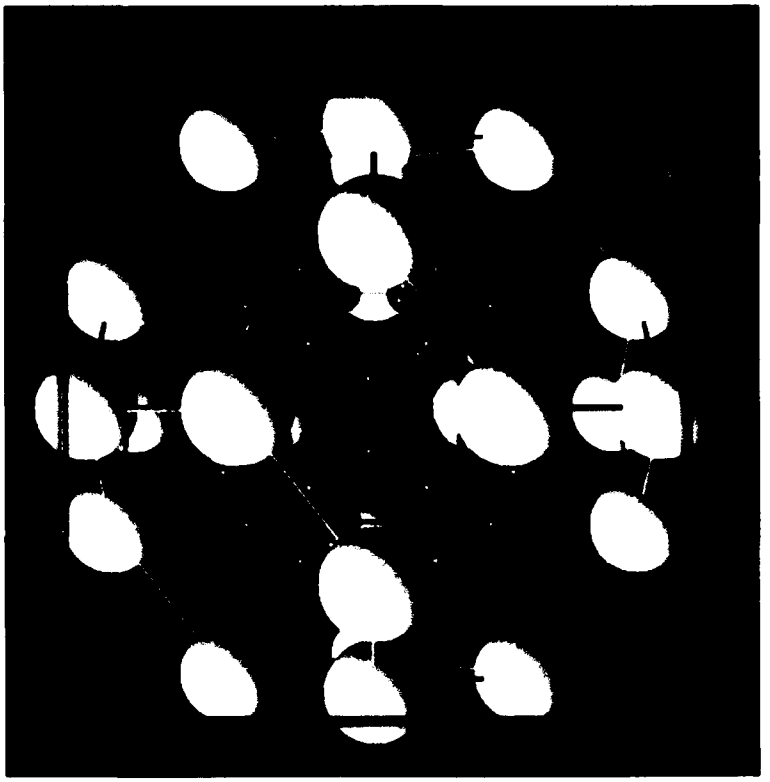

Fig. 13 — The unit cell of the BCC insulating phase [K_6C_{60}] of the alkali-doped fullerene crystals. We have included the central buckyball and the 24 nearest potassium atoms. The next shell of buckyballs reside at the cube corners.

of the potassium rhombus from what is observed experimentally and illustrated in Fig. 13. Our cluster calculations show that the arrangement of the K atoms is in fact governed primarily by short-range repulsions between themselves and their nearest neighbors rather than the long-range Madelung contributions.

In addition to the insulting phases of fullerides, the K_3C_{60} crystal is found to exhibit both metallic and reasonably high temperature (T_c = 19 K) superconducting behavior. Moreover, the Rb-doped analog (Rb_3C_{60}) has a T_c of 33 K. We have verified that the K_3C_{60} electronic structure is indeed that of a metal; Fig. 14 shows its unusual Fermi surface (the surface in momentum space to which the conducting charge carriers are confined). By combining our calculated velocity of the charge carriers on the Fermi surface (about 2×10^7 cm/s) [8] with the experimental value of the superconducting coherence length, we can ascertain that these materials are of the *strong-coupling* type, rather than of a weak-coupling nature. This is part of the information necessary to guide scientists in identifying the mechanism for superconductivity that seems so unusual in view of the deceptively similar potassium-intercalated graphite, which superconducts at only 0.5 K.

Transition-Metal Doped Fullerene Crystals: In analogy to the dibenzene chromium compounds, we have also investigated the possibility of a chromium-doped BCC fullerene crystal of stoichiometry Cr_4C_{60} [6]. In this structure, the chromium atoms would sit between two six-membered carbon rings of neighboring fullerene molecules. Our calculations show that the energy (per chromium atom) required to remove eight chromium atoms from the six-membered carbon rings of a Cr_8C_{60} molecule is similar to the energy required to remove a single chromium atom from a benzene ring. This calculation suggests that interactions between

Fig. 14 — Repeated-zone representation for the second sheet of the Fermi surface of the metallic K_3C_{60} crystal. The two symmetry-equivalent pieces (shown in different colors) are multiply connected along the cartesian axes; although interpenetrating, they never touch.

six-membered carbon rings and transition metal atoms is not strongly dependent on system size. Since our calculations show that the binding energy between two benzene rings increases by two orders of magnitude when a chromium atom is placed between the rings, we expect that the insertion of chromium atoms into a bulk fullerene crystal will also be strongly exothermic.

Summary: The preceding examples illustrate the power of laser/mass spectrometric research in the production and characterization of new doped fullerene assembled materials and show how the interplay between experimental and theoretical investigations have increased with the advent of supercomputers and accurate quantum-mechanical computer codes. Such studies continue to provide sometimes surprising insights into the properties and potential for the third form of carbon. Mass spectrometry, which was crucial in the early gas-phase carbon cluster studies, will continue to play a critical role in this new area of science.

References

1. R.F. Curl and R.E. Smalley, "Fullerenes," *Sci. Am.* **54** (1991).

2. W. Krätschmer, L.D. Lamb, K. Fostiropoulos, and D.R. Huffman, "Solid C_{60}: A New Form of Carbon," *Nature* **347**, 354 (1990).

3. M.M. Ross and J.H. Callahan, "Formation and Characterization of $C_{60}H_e^+$," *J. Phys. Chem.* **95**, 5720 (1991).

4. S.W. McElvany, "Laser Vaporization Production of Endohedral Yttrium/Fullerene Complexes," submitted to *J. Phys. Chem.*

5. M.R. Pederson and K.A. Jackson, "Variational Mesh for Quantum-mechanical Simulations," *Phys. Rev.* **B41**, 7453 (1990); S.C. Erwin, M.R. Pederson, and W.E. Pickett, "First-principles, General-potential Local-orbital Calculations for Bulk Crystals," *Phys. Rev.* **B41**, 10437 (1990).

6. M.R. Pederson, K.A. Jackson, and L.L. Boyer, "Enhanced Stabilization of C_{60} Crystals through Doping," to appear in *Phys. Rev. B.*

7. S.C. Erwin and M.R. Pederson, "Electronic Structure of Crystalline K_6C_{60}," *Phys. Rev. Lett.* 67, 1610 (1991).

8. S.C. Erwin and W.E. Pickett,"Theoretical Fermi-Surface Properties and Superconducting Parameters for K_3C_{60}," *Science* **254**, 842 (1991). ■

Simulation for a Strategic Surveillance System
Scientific Data/Visualization (Color), *Second Place*
Harry M. Heckathorn

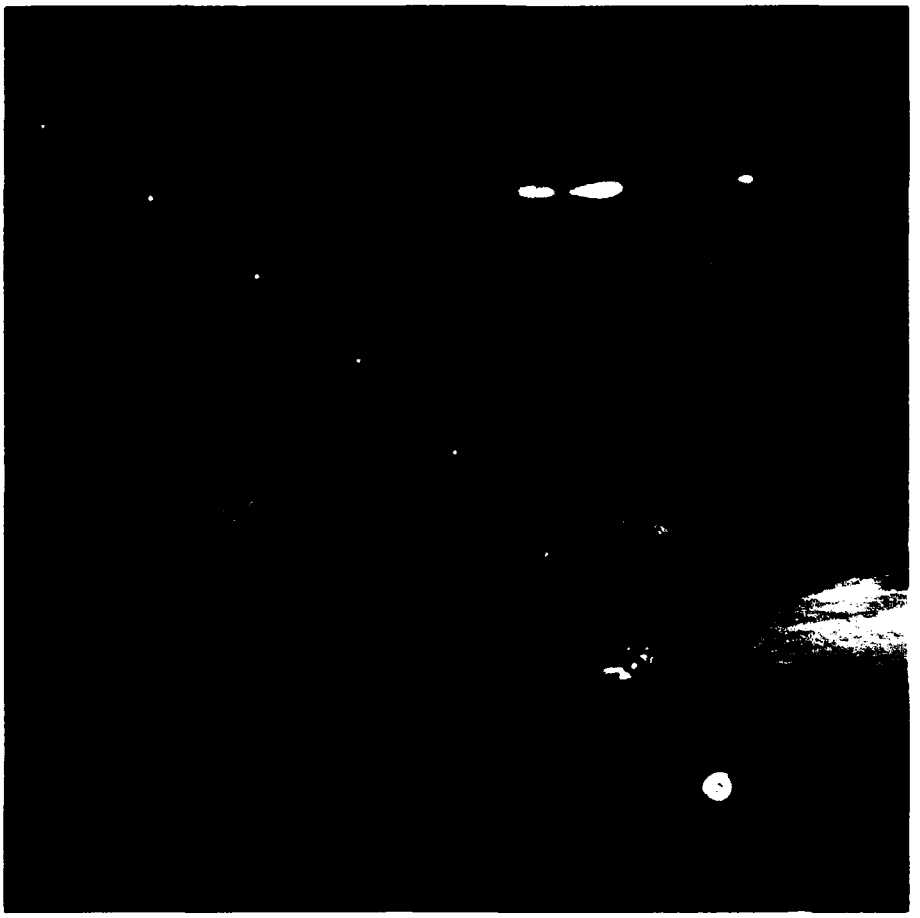

Simulation for a Strategic Surveillance System
Scientific Data/Visualization (Color), *Second Place*
Harry M. Heckathorn
Space Science Division

The panorama is a simulated view of the Earth as seen from an early warning infrared sensor in geosynchronous orbit. The scene includes a ballistic missile during the late launch phase near 100-km altitude. To depict the trajectory of the threat missile system and evolution of the liquid propellant plume, the image is a multiple exposure taken at a constant framing rate. A variety of naturally occurring backgrounds is visible including the ocean, various types of clouds, the atmosphere, aurora, and celestial sources. The field of view covers some 2000 km and is viewed at a wavelength of 2.3 μm.

ELECTRONICS AND ELECTROMAGNETICS

143 **Single Event Upsets in Space**
Arthur B. Campbell

144 **Visualization Tools for Development of Electronic Warfare Techniques**
Tiziano Ricci and Robert Normoyle

147 **Scale Model Analysis Facility**
Stanley A. Moroz and Ernest S. Mak

149 **A Programmable Antiship Infrared Guidance System**
Elmer F. Williams, Robert H. Evans, and Paul L. Alles

151 **Interfaces in Semiconductor Nanostructures**
Daniel G. Gammon, D. Scott Katzer, and Benjamin V. Shanabrook

Single Event Upsets in Space

A.B. Campbell
Condensed Matter and
Radiation Sciences Division

Introduction: The Combined Release and Radiation Effects Satellite (CRRES), launched in July 1990, contains a number of different experiments to look at the radiation environment of space [1]. Among the experiments is the microelectronics package (MEP) space experiment, which is a computer test system that looks at the effects of radiation on integrated circuits. The idea for the experiment and part of the experimental design came from the Radiation Effects Branch of the Condensed Matter and Radiation Sciences Division. The MEP was designed and constructed by NRL's Naval Center for Space Technology. The experiment is the result of a collaborative effort of many scientists and engineers at various government laboratories, private companies, and universities. Phillips Laboratory, formerly the Air Force Geophysics Laboratory, had overall program responsibility for a majority of the experiments on CRRES. NASA was responsible for the satellite and launch. Among the radiation effects being investigated with the MEP, transient changes in digital circuits are some of the least understood phenomena.

Single Event Upset: These transient changes in stored information or program commands called single event upsets (SEUs) can result from single interactions of energetic ions and elements of integrated circuits. SEUs are the result of energy deposited in the semiconductor material by energetic particles that make up the environment of space. These particles include trapped protons in the Van Allen belt surrounding the Earth, protons from solar flares on the Sun, and cosmic ray ions present throughout the universe. Energy can be deposited either by direct ionization or through nuclear reaction products. SEUs can result in corrupted data and erroneous spacecraft computer operation and have been unintentionally observed in many spacecraft.

CCRES MEP: The CRRES orbit is highly elliptical, inclined at 18.2°, with a perigee of 348 km and an apogee of 33,582 km. The CRRES satellite drops to altitudes below and traverses the heart of the proton belts and extends to altitudes near the orbits where geosynchronous communications satellites are located. Depending on the orbital position, the MEP is looking at SEUs either in the proton environment of the belts or out beyond the trapped particle belts where the main radiation source is cosmic rays. This allows one to divide SEUs as to the source of the energetic particles that are the cause of the disturbance leading to a change in logic state. Energetic protons can cause upsets in most devices only by nuclear reactions, since the energy deposition rate for protons is too low. Cosmic ray heavy ions can cause SEUs by direct ionization. There are 40 device types in the MEP that are being tested for SEUs, including random access memories (RAMs), microprocessors, gate arrays, and programmable read-only memories (PROMs). Analyses for this article include 590 orbits or 242 days' worth of data, from 27 July 1990 through 26 March 1991.

Results: Table 1 is a summary of MEP data for eight RAM device types. The total number of SEUs is 13,277 in the 242-day period, for an average of 55 SEUs per day. Variations in the overall SEU rate with device type are dramatic, varying by about three orders of magnitude. We see that the majority of the SEUs are caused by proton events. For these eight device types, only 7.2% of the SEUs are caused above the proton belts, in spite of the fact that the CRRES orbit results in the satellite spending 89% of its time at altitudes above the proton belts.

Summary: The fact that most of the SEUs observed are probably caused by proton reaction products is one of the more surprising new results from the CRRES MEP experiment. Variation in SEU sensitivity among device types is the topic of

Table 1 — Data Summary for Eight RAMs

Device type	Number of bits tested	Proton number of SEUs in proton belts	Cosmic ray number of SEUs at altitude above proton belts	SEUs/Kilobit/Day (overall SEU rate)
93422	4096	2418	173	2.29
92L44	32768	514	61	0.0261
93L422	4096	1819	156	1.82
82S212	8192	957	90	0.385
6116	98304	43	1	0.00185
21L47	40960	375	38	0.0355
71681	98304	74	5	0.00286
4164	655360	6125	428	0.0346

further research looking at SEU models based on ground testing data by using ion accelerators. This data will be used to improve models of SEU in space [2,3].

[Sponsored by SPAWAR]

References

1. M. Gussenhoven, E. Mullen, and R. Sagalyn, "CRRES/SPACERAD Experiment Descriptions," Air Force Geophysics Laboratory Environmental Research Paper No. 906, AFGL-TR-85-0017, Air Force Geophysics Laboratory, Hanscom AFB, MA, 24 Jan. 1985.
2. E. Petersen, P. Shapiro, J. Adams, and E. Burke, "Calculations of Cosmic-Ray Induced Soft Upsets and Scaling in VLSI Devices," *IEEE Trans. Nucl. Sci.* **NS-29**, 2055-2063 (1982).
3. E. Petersen, "Radiation Induced Soft Fails in Space Electrons," *IEEE Trans. Nucl. Sci.* **NS-30**, 1638-1641 (1983). ■

Visualization Tools for Development of Electronic Warfare Techniques

T. Ricci and R. Normoyle*
Tactical Electronic Warfare Division
**QuesTech Inc.*

Antishipping missiles represent a serious threat to U.S. Navy ships. To successfully defend against this threat, effective electronic countermeasures (ECM) must be developed that disrupt a missile's ability to track and strike its intended target. To facilitate and expedite the ECM development process, visualization tools have been developed that permit the scientist to visually analyze large data sets and to recognize conditions and patterns within this data that make a missile seeker susceptible to an ECM technique.

ECM Development: The development of ECM techniques normally requires numerous experiments that are designed to measure a missile seeker's response to ECM excitations. These experiments include open-loop characterizations, closed-loop simulations, and field tests. By using the automated data collection procedures included with the visualization tools, scientists can successfully capture all of the necessary characterization data. These data represent a system's detailed response from which a three-dimensional, highly interactive display of the seeker and antenna responses can be created on a graphics workstation.

The guidance and tracking system of a missile is a function of several independent channels of data from the seeker's radar. Figure 1, which represents just one channel of over three megabytes of characterization data, is a display generated by using collected seeker data. Figure 2 portrays the same seeker with the signal received by the seeker antenna polarized orthogonal to the seeker's normal transmit polarization. From these

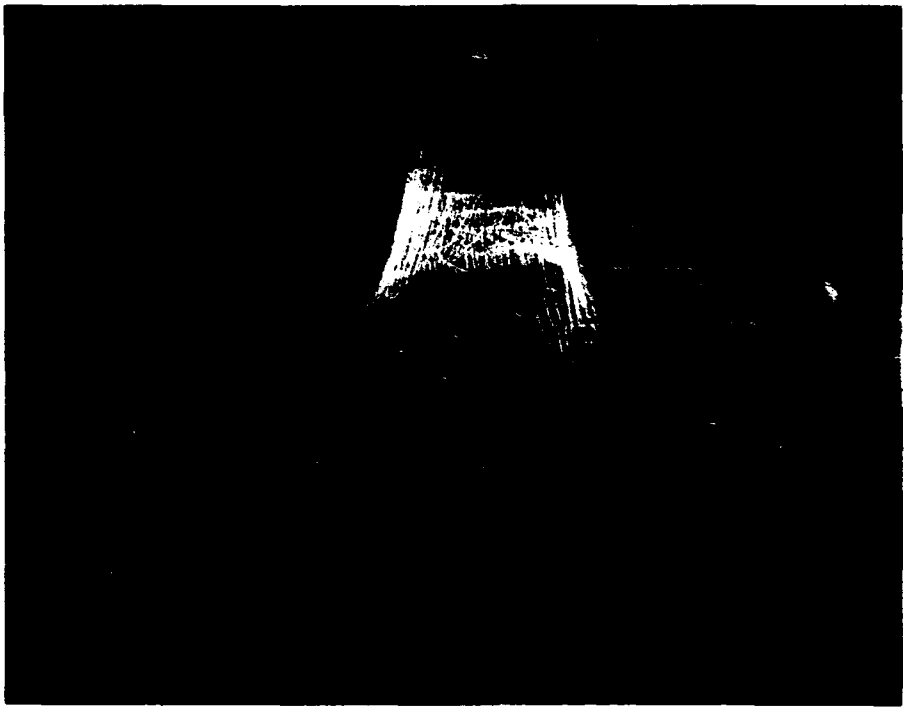

Fig. 1 — Nonpolarized antenna pattern display

Fig. 2 — Orthogonal polarized antenna pattern display

Fig. 3 — Antenna tracking patterns display

two images, it is obvious that by altering the polarization of the returned signal, the seeker's response is radically different. By using the display in conjunction with the antenna tracking patterns display (Fig. 3) (which indicates the path an antenna would travel to obtain a stable tracking point), the scientist can sift through megabytes of system characterization data instantaneously to determine properties within the data that can be exploited to develop effective ECM techniques.

Visualization Advantages: There are several advantages to using these visualization tools. These tools present characterization data to the scientist *visually*, making analysis and comprehension of the underlying phenomena more intuitive. Once the scientist has observed a region of particular interest, these data can be interactively enlarged and manipulated for more detailed analysis.

To determine which is the most effective, the scientist no longer has to rely upon an iterative "trial and error" laboratory method but can quickly establish a starting point from which to try other ECM techniques. In addition, the visual representation allows the scientist to rapidly see the correlation of several independent channels of a seeker's response.

Cost and time savings are realized because the duration of the data collection and simulation processes have been substantially reduced while simultaneously making the data more manageable and understandable. These visualization tools can be used with any generic data set as well as most types of ECM and missile seekers. Additionally, progress is being made to develop an expert system capable of identifying these regions of potential exploitation within the data.

N.J. Chandler of QuesTech Inc. and Andrew Hosmer of NRL continue to provide significant contributions to this research effort.

[Sponsored by ONT] ■

Scale Model Analysis Facility

S.A. Moroz and E.S. Mak
Tactical Electronic Warfare Division

Introduction: Detailed measurement of the radar cross section (RCS) of existing ships is very difficult due to unpredictable factors ranging from ship scheduling to weather and sea state conditions. In the case of new ship designs, it is totally impractical to construct full-sized mock-ups of sufficient quality to perform RCS studies. The Scale Model Analysis Facility (SMAF) has been established at NRL as a low-cost method of measuring and analyzing the RCS of objects through an accurate scaling of the object, the radar system, and the environment. The scaling factor of the model is determined by the source frequencies that can be generated and the desired base frequency. For the SMAF that operates in the submillimeter (SMM) region and is designed to study ships and large ship structures, the achieved scale factors range from 70:1 to 200:1 for a mid-X-band base frequency. Higher ratios allow the measurement of the entire ship with the consequent interaction of the various structural features with reasonable size models of 0.5 to 2 m. Lower scaling ratios permit a more detailed study of individual structures, such as radars or weapon systems. However, SMAF can accommodate rather large targets so that even at 70:1 scaling ratio full ship models can be accommodated.

Facility Features: SMAF has evolved from the development lab where technical implementation and integration issues were resolved to a production facility with continuing improvements in all phases of operation (Fig. 4). These are the main features of the system:

- The radar analog is a homodyne system with an optically pumped, continous wave SMM laser transmitter and a liquid helium cooled, hot electron bolometer receiver. Homodyne detection is accomplished by mixing the received signal beam with the local oscillator, which is phase modulated by a sinusoidally driven piezo translator. This detection scheme, which permits phase and amplitude measurements, has demonstrated a significant improvement of system sensitivity over video detection.
- Three imaging modes are available for studying RCS contributions from various levels of target details (Fig. 5). Localized target imaging is used to measure the RCS contribution of each localized region on the target. In extended target imaging, an extended collecting aperture captures radiations resulting from interactions among individual scatterers. Full target illumination is set up as a compact range for measuring total RCS of the entire target for a specific orientation.

Fig. 4 — Scale model analysis facility

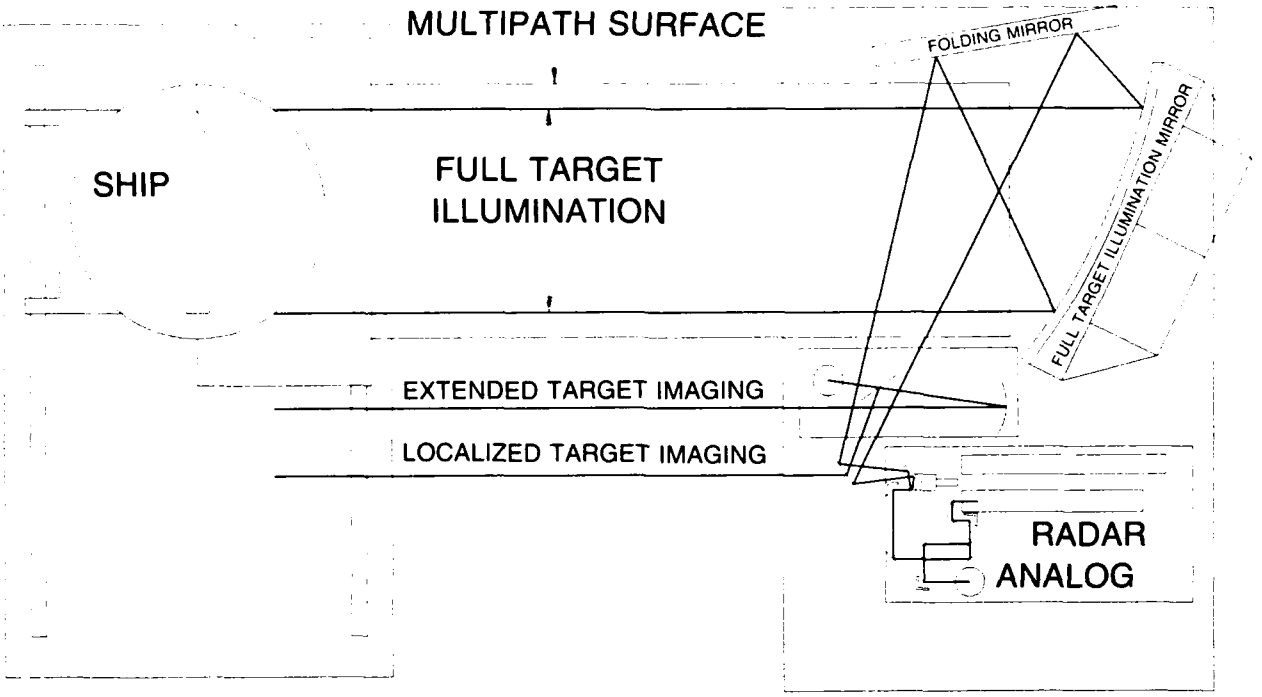

Fig. 5 — SMAF facility layout (plan view) (with multipath surface)

- An SMM sea-water analog has been developed to include measurement of the multipath effect reflecting the complicated interactions between the target and the sea. Isolation of the four paths that make up the separate multipath elements is critical and was a nontrivial problem. A technique that makes use of bistatic optical configuration has been devised so that these four elements can be isolated and measured individually.

- A large, precision, six-degree-of-freedom positioning stage provides several functions in addition to orienting the object. In the localized and extended target imaging modes, where a small phase front spot is fixed in space, the positioner moves the target in a raster pattern from which the far-field RCS can be constructed.

- Wool carpet, which has a good absorption characteristic in the SMM region, is currently used as the radar absorption material (RAM) in the anechoic chamber of the SMAF. RAM of higher quality is available but has been too costly for extensive application. A recent breakthrough in the manufacture of a new SMM analog RAM by the Lowell Research Foundation that is at least 40 dB better than the wool carpet will permit very low RCS analyses.

- A stereo lithography system, a recently added feature of SMAF, is able to grow precision plastic parts directly from CAD drawings. This capability offers a quick way of transforming design ideas to physical forms and is an extremely useful tool for performing "what if" evaluations.

Benefits: Scale model RCS measurements and analyses permit design studies of objects too large or too costly to prototype full scale (for instance, a ship). Now refinements to existing objects, new designs, and designs of notional objects based on the prediction can be modeled and evaluated in the SMAF.

[Sponsored by NAVSEA] ■

A Programmable Antiship Infrared Guidance System

E.F. Williams, R.H. Evans, and P.L. Alles
Tactical Electronic Warfare Division

Accurate and full evaluation of electronic warfare ship defense systems against infrared (IR) missile seekers requires a generic hardware guidance unit. Such a system was developed by NRL. It uses programmable parameters that allow testing of countermeasures providing a defense for the Fleet during a missile attack. The system allows the study of detection, acquisition, and tracking of ship targets in sea clutter. The effects of sensor field-of-view, resolution, sensitivity, scan rate, search area, target characteristics, atmospheric conditions, and data processing algorithms are evaluated for the impact on the detecting, identifying, and tracking ship targets.

System Operation: The IR seeker and data collection system is operated from an NRL EP-3B aircraft and is flown against actual ship targets. The system operator can modify numerous parameters during a mission to examine system performance changes and to optimize the data collection.

A typical scenario starts with the EP-3B carrying the IR guidance unit several miles from a ship target. Once the fly-in is started, the seeker must detect, identify, acquire, and track the target through the run. The seeker searches for targets from slightly in front of the aircraft to the horizon, with an azimuth width of 5° to 30°. During the approach, the target grows from a point source to a large, extended object. On each run, video and signal recorders collect target and sensor data and system configurations for postmission analysis.

The infrared guidance unit uses two independent programmable IR sensors. One sensor is a vertical detector array mounted in a gimbal and scanned horizontally across the target area. This provides excellent sensitivity against point source targets and permits programmable scan rates and scan angles. The second sensor is a wide field-of-view IR imaging camera that permits target and background data collection throughout the run; it also provides the capability to rapidly search a large area. The multiple processor compter continuously collects data from each sensor, implements the detection, identification, acquisition, and tracking algorithms, and changes the sensor's parameters to optimize the target's signal data.

Hardware Configuration: Figure 6 shows the system pod and operator rack, which are

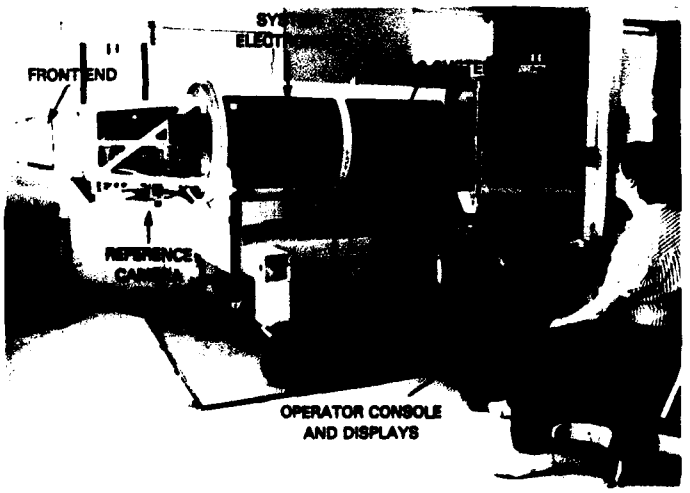

Fig. 6 — Pod and operator rack

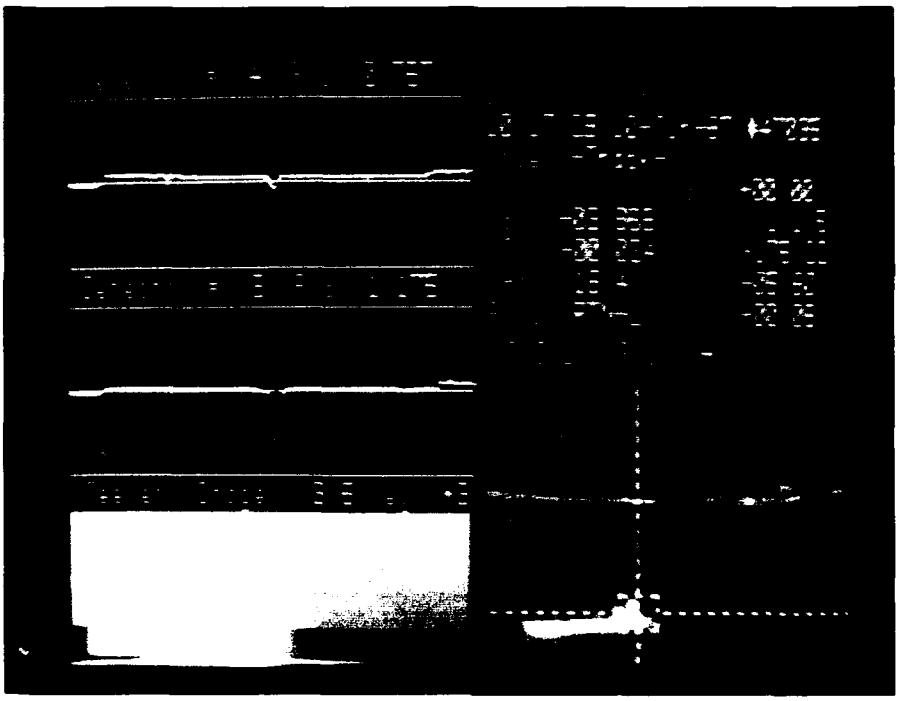

Fig. 7 — Operator display

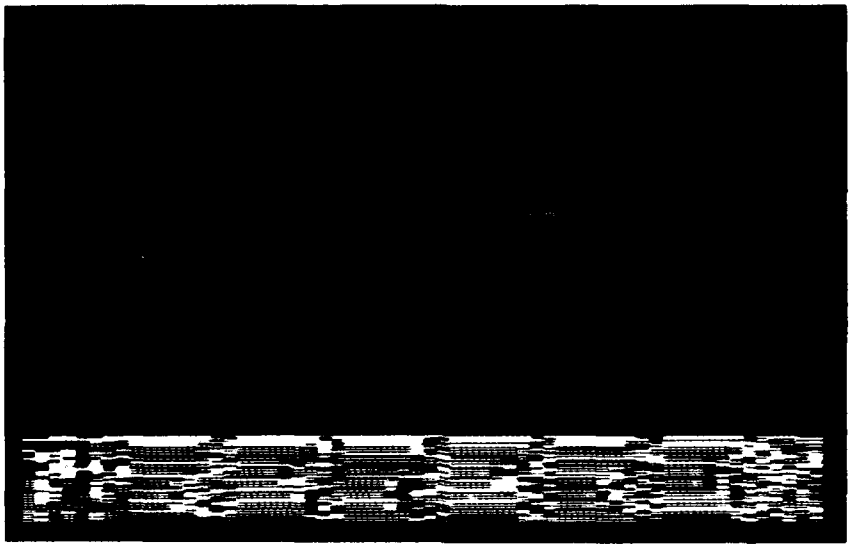

Fig. 8 — IR image with encoded data

normally mounted on the NRL EP-3B aircraft. Located in the pod is the IR seeker line scanner, the IR imaging camera mounted in a separate gimbal, an inertial reference system, the multiple processor computer, a nitrogen gas system for sensor cooling, a video recorder, the pod temperature control system, and the power supplies.

An operator rack is mounted inside the aircraft and is interfaced to the pod equipment by cables in the aircraft wing. Operator displays include images from the camera as well as the data from the line scanner. Figure 7 is a typical display that provides the operator with the scene image, seeker track point, and other system status information. The operator uses a rack-mounted computer to modify the program code, download new algorithms, and communicate operator control commands to the multiple processor computers in the pod.

All data from both sensors are recorded on video tape by the processors. Using a separate data reduction computer system provides the powerful capability to replay mission scenarios in the laboratory. Figure 8 shows an IR camera image as it is stored on video tape. At the bottom of this image are several lines of encoded information containing raw detector data and system operational parameters. This encoded data can be used after the test to examine new algorithms against the actual at-sea conditions.

Combining the data from a slow-scanned, high-sensitivity seeker array with a wide field-of-view IR imager provides the capability for quantitatively evaluating the requirements and techniques associated with the ship target acquisition and tracking problems. This system has been deployed on many ship tracking and decoy evaluation field tests for the U.S. Navy and for other nations. Ongoing modifications to the configuration are being applied to enhance image analysis and understand features of the system.

[Sponsored by NAVAIR] ■

Interfaces in Semiconductor Nanostructures

D.G. Gammon, D.S. Katzer, and B.V. Shanabrook
Electronics Science and Technology Division

Heterostructures composed of different semiconductors provide very versatile building blocks for electronic and optical device engineering. With today's growth technologies (such as molecular beam epitaxy), it is possible to grow structures with elements that have dimensions on the order of a nanometer. For example, it is possible to grow within one semiconductor a layer of a second semiconductor that is only a few atoms thick. The ultimate limits are determined by the structural disorder of the interfaces, and complete control of the structure requires the interface to be perfect on the atomic scale. We are, in fact, very close to achieving this.

GaAs/AlAs Heterostructures: The prototype for the semiconductor-semiconductor heterostructure is GaAs/AlAs grown along the [001] axis. This system consists of alternating layers of anions (As) and the cations (Ga or Al) in the zinc-blende crystallographic structure. Disorder originates in intermixing the Ga and Al atoms, and an interface thus consists of the region over which the structure changes from pure Ga layers to pure Al layers. In the highest quality samples available, the interface thickness is limited to approximately one monolayer (0.28 nm). These samples grown at NRL have allowed us to establish the character of this interfacial roughness with optical spectroscopy [1]. It is found that within this monolayer, there exists *lateral* disorder that consists surprisingly of both large and small scale structure, i.e., monolayer-high islands with large diameters ($>>20$ nm) within which is a large amount of very fine structure ($<<20$ nm). These optical experiments provide confirmation of this fine structure, the existence of which has been very

controversial since the first indication of it was reported three years ago by an AT&T Bell Labs group using a novel electron microscopy technique (chemical lattice imaging) [2].

Optical Characterization: Advances in growth techniques require detailed characterization of the material. Unfortunately, atomic scale structure of buried interfaces is very difficult to probe. Perhaps the most important characterization technique for studying GaAs/AlAs interfaces has been photoluminescence (PL). With PL, a sample is excited with laser light and the resulting luminescence is spectroscopically detected. The PL spectrum is dominated by peaks arising from the recombination of *excitons*. Briefly, an exciton in this system is an electron and hole that are bound together by the Coulomb interaction and exhibit a Bohr diameter (average electron–hole separation) of about 20 nm. The exciting laser light creates energetic electron–hole pairs with the same energy as the laser. The electrons and holes cool down by giving up their kinetic energy to the lattice. These electrons and holes then form excitons with an energy characteristic of the semiconductor structure. The luminescence arises when the electron and hole making up the exciton annihilate and emit light with the characteristic exciton energy. This exciton energy is sensitive to the parameters of the sample structure. This is particularly true if the structure is grown with a thin GaAs layer sandwiched between two AlAs layers. In such a structure, the lowest energy excitons are confined to the GaAs layer because of the larger band gap of AlAs. The GaAs layer then acts as a quantum well for the excitons, and the AlAs layers act as barriers. Because the exciton is confined to a very thin quantum well, its energy is increased. If the layer is made very small, the exciton energy becomes very sensitive to the width of the GaAs layer and to the structure of the two interfaces. Through this sensitivity, the exciton (and therefore, the PL spectrum) provides a useful probe of the interface roughness.

Interface Islands: The most important feature of the exciton is its diameter. The energy of any given exciton is determined by an average of the interfacial structure over the Bohr diameter. Therefore, any interface roughness that has a length scale much smaller than the exciton diameter of 20 nm is averaged over. In this case, the exciton peak remains narrow, and its energy depends on the density of the fine structure. However, if the interface structure includes very large islands, the exciton spectral peak splits into multiplets (Fig. 9). From calculations, the energy separations between the peaks in the multiplets are found to correspond to differences in GaAs layer thicknesses of only a single monolayer.

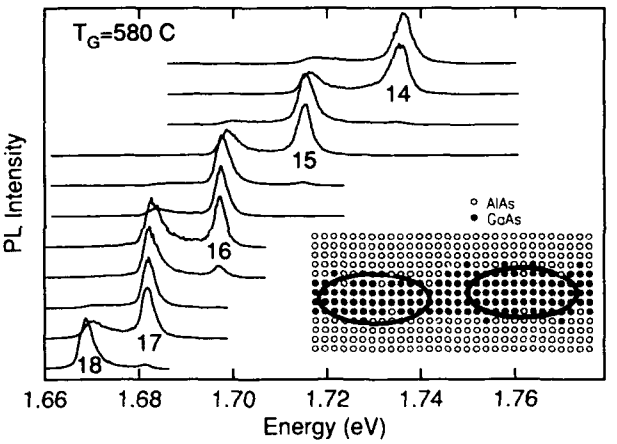

Fig. 9 — Photoluminescence spectra obtained by moving the laser spot across a nonhomogeneous sample. Each exciton peak is labeled by the corresponding GaAs layer thickness. The inset schematically shows excitons confined in a GaAs quantum well. The interfaces have small-scale disorder superimposed on the large islands.

Figure 9 shows a set of PL spectra obtained by moving a focused laser spot of 200 μm diameter across a quantum well sample in steps of 300 μm. Because the average GaAs layer thickness changes monotonically across the sample, the exciton peaks shift as the laser spot is moved across the sample (i.e., the confinement energy changes). Notice that the energies change in a quantized way. In other words, as the GaAs layer thickness is decreased, the higher energy part of the doublet increases in intensity at the expense of the lower until, finally,

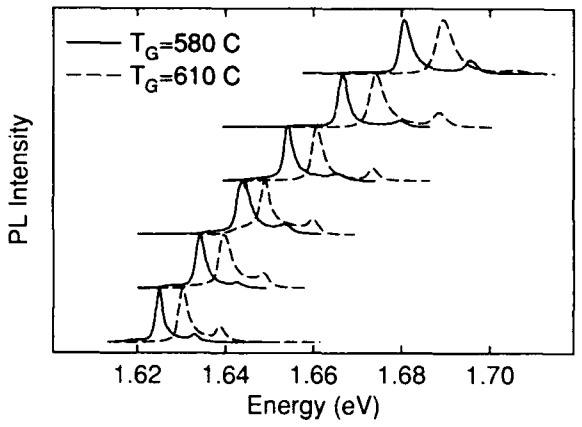

Fig. 10 — Two sets of photoluminescence spectra from two different samples that were grown at different temperatures T_G. The shift between the two sets of peaks indicates the existence of the small-scale disorder within the large islands.

the lower disappears and a new peak appears at higher energies. The figure gives the quantum well width in monolayers for each exciton peak. The occurrence of exciton doublets with energy separations corresponding to one monolayer difference in quantum well width, plus the quantized movement of the exciton peaks as the well width is changed, is clear evidence of the existence of large, monolayer-high islands. It has been taken as evidence for nearly a decade that the interfaces are perfect within the large islands. We have shown that this is an incorrect conclusion. Figure 10 shows two sets of PL spectra from two different samples. These two samples are identical except that they were grown at slightly different temperatures. There is a clear energy shift between the exciton peaks in the spectra from the two samples. Note, however, that if the interface were perfect within the large islands, the exciton energies would be a function only of the number of monolayers in the GaAs layers, and therefore, these energies would be the same in all samples. The fact that these energies differ proves that fine structure ($<<20$ nm) exists within the large islands, and that this fine structure depends on the growth temperature.

Conclusion: It is possible to grow layered semiconductor heterostructures with nearly perfect interfaces. However, optical spectroscopy shows that there still remains a monolayer of disorder even in the highest quality samples available in the world today. We now have a good idea of the nature of this disorder, and we have even learned how to alter it. It remains to be determined whether truly perfect structures can be achieved.

[Sponsored by ONR]

References

1. D. Gammon, B.V. Shanabrook, and D.S. Katzer, "Excitons, Phonons, and Interfaces in GaAs/AlAs Quantum Well Structures," *Phys. Rev. Lett.* **67**(12), 1547 (1991).

2. A. Ourmazd, D.W. Taylor, J. Cunningham, and C.W. Tu, "Chemical Mapping of Semiconductor Interfaces at Near Atomic Resolution," *Phys. Rev. Lett.* **62**(8), 933 (1989). ■

Conical Section of the Anechoic Chamber
Facilities/Project Photos, *Second Place*
Frederick R. Domer

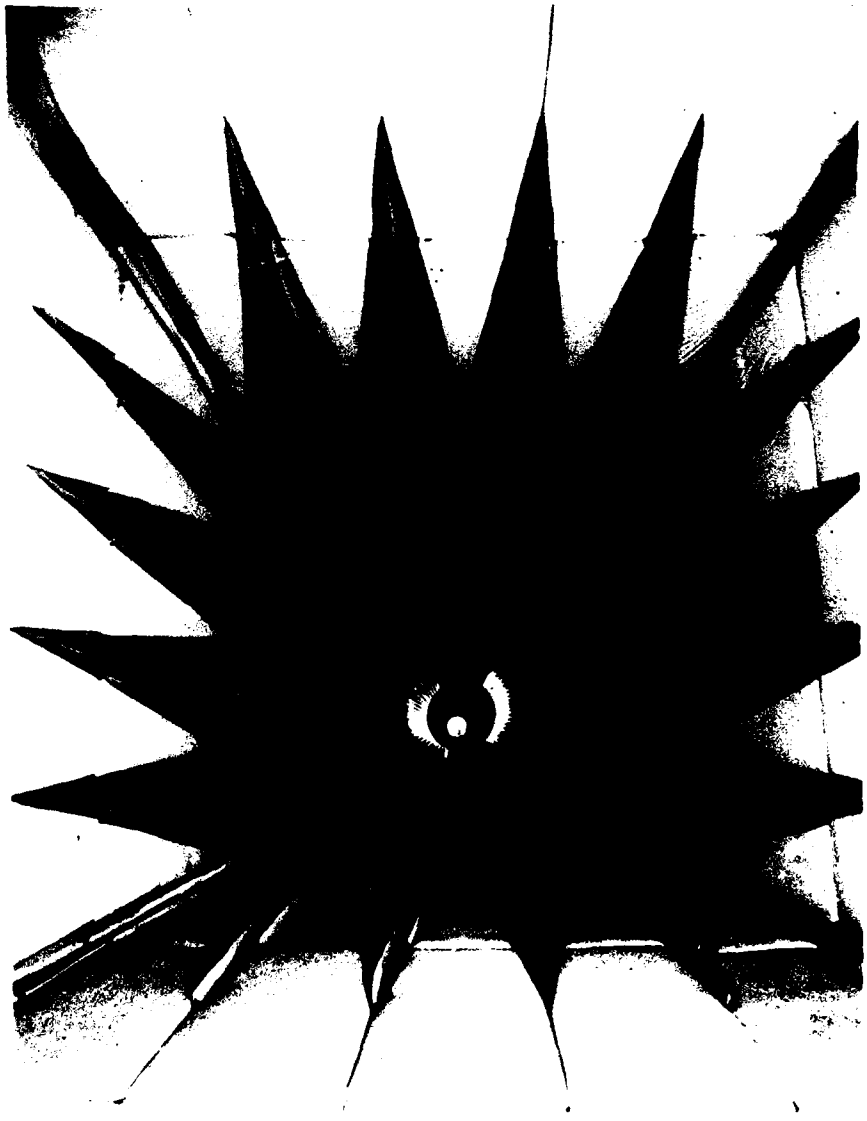

Conical Section of the Anechoic Chamber
Facilities/Project Photos, *Second Place*
Frederick R. Domer
Space Systems Development Department

Shown is the conical end of the large 120-ft tapered anechoic chamber used to design and test antennas, both individually and on RF models, for satellite and ground use by the Naval Center for Space Technology. Source antennas (generally transmitting) are placed through side doors in the conical section shown, which consists of wedge-shaped (gray) absorbing material. Where the wedge material meets the white material, the chamber cross section gradually changes shape from circular to square. As can be seen, the absorbing material also makes a gradual transition from wedge to block material.

ENERGETIC PARTICLES, PLASMAS, AND BEAMS

157 **Brightest X Rays Used to Probe Smallest Crystals**
Earl F. Skelton, Syed B. Qadri, and Jack D. Ayers

159 **Atomic Physics in Ultrastrong Fields**
Jack Davis, Robert W. Clark, and John L. Giuliani, Jr.

162 **Monolithic GaAs Antenna/Detector Array for 94 GHz Imaging**
William M. Waters

164 **Ultrawideband Radar**
Grealie A. Andrews, J. Peter Hansen, and Karl Gerlach

Brightest X Rays Used to Probe Smallest Crystals

E.F. Skelton and S.B. Qadri
Condensed Matter and Radiation Sciences Division

and

J.D. Ayers
Materials Science and Technology Division

A critical link in the chain of understanding the behavior of materials for use in Navy applications and elsewhere is a knowledge of the spatial arrangement of the constituent atoms. Atomic configurations, or crystal structures as they are commonly called, are determined most efficiently from X-ray diffraction measurements. The required X-ray data are usually obtained by scattering monochromatic X rays produced by laboratory X-ray generators from crystal samples having volumes of a few hundred μm^3.

By using one of the brightest sources of X rays in the world, it has been demonstrated that useful X-ray data can be obtained from crystal volumes as small as 0.028 μm^3 (= 28 attoliters), orders of magnitude smaller than sizes normally used. Since there are some materials that can only be produced as crystals with submicrometer dimensions, it is expected that this may open a new vista in materials research.

Submicrometer-diameter Filaments and a Very Bright X-Ray Source: A novel materials fabrication process, recently developed by one of the authors [1], has led to the production of glass enshrouded metallic filaments with submicron diameters. Previously, very fine wires of metals could be drawn at a temperature where the metal is molten and confined within a softened glass capillary; the capillary is drawn into a fiber containing an axial metal filament. By cascading the process and by using glasses with different softening temperatures, metallic filaments have been produced with diameters of only a few hundred Å, smaller than the wavelength of visible light. Because of the minute quantity of material present in the sample and the surrounding glass, efforts to determine the crystallographic properties of single filaments by using conventional X-ray sources have been unsuccessful.

Concomitant with the development of this processing technique, a team headed by NRL has been involved in the construction of a new beam line at the National Synchrotron Light Source (NSLS), Brookhaven National Laboratory. On this line, the X rays are generated by passing the 2.5 GeV electrons orbiting in the synchrotron through a six-pole superconducting magnet, a so-called *wiggler* device. The effect of the multiple trajectory changes caused by the wiggler is the emission of an X-ray beam with a continuous range of energies exceeding 100 keV and a brightness greater than that available on most synchrotron bending magnets. This is significantly greater than that available from any conventional X-ray generator. Thus, a difficult technical problem and a tool to solve it came into being at about the same time.

Energy Dispersive Diffraction Spectra: Glass enshrouded filaments made of elemental bismuth with diameters less than 1 μm were mounted on a computer-controlled, four-circle goniometer. A portion of each sample was than bathed in the polychromatic X-ray beam emanating from the aforementioned wiggler magnets at NSLS. The beam was apertured to a square cross-section, typically 50 to 100 μm on an edge, but for measuring spectra, this was reduced to 10 or 30 μm.

The scattered radiation was detected with an intrinsic Ge energy-sensitive detector positioned at a fixed, but adjustable, 2θ angle. All of the Bi filaments examined to date have been found to consist of either one or a very limited number of crystals within the beam. Figure 1 shows an energy dispersive diffraction spectrum from a 0.22 $\pm$ 0.05-μm-diameter sample.

All samples with diameters of 0.09 μm or larger were found to have the normal rhombohedral lattice of Bi-I, and each crystal was found to

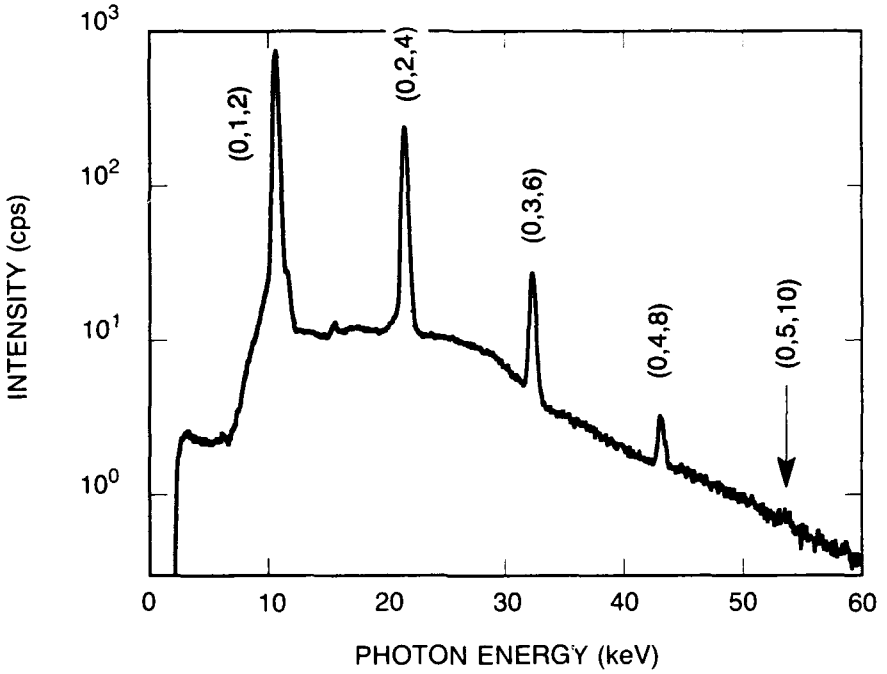

Fig. 1 — Energy-dispersive diffraction spectrum of the (0, *k*, 2*k*) class of reflections from a 0.22 ± 0.05-μm-diameter Bi filament recorded at $2\theta \approx 20.00°$ for a period of 5 m

have grown with its [1,0,4] reciprocal lattice vector approximately normal to the fiber axis.

Once a filament was aligned and its orientation matrix determined, a number of independent reflections were measured. By examining the interplanar distances (so-called *d-spacings*) computed from these reflections, it was found that there was a systematic variation between $\Delta d/d$ and χ, where Δd is defined as the difference between the value calculated by using the accepted lattice parameters for Bi and the measured value; χ is the angle between the normal-to-the-fiber axis and the reciprocal lattice vector associated with the specific reflection. This systematic variation amounted to a linear strain of about 2.0 ± 0.5% on those planes whose normal was perpendicular to the fiber axis. We interpret this strain as resulting from the stress from the encapsulating glass, noting that bismuth expands upon solidification and must do so against the containing glass. Additional details about this are given in Ref. 2.

New Phase of Bismuth: Contrary to our experience with the larger diameter samples, the data obtained from a 0.067-μm-diameter sample showed a large number of diffraction peaks that could not be associated with the rhombohedral structure of Bi-I. These data also are incompatible with all known phases of bismuth. We believe the explanation lies in a new phase of the element, one that we have provisionally identified as Bi-X (since nine other phases of Bi are known to exist). Our data from Bi-X can be referenced to a face-centered cubic lattice with a unit cell parameter of 10.65 ± 0.05 Å and belonging to the space ground F-43m. Efforts are presently under way to complete the structure determination of Bi-X.

Summary: Useful X-ray diffraction data have been obtained from crystal volumes as small as 28 attoliters. Filaments of submicrometer-diameter bismuth consist of single crystals and exhibit the normal rhombohedral structure of Bi-I for diameters of 0.091 μm and larger. For every Bi-I sample measured, the [1,0,4] reciprocal lattice vector has been found to be aligned approximately normal to the fiber axis and the

samples are confined under a residual hoop stress from the encapsulating glass. The 0.067-μm-diameter sample contains crystals that appear to be a new phase of bismuth, provisionally identified as Bi-X.

[Sponsored by ONR]

References

1. J.D. Ayers, "Glass Fibers with Metallic Cores," *1990 NRL Review*, pp. 94-96.
2. E.F. Skelton, J.D. Ayers, S.B. Qadri, N.E. Moulton, K.P. Cooper, L.W. Finger, H.K. Mao, and Z. Hu, "Synchrotron X-Ray Diffraction from a Microscopic Single Crystal Under Pressure," *Science* **253**, 1123 (1991). ■

Atomic Physics in Ultrastrong Fields

J. Davis, R.W. Clark, and J.L. Giuliani, Jr.
Plasma Physics Division

Introduction: Recent developments in laser, technology have produced a new class of lasers, commonly referred to as Table Top Terrawatt (T^3) lasers. The T^3 lasers are so powerful that they generate electric field strengths 10 to 100 times the Coulomb field binding electrons to atoms and molecules. The interaction of these ultrabright intense lasers with matter produces a variety of new, exciting, and challenging problems and unlimited possibilities in the applications area. Research at NRL, and in particular the Plasma Physics Division, naturally divides into three broad categories. In the first—the laser-atom interaction regime—the focus is on how the intense laser field interacts with and perturbs individual atoms and molecules. This interaction is at the fundamental physics level and involves such processes as multiphoton ionization, above-threshold ionization (the modern-day version of the Einstein photoelectric effect), newly formed excited atomic and molecular states, and harmonic generation, as well as basic questions related to the quantum electrodynamics of atoms and interacting fields. In the second—the laser-particle regime—the thrust of the research shifts to nonlinear processes involving beam propagation and focusing, new types of accelerators, relativistic plasma physics, and novel radiation sources. In the third—the laser-solid interaction regime—one enters the region of strongly coupled plasmas, generation of laboratory astrophysical plasmas, subpicosecond X-ray radiation sources, subnanosecond photography, X-ray lasers, and possibly, laser-induced fusion.

Laser-Atom Interactions: Almost everyone who has studied quantum mechanics has encountered the so-called Stark effect characterizing the influence of an externally imposed electric field on the eigenvalues and eigenstates of an atom. Generally, the electric field is weak in comparison with the electrostatic field binding the atomic electrons so that the interaction can be treated in perturbation theory. However, with the appearance of the T^3 laser, the "perturbation" is of the same order of magnitude or greater than the electrostatic field and, as such, vitiates the use of conventional perturbation theory. How can this type of strong interaction be mathematically characterized? What new methods and techniques will describe adequately the behavior of atoms and molecules in such enormous potential fields and hostile environments? These issues are currently under intensive experimental and theoretical investigation globally. NRL is a recent entrant into this maelstrom of excitement and activity. Our approach is based on the assumption that before exposure to the laser field, the atom is characterized by its field-free Hamiltonian and is described by conventional wisdom. As the laser field turns on and increases in intensity to its peak value in about 100 fs, the atom undergoes a complete metamorphosis. The metamorphosis can occur in several ways, including multiphoton ionization, tunneling or the Keldish effect, above-threshold ionization, collective oscillations followed by inner shell excitation and X-ray

emission, and harmonic generation. Of course, during the laser pulse, the atom undergoes severe, dynamic Stark shifts and ionization lowering. Obviously, the complete solution describing the atomic structure involving the full, relativistic Hamiltonian is a challenging and monumental undertaking.

Laser-Solid Interaction: The laser-solid target interaction generates a plasma where not only is the atomic structure crucial but the various atomic processes (such as collisional excitation and ionization, radiative, dielectronic, and collisional recombination, inner shell, and collective processes) must be described to characterize the evolving plasma. These processes are required if one is to unfold, analyze, interpret, and understand experimental data. Figure 2 shows the phenomena occurring when an intense, short pulse laser interacts with a planar solid target. In contrast to laser pulses longer than about 1 ps where there is time for significant hydrodynamic expansion of the illuminated surface, short-pulse laser illumination produces density gradients shorter than the penetration skin depth and interferes with the coupling of the incident laser energy to the target. Under these circumstances, most of the laser energy is delivered before there is any noticeable expansion of the leading edge. In addition, since the magnitude of the electric field associated with the laser pulse is very large, the ponderomotive force competes with the gas pressure in determining the expansion of the front surface.

Primary induced laser breakdown is initially caused by tunneling and multiphoton ionization. Once the first few electrons are produced, the bulk of the absorption of the incident laser energy occurs via inverse bremsstrahlung. The magnitudes of the incident, reflected, and transmitted electric fields are determined from a solution of the Helmholtz wave equation. However, because of the shortness of the pulse, most of the incident wave is reflected so that only a fraction of the laser energy actually heats the plasma. At this time, the bulk plasma is essentially heated by thermal

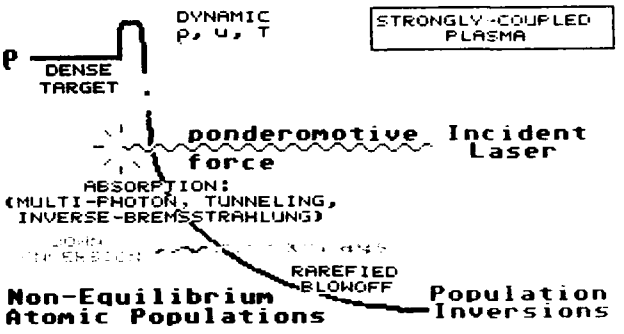

Fig. 2 — Short-pulse laser/plasma interaction

conduction. The early-time plasma is strongly coupled in the sense that it is still relatively cold and at or above solid density. This means that the potential energy is greater than the kinetic energy of the particles, i.e., the electrons are correlated and ordered rather than dominated by random motion. At the end of the laser pulse, the plasma has become hot enough to emit X rays and expand outwardly. It is in the expanding plasma that conditions conducive to population inversion and X-ray lasing are likely to occur.

As an example, consider a KrF laser incident on a planar fluorine target. The laser intensity is 3×10^{17} W/cm^2 and has a pulse width of 650 fs. We illustrate the influence of the laser field on the evolution of the plasma by focusing only on one aspect of the interaction—the influence of the ponderomotive force. The ponderomotive force arises as a result of the electric field of the laser pulse interacting with the electrons in the plasma causing the electrons to experience a force that pushes them away from regions of high field pressure. This ponderomotive force plays a role similar to ordinary pressure. In Figs. 3 and 4, the influence of the ponderomotive force on the mass density is shown as a function of distance (horizontal axis) and time (vertical axis). These results were obtained by using a 1D non-LTE radiation hydrodynamics model self-consistently coupled to a Helmholtz wave equation using nonclassical electrical conductivities. The color scale on the right of the figures represent $\log_{10}$ density (g/cm^3).

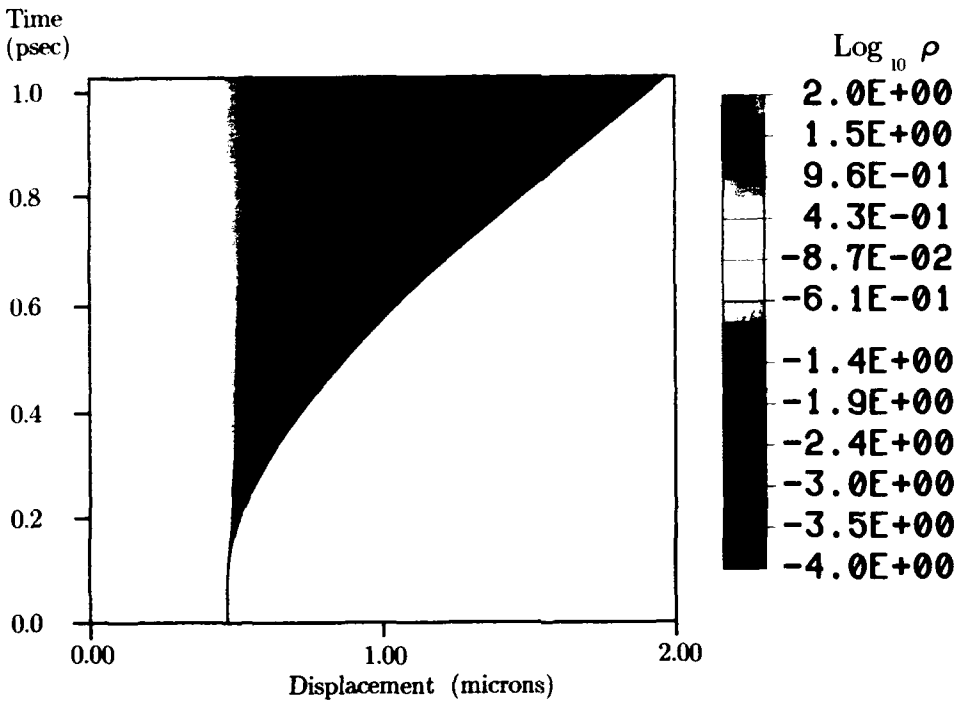

Fig. 3 — Mass density as a function of space and time (without ponderomotive force)

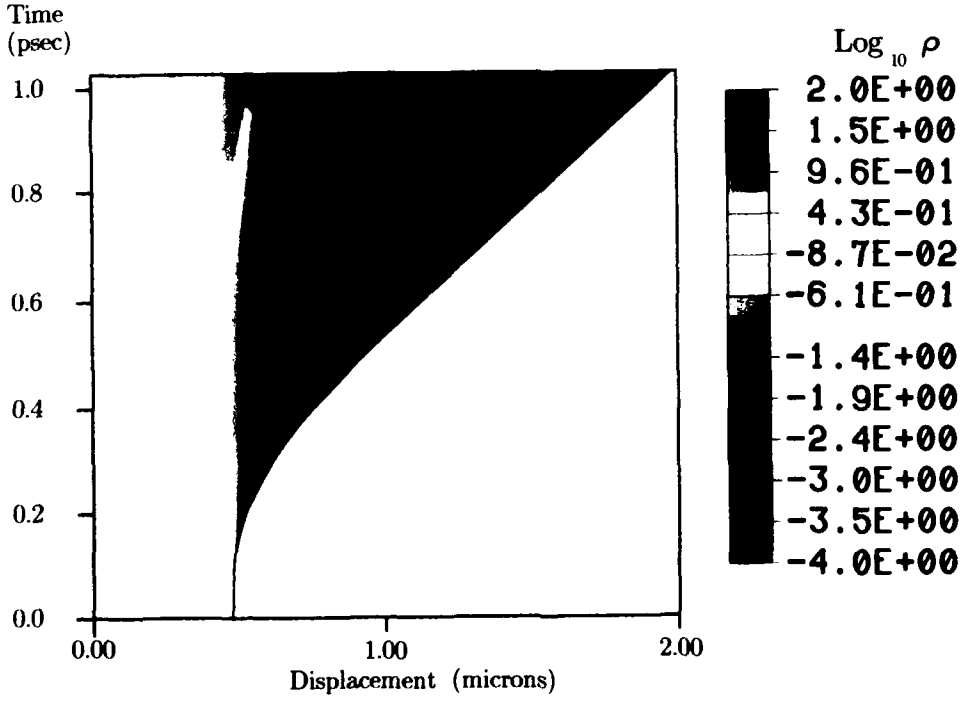

Fig. 4 — Mass density as a function of space and time (with ponderomotive force)

With the ponderomotive force included, there is a pronounced steepening of the density profile in the vicinity near the ablation front, and a corresponding flattening of the profile near the critical surface. Near the peak of the laser pulse (around 300 fs), there is structuring of the density for this case (evidenced by the green contour). Note the shock wave (orange contour) propagating into the target in both cases. The ponderomotive steepening is accompanied by a more-pronounced modification of the temperature profiles, and the ionization and radiation dynamics are substantially altered.

This is a rapidly evolving research area; current issues of *Physical Review A* contain the latest research.

[Sponsored by SDIO and ONR]

Monolithic GaAs Antenna/Detector Array for 94 GHz Imaging

W.M. Waters
Radar Division

Microwave and millimeter wave sensors capable of forming images have been of interest for at least three decades. Energy in this segment of the electromagnetic spectrum suffers far less attenuation in clouds, fog, smoke, and blowing sand than IR and visible light. On the other hand, longer wavelengths lead to larger apertures for the same angular resolution. Hence, microwave and millimeter wave sensors find applications where ranges are short and targets are large, as in airborne weapon delivery, aircraft landing, ship wake detection, and base perimeter monitoring.

Synthetic arrays can be quite large, but because the data rate is limited, target recognition may be difficult. Both synthetic aperture radar (SAR) and inverse SAR (ISAR) acquire data sequentially in contrast with focal plane arrays (Fig. 5), which acquire data from the entire angular field in parallel.

94 GHz Focal Plane Array: Work at NRL began in 1984 in support of the automatic carrier aircraft landing system [1]. In 1989, under an NRL contract, Westinghouse developed and tested a 4 × 4 array of antenna/detector elements fabricated on a wafer of semi-insulating (SI) GaAs [2]. This tile, shown in Fig. 5, will be assembled with other identical tiles to form a much larger array of thousands of pixels consistent with 94 GHz optics and specific applications.

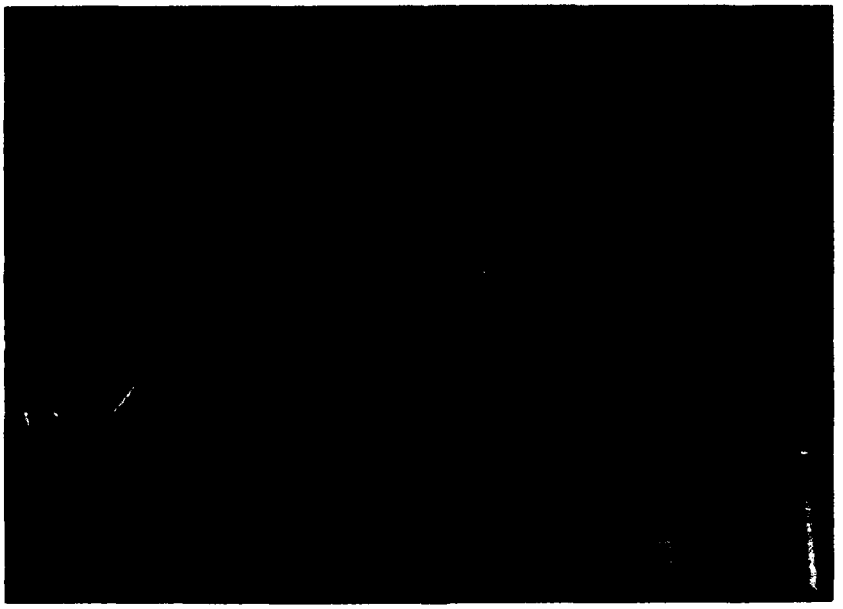

Fig. 5 — Monolithic Ga/As antenna/detector array (slot antennas on opposite side)

50	48	51	51
49	48	50	---
---	50	49	---
---	---	45	---

TSS (– dBm) f_{RF} = 94 GHz

49	47	49	49
49	48	48	---
---	50	48	---
---	---	47	---

TSS (– dBm) f_{RF} = 95 GHz

Wafer: 1280 – 1
f_v = 100 kHz
BW_v = 10 to 1000 kHz

Fig. 6 — Tile maps of tangential sensitivity

An element (pixel) consists of a slot antenna in a ground plane on the face opposite to that shown in the figure, each of which is oriented orthogonal to and approximately centered on a microstrip circuit visible in the blow-up of Fig. 5. This circuit was designed for optimum coupling and impedance match between the slot antenna and diode detector.

A Schottky barrier diode is formed in the microstrip by implanting silicon ions into the SI GaAs separating an anode finger from the boundaries of the cathode channel, both of which are formed by appropriate metalization on the GaAs substrate. Anode and cathode are separated by about 1 μm.

Considerable effort was devoted to diode and circuit development, since significant variations of diode parameters over the face of a focal plane array could not be tolerated. Diode cut-off frequencies in the range from 500 to 700 GHz were achieved; Fig. 6 shows the overall influence of parameter variations on the tangential sensitivity. At frequencies spanning 1 GHz, measured sensitivity varied less than 2 dB from –49 dBm over 9 of the 16 pixels.

Active/Passive Millimeter Wave Sensor: An important feature of a sensor based on this focal plane array is that it will operate in either active or passive modes. By illuminating the array of Fig. 5 with a local signal, the diodes become synchronous mixers that are orders of magnitude more sensitive [3], thereby making possible staring-beam radars and radiometers capable of detecting otherwise undetectable targets.

[Sponsored by ONT]

References

1. W.M. Waters, "On Strengths and Weaknesses of the Automatic Carrier Landing System," NRL Memorandum Report 6198, June 1988.

2. H.G. Henry, R.G.Frietag, R.R. Shaller, M. Cohen, and A.S. Jensen, "Millimeter Wave Vidicon," Westinghouse Final Report on Contract N00014-87-C-2343, Aug. 1990.

3. M.E. Brodwin, C.M. Johnson, and W.M. Waters, "Low Level Synchronous Mixing," Proceedings of the IRE, Aug. 1953, pp. 969-970. ■

Ultrawideband Radar

G.A. Andrews, J.P. Hansen,
and K. Gerlach
Radar Division

The development of ultrawideband (UWB) radar is an area of growing interest in the radar community because of its potential for extremely high-resolution electromagnetic measurements of conducting bodies, dielectric materials, and the environment. The applications of this technology that are becoming evident to radar researchers include the detection of moving targets and the rejection of clutter without relying on Doppler, the resolution of multipath to measure target height, the ability to obtain accurate measurements of target range, velocity, and range profile for target recognition, and the rejection of many types of electronic countermeasures (ECM). As a research tool, this technology will allow transient/impulse electromagnetic probing and extremely high resolution imaging of the sea surface, terrain, weather, the atmosphere, and man-made objects.

Radars have conventionally been developed as relatively narrowband systems. Even the highest resolution radars are usually on the order of 10% to 15% bandwidth; therefore, high resolution can be achieved only with a relatively high transmit frequency. UWB radar has been defined as having >25% bandwidth up to and including 100% bandwidth (impulse radar). In the fifty-plus years of radar history, a tremendous quantity of radar theory has been developed that has inherently included narrowband assumptions. This theory is being re-examined, and a new, more complete understanding is evolving in both electromagnetics and signal analysis to allow the potential of this new technology to be realized.

Characteristics of UWB Radar: Since the information content of a waveform is determined by its bandwidth, the information gathered by UWB radar is an order of magnitude greater than that gathered by current operational wideband (high-resolution) radars, such as the AN/APS-137, and at least two orders of magnitude greater than current search radars. The ultrahigh range resolution (UHR) corresponding to the UWB waveform reduces the interference between closely spaced scatterers and, therefore, effectively increases the energy scattered from the target as compared to conventional narrowband radars. Optimum signal processing algorithms can use this effect to increase the detectability of low-cross-section targets. The vast amount of information gathered on targets allows false alarms to be efficiently rejected by applying multidimensional detection algorithms that include not only the magnitude of the energy scattered from the target but also range profiles, velocity, target height, and the change in the magnitude of the scattered energy with range.

For effective processing and use of UWB radar returns from manmade objects or environmental scatterers, it is necessary to characterize the UWB signal after the effects of radiation, propagation, scattering/reradiation, repropagation, and reception have been applied to the waveform. Thus, an understanding of the electromagnetic phenomena and the relationship with physical characteristics of the target or environment is essential for developing an accurate signal processing theory for UWB radar. To design radar systems aimed at measuring specific propagation or scattering phenomena for assessing the environment or recognizing a manmade target, it is necessary to characterize the physical phenomena deterministically to the extent possible, and resort to statistical characterization when necessary to estimate the parameters of interest.

Applications of UWB Radar: Detailed design and performance predictions of UWB radar for specific applications are limited because very little experimental data exists on targets or the environment. *Data on forward scattering* and ground and rain backscatter as well are completely

lacking for UWB waveforms. NRL recently conducted experiments to understand backscatter from the sea surface. NRL researchers first used a laboratory wave-tank and then looked at the Chesapeake Bay with the laboratory radar equipment shown in Fig. 7. Figure 8 shows the UWB transmitted waveform resulting from a stepped voltage response of a wideband traveling wave tube operating at 10 GHz with a nomina! bandwidth of 3 GHz.

Data taken during these experiments support the expectation that UHR signals backscattered from sea surface would be much more stable than with conventional radars because the higher resolution results in less interference between closely spaced scatterers. This increased stability of clutter and the similar increased stability of moving targets results in significant increases in moving target indication/detection (MTI) and clutter rejection. Area MTI that simply requires that the target moves between range cells rather than relying on Doppler becomes practical because of the ultrahigh range resolution and is being demonstrated with these data. Since this UHR waveform resolves individual scatterers on the target, this range profile is being used for target recognition of small targets in a manner similar to that used by the Naval Weapons Center to recognize ships. Matched filter concepts are being developed to optimally combine the UHR data that, along with the increased *effective backscattered energy* described previously, significantly enhance the detectability of small targets.

Fig. 7 — Setup of the UWB radar experiment at the Chesapeake Bay Detachment

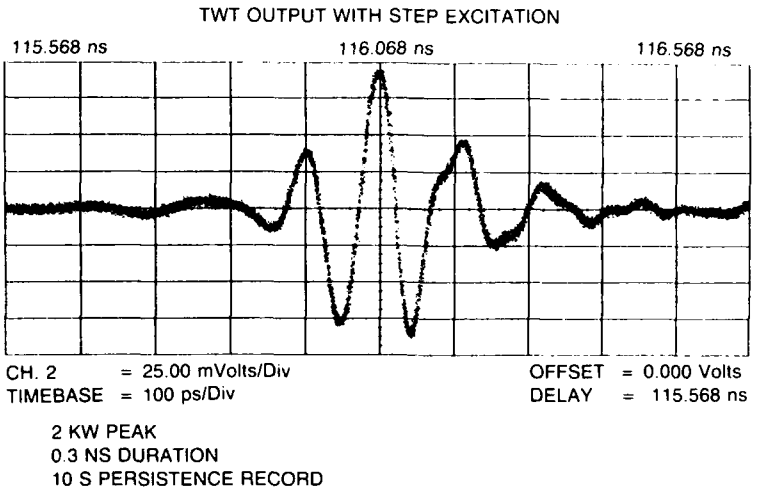

Fig. 8 — The transmitted waveform of a wideband traveling wave tube transmitter with a stepped voltage excitation. Nominal bandwidth: 3 GHz. Center frequency: 10 GHz.

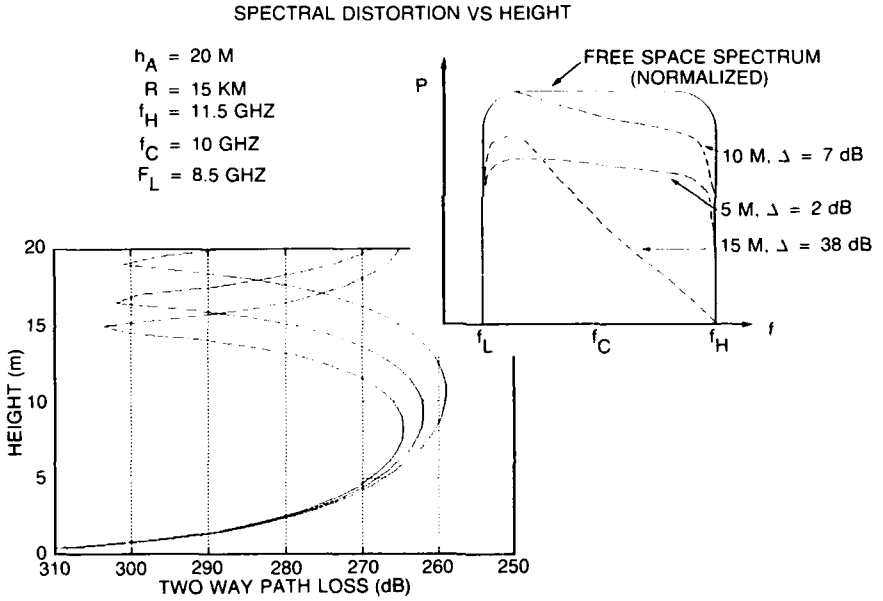

Fig. 9 — Effect of multipath on the spectrum of the transmitted signal for an antenna height of 20 m and a range of 15 km is shown on the left-hand side. f_C. f_L, and f_H are the center of the spectrum, the low end of the band, and the high end of the band, respectively. The change in the spectral distortion with target height is illustrated on the right-hand side.

Figure 9 shows the effect of interference between the signal backscattered from a low-flying target and the multipath signal from the target reflected off the sea surface. The variation in frequency response with altitude must be included in the receiver design and is also being used to estimate target altitude. This information, along with accurate velocity measurements and target recognition, is being used in the development of multidimensional detection algorithms to open up a new realm of target detection radar applications.

[Sponsored by DARPA] ■

CRRES Chemical Release
Artist's Concepts/Illustrations, *Second Place*
Mark M. Baumback

CRRES Chemical Release
Artist's Concepts/Illustrations, *Second Place*
Mark M. Baumback
Plasma Physics Division

The artist's concept shows a chemical release from the NASA/DoD Combined Release and Radiation Effects Satellite (CRRES). Alkaline Earth metals, such as sodium, barium, calcium, and lithium have the property that when they are released into the space environment, they are ionized by sunlight and glow with a unique color. Since these glowing ions gyrate around the magnetic field, they in effect paint a picture of the magnetic fields in space with clouds of glowing ions. In addition to studying the Earth's magnetic field, CRRES chemical releases will be used to study the formation of irregularities in the ionosphere and to create depletion regions that can be used to focus the beam of high-powered radio transmitters into the ionosphere.

INFORMATION TECHNOLOGY AND COMMUNICATION

169 **A Networking Technology Demonstration for Naval Tactical Communications**
Dennis N. McGregor, Dennis J. Baker, and James P. Hauser

172 **A Graphical User Interface Design for Shipboard Damage Control**
David L. Tate

174 **Nonlinear Signal Processing for Detection in Chaotic Backgrounds**
Sheldon B. Gardner

A Networking Technology Demonstration for Naval Tactical Communications

D.N. McGregor, D.J. Baker, and J.P. Hauser
Information Technology Division

Background: A distributed, self-organizing, adaptive networking architecture, called the linked cluster architecture (LCA), is being developed by NRL for application to Naval Intratask Force (ITF) communication services [1]. This network architecture offers the benefits of improved timeliness and information throughput, the ability to adapt to dynamic stressed situations, enhanced survivability/jam-resistance, and support for virtual circuit setup and maintenance. A seven-node hardware demonstration of this networking architecture (involving a ship, an aircraft, and five land-based nodes) was successfully performed as part of the Unified Networking Technology (UNT) project.

Field-Test Demonstration: Figure 1 shows the geography for the test network. Land-based nodes are located at the Naval Ocean Systems Center (NOSC) in San Diego, San Clemente Island (SCI), San Nicolas Island (SNI), Seal Beach (SB), and Point Mugu (PM). Figure 1 also shows the node numbers, transmit frequencies used by each site, and a qualitative assessment of the communication links as they existed during the test period. Tests were designed in such a way that they could be duplicated in the lab. The HF ITF network was tested in two modes of operation. In one mode of operation, traffic was forced into the network to the point that the network was overloaded, and message delays built up to

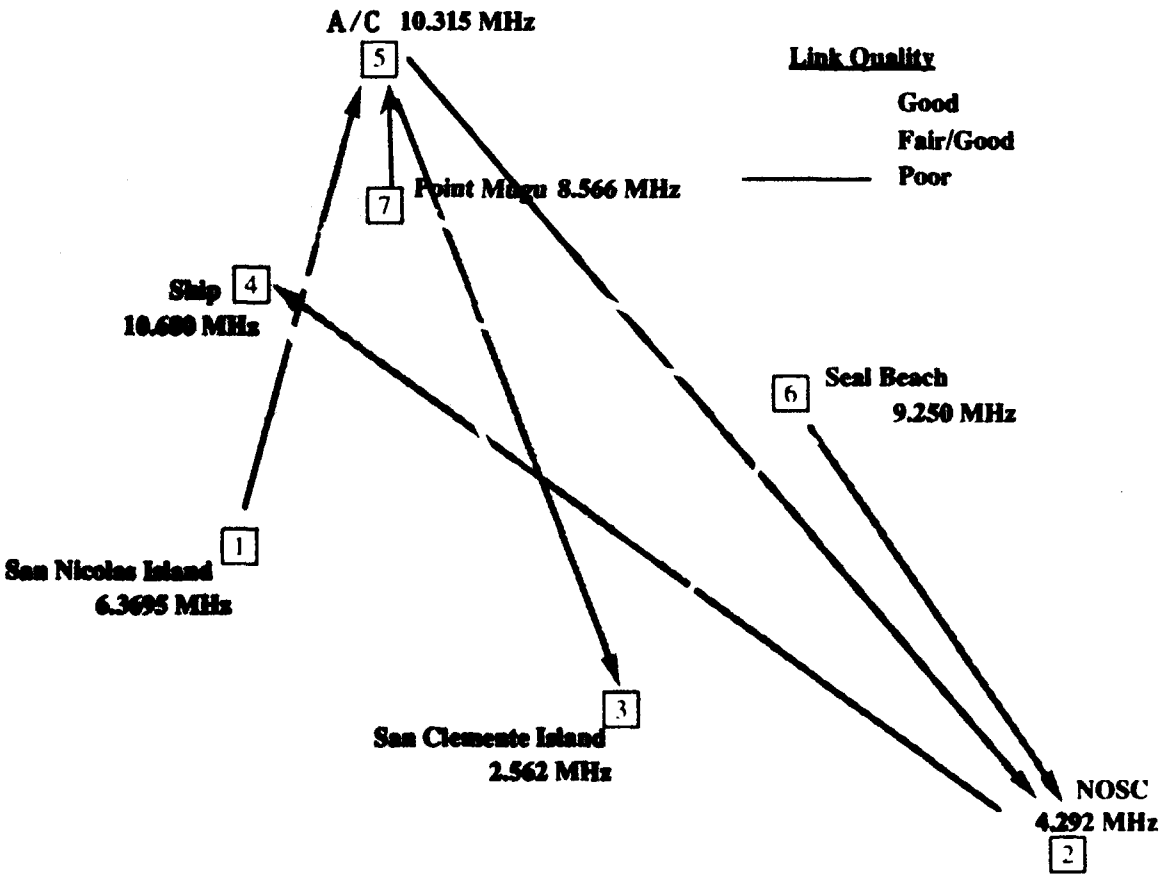

Fig. 1 — Network geography and communication link qualities for NRL UNT tests

unacceptable levels. This mode was used to find the performance limits of the network. In the other mode of operation, the network's congestion control algorithm was allowed to function so as to throttle input traffic and maintain acceptable message delay levels. This latter mode of operation tested the network's ability to operate in an efficient and stable manner.

Despite the limited number of nodes in the UNT tests, the performance of the NRL HF ITF communication network was observed over a wide range of topologies, including topologies that resulted from nodes going on and off the air. Close to 500 topology changes were observed during the course of an 8-hour test period. Of these topologies, 174 were unique. Analyses of the test results show that the network control algorithms allow an LCA network to self-organize in response to topology changes and maintain viable network control structures. The resulting data analyses also indicate that the field test results of network performance are in excellent agreement with NRL's previous simulation experiments.

The LCA uses distributed control techniques to structure itself in response to connectivity changes. Figure 2 shows how the test network self-organized in response to node and link changes during a sample half-hour test segment. Each panel displays the Greenwich Mean Time (GMT) corresponding to the time that a particular network structure occurred. Only reliable, bidirectional links are shown in this figure. The network probes every 18.2 s for the existence of such links and creates a structure based on the link qualities. Nodes assume one of three roles in this architecture—namely clusterheads, boundary nodes, and terminator nodes. Clusterhead nodes serve as dynamically selected regional coordination and broadcast centers and are shown as the solid-filled squares in Fig. 2. Boundary nodes are denoted by solid-filled diamonds and act as relays to send traffic between clusterheads. Solid-filled circles denote terminator nodes, which play only a minor role in network control. The unfilled circles denote nodes that were not operational at that time.

Duplicating Field-Test Results in the Laboratory: The NRL HF network controller (NC) software for UNT was unique in that the software used in simulation studies was used also in the target (i.e., UNT field test) system. Thus, throughout the life cycle of the HF NC software, only one implementation had to be maintained. As a result, each software coding error that was discovered during the simulation phase, which preceded the field tests, meant one less software error to be debugged in the target system. Any changes made in the network control algorithms in the simulation model were, at the same time, changes made to the target system. Because the simulation model and the target system shared a common implementation of the NC software, it is not surprising that the entire UNT test is reproducible in the laboratory. Nevertheless, careful attention was given to the design of the field tests, and some enhancements were made to the simulation support system to ensure that the field test results could be duplicated in the laboratory.

The NRL UNT tests were designed so that all significant inputs to the HF NC software from its environment could be duplicated in the laboratory. The HF NC had two external interfaces that had to be considered. The upper interface connected to the source of traffic at the node. The lower interface received 176-bit blocks of data from the modem, along with information about whether or not a received block contained a transmission error. In the tests, we generated traffic by using the same traffic sources as in the simulation studies. This guaranteed reproducibility between the field tests and the laboratory tests across the upper interface. To guarantee reproducibility of inputs from the lower interface, the NRL HF NC archived data for each transmission block. These data included whether the block was received at a node, and if it was received, whether it was received without a checksum error. The HF NC only interpreted control data if it were received without errors.

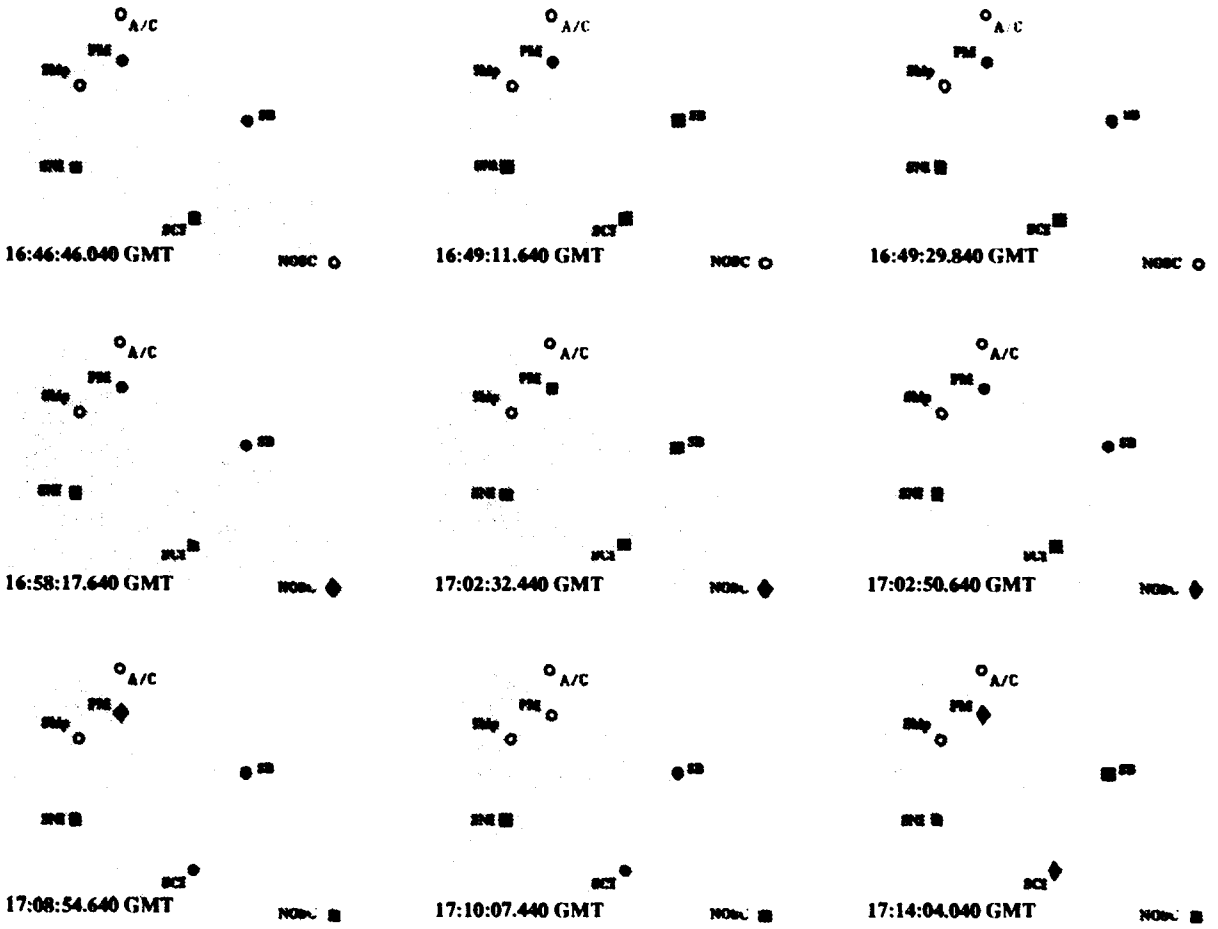

Fig. 2 — Network structural changes during sample half-hour period of tests

A Unique Tool for Communications Research: As part of the NRL UNT tests, a database of channel performance data was archived. This database can be used in place of the simulated HF channel of the NRL UNT simulator. This allows researchers to study many different network protocols in an environment identical to that which existed for the NRL UNT field tests. This means that NRL researchers have access to a desktop emulator of the UNT field testbed as it existed for the NRL UNT tests. One of the first uses of this communications research tool was to duplicate the NRL UNT test results in the laboratory. This testbed is presently being used to develop protocols for establishing and maintaining virtual circuits in networks that use the LCA. The ability to handle virtual circuits is needed to support voice communication over linked cluster networks.

Conclusions: The NRL UNT HF ITF communication network experiment was extremely successful. The major accomplishments of this experiment are the following: (1) it demonstrated a robust, multihop network architecture (LCA) that is well suited for intratask-force communication (especially integrated, voice/data communication); (2) it demonstrated the feasibility of a single, integrated, multifrequency network implemented with frequency-agile receivers; (3) it resulted in the collection of detailed information about HF channel conditions during these tests and archived this information for subsequent use in laboratory simulations; (4) it validated the NRL

UNT network simulator; and (5) it led to the development of the laboratory emulator of the UNT field testbed.

Recent studies [2] show that an integrated, multichannel network (the feasibility of which was demonstrated in the NRL UNT tests) has better performance than a comparable system built from multiple, single-channel networks. A multichannel network based on the LCA is especially suited for those applications that require simultaneous, voice/data communication over terrestrial UHF, VHF, or HF networks that are subject to frequent connectivity changes.

[Sponsored by ONR]

References

1. D.J. Baker, J.P. Hauser, D.N. McGregor, and William A. Thoet, "Design and Performance of an HF Multichannel Intratask Force Communication Network," NRL Report 9322 (1991).

2. W.A. Thoet, D.J. Baker, and D.N. McGregor, "Comparison of Two Transmission Strategies for Use in Survivable Radio Networks," Proceedings of the 1991 IEEE Military Communications Conference, Nov. 4-7, 1991, pp. 38.1.1-5. ■

A Graphical User Interface Design for Shipboard Damage Control

D.L. Tate
Information Technology Division

The combat effectiveness and survivability of Navy ships are directly affected by the ability of the vessel to detect, analyze, report, and control the effects of damage from either accident or hostile action. To respond quickly to various kinds of damage, it is important that information from the damage control sensors be presented in a way that helps damage control personnel make a quick and accurate assessment of the nature and extent of the damage. The Information Technology Division's Human Computer Interaction Laboratory has developed a method of graphically displaying information from shipboard damage control sensors and using the graphical display for operator control of selected equipment and system functions [1].

Approach: Shipboard damage control systems use sensors, equipment, material, and techniques to control damage associated with fire, flooding, hull damage, and chemical, biological, and radiological warfare. Historically, most sensors were connected to alarm systems that operated locally or through point-to-point connections to Damage Control Central or one of the ship's repair stations. Damage control requirements of the future will render dedicated alarms and indicators obsolete as the number and sophistication of sensors increases.

The damage control information display systems (DCIDS) is a graphical information retrieval and equipment control system that is designed to be used in a network environment of remotely controlled sensors, detectors, information resources, and communications equipment. This system is to provide the damage control assistant (DCA) with the ability to detect, analyze, and combat any type of shipboard damage. Computer-based decision aids will also be used, where appropriate, to provide recommendations or automated functions to reduce the workload of the damage control personnel. By using a networked system of sensors, data multiplexers, and workstations, an integrated reconfigurable flexible system is created that allows the DCIDS to be operated anywhere on the ship where access to the network exists.

User Interface Considerations: The DCIDS uses a computer workstation with a large color monitor and graphical input device, such as a trackball. The users of DCIDS, however, are not typical computer users. Special consideration for the intended users' lack of computer experience has led to a novel technique for providing easily

recognized graphical cues for distinguishing graphical control structures from informational displays. Easily recognized graphical devices allow the operator to initiate actions quickly, while information is presented to the operator in an obvious, uncomplicated way.

The careful use of shading and positioning of graphics is used to create a three-dimensional (3D) appearance and apparent motion for the controls, while information-only displays are drawn in a featureless two-dimensional (2D) plane. This technique causes the graphical controls to resemble typical equipment controls in their appearance and response to operator action. Figure 3 shows how a typical control panel for configuring options or selecting views is constructed.

Graphical displays of the deck plans provide an overview of the ship, with the sensors shown in their appropriate locations. Since sensors are distributed throughout the ship, the 3D appearance of the controls permits the operator to quickly recognize and access the sensor controls. Positioning the trackball pointer (cursor) over one of the 3D sensor graphics and clicking the button causes a pop-up panel to appear that shows the sensor information and controls. The information includes status, location, and identification data, and the controls may provide operational push-button switches, alarm enable check-boxes, or variable position sliders. Figure 4 shows how the information for an adjustable heat detector might appear on the screen.

Display Formats: Various display formats of the deck plans of the ship are used to provide maximum display of information without unnecessary clutter. The fire mains system on a ship is not excessively complex and lends itself to a

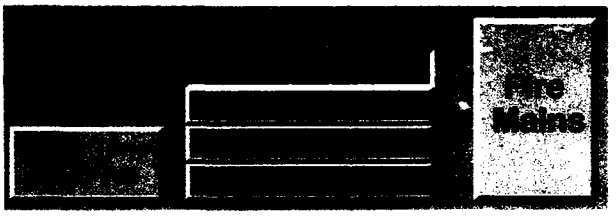

Fig. 3 — Control panels use 3D push-buttons to emulate conventional equipment controls

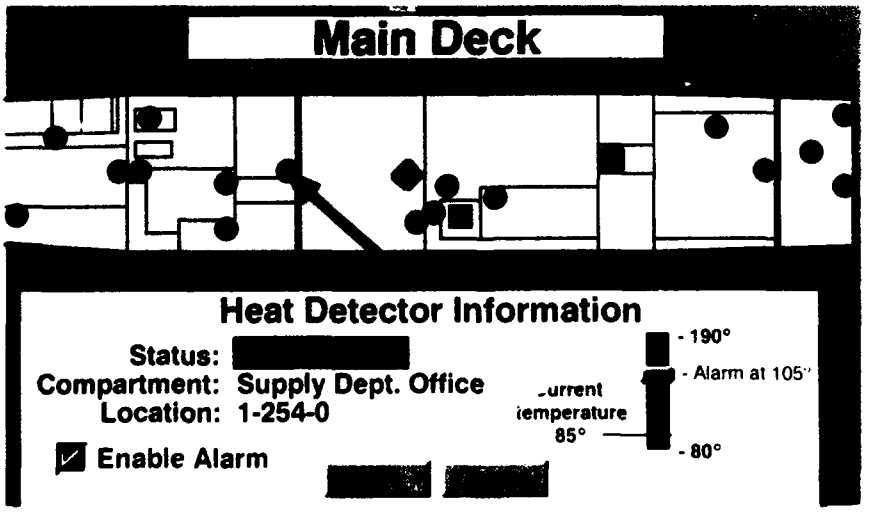

Fig. 4 — Pop-up panels display detailed monitoring information and adjustable graphical controls for advanced detectors, such as this reconfigurable heat detector

3D perspective display, where the fire mains, pumps, and valves can be shown on a single screen. Because newer ships have a large number of sensors for smoke, heat, flame, and flood, separate displays for each deck and sensor type are required. This display format uses a side view of the ship for selection of the desired deck with the selected sensors shown in a plan view of that deck. A simple control panel using push-button selectors controls which sensor type is displayed.

The DCIDS is an experimental prototype that is currently in the exploratory development stage. Further development of the implementation, interface requirements, and transition to Fleet use are planned.

Summary: The DCIDS graphical user interface can improve the performance of damage control personnel through the use of intuitive, easy-to-use graphical displays and controls. It represents a significant improvement to current methods of combatting damage and provides the ability to easily integrate future damage control sensors and equipment.

[Sponsored by the Navy Technology Center for Safety and Survivability and ONT]

Reference

1. D. Tate, "A Graphical User Interface Design for Shipboard Damage Control," NRL Report 9355, Aug. 1991. ■

Nonlinear Signal Processing for Detection in Chaotic Backgrounds

S.B. Gardner
Space Systems Technology Department

Introduction: Nonlinear signal processing based on synthesis of a polynomial neural network (PNN) can be used to detect threshold signals in chaotic backgrounds. The PNN can be trained to predict a chaotic background and detect threshold signals by subtracting a predicted background from the signal plus background. By using a solution of the Mackey-Glass equation as a chaotic background, we synthesize a nonlinear PNN processor that produces a threshold signal-to-background improvement of over 20 dB [1].

The origin of polynomial neural networks can be traced to the work of Ivakhnenko in the Soviet Union [2]. Ivakhnenko developed an algorithm called GMDH (group method of data handling) for the modeling of communication and control of complex systems. The GMDH algorithm is a technique for nonparametric multiple regression that uses an approximate solution of the complete Kolmogorov-Gabor polynomial. The complete Kolmogorov-Gabor polynomial, which describes the relationship between an output y and an input vector $\{x_i, x_j, x_k, \cdots\}$, can be written as

$$y = a + \sum_{i=1}^{m} b_i x_i + \sum_{i=1}^{m}\sum_{j=1}^{m} c_{ij} x_i x_j + \sum_{i=1}^{m}\sum_{j=1}^{m}\sum_{k=1}^{m} d_{ijk} x_i x_j x_k + \ldots \quad (1)$$

In computer implementations of the GMDH algorithm, the Kolmogorov-Gabor polynomial in Eq. (1) is replaced by a composition of lower order polynomials. For computational purposes, the single, double, and triple elements of the PNN can be represented by third-order polynomial transfer functions S, D, and T, as shown in Fig. 5.

The architecture of Fig. 5 describes a neural network with nodes (neurons) having a polynomial transfer function instead of the usual sigmoid. Therefore, the PNN is a neural network with the sigmoid transfer function replaced by a Taylor series centered about the origin. We note that in the limit where the nonlinear terms in S, D, and T are zero, the PNN reduces to a linear, feed-forward neural network.

Mackey-Glass Delay Differential Equation: As an example of a chaotic time series suitable for simulation of a chaotic background, we

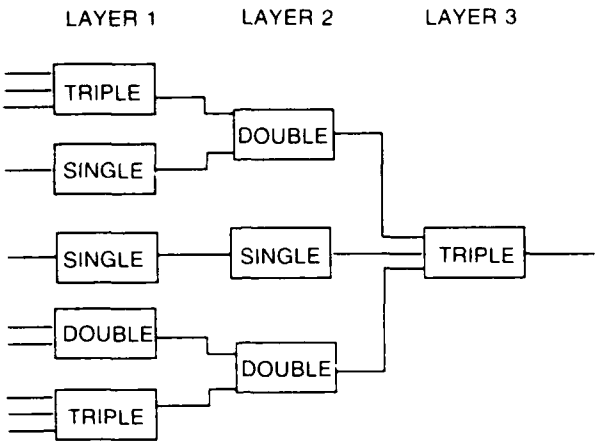

$$S = u_0 + u_1x_1 + u_2x_1^2 + u_3x_1^3$$

$$D = v_0 + v_1x_1 + v_2x_2 + v_3x_1^2 + v_4x_2^2 + v_5x_1x_2 + v_6x_1^3 + v_7x_2^3$$

$$T = w_0 + w_1x_1 + w_2x_2 + w_3x_3 + w_4x_1^2 + w_5x_2^2 + w_6x_3^2 + w_7x_1x_2 + w_8x_1x_3 + w_9x_2x_3 + w_{10}x_1x_2x_3 + w_{11}x_1^3 + w_{12}x_2^3 + w_{13}x_3^3$$

Fig. 5 — Three-layer PNN with 10 inputs, 1 output

use a first-order, nonlinear delay differential equation introduced by Mackey and Glass [3].

$$\frac{dx(t)}{dt} = \frac{ax(t - \tau)}{1 + x(t - \tau)^c} - bx(t). \quad (2)$$

Equation 2, the Mackey-Glass equation, describes the flow of blood in the human physiological control system. The parameter τ represents the delay between the initiation of cellular production in the bone marrow and the release of mature cells into the blood.

Detection of a Threshold Pulse Signal in a Chaotic Background: We demonstrate that it is possible to train a PNN to detect a pulse signal buried in a chaotic background by subtracting the predicted background from the signal plus background. Figure 6(a) shows a solution of the Mackey-Glass equation for $\tau = 30$, $a = 0.2$, $b = 0.1$, and $c = 10$. By using this solution as a chaotic background, we synthesized a predictive PNN with a set of rules that balance complexity and accuracy [1]. The process of capturing the information contained within a finite dimensional time series, which is called time delay imbedding, was put on a firm mathematical foundation by Takens [4]. Briefly, if $x_0(t)$ represents the time series, we construct $\{x_0(t), x_0(t + \tau), x_0(t + \tau), x_0(t + 2\tau), x_0(t + 3\tau), \ldots, x_0(t + (n - 1)\tau)\}$. Takens showed that if r is the dimension of the manifold containing the invariant subset where trajectories stay bounded (i.e., the 'attractor'), then $n = 2r + 1$ is sufficient to imbed the attractor. For this simulation, time delays of 6 units over a total delay range of 42 units were chosen together with a prediction time of 6 units. Delay values of 6, 30, and 36 units were selected for the network synthesis procedure. The sample set of 3000 was arbitrarily split into a training set of 2100 samples and an evaluation set of 900 samples. The results indicated that the standard deviation of the PNN prediction error was about 2%.

Figure 6(b) shows an input pulse signal with a peak value of 0.1. This signal was embedded in a chaotic background, as shown in Fig. 6(c). The statistics of the background are a minimum value of 0.22 and a maximum value of 1.36, with an average level of 0.9. On the basis of these statistics, the signal-to-background ratio is ≈ -20 dB. Processing consisted of subtracting the predicted PNN background (6 units prediction) from the input background plus signal shown in Fig. 6(c). Background samples were generated as a different realization of the chaotic process and did not include samples used for network training. Figure 7(b) shows the PNN processor output. For reference, the input pulse signal is shown in Fig. 7(a). Figure 7(c) shows the processor output on an expanded scale, indicating clearly the presence of the signal. We estimate that the PNN processor has produced an improved signal-to-background ratio of at least 20 dB. Note that by comparing Fig. 7(b) with Fig. 6(a), the PNN output is significantly 'whiter' than the input, as expected.

Summary: We have demonstrated by means of simulation that nonlinear signal processing

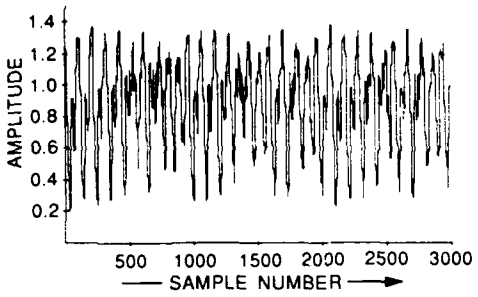

Fig. 6(a) — Mackey–Glass chaotic background (τ = 30)

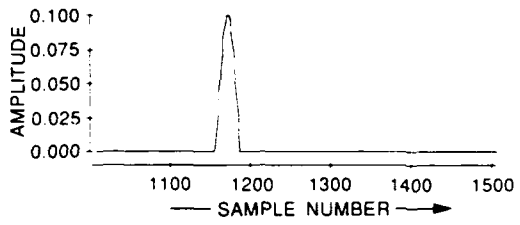

Fig. 6(b) — Input pulse signal

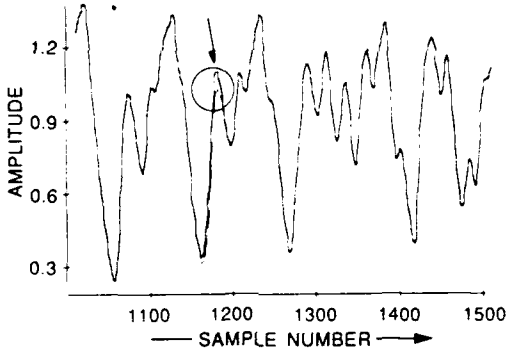

Fig. 6(c) — Pulse signal embedded in a chaotic background

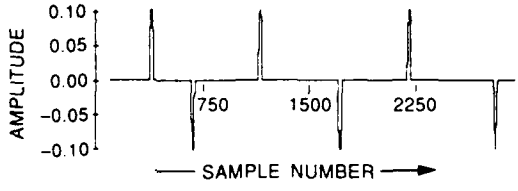

Fig. 7(a) — Input pulse signal

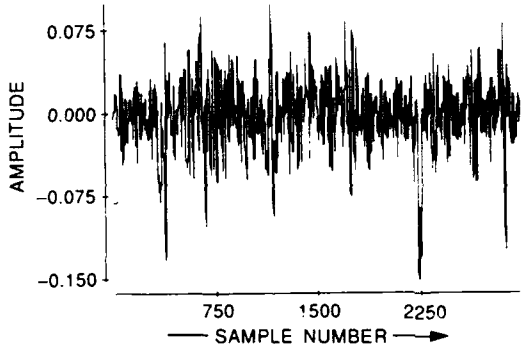

Fig. 7(b) — PNN processor output

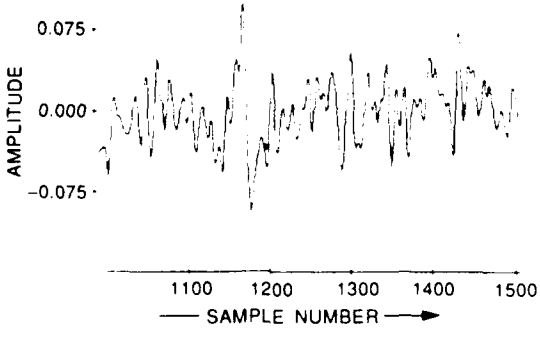

Fig. 7(c) — PNN processor output (expanded scale)

based on PNN synthesis has a potential value in the improved detection of threshold signals in chaotic backgrounds. The PNN synthesis method should be applicable in a variety of natural backgrounds, such as radar clutter and underwater acoustic signal processing. The extension of these methods to multidimensional signal processing (e.g., image processing) is the subject of ongoing research.

References

1. S. Gardner, "Polynomial Neural Nets for Signal and Image Processing in Chaotic Backgrounds," Proceedings of the SPIE International Symposium on Optical Science and Engineering, San Diego, California, July 1991.

2. A. Ivakhnenko, *Self Organizing Methods in Modeling*, S.J. Farlow, ed. (Marcel Dekker, New York, 1984), Ch. 5, pp. 105–119.

3. M.C. Mackey and L. Glass, "Oscillation and Chaos in Physiological Control Systems," *Science* **197**, p. 287 (1977).

4. F. Takens, *Dynamical Systems and Turbulence*, D. Rank and L.S. Young, eds. (Springer, New York, 1981). ■

Magnetospheric Barium Cloud Simulation
Computer Graphics, *Third Place (Tie)*
Joseph D. Huba

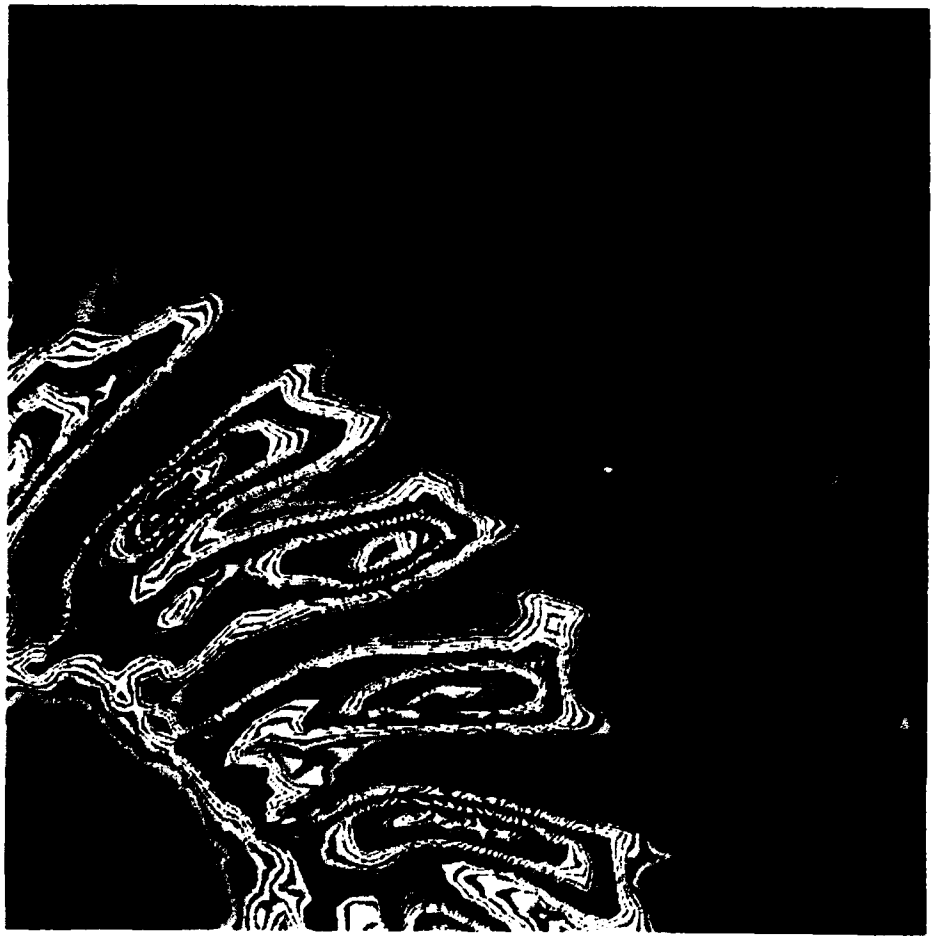

Magnetospheric Barium Cloud Simulation
Computer Graphics, *Third Place (Tie)*
Joseph D. Huba
Plasma Physics Division

As part of the NASA CRRES mission, a series of high altitude barium releases has recently been made. The scientific objectives of these releases are to better understand the formation of diamagnetic cavitities, the coupling of the barium plasma to the ambient plasma and magnetic field, and the attendant plasma instabilities associated with this coupling. This picture is a color-coded representation of the barium ion density of one of the releases and is based on a 2D MHD simulation code. Large-scale structuring of the barium shell is clearly evident, which is consistent with observational data.

MARINE TECHNOLOGY

181 **High Resolution Remote Sensing**
Richard P. Mied, Farid Askari, George O. Marmorino, Gaspar R. Valenzuela, and Dennis B. Trizna,

183 **Atmospheric Aerosol Size Distributions in the Marine Boundary Layer**
James W. Fitzgerald and William A. Hoppel

187 **Acoustic Backscattering from the Sea Surface**
Peter M. Ogden and Fred T. Erskine

High Resolution Remote Sensing

R.P. Mied, F. Askari, G.O. Marmorino, and G.R. Valenzuela
Center for Advanced Space Sensing
and
D.B. Trizna
Radar Division

Background: Ocean remote sensing provides the ability to observe events on the ocean surface and challenges us to infer the underlying physics from the remotely sensed images. Of particular interest to the Navy is the interpretation of submesoscale near-surface motions, i.e., those having horizontal length scales of 100 m to 10 km. This requires meeting a two-fold objective: understanding the fluid dynamics of these motions as well as the radar imaging mechanisms. To address these questions, the High Resolution Remote Sensing Accelerated Research Initiative (FY91-95) employs the disciplines of remote sensing, oceanography, meteorology, and microlayer physics. About 30 investigators from three NRL organizations (the Atmospheric/Ocean Sensing Branch, the Imaging Systems and Research Branch, and the Radar Division's Propagation Staff) and the ONR Remote Sensing Program are participants.

Program Focus: Two field experiments provide a focus for the program. The first experiment was conducted during 10 to 25 September 1991, off Cape Hatteras, North Carolina. That experiment employed synthetic and real aperture radars (SAR and RAR) as well as a variety of in-situ oceanographic and meteorological instruments to sample the near-surface ocean and the marine atmospheric boundary layer. Measurements were made at the inshore edge of the Gulf Stream, an area that is rich in submesoscale current features and provides a persistent ocean feature where the effects of current shear, thermal jumps, and changing drag coefficient for the atmospheric boundary layer can be studied at one convenient location. A secondary focus was the adjacent continental shelf, where previous SAR images show an abundance of apparent biogenic surfactant slicks and high backscatter curvilinear filaments. Both low and high wind conditions were sampled.

An example of one such high backscatter filament (Fig. 1) was sampled on 17 September on this continental shelf. The area of strongest return is the wavy red filament oriented east-west and having a width of no more than 100 m. In addition, we see that the corrugations are not smooth, but cusped. They have a typical length scale of 1 km, but there are areas (e.g., at the 9-km azimuth distance mark) where the spacing between cusps is $\leq$ 200 m. The waviness is possibly caused by an instability in the frontal flow. Figure 2 shows a RAR image of the immediate area taken for near grazing angles by the X-band HH polarized radar aboard the USNS *Bartlett*. This plan view of normalized backscatter shows two interesting phenomena. First, the region to the south of the front has higher average backscatter than the region to the north. This is because the ambient wave field is of greater amplitude toward the south where the incoming current (measured with an acoustic current Doppler profiler) provides a convergence and flows under the fluid to the north. The surface waves conserve the action spectral density by steepening. Second, two cusps of the type in Fig. 1 are also seen in the RAR image. The near-surface temperature structure of the local water column (Fig. 3) was obtained with a conductivity-temperature-depth (CTD) instrument and shows a layer of lighter, density-stratified fluid overlying a warmer, saltier, heavier layer of nearly homogeneous fluid; the overall depth of the water is 32 m. Water entering from the left is subducted under the lighter fluid.

Current Research Directions: Although convergence fronts are not uncommon, details of their dynamics remain to be discovered. In particular, the origin of this feature and its relation to the nearby Gulf Stream is obscure. Moreover, the sources of the cusps in Figs. 1 and 2 and the

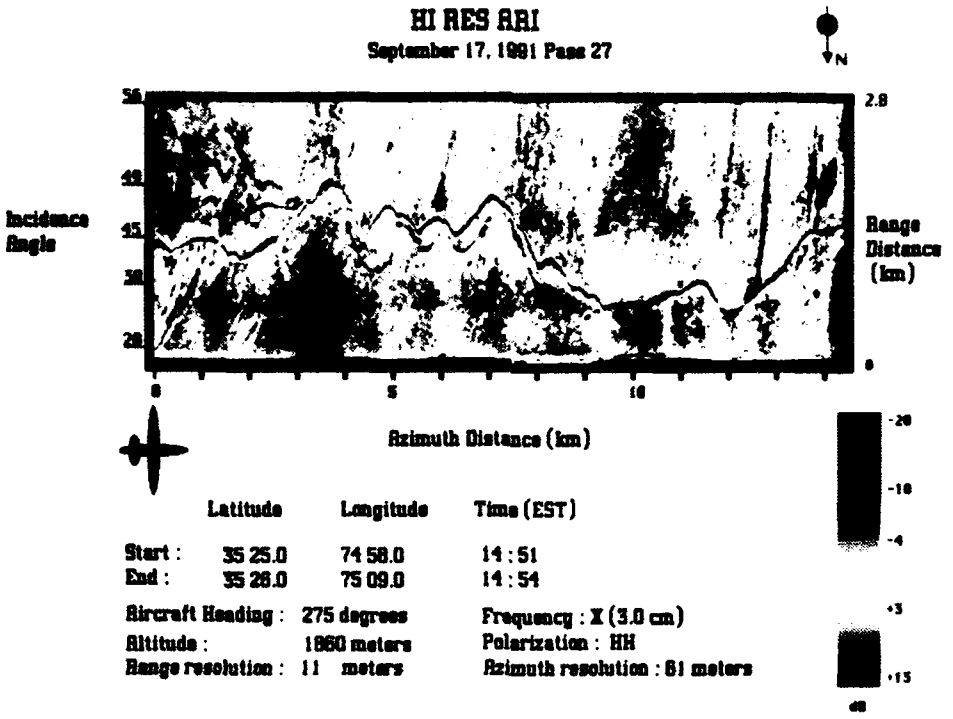

Fig. 1 — A RAR image of the high backscatter filament (shown in red) on the continental shelf. The scale is in decibels (relative power) and is given in the color bar. The paired blue/red areas at the 3.5 and 10 km azimuth *distance points are caused by airplane roll.* The smaller-width blue streaks represent areas of low backscatter and are likely due to the presence of surfactants. North is indicated by the small arrow, and the direction of airplane flight is given by the aircraft outline.

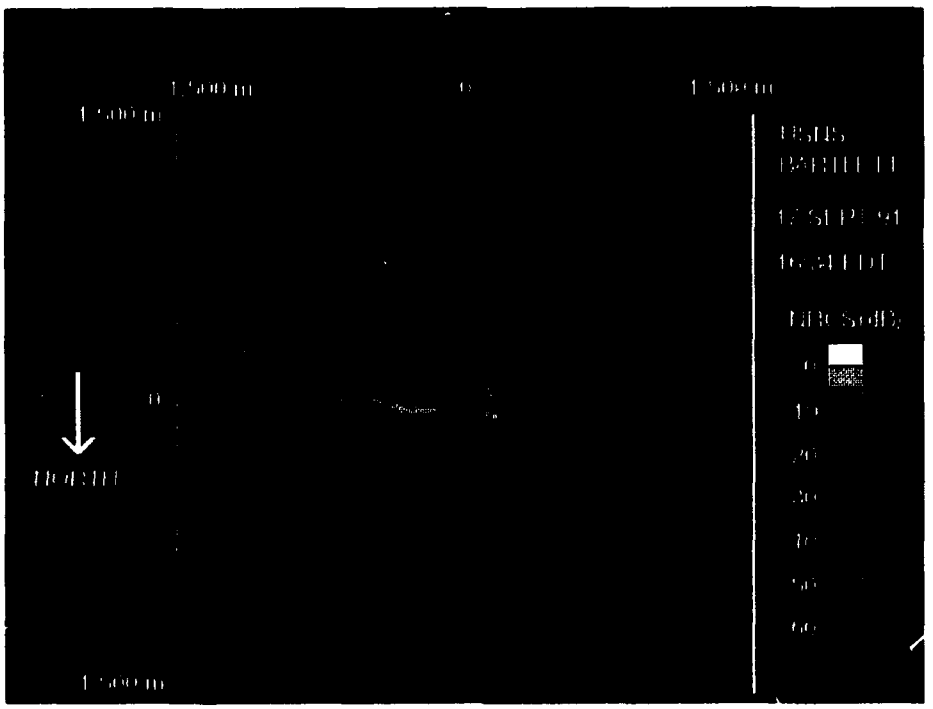

Fig. 2 — The shipborne X-band, HH polarized grazing angle radar image of the convergence front. The brightest areas indicate high backscatter.

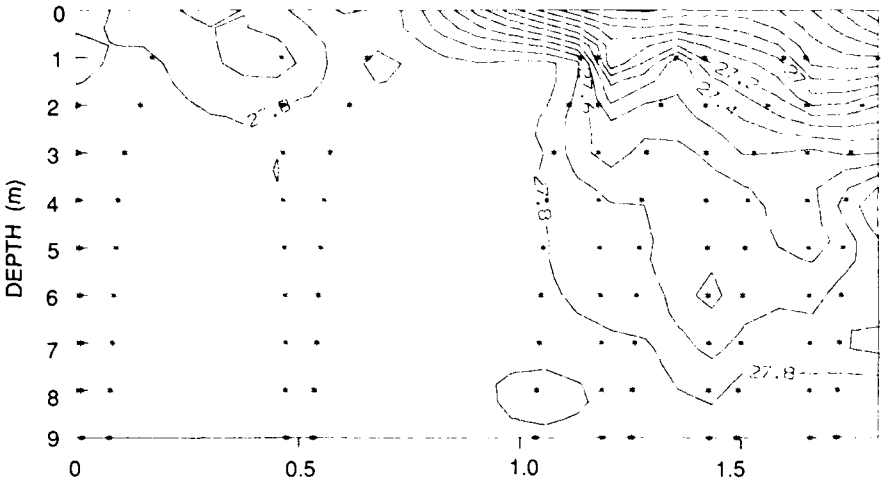

Fig. 3 — A vertical temperature section based on CTD measurements (shown by asterisks) made with the ship underway. A cold but buoyant lens of water (on the right) moves to the left relative to the ambient isothermal fluid (on the left and below 9-m depth). The total water depth is 32 m. The edge of the lens corresponds to the high backscatter areas seen in Figs. 1 and 2.

blue-colored streakiness (possibly related to the presence of surfactants) are not known. In addition, the flow around the cusps and underneath the front provides a compact three-dimensional velocity field that serves as a laboratory in which to study strongly nonlinear wave/current interactions, wave breaking, and the role of surfactants as each contributes to the nature of the backscattered electromagnetic field. In particular, mechanisms responsible for large incidence angle scattering are poorly understood, as are the effects of surface wave nonlinearities on the Doppler spectrum. The experiment affords us the opportunity to assess existing hydrodynamic and electromagnetic theories with the experimental data and to refine those theories where necessary.

Future Research Directions: A second experiment will be conducted in mid-1993 in higher winds in the open ocean. These conditions should provide for removal of the surfactant by vertical mixing and give rise to a richer, more fully developed surface wave spectrum. This would be conducive to a broadening of the Doppler spectrum and would yield a more complicated SAR representation that is more difficult to interpret. The timing of this second experiment will allow for a refinement of theories of the ocean dynamics, wave/current interactions, and EM scattering in light of the present experiment.

Acknowledgments: Additional NRL researchers who have made significant contributions to the program are S. Chubb, A. Cooper, R. Hill, J. Kaiser, W. Keller, G. Lindemann, C. Shen, C. Trump, and L. Wetzel.

[Sponsored by ONR] ■

Atmospheric Aerosol Size Distributions in the Marine Boundary Layer

J.W. Fitzgerald and W.A. Hoppel
Center for Advanced Space Sensing

Understanding the sources, sinks, and size distribution of aerosols in the marine atmosphere is important to the Navy for three reasons: first for evaluating and predicting the effects of aerosols on the extinction of signals from electro-optical systems. Second, to the climate change community for evaluating the effect that changing aerosol concentrations have on radiative transfer, either directly, or more importantly, through the aerosol's influence on the size and number of cloud

droplets and hence, on cloud radiative properties; third, to atmospheric chemists for understanding the removal of trace gases by gas-to-particle conversion.

Background: Marine aerosols were previously thought to be the remnants of aerosols formed over continental regions and advected into the marine environment with the addition of sea-salt aerosol generated by bursting air bubbles (from whitecaps) and ocean spray. Optical methods have long been available to measure particles larger than 0.5 μm radius, either by impaction of particles and subsequent microscopic examination or by light-scattering, optical particle spectrometers. Optical and chemical identification of particles larger than 0.5 μm are consistent with the assumption that these larger particles are of continental or sea-surface origin.

It has been known for decades, from expansion cloud chamber measurements of total particle concentrations, that particles smaller than 0.5 μm are far more numerous than larger particles, even in remote ocean regions. Until new measurement techniques were developed at NRL, efforts to measure the size distribution of these submicron particles were unsuccessful because they were too small for optical detection and too volatile to be detected in the high vacuum environment of the electron microscope.

Aerosol Size Distributions: In the early 1980s, NRL developed the differential mobility size spectrometer (DMA) based on measuring the mobility of the charged fraction of aerosol particles. This instrument made it possible to achieve accurate in-situ measurements of the aerosol size distribution in the 0.005 to 0.5 μm radius range. In the mid-1980s, shipboard measurements of the aerosol size distribution were made over the remote Atlantic and Pacific Oceans by using this new instrument.

Figure 4 shows typical size distributions observed over the remote tropical Atlantic and Pacific Oceans [1]. From these data and complementary data on the volatility and chemistry

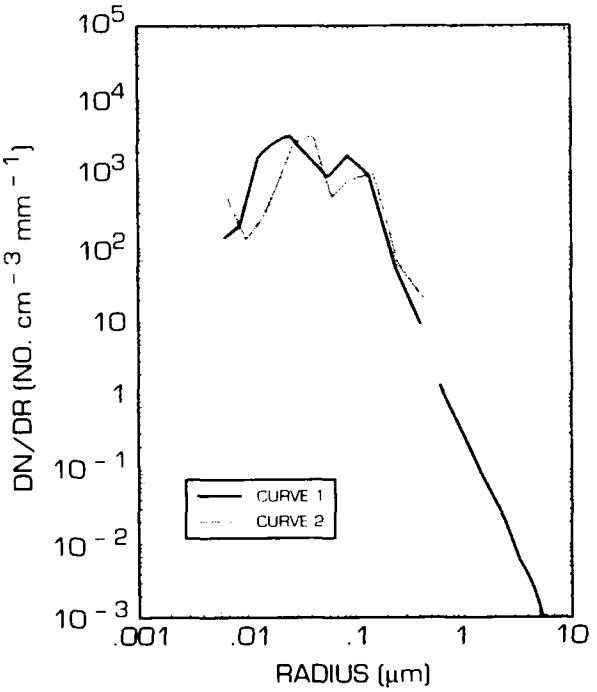

Fig. 4 — Typical size distributions measured in the remote tropical Atlantic (1) and tropical Pacific (2). Particles larger than 0.5 μm are measured by optical means; smaller particles are measured by the DMA.

of the particles, it has been deduced that particles smaller than about 0.3 μm radius are primarily sulfate (sulfuric acid and ammonium sulfate), with only a small fraction being sea-salt particles. A major effort has been made to understand the origin of these sulfate particles and to explain the biomodal character of the submicron size distributions shown in Fig. 4. The data indicate that these particles are most likely formed spontaneously from the gas phase by homogeneous nucleation of trace condensable species, such as sulfuric acid vapor. The newly formed embryos then grow slowly by condensation until they attain a size observable by the DMA. The source of the sulfate is now believed to be dimethyl sulfide (DMS), an insoluble gas given off by phytoplankton. DMS is rapidly photolyzed in the atmosphere, resulting in the formatin of SO_2, methanesulfonic acid, and H_2SO_4, the latter arising from the photolysis of SO_2. Recent measurements by others of the global DMS flux from the oceans have shown that it rivals in magnitude the global input of SO_2 from anthropogenic sources.

The explanation of the bimodal character of the size distribution shown in Fig. 4 initially posed a problem to NRL scientists. After consideration of four possible mechanisms that might cause the bimodal character, it became evident from aerosol modeling that this bimodality could best be explained by aerosol transformations that take place in nonprecipitating clouds. When air enters a cloud, a subset of the aerosol population called cloud condensation nuclei (CCN) are activated and become cloud water droplets. Cloud droplets absorb soluable trace gases and oxidants; subsequent chemical reactions between these reactants (e.g., sulfur dioxide and ozone) form sulfates that remain as additional residue after dissipation of the cloud and evaporation of the droplets. The additional residue acquired during the cloud phase increases the mass of the CCN, causing the observed separation in the size distribution between the smaller, unactivated particles and the CCN. Since only about one out of ten clouds develops precipitation, and since precipitation scavenging is the primary process that removes CCN-sized particles from the atmosphere, CCN are processed through many nonprecipitating clouds, on average, before being removed by precipitation.

Marine Aerosol Model: A numerical model describing aerosol dynamics and gas-phase chemistry in the marine boundary layer has been developed as a useful tool to understand how different aerosol processes affect the aerosol size distribution and to study the sensitivity of the size distribution to input parameters, such as the DMS flux rate into the boundary layer. The model simulates all of the processes believed to influence the marine aerosol and predicts the temporal evolution of the aerosol size distribution as well as the concentrations of the important trace gases, such as DMS, SO_2, and H_2SO_4.

Figures 5 and 6 are model simulations that show the important effect that precipitation scavenging of aerosols has on the size distribution.

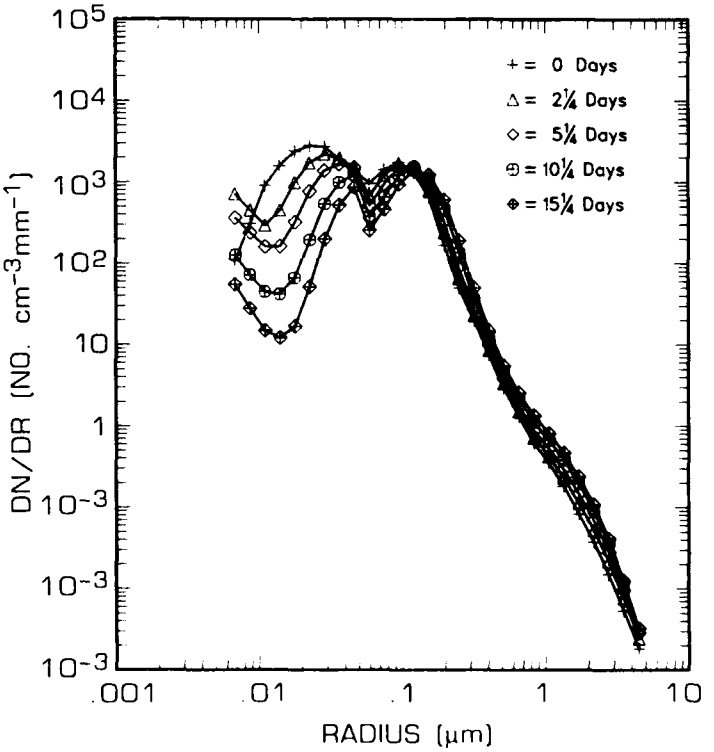

Fig. 5 — Model predicted evolution of the marine aerosol size distribution over 15-day period when there is no precipitation scavenging of aerosol

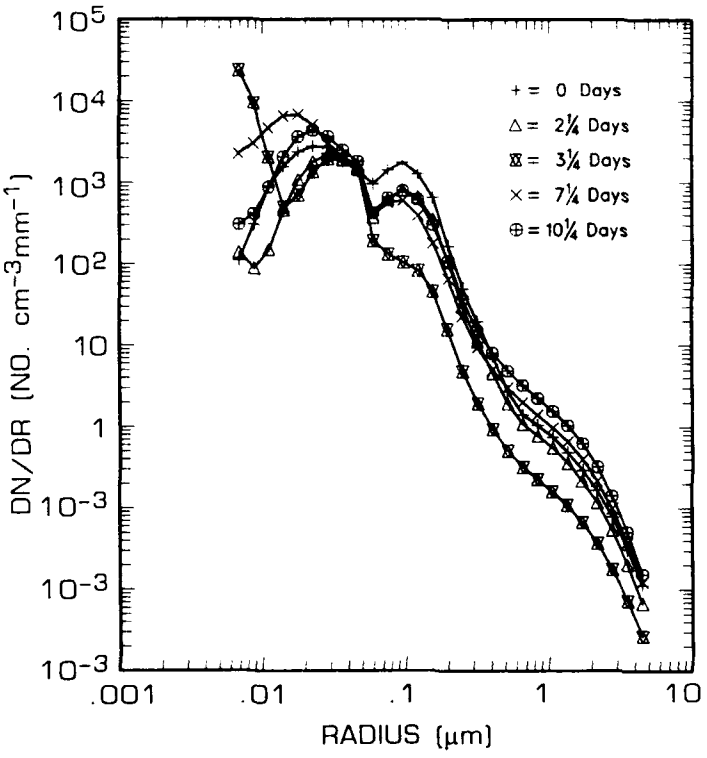

Fig. 6 — Model predicted evolution of the size distribution over 10-day period when there is precipitation scavenging of aerosol on day 3

The initial distribution (0 days) is typical of the size distributions measured over the remote, subtropical oceans. Figure 5 shows how the size distribution would evolve over 15 days when there is no removal of CCN ($r > 0.05$ μm) by precipitation. In this case, condensation of H_2SO_4 vapor on particles is a sufficiently large sink of H_2SO_4 (due to the total surface area of the particles) that the homogeneous nucleation rate of new sulfuric acid particles ($r = 0.006$ μm) is not high enough to compensate for the decrease in the concentration of small ($r < 0.05$ μm) particles due to coagulation and growth by condensation to larger sizes. The model predicts a large depletion of small particles within 10 days, which is not in accord with observations. Figure 6 shows, however, that if there is scavenging of particles by precipitation (in this case, on day 3 of simulation), there is a decrease in the sink of H_2SO_4 vapor due to condensation, ambient H_2SO_4 concentrations, and nucleation rates increase, and the population of small particles can be sustained. When precipitation ceases, the generation of sea-salt particles at the surface starts to replenish the particles removed by precipitation, and H_2SO_4 vapor concentrations and nucleation rates begin to decrease. The modeling suggests that periodic "nucleation events," perhaps as a result of the cleansing of the air by precipitation, are necessary to sustain the population of small particles.

Summary: Through the development of new measurement techniques and sophisticated aerosol models, NRL scientists have made important advances to our knowledge of the size distribution of submicron aerosol particles over the ocean and to our understanding of the atmospheric processes that shape the size distribution. The advances improve our capability to predict marine aerosol characteristics and will help to quantify the relationship between the source strength of DMS gas emitted by the ocean and the number of cloud active nuclei. The quantification of this relationship is crucial to evaluate the climatic

effects of changes in DMS emissions from the ocean, a subject of current scientific interest.

[Sponsored by ONR]

Reference

1. W.A. Hoppel, J.W. Fitzgerald, G.M. Frick, R.E. Larson, and E.J. Mack, "Aerosol Size Distributions and Optical Properties Found in the Marine Boundary Layer over the Atlantic Ocean," *J. Geophys. Res.* **95,** 3659 (1990). ■

Acoustic Backscattering from the Sea Surface

P.M. Ogden and F.T. Erskine
Acoustics Division

Acoustic reverberation from the sea surface is one of the principal sources of background noise for low-frequency active sonar systems. When acoustic energy strikes the sea surface, most of the energy is reflected in the specular direction. But because the ocean surface is rough, some of the energy is scattered in all directions—in particular, some is scattered back toward the sonar system. Under some environmental conditions, this backscattered reverberation can be a significant source of interference for the sonar. The quantity that describes the amount of backscattering is scattering strength, which is the ratio of the acoustic intensity scattered in a particular direction to the incident intensity. Scattering strengths are measured as a function of grazing angle (the angle of the incident energy with respect to the surface) and environmental descriptors of the roughness of the surface, such as wind speed. These scattering strength values are then entered into computer models that predict the amount of reverberation that a particular sonar system will see under a given set of environmental conditions.

In virtually all Navy depictions of reverberations, surface scattering is modeled through the use of measured results obtained by Chapman and Harris [1] in 1962. These results were obtained at high grazing angles (30°) over a brief period of time and have since been extrapolated for use in frequency, grazing angle, and wind speed regimes, where the validity of the extrapolations is unknown. What is known, however, is that theoretical predictions of scattering from rough surfaces is in substantial disagreement with the Chapman–Harris results.

Scattering Strength Measurements: In a series of at-sea tests carried out in a variety of environmental conditions, we used signal underwater sound (SUS) explosive charges and a horizontal line array receiver to measure surface scattering strengths over a range of frequencies from 70 to 1000 Hz and a range of grazing angles from 30° down to about 5°. During each experiment, SUS charges are deployed from the aft end of the research ship, from where they descend to their preset detonation depth. At the time of detonation, the motion of the research ship has pulled the line array directly over the SUS charge, thereby achieving a nearly monostatic geometry. We then combine the surface returns that result from the explosion with geometrical factors, such as transmission loss and grazing angle, to get scattering strengths as a function of grazing angle, frequency, and sea surface conditions. Figure 7 shows some of these results. These scattering strengths were measured for a wind speed of 28 knots and a sea state of about 4.5. The figure shows scattering strengths for a range of frequencies, and it also shows three reference curves: Chapman–Harris curves for the highest and lowest frequencies measured and a theoretical prediction using a perturbation theory that should be roughly appropriate for all frequencies measured.

Scattering Mechanisms: After measuring scattering strengths over a wide range of frequencies and sea surface conditions, it became clear that more than one physical mechanism is responsible for surface scattering. The results of many SUS tests were combined to produce the chart shown in Fig. 8. This chart divides surface scatter results into three regimes. The first applies

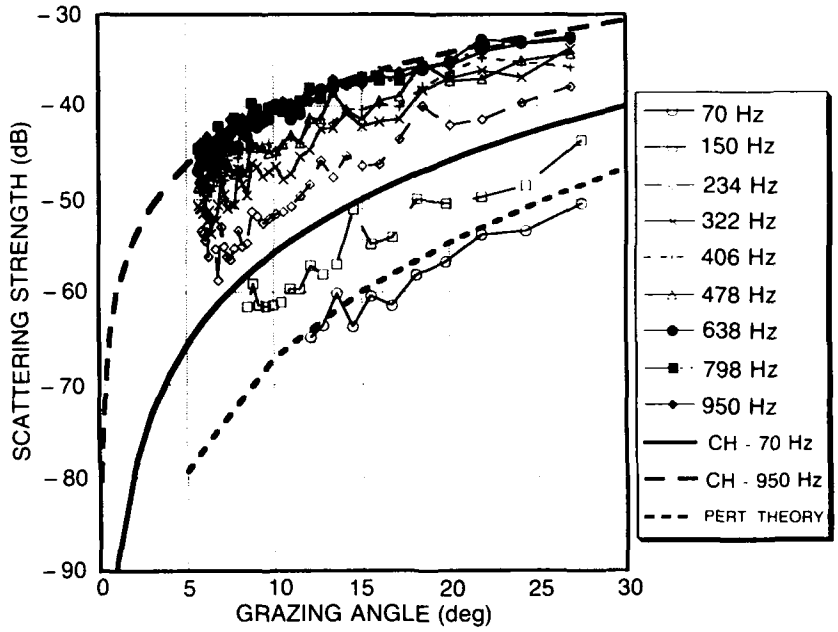

Fig. 7 — Measured surface scattering strengths for a wind speed of 28 knots and a sea state of 4.5

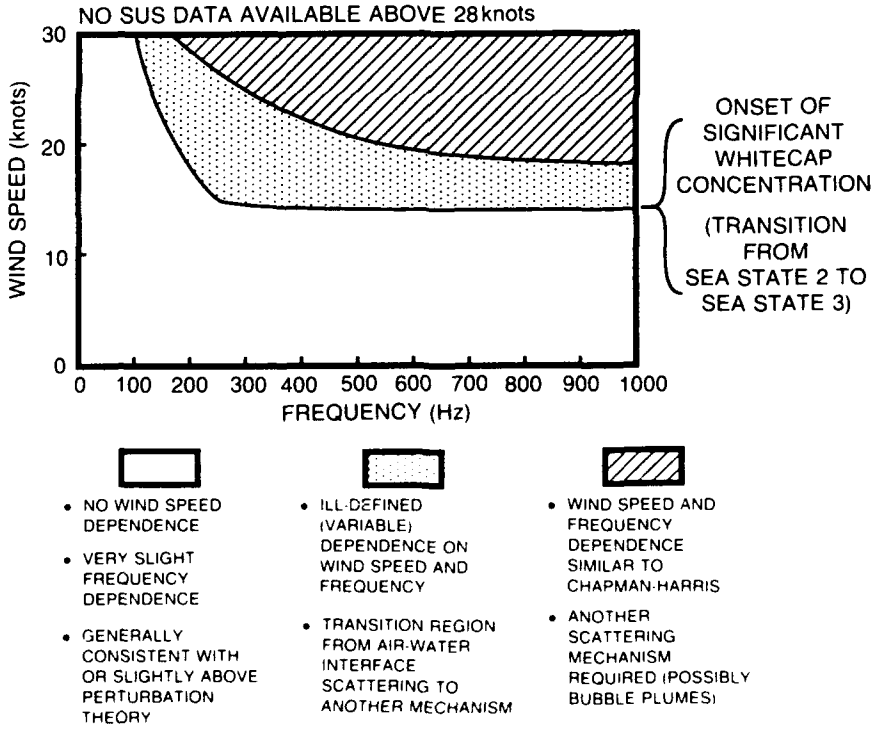

Fig. 8 — Surface scattering mechanisms that dominate for a particular choice of frequency and sea surface conditions

for relatively calm seas at high frequencies and for increasingly rougher seas as frequency decreases. In this regime, the predictions of perturbation theory as it is applied to scattering from rough surfaces appears to describe adequately the surface scattering returns (as in the lowest-frequency case in Fig. 7, for example). In contrast, at high sea states and high frequencies, our scattering results are in reasonable accord with Chapman-Harris. It is widely believed that scattering in this regime is caused by the presence of subsurface bubble clouds that can significantly enhance reverberation from the near-surface over that arising from rough-surface scattering. The third regime is a transition region between rough-surface scattering and subsurface bubble scattering. For frequencies and surface conditions in this regime, scattering strengths are more difficult to predict and appear to depend on the details of the wind history in a not-yet-understood way.

[Sponsored by SPAWAR]

Reference

1. R.P. Chapman and J.H. Harris, "Surface Backscattering Strengths Measured with Explosive Sound Sources," *J. Acoust. Soc. Am.* **34**, 1592 (1962). ■

Waves in Transit—Ducted Sound Waves Broken Up by Dispersed Scatterers

Computer Graphics, *Third Place (Tie)*

Rudolph A. Krutar

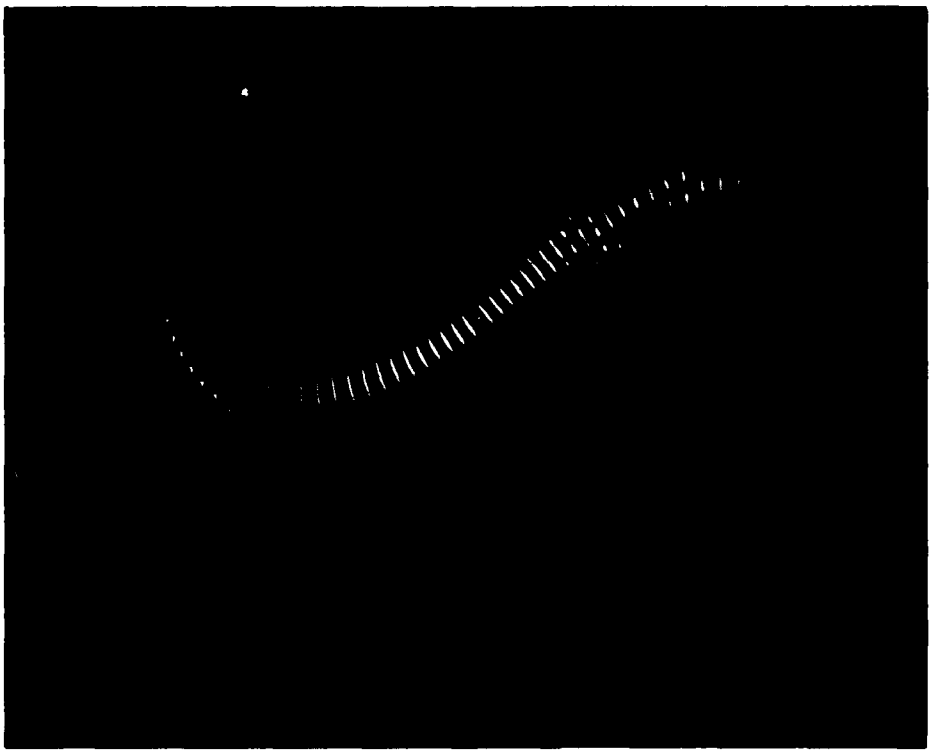

Waves in Transit—Ducted Sound Waves Broken Up by Dispersed Scatterers
Computer Graphics, *Third Place (Tie)*
Rudolph A. Krutar
Acoustics Division

This simulation was produced by an acoustic-wave model developed on the Connection Machine. The model is a cellular automaton, a computational system that generates global behavior from the interaction of the immediate neighbors of each point in the field to be modeled. In the acoustic wave model, the rule that is broadcast across all points is a central finite difference solution to the wave equation. The model produces the time evolution of the field and the illustration is a snapshot at some point in time. The power of the cellular automaton method is the ability to handle complexity. Once a phenomenon is correctly modeled, it can be replicated anywhere in the field—gathered into irregular shapes or dispersed as individual points. In this illustration, a beam of sound propagating in a duct is scattered by pressure release points. The presence of scatterers in a variable environment makes the problem difficult to solve by more traditional computational or analytical methods.

MATERIALS SCIENCE AND TECHNOLOGY

193 **Vertex Simulation of Two-dimensional Grain Growth**
Steven P. Marsh, Robert A. Masumura, and Chandra S. Pande

195 **Structural Mapping of Ultrathin Films**
Yves U. Idzerda, Gary A. Prinz, and David E. Ramaker

196 **A Process to Make Ultrafine Metal Powders**
Khershed P. Cooper and Jack D. Ayers

200 **Advances in the State-of-the-art Growth of InSb by Using Molecular Beam Epitaxy and Organometallic Vapor Phase Epitaxy**
D. Kurt Gaskill, Phillip E. Thompson, John L. Davis, and Gregory T. Stauf

Vertex Simulation of Two-dimensional Grain Growth

S.P. Marsh, R.A. Masumura, and C.S. P nde
Materials Science and Technology Division

The properties of a material are not determined solely by the elements and compounds from which they are made; the microstructure also plays a key role in influencing the performance of a given material component. Virtually all crystalline materials are composed of an array of tiny crystals packed together to form the bulk material. The sizes and shapes of these grains are determined by the way the material was formed as well as subsequent thermal and mechanical processing. Grain growth, in which the mean grain size of a material increases, is driven by a reduction in the excess free energy associated with the total grain boundary area. The ability to model and predict the dynamics of grain growth represents a key opportunity to optimize and control the properties of a wide variety of technologically important materials. An overview of the physics of grain growth and of various modeling approaches is presented in Ref. 1.

Thin-film Grain Networks: Many processes of interest involve the deposition of thin films on a substrate by various methods, including chemical vapor deposition and epitaxial growth. The grain structure in these films appears as a plane-filling array of polygonal domains with slightly curved boundaries. The lines separating adjacent grains are the grain boundaries that pass vertically through the film, so the structure can be treated as a two-dimensional array. These boundaries meet at corners (or vertices) in groups of three. The dynamics of the grain structure result from a complex interaction in which the curvatures tend to flatten, and the angles between adjacent edges simultaneously tend to approach 120° at each vertex.

Simulation Approach: Computer modeling of grain growth in thin films requires a description of the geometry of the grain array and how it is continuously related to the dynamical behavior. We are developing a powerful approach based on the motion of the vertices in the structure. The fundamental information of grain size and shapes is specified by tracking the location of each vertex in the structure, as well as by the identity of the three neighboring vertices and of the three grains that meet at the vertex. However, this information is not enough to determine the dynamical behavior of the grains. We have developed a novel geometric algorithm based on observations in real structures to calculate implicitly the boundary curvatures from the locations of vertices adjacent to each boundary.

The instantaneous velocity of each vertex is determined from the sum of the forces imposed by the curvature of the adjacent boundaries. These motions are then applied simultaneously in a single time-step. One advantage of the vertex simulation is that the time-step is scaled to the average vertex velocity in the structure. This maintains the computational efficiency of the simulation, even though the grain growth slows down in real time as the average grain size increases. Furthermore, the computational time required for this method increases linearly with the number of vertices in the network. This allows us to simulate large numbers of grains with only moderate increases in computational time.

Topology and Dynamics: Two fundamental topological operations can occur during two-dimensional grain growth. The first is elimination, illustrated in Fig. 1(a), where a three-sided grain disappears and is replaced by a single vertex. The second process, illustrated in Fig. 1(b) is "neighbor switching." This results when two adjacent vertices meet and immediately separate to create a new boundary. The grains in contact across this boundary change during this process. Both of these events have been observed in real grain structures. The simulation accounts for these events by manipulating the identities of neighboring grains and vertices appropriately when two vertices meet during a time-step. More

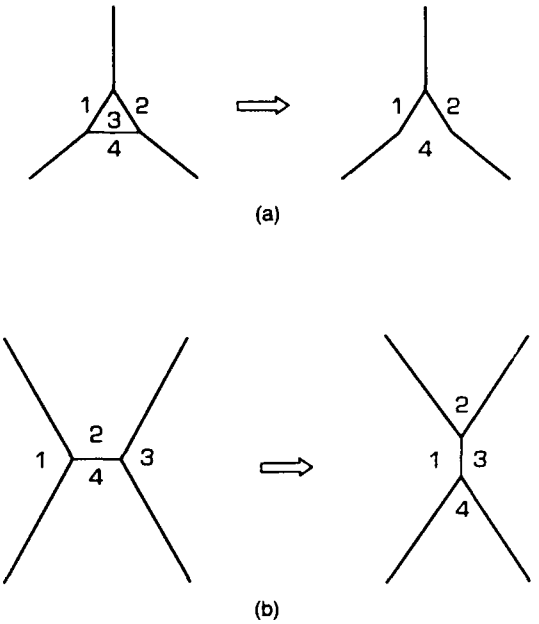

Fig. 1 — (a) A grain disappearance event, and (b) a grain "switching" event. Note that grains 2 and 4 are initially in contact, and grains 1 and 3 are in contact after the switch occurs.

complex interactions (such as the collapse of a four-sided grain to a single edge) can be obtained as a combination of these two elementary processes.

The initial grain structure in the simulation is set up in a square cell with periodic boundary conditions. This standard technique mimics an infinite structure and avoids edge effects. An example of a typical structure is shown in Fig. 2(a). The dark square is the unit cell, and the periodic boundaries match grains extending beyond the cell edge to those entering from the other side. The boundary curvatures are not shown in this figure, which only illustrates the location and connectivity of the vertex network. This structure was allowed to aged for about 150 time-steps. The aged structure, shown in Fig. 2(b), is a bit more equiaxed (the grains are less elongated), and a few grains have disappeared. This trend is typical during grain growth, and the change in structure over this relatively short simulation further suggests that the simulation approach presented here is extremely efficient.

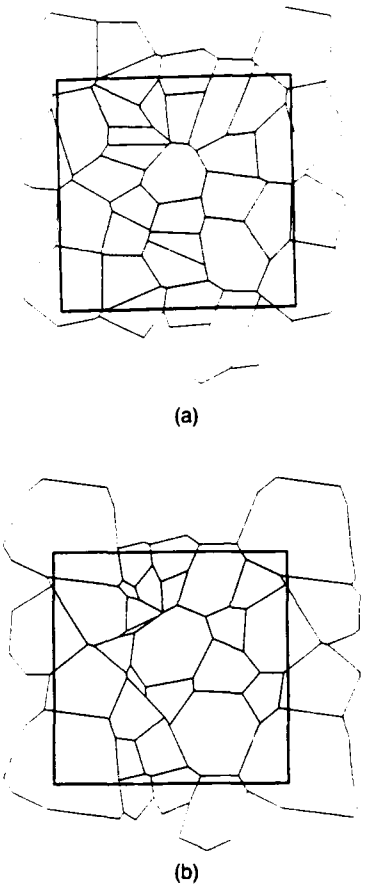

Fig. 2 — (a) The initial grain network used in the simulation, showing the periodic boundary condition, and (b) the same grain network after 150 time-steps

Future Plans: We have tested and verified the algorithms; we now will extend the size of our simulations to obtain statistical data on grain size distributions and global kinetics. We will also use recent data from an experimental vertex array to initialize a simulation and compare our results with those that occur in the experiments. This will provide an excellent test of the modeling approach and an opportunity to finely tune the geometric algorithms. We will also apply this vertex model to simulate three-dimensional grain structures.

[Sponsored by ONR]

Reference

1. H.V. Atkinson, "Serial of Normal Grain Growth in Pure Signal Phase System," *Acta Metal.* **36**(3), 469 (1988). ■

Structural Mapping of Ultrathin Films

Y.U. Idzerda and G.A. Prinz
Materials Science and Technology Division
and
D.E. Ramaker
Chemistry Division

As films become ultrathin (only a few atoms thick), they can exhibit unique and extraordinary properties. To understand the basis for their behavior, a detailed and complete structural description of the film/substrate system must be determined. This description of the relationship of the overlayer atoms with each other and with the atoms of the substrate on which they are deposited is a very difficult task. Recent advances in extracting this information from the angular resolved intensity mappings of high energy (>500 eV) Auger electrons and photoelectrons emitted from the ultrathin film have made possible a complete determination of the structure and method of growth of the film.

Mapping Structures: Electron forward scattering is a recently developed technique that exploits an aspect of the quantum mechanical scattering of electrons by neighboring atoms [1]. An electron emitted from an atom can scatter off the neighboring atoms on its way to the electron detector. For those special instances when a nearby atom is directly in the path between the emitting atom and the detector, the attractive atomic potential of the scattering atom "focuses" all nearby electron paths into the forward direction (Fig. 3). For an electron detector with sufficient angular resolution, this results in a large increase in the electron intensity for detector positions corresponding to atom-atom directions. Measuring the angular placement of these intensity enhancements creates a mapping of the internuclear directions within the film. From this mapping, an accurate and complete structural model of the film can be made. For a film with more than one element, the chemically specific

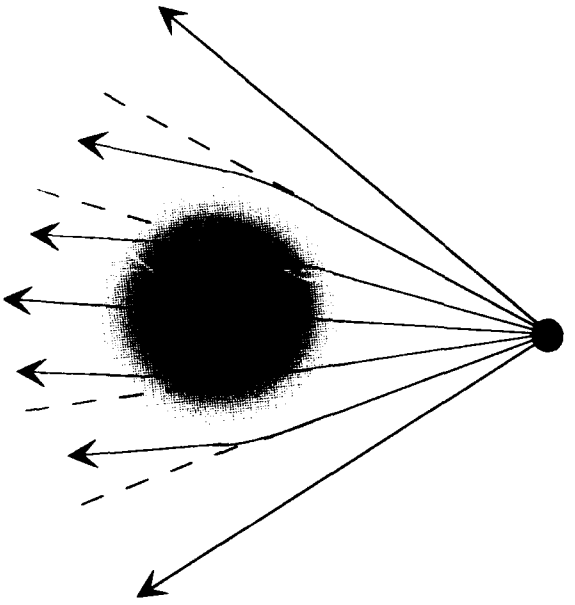

Fig. 3 — Intuitive picture of electron intensity enhancement caused by forward scattering from a nearby atomic potential

nature of Auger electrons and photoelectrons can be exploited to allow for the independent determination of the local structure of each chemical species in the film. At NRL, the experimental structural determination is complemented by extensive theoretical work to understand the mechanisms underlying electron forward scattering.

Determining Film Growth: Another important aspect in the development of ultrathin films is the mode of film growth. The properties of a film that grow in a three-dimensional island form and a film that grows in a layer-by-layer form can be very different. Because the local structure of a one atomic layer film, a two atomic layer film, and a three atomic layer film are distinctly different, electron forward scattering can be used to determine the mode of film growth. As an example, we show in Fig. 4 the complete angle-resolved intensity mapping of the Ni LMM Auger electron (835 eV) for Ni deposition on Cu(001). For one atomic layer of Ni, no atoms exist above the emitting atoms, so no forward scattering occurs; only a uniform background intensity is observed. (Actually some weak

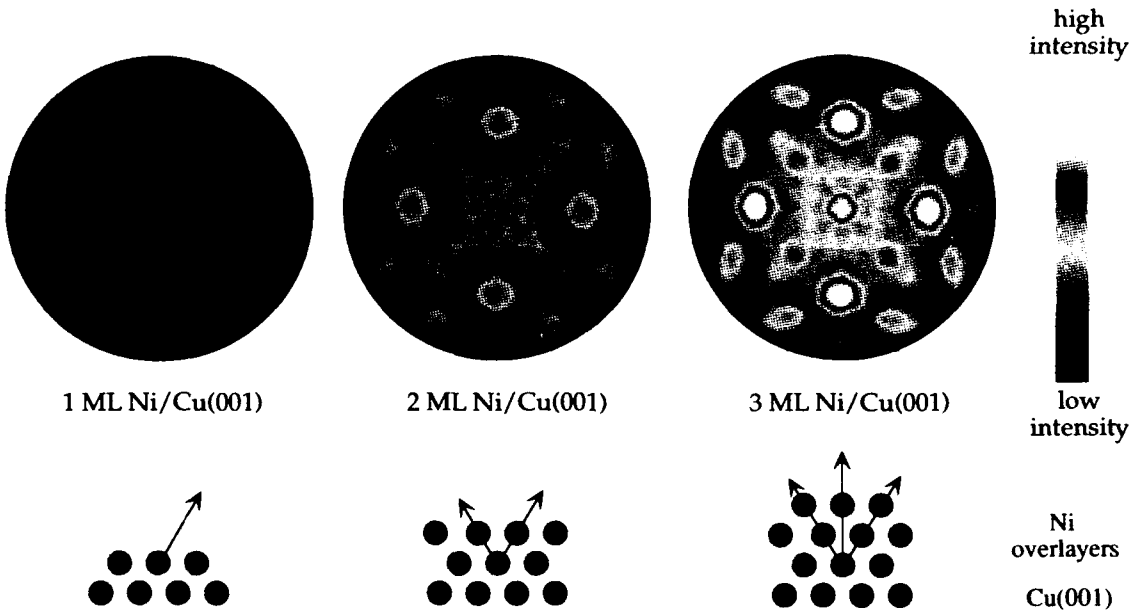

Fig. 4 — Measured Ni LMM Auger electron angular intensity mapping for one, two, and three atomic layers of Ni deposited on Cu(001). Complete film structure and film growth mode can be determined from intensity mappings.

features are present due to the backscattering of emitted electrons from the Cu(001) substrate.) For two atomic layers of Ni, atomic sites above some emitting atoms are occupied. This is seen from the presence of the high-intensity peaks located in the internuclear directions present for a two-layer film. Finally for the deposition of a third atomic layer of Ni, new intensity maxima associated with the occupancy of third-layer sites are observed. The presence or absence of these peaks can be used to infer layer-by-layer growth. For instance, if the exact number of atoms that corresponded to two atomic layers of Ni were deposited but scattering peaks indicative of the occupancy of third layer sites were observed, then this would demonstrate that the films grow in islands, where the third layer of the film begins to develop prior to completion of the second layer. If these peaks are absent in the intensity mapping, as for Ni/Cu(001) deposition, then we can conclude that the film grows in a layer-by-layer manner. In addition to the growth mode determination, the structure of the three-layer Ni film can be determined from the intensity mapping. We find the Ni film is face-center cubic (fcc), matched to the Cu(001) surface net, but contracted by 5% in the direction perpendicular to the film.

[Sponsored by ONR]

Reference

1. S.A. Chambers in *Advances in Physics*, S. Doniach, ed.(Taylor and Francis, London, 1991). ■

A Process to Make Ultrafine Metal Powders

K.P. Cooper and J.D. Ayers
Materials Science and Technology Division

Ultrafine metal powders are desirable for metal injection moulding, magnetic recording tapes, ferrofluids, conductive and capacitative pastes for electronics, and conducting plastics—all applications vital to the Navy. Melt processing with energetic fluids (e.g., gas and water atomization) is one way to produce bulk quantities

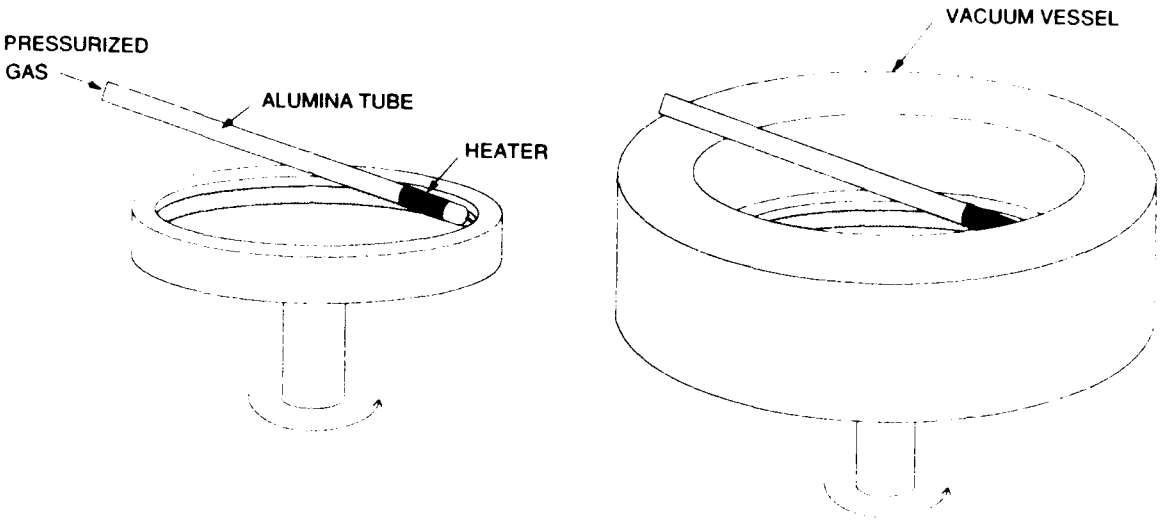

Fig. 5 — The rapidly spinning cup atomizer

of fine-scale metal powders [1]. more promising technique is rapidly spinning cup atomization [2], which has the potential to produce finer powders than is possible with gas atomization and to produce a more contaminant-free powder than is possible with water atomization. This method also serves as a basic research tool to obtain a fundamental understanding of the melt breakdown process.

Rapidly Spinning Cup Atomization: This process consists of introducing molten metal into an atomizing fluid contained within a rapidly rotating cup. The process variation employed in this study, illustrated schematically in Fig. 5, introduces the melt as a fine stream ejected under pressure from a nozzle. As the melt penetrates the atomizing fluid or quenchant, it is sheared into droplets, which solidify rapidly into powder (Fig. 6). The atomizing apparatus employed in this study includes a means to evacuate both the atomizing vessel or chamber and the reservoir containing the quenchant. This assures that the chamber and the quenchant, which is usually a nonreactive oil, are free of oxygen. This bench-top atomizer is used to fragment molten tin to provide an understanding of the fluid dynamical interactions between the liquid metal and the processing fluid and to determine the atomizing conditions that would produce the highest yield of the finest powder.

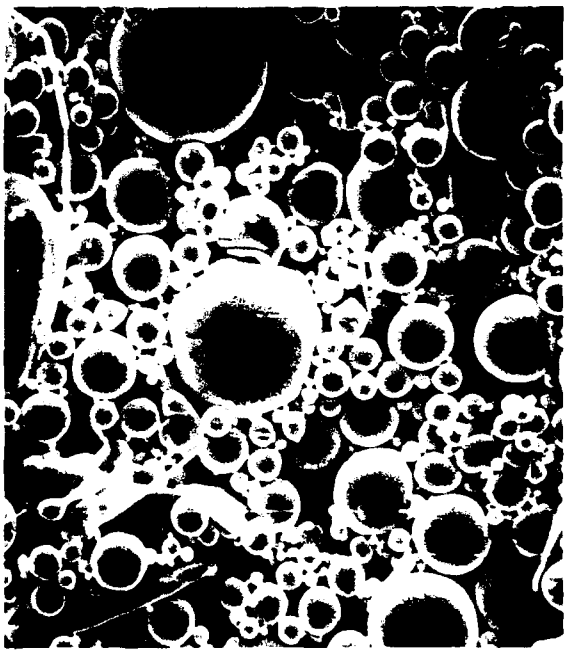

Fig. 6 — Typical morphology of the < 30 μm fraction powder that makes up nearly 90 weight percent of the total yield

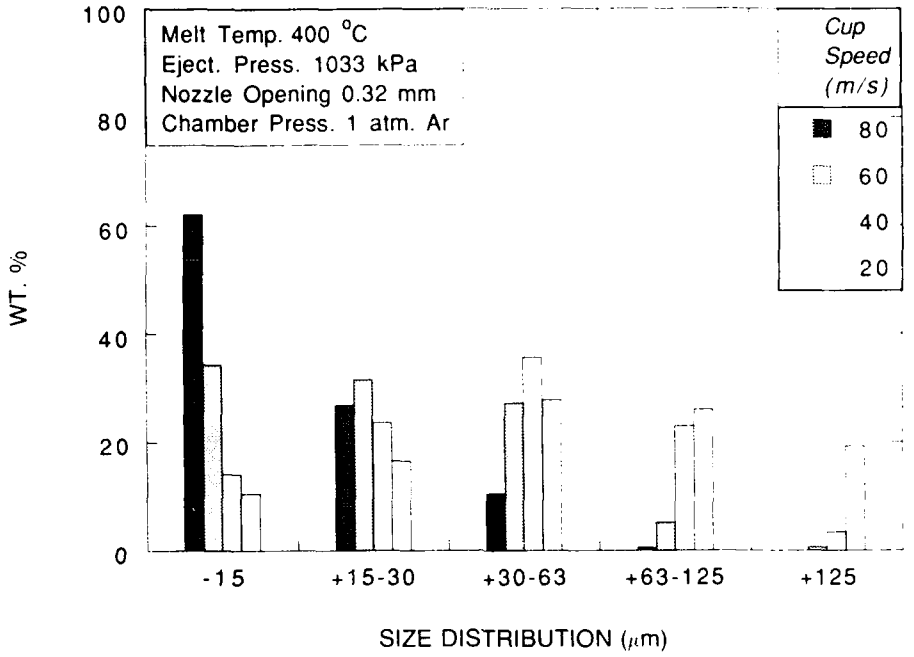

Fig. 7 — The effect of cup rotational speed on particle size distribution

Optimization of Processing Parameters: It has been found that the most direct way of achieving particle size refinement is to increase the cup rotational speed. This effect is graphically illustrated in Fig. 7. Increased cup speed enhances the shearing capability of the atomizing fluid, and the incoming melt stream is more effectively atomized. Another factor that results in finer particles is the use of a melt ejection nozzle with a smaller opening. When compared to a large opening, a small opening produces a narrow melt stream and a higher ejection velocity. Both factors improve comminution of the melt stream by the atomizing fluid. It has also been found that for liquid tin, melt temperatures of 400° and 500°C produce finer particles than a melt temperature of 300°C. Since the breakdown of the melt stream involves the formation of thin liquid metal sheets [3], at lower superheat, these do not have the sufficient time to spherodize into droplets and therefore freeze as small splats. Being greater in width than the diameter of a droplet of equivalent volume, these splats tend to skew the measured particle size distribution to coarser regimes. Very thin splats with greater superheat can break up into more than one droplet during the spheroidization process, thus permitting a real, rather than an apparent, particle size refinement.

With the apparatus employed here, atomizing can be done in vacuum (about 50 mTorr) or with the chamber backfilled with an inert gas. We observe that the processing atmosphere and melt ejection pressure have a complex influence on particle size distribution. As shown in Fig. 8, the highest yields of $< 15\ \mu m$ powder occur with high ejection pressure when the chamber is filled with argon and with low ejection pressure in a vacuum environment. These results are explained as follows. When the chamber is backfilled, a gas boundary layer forms in front of the rapidly spinning quenchant. This boundary layer acts as a primary atomizing fluid that breaks down the melt stream into coarse droplets, which are further atomized into fine droplets by the quenchant. When the ejection pressure is low, the melt stream is decelerated by the boundary layer, the droplets enter the quenchant with reduced momentum, and less effective secondary atomizing occurs. When

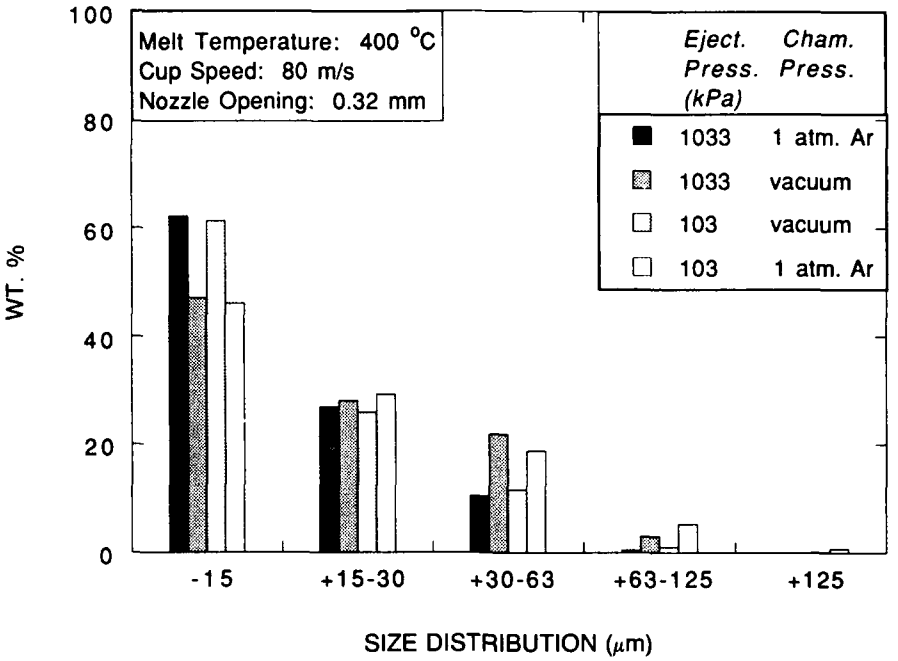

Fig. 8 — Size distribution of the powder as a function of melt ejection pressure and chamber pressure

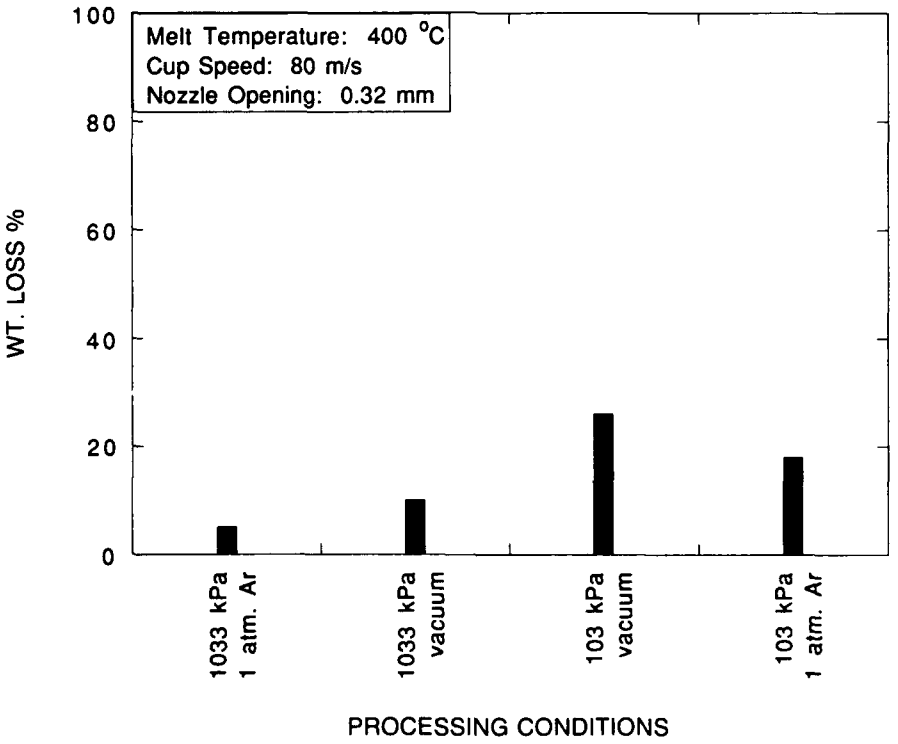

Fig. 9 — Metal weight loss under different processing conditions

the ejection pressure is high, the fragmented droplets enter the quenchant with high momentum, and more effective secondary atomizing occurs. In vacuum, the gas boundary layer is absent or negligible, and the melt stream exiting the nozzle remains relatively unbroken. With high ejection pressure, the stream penetrates the quenchant deeper, and this appears to be detrimental for effective atomizing as evidenced by the lower yield of the finest size fraction. With low ejection pressure, penetration of the stream into the quenchant is shallow, and this appears to be more effective in atomizing as evidenced by the high yield of the finest size fraction. This suggests that the most effective atomizing occurs in the surface layers of the rapidly spinning quenchant.

A benefit of high ejection pressure is reducing metal loss, which occurs when a portion of the melt stream bounces off the surface of the quenchant. As shown in Fig. 9, the weight of metal lost is consistently higher with low ejection pressure than with high ejection pressure. Metal loss appears to be lower when the chamber is backfilled because the gas boundary layer helps minimize bouncing of the melt stream off the quenchant surface.

Conclusions: It is found that the highest cup rotational velocity and the highest ejection pressure possible with a given rapidly spinning cup atomizer, combined with the smallest orifice diameter that would allow unhindered melt flow, yield the finest powder with the least metal loss. With a cup rotational velocity of 80 m/s, a melt ejection pressure of 1033 kPa, and ejection nozzle opening of 0.32 mm, a yield of 62 weight percent of the < 15 μm fraction is achieved with only a 5 weight percent metal loss. This is some of the finest powder produced by melt processing with energetic fluids. Insights gained from this study are being applied to the construction of a scaled-up atomizer designed to spin with speeds greater than 80 m/s and designed to atomize large quantities of ultrafine metal powders.

[Sponsored by ONR]

References

1. J.D. Ayers and I.E. Anderson, "Very Fine Metal Powders," *J. Metals*, **37**(16) (1985).

2. R.V. Raman, A.N. Patel, and R.S. Carbonara, "Rapidly Solidified Powders Produced by a New Atomization Process," *Metal Powder Rep.*, **39**(106) (1984).

3. J.D. Ayers and K.P. Cooper, "Counter Rotating Fluid Atomization of Tin," Proceedings of the Second International Conference on Rapidly Solidified Materials, ASM International, Materials Park, Ohio, 1988, p. 199. ■

Advances in the State-of-the-art Growth of InSb by Using Molecular Beam Epitaxy and Organometallic Vapor Phase Epitaxy

D.K. Gaskill, P.E. Thompson, J.L. Davis, and G.T. Stauf*
Electronics Science and Technology Division
**NRC-NRL Associate*

Epitaxial InSb-containing films are important in meeting the Navy's mission of developing III-V compound semiconductor technology for use in long wavelength (8 to 14 μm) detectors and high-speed devices. At NRL, research has focused on the long wavelength detector goal, where two approaches have been undertaken. For the first approach, superlattices consisting of alternating $InAs_xASb_{1-x}$ and InSb layers are grown such that the strains in each constituent layer give rise to an appreciable absorption coefficient in the wavelength range of interest. The second approach entails alloying Bi into InSb, dilating the lattice, and thereby reducing the band gap. For both approaches, the epitaxy of high quality InSb is essential. This article presents a summary of recent

advances in the state-of-the-art growth of InSb by using molecular beam epitaxy (MBE) and organometallic vapor phase epitaxy (OMVPE).

Organometallic Vapor Phase Epitaxy: High quality InSb layers were grown that exhibit crystallinity and electronic transport properties superior to past efforts of other research groups when a modified version of the quartz reactor, designed to minimize thermally driven gas recirculation loops, was installed. Figure 10 displays electronic Hall transport results for an *n*-type film grown on high resistivity, *p*-type InSb substrates. These transport measurements are very similar to those of the bulk materials, indicating a backgound impurity concentration in the low 10^{15} cm^{-3}. These results were confirmed by cyclotron resonance measurements at 4 K. Additionally, the high quality of the layers was confirmed from measurements of excess carrier lifetime at 77 K on a sample similar to the one used in Fig. 10, and the results were equal to or exceeded similar measurements on an undoped, high purity, *n*-type InSb substrate.

Incorporation of Bi into InSb epilayers requires low growth temperatures to minimize the formation of undesirable crystalline phases. The organometallic Sb source employed in the work described above was unable to meet the growth temperature requirement, and hence a new source was needed. Through the ONR 6.2 Electronic Materials Program, synthetic chemists at the Naval Weapons Center (NWC) developed a new Sb compound that was tested at NRL. InSb epitaxial films were successfully grown at temperatures 100°C lower than ever before and they exhibited good crystallinity and transport properties. This new organometallic source and a second source recently synthesized at NWC are being used and evaluated by the Hughes Aircraft Company, Sandia National Laboratories, University of Utah, and Oxford University.

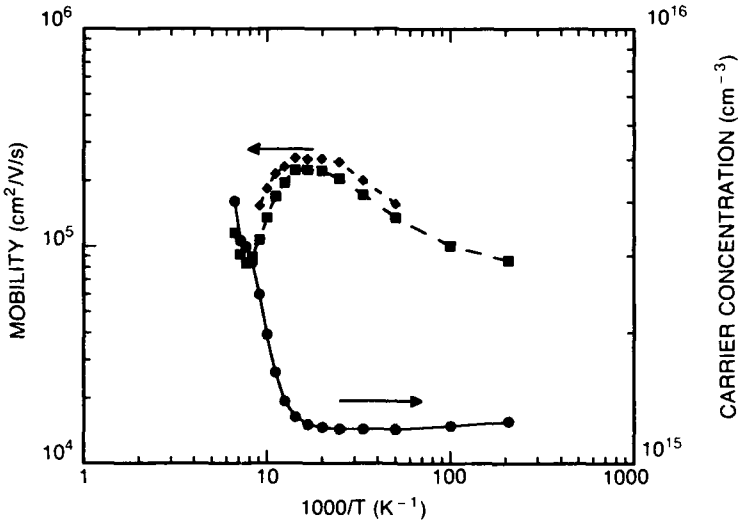

Fig. 10 — Electronic Hall transport measurements of carrier concentration and mobility as a function of inverse temperature for an InSb epilayer grown on a high-resistivity *p*-type InSb substrate at 450°C. The ●, ■, and ◆ correspond to *n*-type net carrier concentration at 2000 G, mobility at 2000 G, and mobility at 500 G, respectively. At temperatures above 130 K, the resistivity of the substrate becomes small and dominates the measurement, masking the film properties.

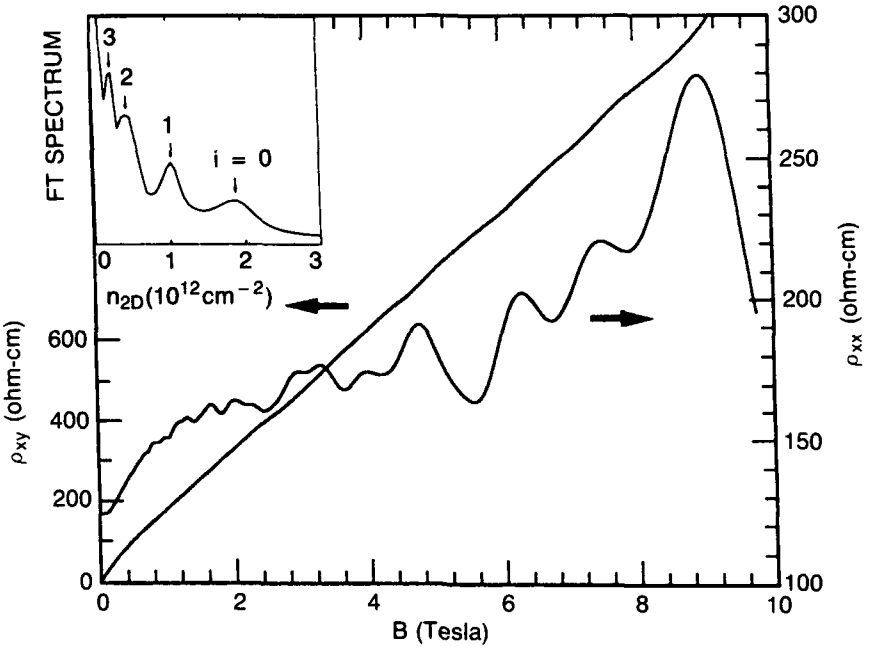

Fig. 11 — Transport coefficients ρ_{xx} and ρ_{xy} vs magnetic field B. The inset shows the Fourier transform spectrum of ρ_{xx} vs B^{-1}, where i labels different 2DEG subbands.

Molecular Beam Epitaxy: To achieve the intial goal, the preparation of InSb layers on GaAs substrates, the dislocations, and defects resulting from the 14% lattice mismatch between film and the substrate had to be overcome. To this end, a new approach using atomic layer epitaxy (ALE) was employed to initiate InSb growth on GaAs. ALE involves the alternate shuttering of the group III and V sources so that, at a given time, only one constituent is incident upon the substrate. In the absence of one element, atoms of the other element are free to move on the surface of the growing film until they find an appropriate site to bind. In-situ reflection, high-energy electron diffraction spectra were used to determine when the initial island growth of the film became two-dimensional, at which point normal epitaxial growth was started. Films grown by using ALE were superior in quality to previous attempts by other researchers and nearly equal to the homoepitaxial quality described in the OMVPE section.

Optimum growth conditions for Si doping were determined, and Si delta-doped layers were grown whereby an undoped film is grown, growth is stopped, and the surface is exposed to the Si atomic beam for a short time; then growth continues. Figure 11 plots the transport coefficients ρ_{xx} and ρ_{xy} as a function of magnetic field B taken from a sample grown on a high resistivity p-type InSb substrate. The slope of ρ_{xy} vs B yields the total electron density, which was consistent with the concentration of Si in the delta-doped layer. The features in ρ_{xx} vs B are due to a two-dimensional electron gas (2DEG) centered on the delta-doped layer. A Fourier transform of the ρ_{xx} data, shown in the inset of Fig. 11, reveals four occupied subbands of the 2DEG.

Summary: By using new approaches to expitaxial growth, OMVPE and MBE researchers at NRL have advanced the state-of-the-art for the growth of InSb epitaxial films. Future work will concentrate on the reduction of threading dislocations into the superlattice by the use of dislocation filters and on incorporating Bi into InSb while maintaining good crystallinity and transport properties.

Acknowledgments: Dr. M.J. Yang, SFA Inc., and Dr. R.W. Gedridge, Jr., NWC, are recognized for the contributions to this work.

[Sponsored by ONR]

References

1. D.K. Gaskill, G.T. Stauf, and N. Bottka, "High-Mobility InSb Grown by Organometallic Vapor Phase Epitaxy," *Appl. Phys. Lett.* **58**, 1905 (1991).

2. P.E. Thompson, J.L. Davis, J. Waterman, R.J. Wagner, D. Gammon, D.K. Gaskill, and R. Stahlbush, "Use of Atomic Layer Epitaxy Buffer for the Growth of InSb on GaAs by Molecular Beam Epitaxy," *J. Appl. Phys.* **69**, 7166 (1991).. ■

A Corrosion Pit on Aluminum Ion Implanted with Niobium
Scientific Data/Visualization (B&W), *Third Place*
Paul M. Natishan

A Corrosion Pit on Aluminum Ion Implanted with Niobium
Scientific Data/Visualization (B&W), *Third Place*
Paul M. Natishan
Materials Science and Technology Division

The micrograph illustrates the fourth stage in the blister formation and rupture mechanism of pitting corrosion. Briefly, the mechanism states that a small crack or pore in the oxide film provides a path for solution to reach the oxide/metal interface; metal dissolution and hydrogen gas production then occur at the oxide/metal interface. With time, the hydrogen accumulates and produces a pressure that causes the mechanical failure of the protective oxide film. The micrograph shows that the oxide film has been push upward and that crystallographic dissolution of the metal has occurred beneath the oxide film. This and similar micrographs, along with determinations of hydrogen pressure that use both thermodynamic and Griffith type calculations, were used to develop the blister formation and rupture mechanism.

NUMERICAL SIMULATING, COMPUTING, AND MODELING

207 **Skywave Over-the-horizon Radar Performance Model**
Benjamin T. Root

209 **Decision Support for Operational Logistics**
James B. Hofmann

Skywave Over-the-horizon Radar Performance Model

B.T. Root
Radar Division

HF skywave radar is the only kind of radar that can see over the horizon, illuminating thousands of square miles at a time under all weather conditions. It operates by using the ionosphere as a kind of mirror in which the radiated energy is refracted by the electron plasma. This requires frequencies in the 5 to 30 MHz range and large antennas on the order of a kilometer. These radars are therefore expensive, and it is desirable to predict their performance in a given geographical location before installing them. To do this, we need a model that, in effect, simulates the radar equation. All important gains and losses in the round-trip path of the energy from transmission to target and back to detection must be accounted for. Many of the environmental factors can only be predicted by a statistical database. A typical output is a two-dimensional map of the clutter-to-noise ratio vs range and frequency (Fig. 1). NRL, in collaboration with the Institute for Telecommunication Science, pioneered such HF performance models, starting in the mid-1960s. The specifications set by these early efforts have endured as the basic standard for current models. NRL's model is revised as the need arises. Currently, data from the new Navy radar at Amchitka in the Aleutian Islands is being analyzed for this purpose.

Radar Performance Model: The environmental database includes a description of the ionospheric and the external and man-made noise. On a large scale, the electrons of the ionosphere are concentrated in approximately parabolic layers ranging in height from 100 to 300 or more kilometers. The height, thickness, and density of these layers are influenced by many factors, such as the angle of the Sun, the solar wind, the geomagnetic field, induced ionospheric currents, and even the weather. Therefore, the ionospheric model is a hybrid of deterministic and statistical components. The statistical part was determined by measurements from a network of sounders sparsely distributed over the Earth with large gaps over the ocean. Data were taken during a quiet and an active part of the solar cycle, and the current sunspot number is used to extrapolate in between. The external and man-made noise component of the database is entirely statistical and was recently revised.

Once we have obtained a prediction of the current ionosphere from the database, we then calculate the propagation path for the radar energy. The radar beam is considered as a bundle of rays, and the path of a ray varies with frequency and elevation angle. We use approximate closed-form solutions over one or two hops between Earth and ionosphere, and we account for geometrical spreading, losses, and absorption. Recently, spectral distortion caused by irregularities in the ionosphere (spread-Doppler clutter) has become a major issue, and we are accounting for this. Also, we are incorporating a more accurate model of the reflectivity of the Earth and sea, based in part on data from other sensors, such as buoys.

Finally, we must include the effect of the radar system itself. There are losses and thermal noise in the antenna and cables but also gains in the signal processor. There are many possible types of waveforms, for a variety of purposes, and a performance model helps to optimize the choice of waveform. Frequency management is critical to obtain good propagation and to avoid other users in the cluttered HF spectrum; performance models are useful here, too. Furthermore, a performance model helps to verify that a new and complex radar system is performing as expected.

Current Research: The data from the radar at Amchitka contain 10 days of observation from each of the four seasons of the year. We are comparing subclutter visibility (a measure of how weak a target can be detected) predicted by our model and measured by the radar. The target masking effects of spread-Doppler clutter are

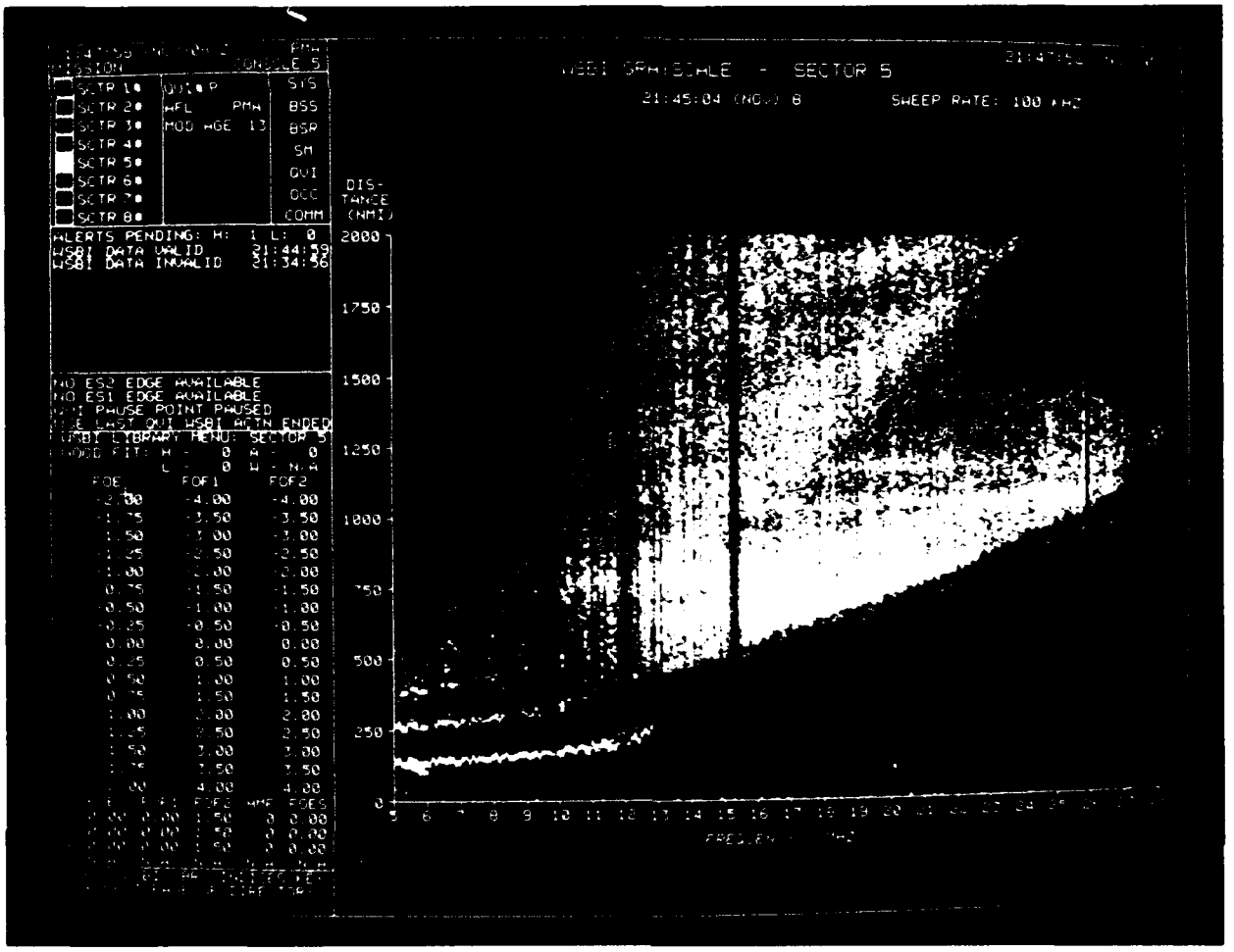

(a)

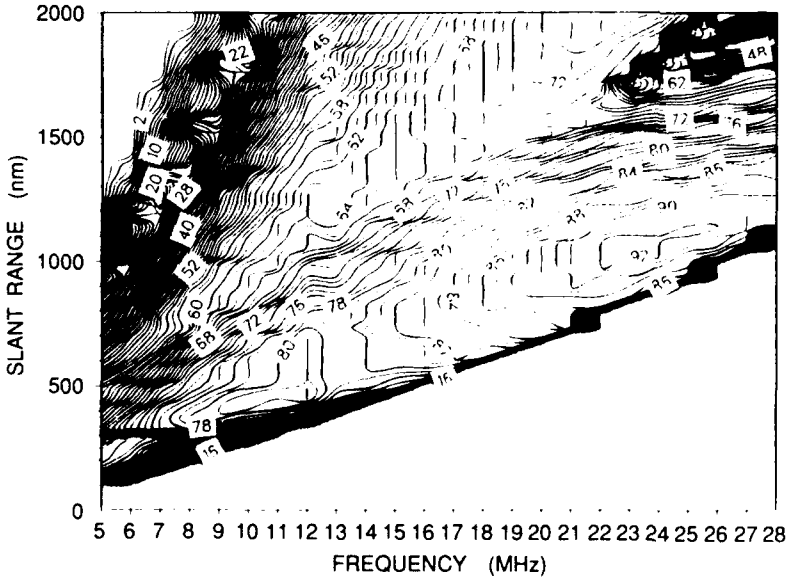

(b)

Fig. 1 — (a) *Wide-sweep backscatter ionogram* from radar. This plot provides a complete view over range and frequency of the propagation conditions during operation. The radar operator selects one of the brighter regions, provided there is no interference (vertical lines); and (b) simulated wide-sweep backscatter ionogram for same time and location as Fig. 1(a). Differences with Fig. 1(a) are partly accounted for by the statistical nature of the ionospheric database.

more important than at previous radar locations, and the data will help in analyzing this problem. The large amount of land in the coverage area of the radar requires corrections in the surface reflectivity coefficient.

The corrections and adjustments to our performance model will contribute to the solution of a radar problem that is both complex and in need of more complete environmental data.

[Sponsored by SPAWAR] ■

Decision Support for Operational Logistics

J.B. Hofmann
Information Technology Division

Introduction: Naval operational logistics is the science of keeping afloat platforms sustained in order to complete their prescribed tactical mission. Logisticians for battle groups, battle forces, and Fleets face an enormous job keeping each platform replenished and operational. However, it was not until the late 1980s that benefits of the application of computer technology for this problem were recognized.

Background: Captain Raymond B. Wellborn, in a speech to the American Society of Naval Engineers, first pointed out the opportunity to apply computer technologies to the operational logistics problem [1].

The Naval Postgraduate School responded by developing a PC-driven tool known as the Battle Group Logistics Computer Support System (BGLCSS) [2], which incorporates forecasting models to predict future logistical states of fuels and ordnance. BGLCSS was successfully tested and proven during Fleet exercises. This was a major step and encouraged the logistics community to develop state-of-the-art decision aids for at-sea replenishment problems.

In addition, the current and future thrust of the Navy is to support possible extended contingency and limited objective warfare regions located far from supply ports. With the projected diesel submarine and air threat, it becomes too critical to minimize the degradation to the battle group defensive posture by planning and executing at-sea replenishments only when they are needed. Old rules of thumb must give way to the exploitation of technological approaches and command and control assets to respond to new tactical realities.

Decision Support Paradigm: Meanwhile, NRL's Information Technology Division has been developing decision aids for tactical problems, such as antisubmarine warfare, acoustic data management, strike planning, and on-board fire control. Each of these systems has a common decision support paradigm (Fig. 2), which can be applied to many decision support problems. External data, such as sensor and radio reports, are combined with internal knowledge of the problem characteristics and interrelationships to form a real-time picture from which several decision-aiding operations occur. By using a state-of-the-art operator-machine interface, the decision maker can forecast from a real-time picture, perform an assessment of the situation (such as threats and possible future alerts), and generate plans to address any current shortcomings in the problem space. In addition, the decision maker can posit possible events that may have a probability of occurring by the "what if" module and then perform forecasts, situation assessments, and response plans.

Application to Logistics Support: The operational logistics problem can be generalized to the generic paradigm. A logistics picture is generated by inventory and readiness reports and any other exploitable data. Internal knowledge of consumption rates, vehicle capacities, current speed, and tactical state is used to maintain the picture between updates. With the user interface shown in Fig. 3, the operator can immediately access the logistical state of the battle group as a

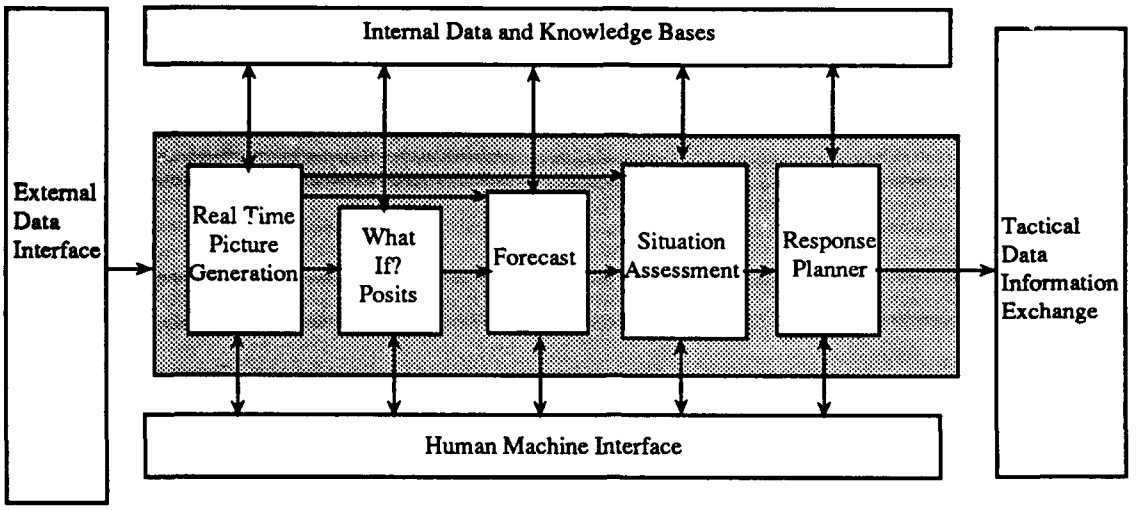

Fig. 2 — NRL generic decision support paradigm

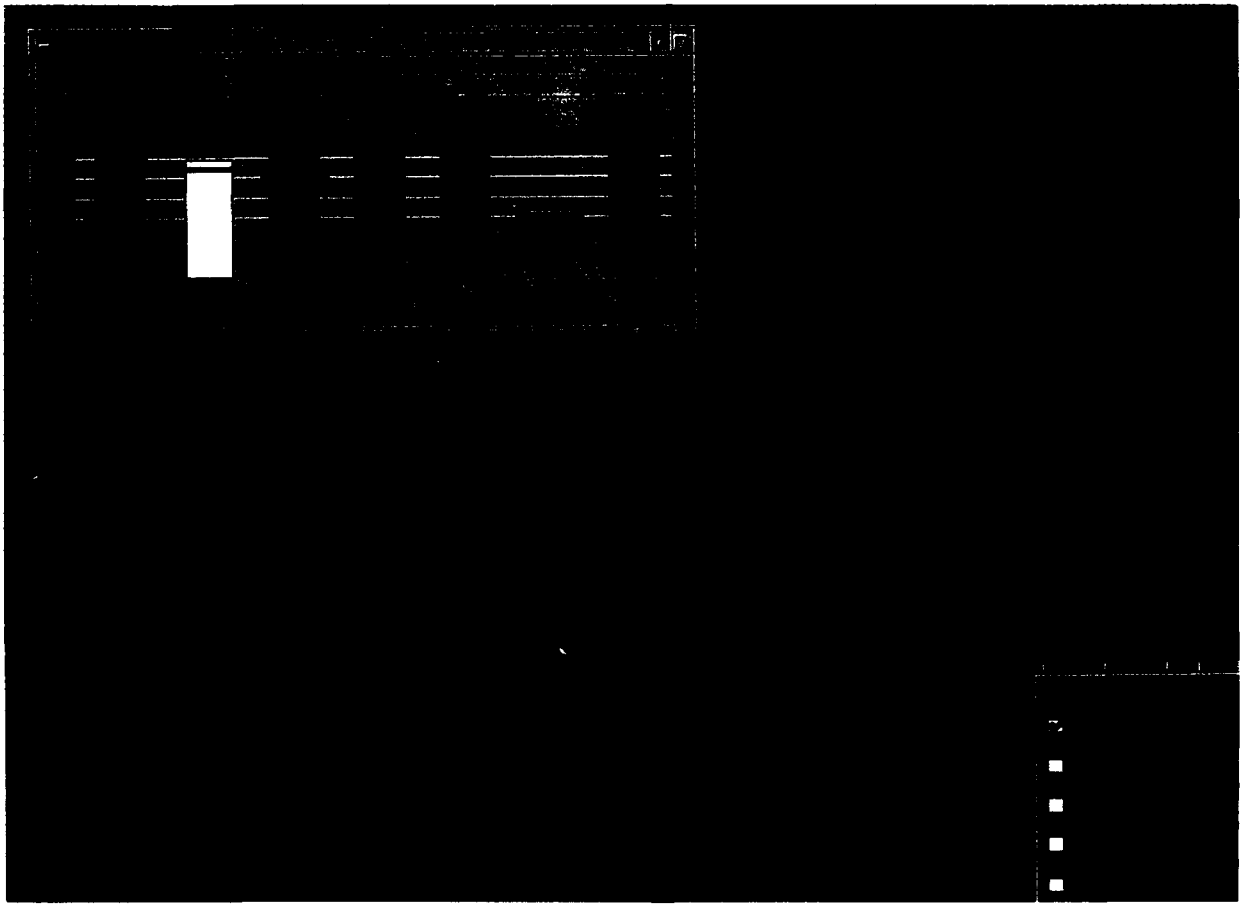

Fig. 3 — Operator machine interface for logistics decision support system

whole, or as an individual platform. The inset (bar chart, upper left) in Fig. 3 shows total battle group assets by fraction of total capacity across fuel and ordnance (divided by threat area). The yellow alert for F-44/JP5 (airplane fuel) indicates that assets have fallen below desired levels, and a red alert (ASW ordnance) indicates that assets have fallen below mandated levels and must be immediately addressed. The decision maker could then enter Situation Assessment (pressing the button at the bottom right of the screen) and pinpoint battle group platforms that are triggering the alerts. Based on this assessment, the decision maker can generate a plan in the Response Planning mode. In another example, the logistics officer is approached by the strike warfare commander and asked whether the battle group can support multiple strikes over the next three days. The logistics officer enters What If? mode and (based on input from the strike commander) enters in the planned strike events and then forecasts over the next three days. The forecasting model could indicate, for example, that the increased sortie rate will significantly affect the airplane fuel on a carrier and, accordingly, the logistics officer immediately schedules the carrier to be topped off.

Future Plans: NRL is working with NAVSUP to develop a decision aid known as Battle Group Operational Logistics Decision Support System (BOLDSS), which will be linked with Navy tactical systems, such as the Joint Operational Tactical System (JOTS), to obtain current positions and speeds of platforms. Eventually, the system will be expanded to aid battle force and Fleet logistics, as well as on-shore planning.

[Sponsored by NAVSUP]

References

1. R.B. Wellborn, "Battle Group Logistics—The Multiplier," presented to The American Society of Naval Engineers, March 1988.

2. D.A. Schrady and D.B. Wadsworth, "User's Guide for the Battle Group Logistics Coordinator Support System (BGLCSS)," and IBM-PC software, February 1991. ■

Reconstruction of Hubble Space Telescope Image of Saturn with the NRL Connection Machine

Scientific Data/Visualization (Color), *Third Place*

Paul L. Hertz

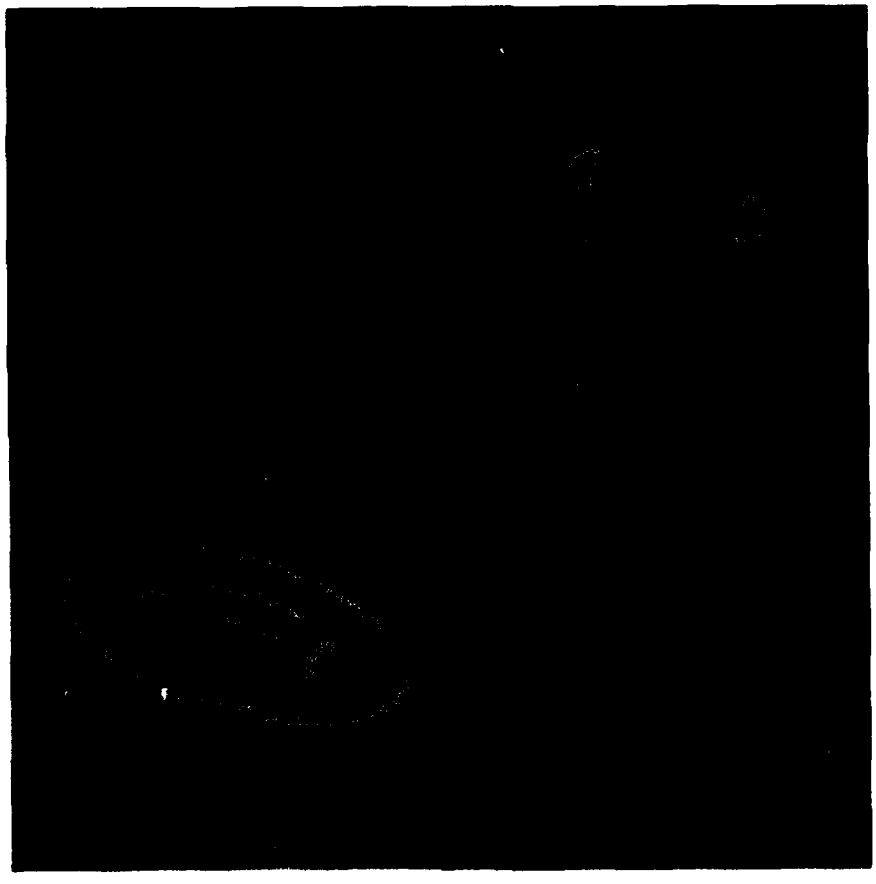

Reconstruction of Hubble Space Telescope Image of Saturn with the NRL Connection Machine
Scientific Data/Visualization (Color), *Third Place*
Paul L. Hertz
Space Science Division

Astronomical images obtained with the Hubble Space Telescope have reduced spatial resolution because of spherical aberration in the primary mirror. By using the NRL Connection Machine and advanced image restoration techniques, most of the lost resolution can be recovered. Shown are a Hubble Space Telescope image of Saturn (upper right), the restored image (upper left), and two measurements of the accuracy of the restoration (lower panels). Saturn image courtesy NASA.

OPTICAL SCIENCE

215 **Subpicosecond All-fiber Laser**
Irl N. Duling III

216 **1.06 μm All-fiber Optic Gyroscope**
William K. Burns and Robert P. Moeller

218 **Heavy Metal Fluoride (HMF) Glass Windows**
Ishwar D. Aggarwal and John M. Jewell

Subpicosecond All-fiber Laser

I.N. Duling III
Optical Sciences Division

The need for a compact, efficient, ultrashort-pulse fiber laser spans such diverse areas as high-speed optical communications, optical probing of high-speed electrical circuits, and short-pulse optical sensors. In recent years, the use of optical fibers doped with erbium ions as amplifiers and optical repeaters expanded greatly. Researchers realized that complicated systems of detectors, lasers, and electronic amplifiers could be replaced by a section of fiber with gain spliced into the transmission system. There was no need to convert back and forth between light and electricity when the signal needed amplification. The erbium-doped fiber amplifies optical signals at 1.5 μm, which is in a low-loss window of optical fibers. This amplifier can also be pumped by semiconductor diode lasers. These characteristics make the erbium-doped fiber amplifier (EDFA) a well-suited source of gain for advanced fiber systems.

Fiber Lasers: To complement this new optical amplifier, numerous researchers are trying to make ultrashort-pulsed laser sources by using the EDFA as a gain medium. If successful, this source would not only be useful in communications but would be a compact, efficient source of pulses at 1.5 μm for scientific study of high-speed electrical circuits and optical probing of semiconductor materials. Until the development of short-pulsed fiber sources, the only way to get an ultrashort pulse at 1.5 μm was by using a color center laser (which is a large, costly laser) or by using a modelocked semiconductor diode laser (which generally has a short operating lifetime).

At NRL, we actively research the development of high-speed communications systems and short-pulse laser sources. In this effort, we developed a simple, ultrashort-pulse erbium fiber laser with all-fiber components making it suitable for integration into fiber systems. Since its development, other laboratories duplicated this laser and reproduced the results obtained here. The laser sets the world record for the shortest pulses from an erbium-doped fiber laser, producing pulses as short as 0.3 ps (3×10^{-13} s) in duration.

Figure 1 is a diagram of the laser configuration. The shape of the laser cavity suggests the obvious name of "figure-eight laser" (F8L). The laser is based on a 50% fiber coupler with the fibers spliced together on each side. One side contains an EDFA, while the other contains an optical diode and an output coupler.

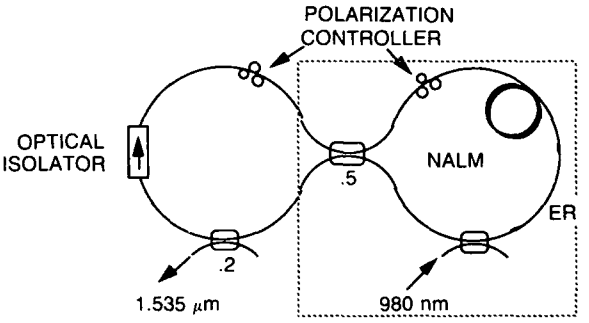

Fig. 1 — Layout of the modelocked all-fiber laser. The components in the dotted line constitute a nonlinear amplifying loop mirror, which serves as the passive modelocker for the laser.

Modelocking Mechanism: The portion of the figure in the dotted line is a nonlinear amplifying loop mirror (NALM) [1]. This simple, all-fiber device transmits high intensity light with less loss than low intensity light while providing gain. Normally a coupler with its outputs fused will act as a mirror, but here light traveling in one direction around the loop is amplified at the beginning, and light traveling in the other direction is amplified at the end. The different counter-propagating intensities make the fiber look slightly longer for the light amplified before propagation because of the intensity dependence of the fiber refractive index. The propagation distance mismatch will cause the phase of the light to be mismatched at the coupler allowing some light to be transmitted to the output port. Since the nonlinear index is intensity dependent, the higher the intensity of the light, the more will be

transmitted. For a pulse of light, this means that the peak of the pulse will transmit through the mirror, while the wings of the pulse reflect.

Using the output of a NALM as its own input creates a laser in which a pulse will form and get shorter with each round-trip of the cavity. It is important to get rid of the reflected wings of the pulse. The optical diode in the feedback loop accomplishes this purpose. By inserting a second coupler in the feedback loop, we can take a portion of the light out of the cavity. The finite gain bandwidth of the EDFA (8.1 nm) ultimately stops the pulse from getting any shorter than about 0.3 ps.

The F8L has already been used for probing high-speed electrical circuits and is actively pursued as a source for high-speed communications. Further investigations into the pulse forming mechanisms, limits to the repetition rate, and laser stability are in progress.

[Sponsored by ONR]

References

1. M.E. Fermann, F. Haberl, M. Hofer, and H. Hochreiter, "Nonlinear Amplifying Loop Mirror," *Opt. Lett.* **15**, 752-754 (1990). ■

1.06 μm All-fiber Optic Gyroscope

W.K. Burns and R.P. Moeller
Optical Sciences Division

Fiber optic gyroscopes are likely to be used for rotation sensing in a wide variety of Navy applications because they will provide better lifetime at a lower cost than present day technology. We report on the development of a new optical source for fiber gyros using a neodymium (Nd)-doped fiber pumped by a high-power laser diode array. A gyro using this source has achieved new levels of sensitivity with improved lifetime and scale factor stability when compared to older approaches using semiconductor sources alone.

In the past, semiconductor superluminescent diodes (SLDs) were used as sources for fiber optic gyroscopes, thereby providing the required broad wavelength emission. These devices tended to have short lifetimes and a large dependence of wavelength on temperature, which in turn caused a gyro-scale factor variation. The Nd fiber source is pumped by a semiconductor diode array at 0.81 μm and emits broadband superfluorescent emission at 1.06 μm. Lifetime is now limited by the lifetime of the pump laser, which is long, and the wavelength dependence on the temperature of the 1.06 μm emission, which is about a factor of ten smaller than that for the SLD.

Fiber Source Implementation: Figure 2 shows our first implementation of the fiber source in a fiber gyroscope [1]. To maintain the fiber in a superfluorescent mode (i.e., to keep it from lasing), isolation from optical feedback to the fiber must be provided. This was provided by a 1.06 μm isolator at the fiber-output end and by a dichroic mirror (passes 0.81 μm and reflects 1.06 μm) at the pump input end. The dichroic mirror keeps the backward-going emission from reflecting off the diode facet and reflecting back into the fiber, causing feedback. In Figure 3, we show a new, integrated implementation that performs the same function. A samarium (Sm)-doped fiber that transmitts 0.81 μm but heavily absorbs 1.06 μm light is used to connect the diode array with the Nd-doped fiber. This provides isolation and allows all the different fibers to be spliced together to form an integrated package.

1.06 μm Gyroscope Performance: Figures 3 and 4 show gyroscope performance with the fiber source. In Fig. 4, the optical scale factor variation over a 17-h run is 15 parts per million (ppm). This is an indicator of the superior wavelength stability of the fiber source. In Fig. 5, the gyro random walk coefficient is shown as a function of detector current. The experimental datum is plotted with theory assuming only shot noise in the detector. The high optical power (10 mW) available from the fiber source allows a high detector power, which

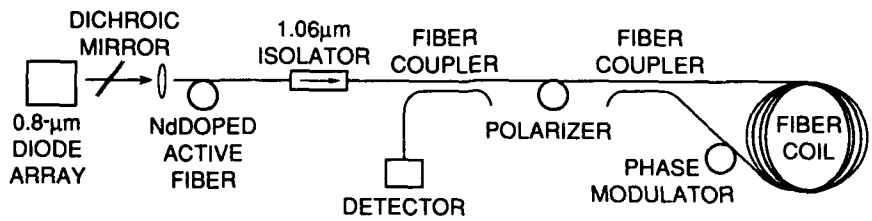

Fig. 2 — Configuration of the fiber gyroscope pumped by an Nd-doped fiber source

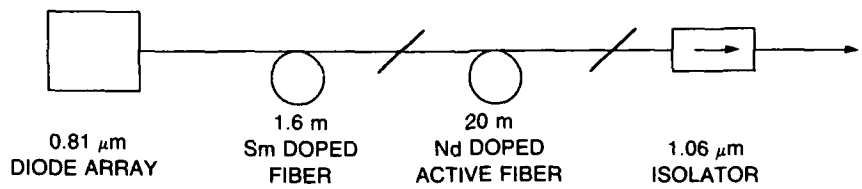

Fig. 3 — All-fiber source configuration using an Sm-doped fiber

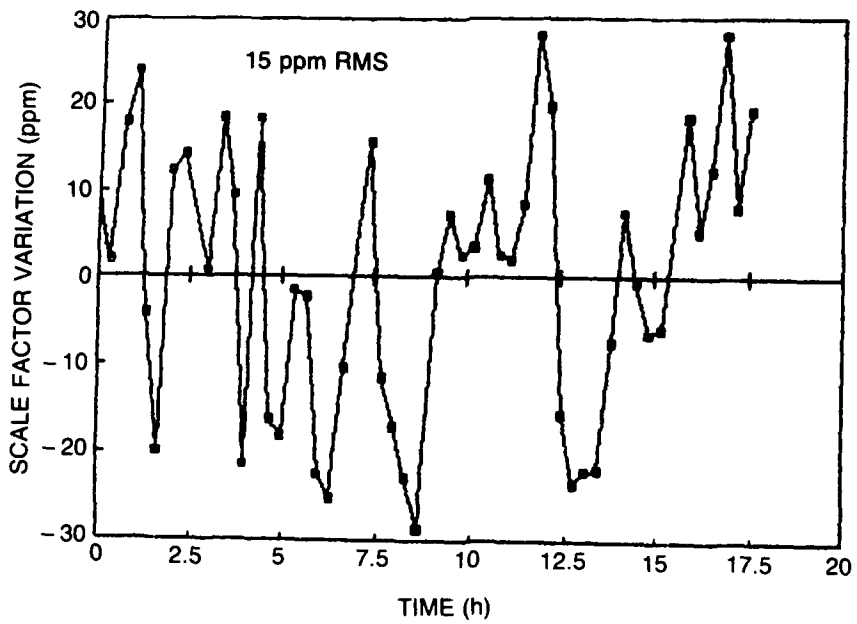

Fig. 4 — Optical sale factor stability

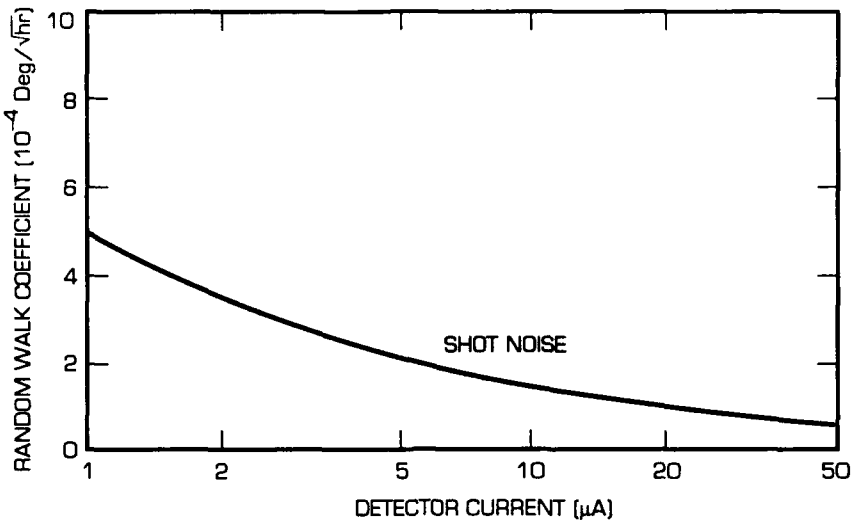

Fig. 5 — Experimental result with shot/noise theory for random walk coefficient

in turn provides a very low value of the intrinsic noise, as expressed by the random walk coefficient.

The case of implementation of the fiber source and its superior performance and lifetime indicates that it is likely to find wide use in fiber optic gyros, which will in turn impact many Navy rotation sensing requirements.

[Sponsored by ONR]

Reference

1. W.K. Burns, R.P. Moeller, and C.A. Villarruel, "1.06 μm All-fiber Optical Gyroscope," OE/Fibers 1991, Boston (1991). ■

Heavy Metal Fluoride (HMF) Glass Windows

I.D. Aggarwal and J.M. Jewell
Optical Sciences Division

Glass formation in the zirconium-based heavy metal fluoride (HMF) glass system was first reported in 1975. Since that time, major research efforts have focused on the development of these materials for ultralow-loss optical fibers [1]. However, HMF glasses also have properties that are very desirable for high-energy laser optical components. In particular, these glasses offer (1) a broad optical transmission window extending from 0.2 to 8 μm; (2) very low optical absorption ($< 1 \times 10^{-4}$ cm^{-1}) between 1 and 5 μm [2]; and (3) the possibility of producing windows that exhibit zero optical phase distortion when heated by laser fluences [3]. Until recently, the advantages that HMF glasses have over other window materials could not be exploited, because these glasses could not be produced in large enough sizes to be of practical use in high-energy laser optical systems.

Glass Melting: Extensive research found that the best glass composition for producing large size fluoride glass windows is $53ZrF_4$, $20BaF_2$, 20NaF, $4LaF_3$, $3AlF_3$ (in mol%). High-quality pieces of this glass can only be produced if the oxygen impurity content of the crystalline raw materials is low. In general, commercially available BaF_2, NaF, and LaF_3 are sufficiently low oxide impurities. ZrF_4 and AlF_3, on the other hand, must be purified through careful sublimation to remove oxygen.

When fluoride glasses are melted, a decrease in volume occurs of more than a factor of two from

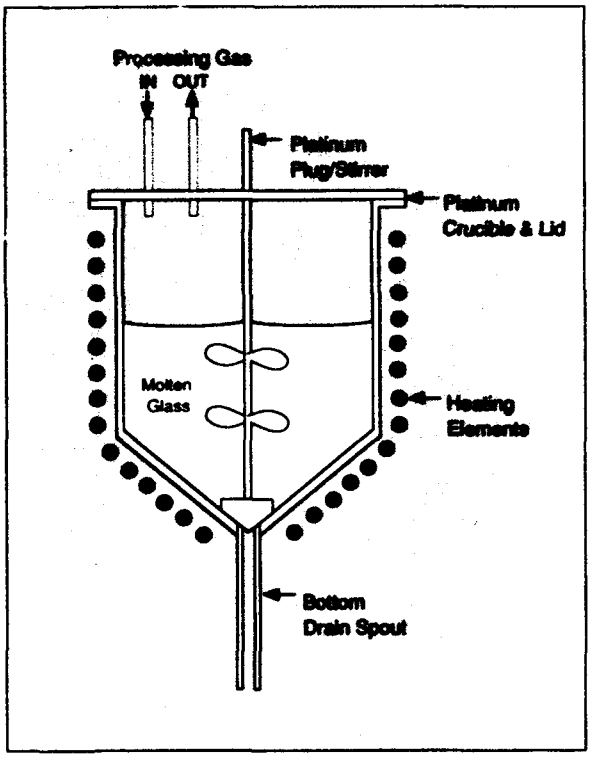

Fig. 6 — Schematic of 90-kg capacity platinum melting/casting crucible

the crystalline batch to final glass. This fact poses little problem for the production of small quantities of glass, but successful large-scale production requires a "premelt/remelt" technique. Small batches of glass (< 500 g) are melted in platinum crucibles under an inert atmosphere to form "cullet" that can be remelted with little change in volume.

When enough cullet has been made for the desired window size, it is charged into a large 90-kg capacity platinum melting crucible. Figure 6 shows a schematic of this crucible. The melting/casting crucible has a bottom drain spout to deliver glass to a mold, a gas inlet and outlet to maintain an inert atmsophere of argon during melting, and a platinum plug/stirrer used to ensure complete homogeneity. A typical melting cylce for a 50-kg window takes 4 days from start-up to cast. A melting temperature of 800°C is maintained throughout with a dry argon flow ranging from 0.75 to 1.5 ℓ/min and stirring rates of 30 to 60 rpm.

Window Casting: At the end of the melting cycle, just prior to casting, the melt temperature is reduced to ~650°C. A lower melt temperature at casting serves two purposes: the viscosity of the melt is higher, reducing turbulent flow during casting; and less heat is removed from the cast by the mold. Figure 7 shows the melting and casting facilities in place at Owens-Corning Fiberglas Corporation, the NRL contractor used for the production of 50-kg HMF windows.

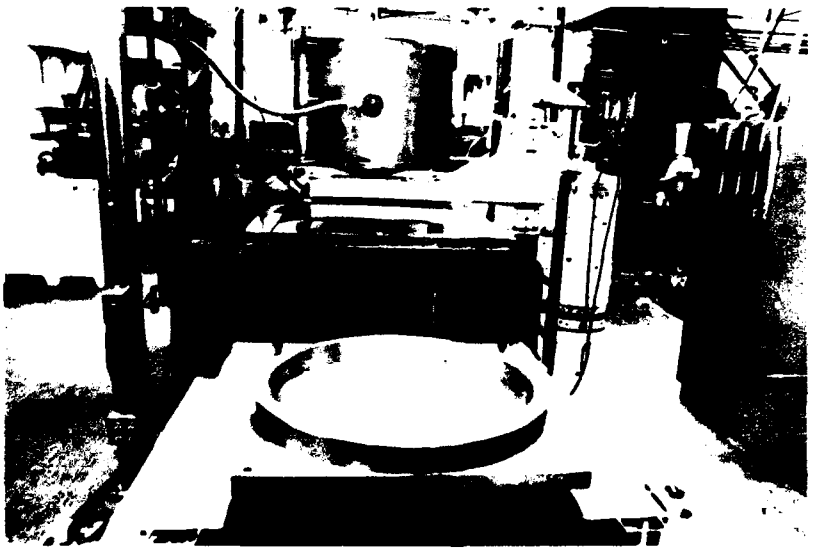

Fig. 7 — Casting facility at Owens-Corning Fiberglas Corporation that was used to produce 50-kg HMF glass windows

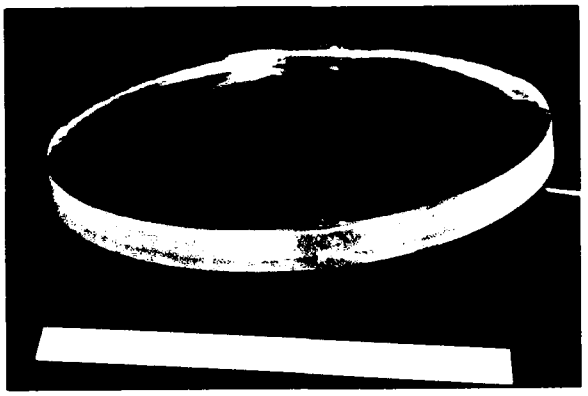

Fig. 8 — Unpolished 50-kg HMF glass window. Ruler is 24 in. long.

Windows are cast by draining the molten glass from the bottom of the crucible into a brass mold. The mold, mounted on a translational stage, is contained in a chamber isolated from the atmosphere and purged with argon. Casting a 50-kg window typically takes from 8 to 10 min. The mold is preheated to a temperature of 60° to 100°C, which allows the final cast/mold temperature to equilibrate at 240°C, i.e., just below the glass transition temperature. The preheating and equilibrium at this temperature ensures that the window will not crack and will be crystal free.

Following the casting and temperature equilibration, the window and mold are transferred into a large annealing furnace preheated to 265°C. The window is annealed over the course of several days and cooled to room temperature at rates not exceeding 3 K/h. Figure 8 shows an unpolished 50-kg window.

Summary: New techniques and glass compositions have been developed at NRL to produce large-scale HMF glass windows. The techniques described here have recently been used to produce 50-kg windows at Owens-Corning Fiberglas Corporation, ranging in size from 3- to 5-cm thick and 45 to 79 cm in diameter. These windows are large enough to be used for ground-based and shipboard high-energy laser systems.

[Sponsored by SPAWAR]

References

1. M.G. Drexhage, "Heavy Metal Fluoride Glasses," *Treatise on Materials Science and Technology*, **26** (Academic Press, New York, 1985), pp 151-243.

2. J.M. Jewell, G. Williams, J. Jaganathan, I.D. Aggarwal, and P. Greason, "Separation of Intrinsic and Extrinsic Optical Absorption in ZBLAN Glasses," *Appl. Phys. Lett.* **59**(1), 1-3 (1991).

3. J.M. Jewell and I.D. Aggarwal, "Control of Parameters Affecting Optical Path Distortion in Heavy Metal Fluoride Glass Windows," *Proc. SPIE* **1327**, 190-7 (1990). ■

Global Imaging of the Ionosphere
Artist's Concepts/Illustrations, *Third Place*
Robert R. Meier

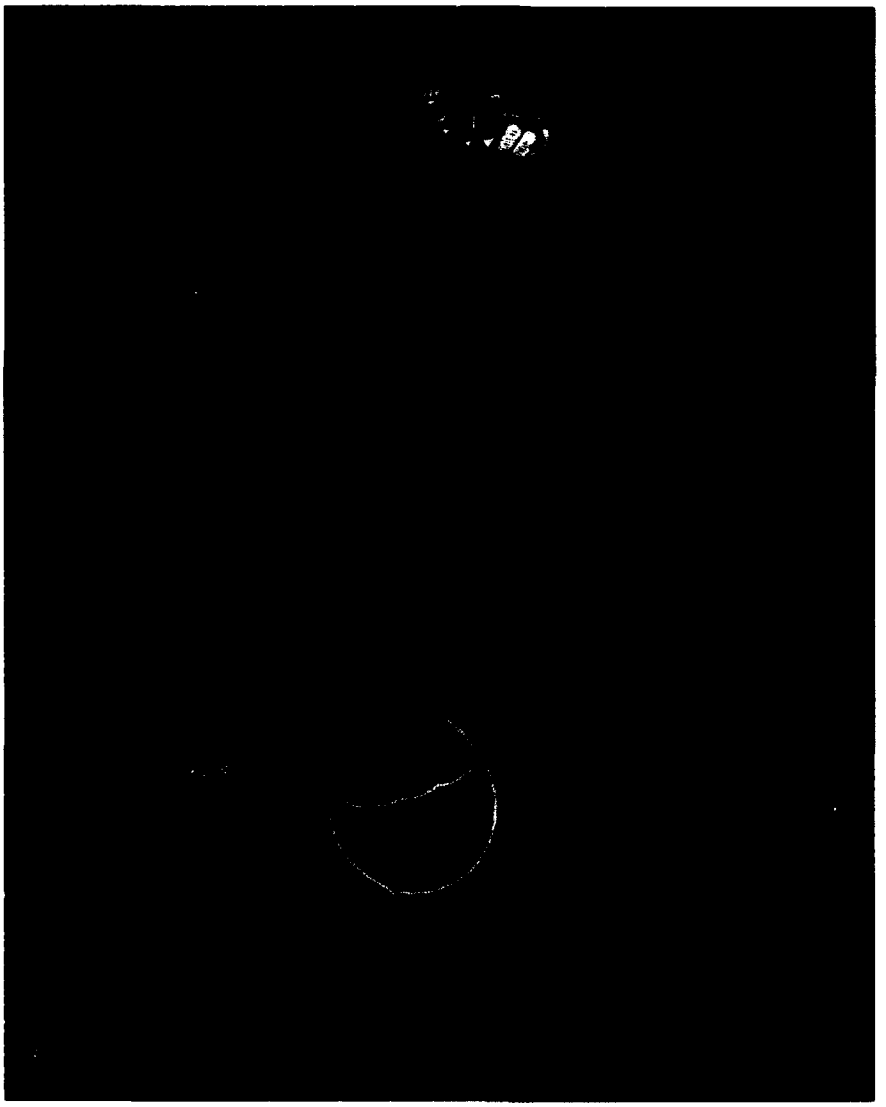

Global Imaging of the Ionosphere
Artist's Concepts/Illustrations, *Third Place*
Robert R. Meier
Space Science Division

The artist's concept illustrates a future Atmospheric and Ionospheric Remote Sensing (AIRS) system operating on a global scale. Images in spectrally pure light of selected ionospheric emissions will be processed and modeled to obtain global pictures of ionospheric conditions. Information on the electron density, ionospheric composition, morphology, and dynamics will be available from such data. Monitoring of "ionospheric weather" will lead to substantial improvement in Navy systems that rely on the propagation of electromagnetic radiation. A proof-of-concept program for AIRS, presently under development at NRL, is the Remote Atmospheric and Ionospheric Detection System (RAIDS) scheduled for 1992.

SPACE RESEARCH AND SATELLITE TECHNOLOGY

223 **Anomalous Cosmic Rays**
James H. Adams, Jr. and Allan J. Tylka

226 **Far Ultraviolet Cameras Experiment on STS-39: Observations of the Far UV Space Environment**
George R. Carruthers

231 **Probing the Magnetosphere by Using Chemical Releases from the Combined Release and Radiation Effects Satellite (CRRES)**
Paul A. Bernhardt, Joseph D. Huba, and Paul Rodriguez

234 **Battery Impedance Effects on Spacecraft Electrical Power System Stability**
Daniel J. Shortt and William E. Baker, Jr.

236 **Ground-based Laser Measurements of Vibration of the LACE Satellite**
Shalom Fisher, Donald Augenstein, and Kenneth I. Schultz

Anomalous Cosmic Rays

J.H. Adams, Jr. and A.J. Tylka
Space Science Division

Cosmic rays have long been known to come from the galaxy and occasionally from the Sun or interplanetary medium. In 1973, anomalous features in the spectra of He, N, and O at energies of ~10 MeV/nucleon were identified as a new component of the cosmic radiation.

Origin: Soon after the discovery, a theory was proposed for the origin of these "anomalous cosmic rays" [1]. According to this theory (Fig. 1), these particles arise from neutral atoms of the interstellar medium that sweep into the heliosphere as the solar system moves through interstellar space. (Only neutral atoms can do this, since the Sun's magnetic field easily deflects charged particles at these low velocities.) When these neutral atoms approach the Sun, they lose a single electron because of the ionization by solar UV photons or by charge exchange with particles of the solar wind. These singly-ionized particles then become entrained in the solar wind that carries them to the solar wind termination shock at the boundary of the heliosphere. Collisions with this standing shock increase the energies of these ions by a factor of ~1000. These energetic ions escape the acceleration region in all directions, and some head back toward Earth.

This theory makes two striking predictions. First, the elemental composition of anomalous cosmic rays should reflect that of the *neutral* local interstellar medium (LISM). Thus, the anomalous component should be strongest in the elements whose first-ionization potential is higher than that of hydrogen. (The atoms can remain neutral in the LISM because hydrogen atoms near the Sun absorb solar photons energetic enough to ionize them.) This first predicition has so far been borne out by observations. Second, the theory predicts that anomalous cosmic rays should be singly ionized. This is the key test of the theory, since galactic cosmic rays, solar energetic particles, and ions accelerated in other ways are completely or nearly completely stripped of electrons.

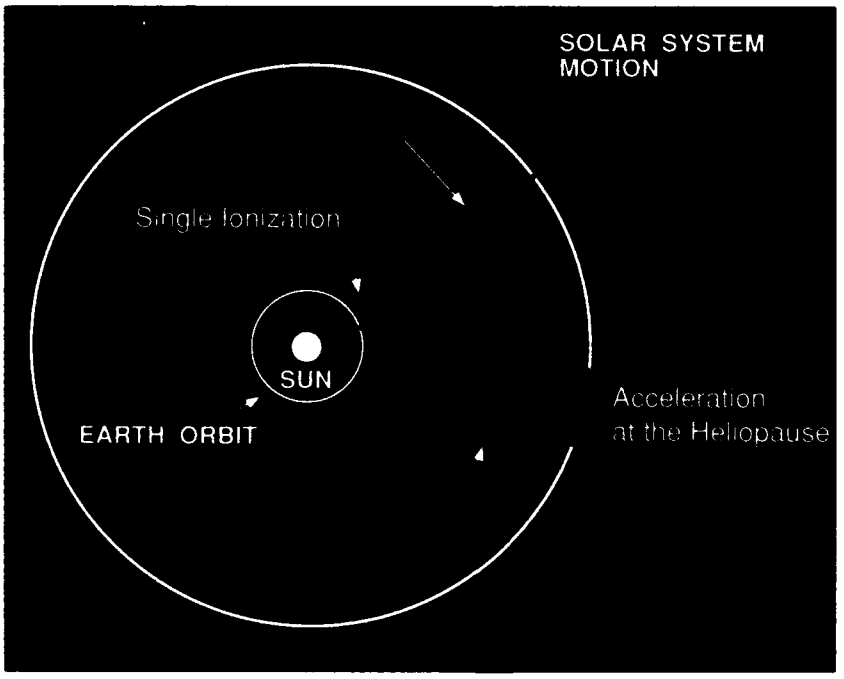

Fig. 1 — Origin of anomalous cosmic rays

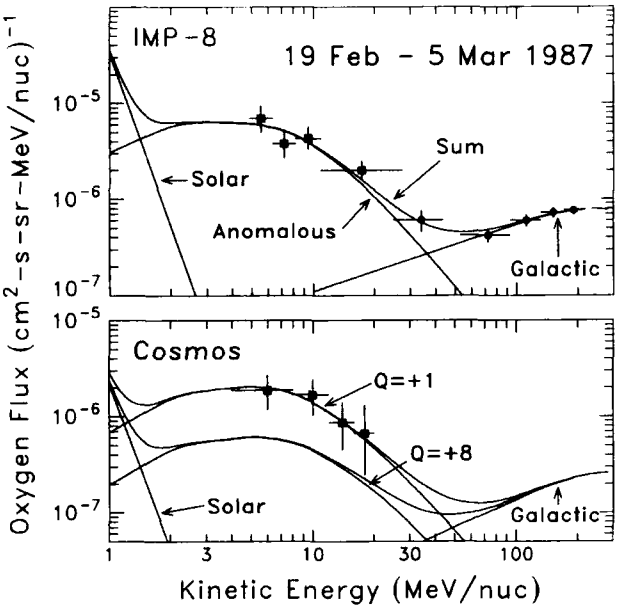

Fig. 2 — Determination of the charge state of anomalous cosmic ray oxygen. The top panel shows flux measurements outside the Earth's magnetosphere made aboard the US IMP-8 satellite. The curves show the contributions of solar, anomalous, and galactic particles to the observed flux. The bottom panel shows simultaneous measurements made inside the magnetosphere aboard a Soviet Cosmic satellite. The curves show the expected fluxes (based on the IMP-8 measurements) if the anomalous cosmic rays are either singly ionized ($Q = +1$) or fully ionized ($Q = +8$). The data clearly favor $Q = +1$, as predicted.

Charge State: A definitive measurement of the ionic charge state of anomalous cosmic ray oxygen was published in 1991 by an international collaboration, organizd and led by NRL [2]. Singly ionized particles are better able to penetrate the Earth's magnetic field than fully ionized ones. The charge state was thus inferred by comparing the observed anomalous cosmic ray flux inside the magnetosphere (which was measured aboard Soviet Cosmos satellites) with that measured outside the magnetosphere in interplanetary space (as measured on the US IMP-8 satellite). Since these fluxes vary with time, these two measurements must be made simultaneously. Figure 2 shows the results from one two-week period in which the comparison was made. By combining observations made over a period of 4 years, during which the anomalous flux varied by a factor of ~ 20, the average charge state of anomalous component oxygen was measured to be $0.9^{+0.3}_{-0.2}$.

Geomagnetially-Trapped Anomalous Cosmic Rays: This singly charged state also has another important consequence [3], as illustrated in Fig. 3. Because the ions are singly ionized, they can penetrate deeply into the magnetosphere and become geomagnetically trapped after being stripped of remaining electrons in the residual atmosphere. Our collaboration has recently reported the discovery of a belt of such trapped ions [4], where the flux of ~ 10 MeV/nucleon oxygen ions exceeds the interplanetary oxygen flux by a factor of ~ 1000.

Significance of Anomalous Cosmic Rays: One of the great goals of cosmic ray astrophysics is to understand the history of nucleosynthesis in the galaxy. The solar system provides us with a sample of matter that is approximately 4-billion years old. Galactic cosmic rays, on the other hand, are generally believed to be only approximately 10-million years old. Since anomalous cosmic rays come from the interstellar medium, they present a third sample of matter younger than the solar system but older than galactic cosmic rays. By comparing the isotopic compositions of these three samples, we can learn how the matter of the galaxy is evolving. We may also find evidence of unique events, such as nearby supernova, that may have triggered the formation of the solar system.

Anomalous cosmic rays are of practical importance as a potential space radiation hazard. Their enhanced access to low-earth orbit makes them the dominant cause of single-event upsets in

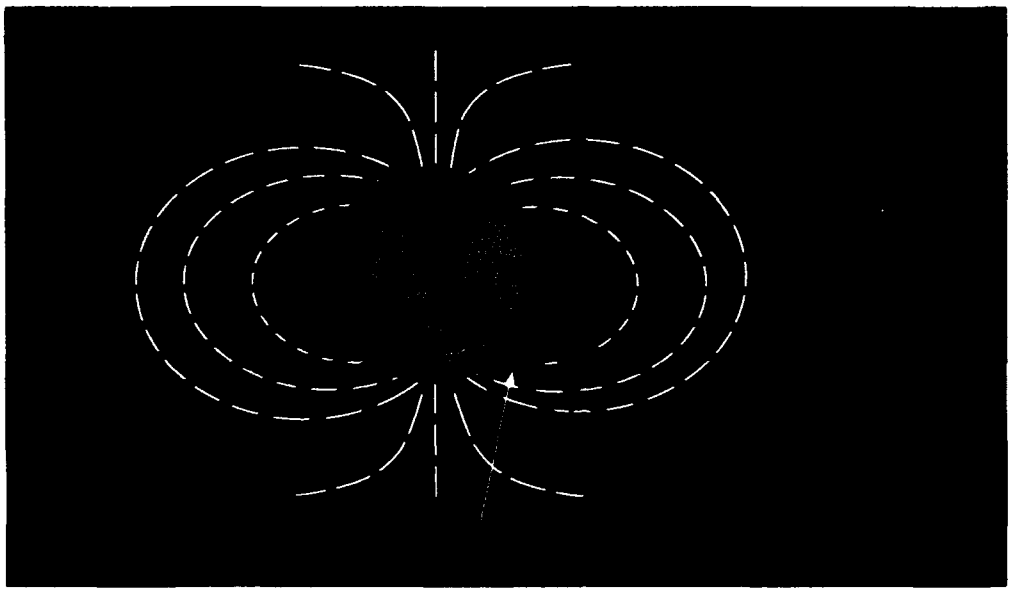

Fig. 3 — Geomagnetic trapping of an anomalous cosmic ray oxygen ion

some spacecraft electronic devices. The trapped anomalous cosmic rays are a new and unexplored radiation hazard for spacecraft that pass through this belt.

Physicists from the Aerospace Corporation, Caltech, University of Chicago, Goddard Space Flight Center, University of Maryland, the Max-Planck Institute for Physics and Astrophysics, Moscow State University, and NRL contributed to the work described here.

[Sponsored by NASA]

References

1. L.A. Fisk, B. Kozlovsky, and R. Ramaty, "An Interpretation of the Observed Oxygen and Nitrogen Enhancements in Low-Energy Cosmic Rays," *Astrophys. J. Lett.* **190**, L35-L37 (1974).

2. J.H. Adams, Jr., M. Garcia-Munoz, N.L. Grigorov, B. Klecker, M.A. Kondratyeva, G.M. Mason, R.E. McGuire, R.A. Mewaldt, M.I. Panasyuk, Ch.A. Tretyakova, A.J. Tylka, and D.A. Zhuravlev, "The Charge State of the Anomalous Component of Cosmic Rays," *Astrophys. J. Lett.* **375**, L45-L48 (1991).

3. J.B. Blake and L.M. Friesen, "A Technique to Determine the Charge State of the Anomalous Low-Energy Cosmic Rays," *Proceeding 15th Intl. Cosmic Ray Conference* **2**, 341-346 (1977).

4. N.L. Grigorov, M.A. Kondratyeva, M.I. Panasyuk, Ch.A. Tretyakova, J.H. Adams, Jr., J.B. Blake, M. Schultz, R A. Mewaldt, and A.J. Tylka, "Evidence for Trapped Anomalous Cosmic Ray Oxygen Ions in the Inner Magnetosphere," *Geophys. Res. Lett.* **18**, 1959-1962 (1991). ■

Far Ultraviolet Cameras Experiment on STS-39: Observations of the Far UV Space Environment

G.R. Carruthers
Space Science Division

The far-ultraviolet (105 to 200 nm) wavelength range is of fundamental importance to astronomy and to studies of Earth's upper atmosphere; it is also of potential significance and use to Deparment of Defense (DoD) applications. This wavelength range contains the resonance emission and absorption spectral features (transitions to and from the ground state) of the common atoms and molecules found in planetary and stellar atmospheres and the interstellar medium. Hence, the far-UV provides better sensitivity and quantitative accuracy in measuring these species than is possible at longer wavelengths. It also provides increased discrimination between hot and cool objects vs the visible and infrared. For DoD applications, a need exists to determine the natural background against which targets of DoD interest would have to be detected. Also, a need exists to directly measure artificial sources of potential DoD interest in the near-Earth space environment.

Up to the present, there have been numerous far-UV spectroscopic studies of Earth's upper atmosphere and far-UV astronomy investigations (such as NASA's IUE, HST, and Astro missions). However, little has been done in wide-field imaging surveys. A major objective of such surveys is to measure and map the naturally occurring far-UV background of point and diffuse sources over the whole (or a large portion of) the sky as observed in near-Earth space. These sources include upper-atmospheric airglow and auroras, celestial diffuse sources and diffuse background, stars, and galaxies.

NRL's far-ultraviolet cameras experiment was one of five experiments making up the Air Force Space Test Program's AFP-675 space shuttle payload. AFP-675 flew on mission STS-39 from 28 April to 6 May 1991. The far-UV cameras objective was to collect—over wide fields of view—imaging and photometric information about natural and artificial sources of far-ultraviolet radiation in near-Earth space. The two cameras were sensitive to the 105 to 160 and 123 to 200 nm wavelength ranges, with auxiliary filters providing narrower bands of 123 to 160 and 165 to 200 nm.

Upper Atmosphere Observations: The experiment observed the Earth's upper atmosphere in imaging of the night horizon airglow and auroras (Fig. 4). Previous investigations have shown that the night sky is very bright in hydrogen Lyman-α (121.6 nm) emission. The horizon, as seen at night by the far-UV cameras in Lyman-α emission, is sharply defined by molecular oxygen absorption in the lower atmosphere at an apparent altitude of about 65 km (Fig. 5 (a)). Stars were also observed as they were occulted by the atmosphere, allowing measurement of the absorption of far-UV starlight by O_2. These latter measurements were made simultaneously in two wavelength ranges (123 to 160 and 165 to 200 nm). These observations demonstrate means for horizon-sensing and for remote-sensing measurements of O_2 density vs altitude in the night-time atmosphere.

The cameras also observed night airglow in the upper atmosphere. In the 165 to 200 nm wavelength range, an airglow layer apparently caused by nitric oxide (NO) band emission is observed centered near 120 km altitude (Fig. 5(b)). Also, a higher-altitude (200 to 300 km) airglow of atomic oxygen emissions (130.4 and 135.6 nm) resulting from recombination of ionized oxygen (O^+) with electrons was observed. Since O^+ is the dominant ion in the F region of the ionosphere, this demonstrated a means for remote sensing of the night ionosphere.

The cameras observed the southern polar aurora in the 105 to 160, 123 to 160, and 165 to 200 nm ranges. Although the observing conditions were not optimal for our objectives, we expect to obtain useful information on the incoming charged particles that produce the aurora by comparing the images in the various wavelength ranges.

Shuttle Glow Observations: Observations of the mysterious shuttle glow were made for the first time in the far UV. The previously observed visible surface glow appears on vehicle surfaces facing the direction of motion, i.e., which impact the ambient atmosphere at the 8 km/s orbital velocity. The far-UV cameras obtained images of one side of the vertical tail of the shuttle while that surface was facing the direction of motion. Little or no glow was observed in the wavelength range below 160 nm, but a definite glow was seen in the 165 to 200 nm wavelength range (Fig. 6). This latter glow is more diffused than that observed in the visible, and it is most likely because of NO band emissions.

Celestial Target Observations: The far-UV cameras observed 12 star fields, each 20° in diameter. The fields included the large and small Magellanic Clouds (our nearest external galaxies), the Virgo cluster of galaxies, and several fields along the plane of our own galaxy (the Milky Way). The cameras also obtained measurements of the diffuse UV background radiation at high- and low-galactic latitudes.

One of the most interesting fields includes the head of the constellation Scorpius, where vast interstellar dust clouds are revealed for the first time in far-UV wavelengths (Fig. 7). Comparisons of the images in the 123 to 160 and 165 to 200 nm ranges and with ground-based images are expected to provide new information regarding the scattering and absorbing properties of dust particles as a function of wavelength; this ultimately may lead to greater insight into the physical properties and chemical composition of the dust particles, as well as the spatial distribution of dust density.

Fig. 4 — The space shuttle mission STS-39 conducted a wide variety of investigations of the near-Earth space environment and of artificial effects associated with the shuttle vehicle. In this photograph, a bright auroral display is visible in the background at the same time as are the plumes of the shuttle's orbital maneuvering system rocket engines.

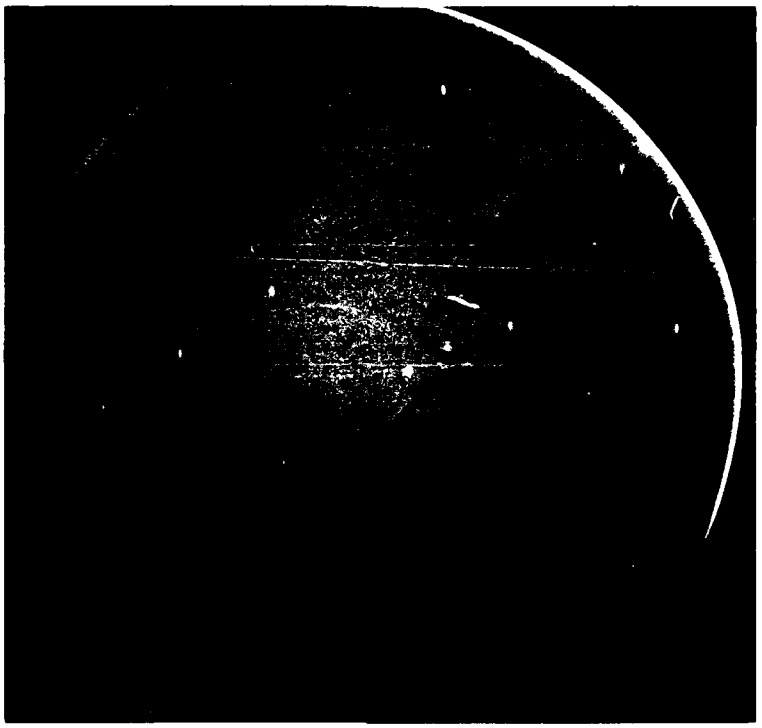

(a)

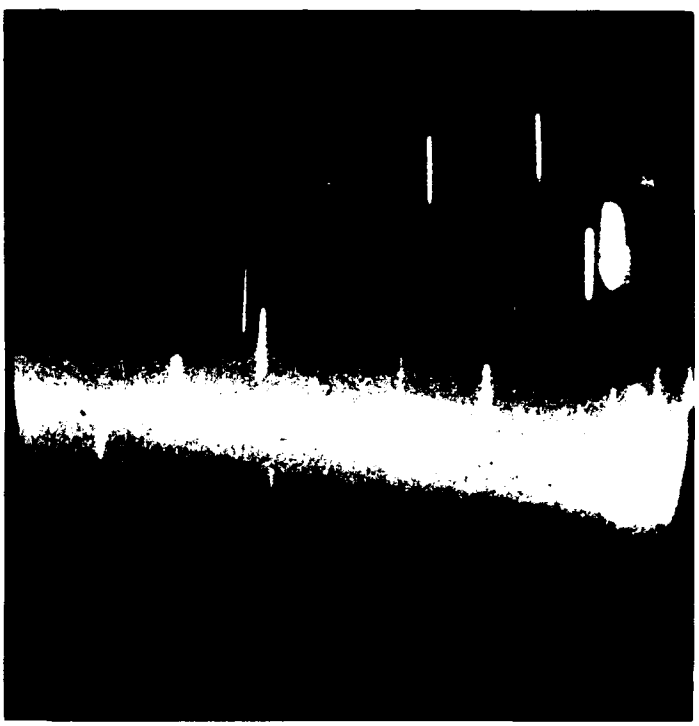

(b)

Fig. 5 — (a) Image of the Earth limb taken with the #1 far-UV camera in the 105 to 160 nm wavelength range (dominated by hydrogen 121.6 nm emission). Note the relatively sharp "horizon," defined by molecular oxygen absorption in the mesosphere; (b) image of the Earth limb taken with the #2 far-UV camera in the 165 to 200 nm wavelength range. Note the airglow layer thought to be caused by nitric oxide band emission. Also note attenuation of trailed star images in this 30-s exposure caused by the molecular oxygen absorption in the mesosphere.

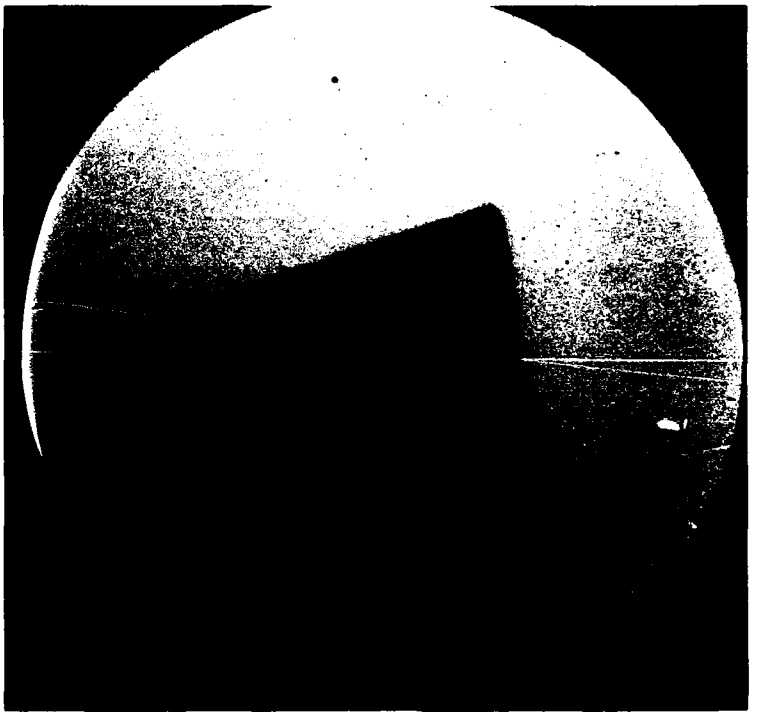

(a)

(b)

Fig. 6 — (a) Image of the shuttle vehicle stabilizer obtained with the #1 far-UV camera in the 105 to 160 *nm wavelength range. The bright* Lyman-α night sky glow is apparent, as is the tail by reflected skyglow. Note that the leading edge of the tail, which is black in the visible, appears to be more reflective in the far-UV than the side of the tail, which is white in the visible; (b) image of the shuttle vertical stabilizer obtained with the #2 far-UV camera in *the 165 to 200 nm wavelength range. A definite* diffuse glow is seen over the tail in this wavelength range, and it is thought to be caused by nitric oxide band emission.

(a)

(b)

Fig. 7 — (a) Image of the northwest portion of the constellation Scorpius obtained with the #1 far-UV camera in the 123 to 160 nm wavelength range. A diffuse glow of dust-scattered far-UV starlight is observed, as well as dark clouds that are silhouetted against this diffuse background. Some of the dark clouds exhibit "bright rim" features (denoted by arrows); (b) as in (a), but taken with the #2 far-UV camera in the 165 to 200 nm wavelength range.

The analyses of the images returned by the far-UV cameras has barely begun and will probably take years to complete. In addition to having scientific value in its own right, however, it is already apparent that much information useful in planning future, more advanced experiments has been obtained.

Acknowledgments: The contributions of many persons, including past and present NRL employees to the development and successful operation of the experiment, are gratefully acknowledged. The Air Force Space Test Program provided the flight opportunity as part of the AFP-675 mission. Support was also provided by Lockheed Missiles and Space Corporation, the Aerospace Corporation, and NASA.

[Sponsored by ONR]

References

1. G.R. Carruthers, "The Far UV Cameras (NRL-803) Space Test Program Shuttle Experiment," in *Ultraviolet Technology* **687**, Proceedings of the SPIE, p. 11 (1986).
2. G.R. Carruthers, "The Naval Research Laboratory's Far-Ultraviolet Cameras and Far-Ultraviolet Imaging Spectrograph Space Shuttle Investigations," Proceedings of Short Wavelength Phenomenology and Applications Conference, Johns Hopkins University Applied Physics Laboratory, Vol. 1, p. 367 (1990). ■

Probing the Magnetosphere by Using Chemical Releases from the Combined Release and Radiation Effects Satellite (CRRES)

P.A. Bernhardt, J.D. Huba, and P. Rodriguez
Plasma Physics Division

CRRES Mission Overview: The CRRES program used the scientific resources of the National Aeronautics and Space Administration (NASA) and the Department of Defense (DoD) to (1) perform chemical release experiments in the ionosphere and magnetosphere, (2) study the natural radiation environment and its effects on electronic circuit components, and (3) probe naturally occurring ionospheric irregularities. The CRRES program was synthesized from the NASA chemical release module (CRM), the AFGL space radiation (SPACERAD) experiments, the NRL low altitude satellite studies of ionospheric irregularities (LASSII) instruments, and the ONR heavy ion detectors. The chemical release segment of the CRRES mission was greatly enhanced by the support provided by the in situ measurements of both the SPACERAD and LASSII instruments.

The CRRES spacecraft was launched on 25 July 1990 at 1921 universal time. Eight small and sixteen large canisters were held by injection tubes located on two side of the satellite. The chemical release experiments were conducted in a geosynchronous transfer orbit with apogee and perigee of 33,600 and 350 km, respectively. The experiments were designed to investigate stimulated electron and ion precipitation, ion transport in the magnetotail, critical ionization velocity (CIV), field line tracing and parallel acceleration, diamagnetic cavity formation and collapse, and plasma instabilities.

LASSII used a pulsed plasma probe (P^3), quadrupole ion mass spectrometer (QIMS), and a very low frequency wave analyzer (VLFWA) to record the effects of the releases below 550-km altitude. The SPACERAD instruments (the medium energy electron and proton spectrometer, low energy plasma analyzer, mass composition instruments, fluxgate magnetometer, search coil magnetometer, Langmuir probe-cold plasma experiment, and passive plasma sounder) were used near apogee. Both sets of instruments were used to determine when the ambient conditions were suitable for release and to record the effects following each high altitude release.

A network of ground-based optical stations were set up around the globe to observe the CRRES releases. NRL's low-light-level cameras

in New Mexico and in the Caribbean recorded images of the ion and neutral clouds from the releases. Figure 8 shows a neutral barium (green) and singly ionized barium (red-blue) 84 s after a release at 6000-km altitude. By using a high resolution telescope, a new type of plasma structure was discovered near the chemical injection point. The source of this structure, called *cycloid bunching*, is being studied with computer models.

Diamagnetic Cavities: All barium releases near 33,000-km altitude contained enough energy to displace the ambient magnetic field to generate diamagnetic cavities. This was expected, since scientists had previously observed this phenomena in space and laboratory experiments [1,2]. During the CRRES mission, diamagnetic cavities were studied with large (10 kg) or small (1.5 kg) releases of barium into regions having a range of magnetic field strengths 5000, 1000, 280, and 125 nT. The effects were measured with in situ SPACERAD instruments on CRRES and with remote optical systems.

A magnetohydrodynamic (MHD) simulation [3] of the CRRES releases has been used to model the CRRES diamagnetic cavities. Figure 9 shows the time history of the magnetic field and electron density for a simulation of one of the CRRES releases. The simulation provides a good match to the observations with the CRRES magnetometer and with ground-based cameras.

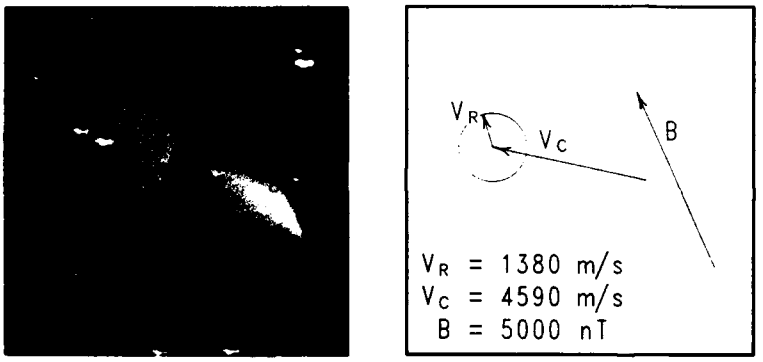

Fig. 8 — Neutral (green) and ion (blue green) clouds from the CRRES barium release. The ions are deposited on the field lines near the release point shown by the red circle. The asymmetric neutral cloud indicates that the initial velocity distribution was not spherical.

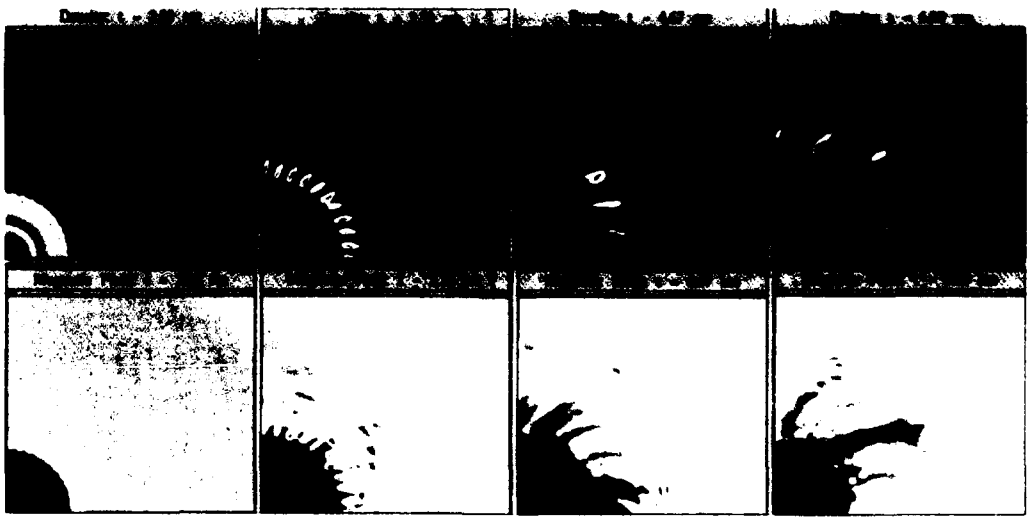

Fig. 9 — MHD simulation of the CRRES barium release in the magnetosphere. The expanding ion cloud forms a diamagnetic cavity with surface irregularities. After the cavity collapsed, the residual structure was measured with satellite instruments and ground-based cameras.

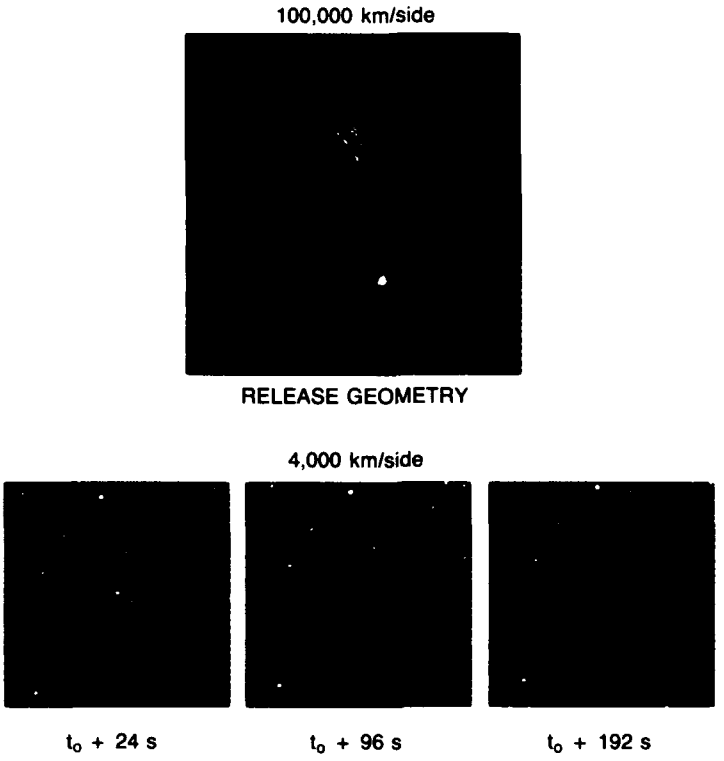

Fig. 10 — Location of the CRRES lithium release into the outer zone radiation belts. The release was designed to produce auroral displays at the foot of the field line. The sequence of photos shows the expanding neutral cloud.

Artificial Aurora: The CRRES releases may have produced artificial aurora by enhancing energetic particle precipitation. The radiation belts in the magnetosphere are composed of energetic particles trapped on geomagnetic field lines. An enhancement of cold plasma density near the equatorial regions of the outer radiation belts can lead to an increase in auroral precipitation.

The CRRES mission used three lithium releases and two barium releases to artificially stimulate particle precipitation (STEP). All of the releases occurred at about 33,000-km altitude in the outer zone radiation belt. The injected neutrals photoionized and the resulting ions flowed along the magnetic field lines enhancing the cold plasma density. Figure 10 shows a schematic of the lithium release on a closed field line and a sequence of images for the neutral lithium cloud. Following both large barium releases, the auroral activity increased within 5 min. These observations were made with low-light-level cameras in aircraft flying near the predicted deposition regions over Canada. Further theoretical and experimental analyses needs to be done before the CRRES scientist can determine if the release caused the aurora.

Conclusions: The CRRES chemical release mission attempted to conduct a complex variety of active experiments by using vapor injections from an orbital spacecraft. Each individual release was efficiently used to satisfy multiple objectives. The CRRES mission was supported by ground based diagnostics and by spacecraft instrumentation. Ongoing analyses of data acquired during the CRRES high-altitude releases should provide a better understanding of the space plasma environment.

[Sponsored by NASA]

References

1. P.A. Bernhardt, R.A. Roussel-Dupre, M.B. Pongratz, G. Haerendel, A. Valenzuela, D. Gurnett, and R.R. Anderson, "Observations and Theory of the AMPTE Magnetotail Barium Releases," *J. Geophys. Res.* **92**, 5777-5794 (1987).
2. B.H. Ripin, E.A. McLean, C.K. Manka, C. Pawley, J.A. Stamper, T.A. Peyser, A.N. Mostovych, J. Grun, A.B. Hassam, and J.D. Huba, "Large-Larmor-Radius Interchange Instability," *Phys. Rev. Lett.*, **59**, 2299 (1987).
3. J.D. Huba, P.A. Bernhardt, and J.G. Lyon, "Preliminary Study of the CRRES Magnetospheric Barium Releases," *J. Geophys. Res.*, (in press) (1992). ■

Battery Impedance Effects on Spacecraft Electrical Power System Stability

D.J. Shortt and W.E. Baker, Jr.
Space Systems Development Department

One of the tasks of the Space Systems Development Department is to accurately determine the performance of power system components under various types of conditions. A typical low-earth-orbit spacecraft's electrical power system consists of a solar array (power generation), batteries (power storage), distribution, instrumentation, and control circuitry. A typical battery model that has been used to examine the stability of an electrical power system is a simple resistor-capacitor network. While this type of model adequately predicts the high-frequency system response (for example, > 100 Hz), it does not accurately predict the low-frequency response.

This paper describes another battery model consisting of passive components, which is more accurate than the previously mentioned model. This proposed battery model is used in a stability analysis to develop the open-loop transfer function and closed-loop transient responses for an electrical power system.

Nonlinear Modeling: The basic modeling technique used in this analysis is the describing function. In this method, the transfer characteristics of a nonlinearity are represented by quasi-linear approximate (describing) functions. A sinusoidal input is normally assumed as the input to the nonlinearity. A requirement for the use of this technique is that the linear part of the system should filter the output of the nonlinearity sufficiently. (See Ref. 2 for a more detailed discussion).

Component Model Development: Figure 11 shows a simplified form of the small-signal model for a spacecraft battery charger. The transfer functions (gain and phase) are derived in Ref. 2.

Battery Characteristics: For the purposes of this analysis, an electrochemical cell can be thought of as an impedance to a small sinusoidal excitation. The rate of an electrochemical reaction can be strongly influenced by diffusion of a reactant towards or a product away from the electrode surface. Whenever diffusion effects completely dominate the electrochemical reaction mechanism, the impedance is called the Warburg impedance [1]. This impedance represents a kind of resistance to mass transfer. By examination, the battery cells of interest are kinetically rather sluggish. (Therefore, the Warburg impedance is assumed to be inductive.)

In contrast to R_S, L_S (wire impedance effects) and C_p (double layer capacitance) (which are nearly ideal circuit elements (Fig. 12)), the components of the Warburg impedance are not ideal; they change with frequency. A given equivalent circuit represents the battery performance at a given frequency but not necessarily at other frequencies. The circuit elements were obtained by a best-guess approach and/or existing available battery data.

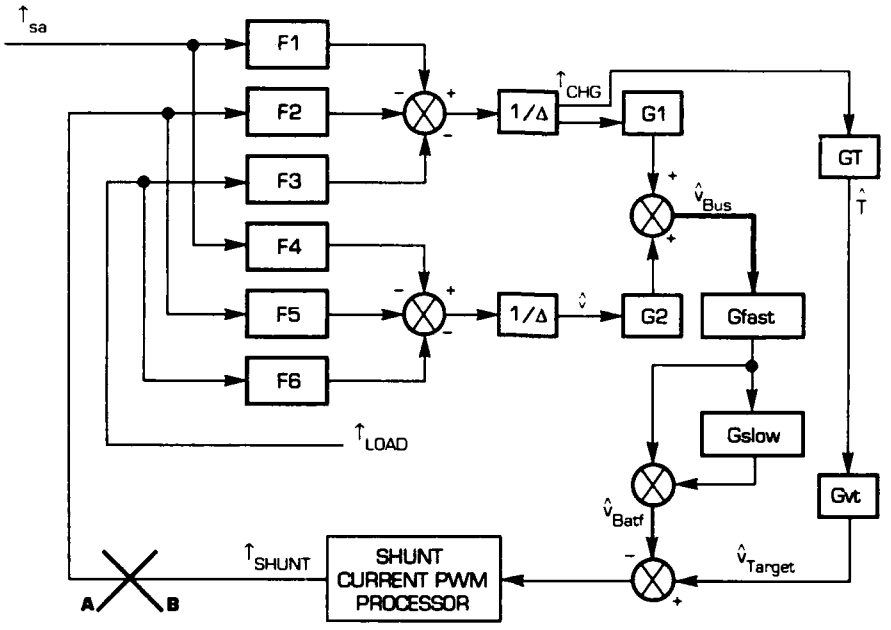

Fig. 11 — Spacecraft battery charger

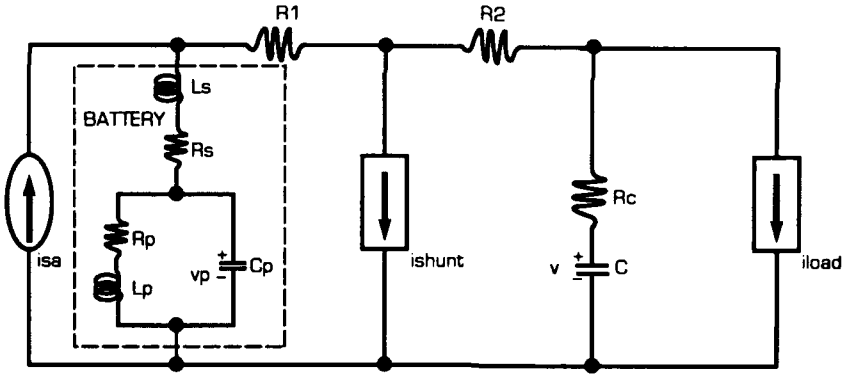

Fig. 12 — Electrical power system

The transfer functions for the battery model were derived by using the circuit model in Fig. 12. From Ref. 2, the equations are put into the following form for the AC model:

$$\dot{\hat{x}} = A\hat{x} + B\hat{u}$$

Using the Laplace transform to solve for $x(s)$ results in the following expression:

$$\hat{x}(s) = [sI - A]^{-1} + B\hat{u}(s).$$

This expression was used to determine the transfer functions shown in Fig. 11 and listed in Ref. 2. The open-loop transfer function is found by opening the control loop and determining the transfer function from A to B (Fig. 11). Note that there are two loops; the expressions for both are shown in Ref. 2.

Simulation Results: Knowing the battery impedance characteristic, as discussed previously, and employing a computer program to compute the frequency dependent battery Warburg impedance

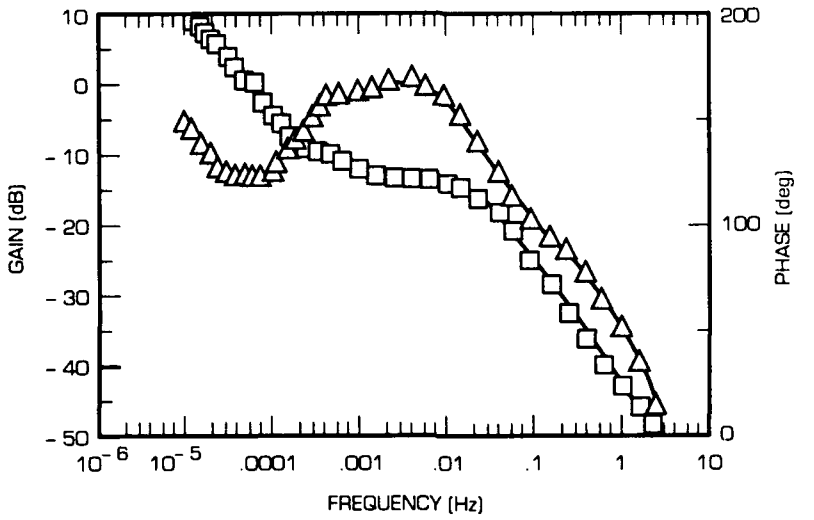

Fig. 13 — Open-loop gain (blocks) and phase margin (triangles)

has enabled a complete open-loop analysis to be simulated. Figure 13 shows the open-loop gain and phase plot. The phase margin is $\approx 120°$ and the gain margin is ≈ 50 dB. This figure represents the V-T charge mode with the battery impedance, as shown in Fig. 12.

Conclusion: A stability analysis has been performed that uses the nonlinear describing function technique. A more accurate battery model has been proposed that includes the effect of the Warburg impedance. This has enabled a complete open-loop analysis; otherwise, the analysis would have had to be performed in a piece-wise linear fashion

The battery model needs to be verified and adjusted to accurately reflect the actual conditions of the proposed system. A testing facility or a test bed should be established so that as the data are collected and evaluated, they can be implemented into the appropriate computer simulation.

[Sponsored by ONR]

References

1. A.J. Bard and L.R. Faulkner, *Electrochemical Methods: Fundamentals and Applications*, (J. Wiley and Sons, New York, 1980).

3. D.J. Shortt and W.E. Baker, "Battery Impedance Effects on Spacecraft Electrical Power System Stability," Proceedings of the 1990 IECEC. ■

Ground-based Laser Measurements of Vibration of the LACE Satellite

S. Fisher
Spacecraft Engineering Department
D. Augenstein
University of Maryland
College Park, Maryland
and
K.I. Schultz
Massachusetts Institute of Technology Lincoln Laboratory
Lincoln, Massachusetts

Vibration signatures from the Low-power Atmospheric Compensation Experiment (LACE) satellite were obtained from the ground-based Firepond coherent CO_2 laser radar operated by MIT Lincoln Laboratory in January 1991. This dynamics experiment was conducted out of a need to obtain structural dynamics data from an orbiting spacecraft. It is well known that the analysis, design, and construction of modern spacecraft

necessary to address Navy, DoD, and NASA requirements demand a thorough knowledge of the response of orbiting systems to structural vibrations generated by antenna slews, by the attitude control system, and by environmental forces. To treat and analyze such structural concerns, sophisticated computer simulation programs and ground-based laboratory experiments have been developed. However, on-orbit data and experience are still required to refine and validate structural dynamics models. Because of the high cost of space experiments, only one on-orbit vibration experiment—the Solar Array Flight Experiment (SAFE) [1]—had been conducted prior to the LACE's dynamics experiment. In the SAFE experiment, a boom similar to the LACE booms was deployed with a solar blanket and attached tension wires. A measurement apparatus on board the space shuttle was used to observe boom vibrations during an 18-h period.

With the LACE's dynamics experiment, on-orbit structural dynamics information is obtained by ground-based laser radar reflections from targets on the spacecraft. Costs were kept relatively low because the LACE satellite was built and launched by NRL and because minimal flight hardware was needed.

Description of the LACE: The LACE satellite was launched on 14 February 1990 into a 540-km altitude circular orbit of 43° inclination. The spacecraft, shown in Fig. 14(a), was built for the Strategic Defense Initiative Organization by NRL. The 1400-kg Earth-pointing LACE spacecraft has three deployable/retractable booms of maximum length 45.72 m. The zenith-directed gravity gradient boom is mounted on the top of the bus with a magnetic damper at its tip; the forward or retroboom is deployed along the velocity vector; the balance boom is mounted and deployed counter to the velocity. Attitude stabilization to within about 1° libration amplitude is accomplished with the magnetic damper and by a constant speed momentum wheel installed in the bus to control roll and yaw motion. Constant-rate boom deployment/retraction maneuvers are remotely controlled through a ground-based telemetry link. At the tip of the forward or retroboom, an array of glass retroreflectors is installed to serve as targets for ground-based lasers in the visible light spectrum. The goal of the LACE experiment is to evaluate atmospheric compensation techniques.

The dynamics experiment is a low-cost "piggyback" experiment secondary to the primary LACE mission. With this dynamics experiment, vibrations of the LACE satellite structure are generated by deployment/retraction maneuvers of the booms. To facilitate ground-based coherent IR laser radar measurements in the dynamics experiment, IR germanium retroreflectors are mounted on the tip of the lead boom, on the bottom of the satellite body, and on the tip of the trailing boom, as shown in Fig. 14(a). The Firepond laser radar targets the germanium reflectors, as shown in Fig. 14(b). Two of the reflectors are illuminated simultaneously to provide differential Doppler measurements of the relative motion between the end of the boom and the spacecraft body. This relative motion is generated by the vibrations of the boom tip relative to the body and by the rigid-body satellite motion and the retraction motion of the boom.

Results and Discussion: The dynamics experiment successfully used laser Doppler methods to measure vibrations of LACE from the MIT Lincoln Laboratory's Firepond Laser Radar facility located near Westford, Massachusetts on 7, 8, and 10 January 1991 (denoted in this article as days 91007, 91008, and 91010). The lead boom was retracted from 24.384 m to 4.572 m during illuminations from the IR laser radar. Forced vibrations of the LACE structure were observed during the retraction, and free-damped system vibrations were observed after the retraction was stopped.

The laser Doppler measurement window of day 91007 observed about 38 s of forced dynamic motion of the lead boom while the boom was being

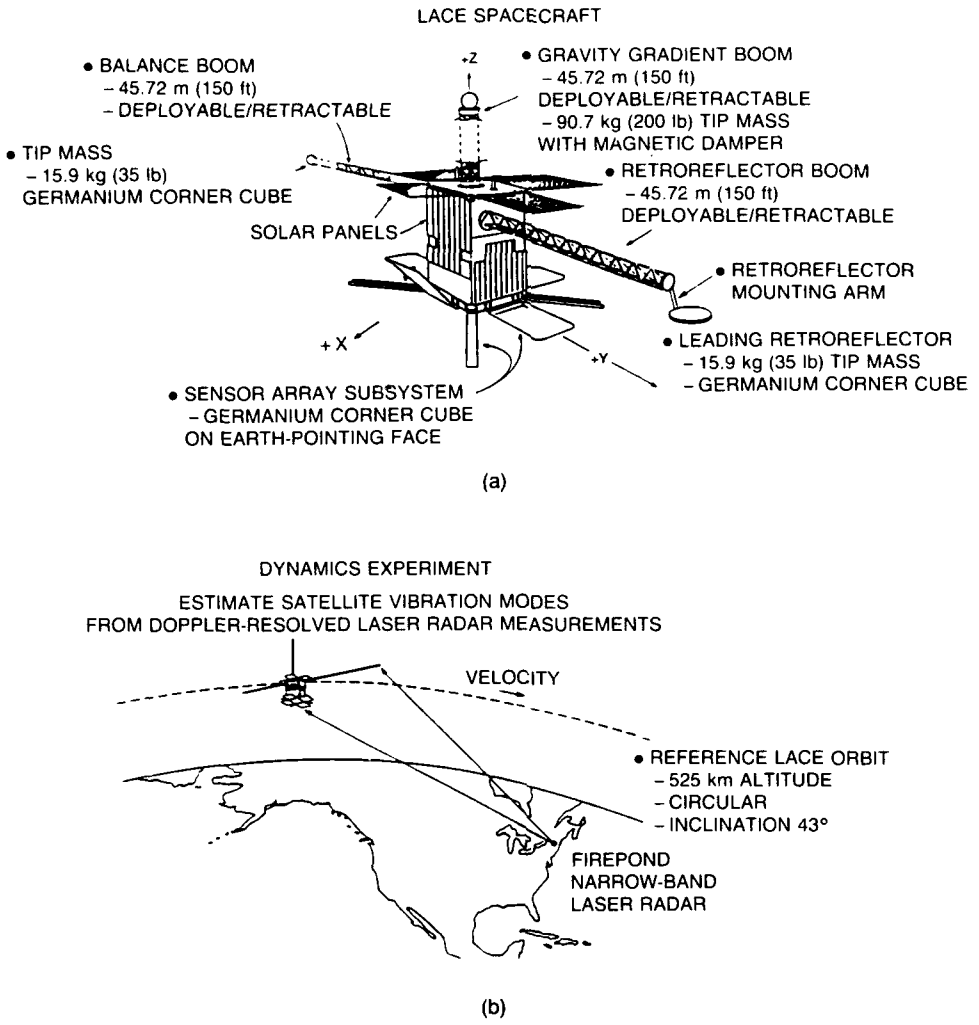

Fig. 14 — (a) LACE satellite and (b) trajectory

retracted. The window of day 91008 contained about 68 s of retraction data and 25 s of free-decay data after retraction was stopped. Although day 91007 data are not presented in this article, the results are consistent with data collected on day 91008. Day 91010 data contained 45 s of useful free-decay data after retraction was stopped.

Finite Element Modeling (FEM): A NASTRAN finite element analysis was performed on the LACE system, modeled according to the postretraction configuration with the gravity gradient and the balance booms at 45.72 m and the retroboom at 4.572 m. This is a "stick" model in which the booms are built as simple beams, rather than as trusses. Modal frequency values derived from this model are given in Tables 1 and 2, where they are compared with modal frequencies identified from the Doppler measurements.

Retraction Analysis: For the data collected during the boom retraction maneuver, the power spectral density (PSD) of a moving Hamming window of length 24 s is computed at 0.1-s intervals. Figure 15 shows a typical PSD of day 91008. Table 1 compares the forced system response with free-system modes obtained by the Eigensystem realization algorithm (ERA) developed by Juang et al. [2] and the minimum

Table 1 — Day 91008 Identification Results: Modal and PSD Frequencies

Model Mode (Hz)	ERA (Hz)	Std. Dev. (Hz)	ERA/MME (Hz)	Std. Dev. (Hz)	PSD Princ. (Hz)	PSD Second. (Hz)
0.1298	0.1225	0.0005	0.1226	0.0005	0.30	0.15
0.3238	0.3245	0.0003	0.3248	0.0006	1.44	1.00
	0.5219	0.0025	0.5201	0.0030		2.40

Table 2 — Day 91010 Identification Results: Modal Frequencies

Model Mode (Hz)	ERA (Hz)	Std. Dev. (Hz)	ERA/MME (Hz)	Std. Dev (Hz)
0.0191	0.0208	0.0033	0.0210	0.0020
0.1298	0.1244	0.0010	0.1245	0.0011
0.3238	0.3312	0.0009	0.3320	0.0008
	0.5115	0.0061	0.5120	0.0064

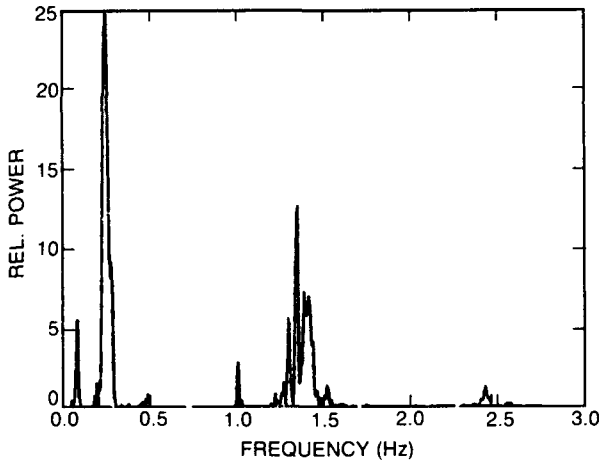

Fig. 15 — Power spectral density, day 91008

model error method (MME) developed by Mook et al. [3] for frequencies with principal and secondary power densities. In Fig. 16, the PSD characteristics are shown as the boom is retracted from 10 m to 4.572 m. The figure shows how the retraction PSDs changed during the retraction process. The heaviest concentration of spectral activity occurs in two dominant bands of ranges 0.1 to 0.7 Hz and 1.2 to 1.6 Hz. It is readily seen from this figure that, with decreasing boom length, there is an increasing trend in the frequencies of the two dominant bands. Between 1.0 and 1.2 Hz, another band of significant amplitude emerges. This band corresponds to the nominal 1 Hz driving frequency of the boom deployment mechanism.

Identification Analysis: The system identification proceeds by attempting to duplicate the structural internal dynamics with an impulse response model. The identification method uses linear system realization theory, which provides error bounds on the model's performance. The algorithms used are the ERA [2] and the MME [3]. Tables 2, 3, and 4 detail the results of this study. Four vibration modes were detected on day 91010, three of which were among the first four pitch plane vibration modes. Three vibration modes were detected on day 91008, two of which were among the first four pitch plane vibration modes. The lowest mode predicted is detectable only when the rigid body motion is removed from the data of day 91010. Day 91008 observation window was only 25-s long, and this observation was too short to collect enough data on the lowest mode (modal period is approximately 50 s).

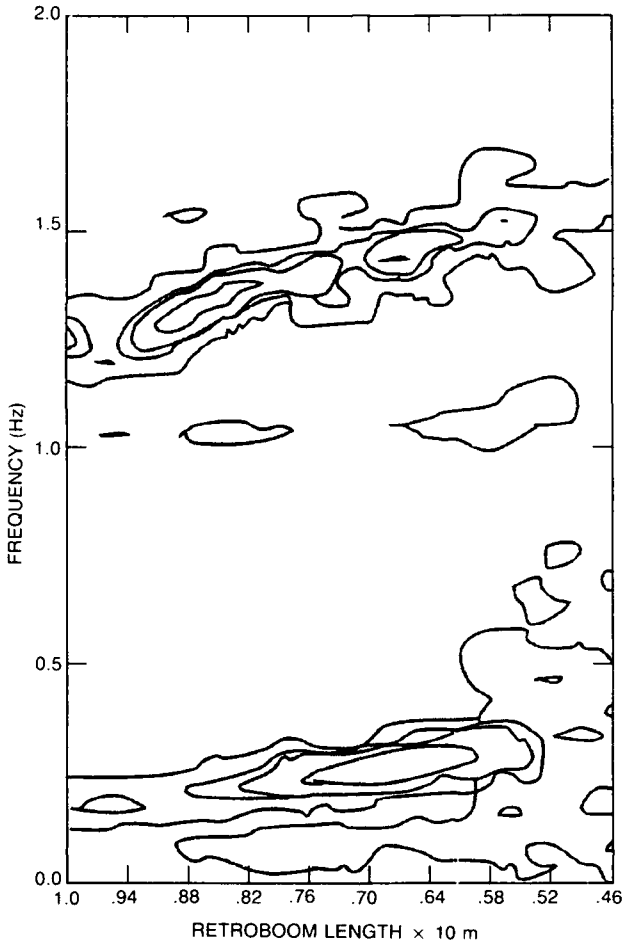

Fig. 16 — Power spectral density vs boom length during retraction

Table 3 — Day 91008 Identification Results: Damping Factors

Model Mode	ERA (%)	Std. Dev.	ERA/MME (%)	Std. Dev
0.1298	—	0.2489	—	0.3027
0.3238	1.4477	0.0410	1.1137	0.0473
	4.8917	0.2984	4.5929	0.2631

Table 4 — Day 91010 Identification Results: Damping Factors

Model Mode	ERA (%)	Std. Dev.	ERA/MME (%)	Std. Dev
0.0191	1.8385	1.8277	1.3937	2.260
0.1298	2.3233	0.5182	2.1029	0.3007
0.3238	2.1114	0.2312	2.0058	0.2971
	10.4537	1.2157	10.7973	1.0233

Both days 91008 and 91010 detected a mode not previously predicted by the FEM model. This moderately damped mode at approximately 0.52 Hz has higher damping than the other derived modes. While the explanation for this mode is yet unknown, it is believed to be due to either unmodeled behavior within the boom canisters or vibrations of the cantilevered retroreflector plate.

Comparison with Ground Tests and the SAFE Experiment: The computed damping is comparable to the values of 1.4% to 2.7% measured for the Voyager magnetometer boom by the Marshall Space Flight Center, Huntsville, Alabama, [4] and the values of 1.2% to 3.5% measured at the Canadian Communications Research Centre, Ottawa, Canada, for an astromast of design similar to the LACE booms [5]. With the SAFE boom, the vibrations measured out of the plane of the solar blanket can be compared to our results. The out-of-plane modes had damping factors of 3% to 6% depending on day/night. This damping was higher than ours, possibly because of the tension wires [6].

Conclusions: The LACE dynamics experiment has established the feasibility of ground-based laser measurements of vibrations, slews, and deployments in orbiting satellites. The technique can be applied to health monitoring of large structures, such as the space station. The experiment has demonstrated that resolutions of 1.8 mm/s are attainable with the current Firepond apparatus.

[Sponsored by SDIO]

References

1. J.N. Juang and R.S. Pappa, "An Eigensystem Realization Algorithm (ERA) for Modal Parameter Identification and Model Reduction," *AIAA J. Guidance, Control and Dynamics* **8**(5), 620-627 (1985).

2. D.J. Mook and J.L. Junkins "Minimum Model Error Estimation for Poorly Modeled Dynamic Systems," *AIAA J. Guidance, Control and Dynamics* **11**(4), 365-375 (1988).

3. Lockheed Missiles and Space Company Report No. LMSC-F087173, "Solar Array Flight Experiment Final Report," Marshall Space Flight Center, Huntsville, Alabama Contract NASA-31352, 1986.

4. G.D. Johnson, "Modal Tests of the Voyager Magnetometer Boom," letter ET53(83-98) to H. Waites, Marshall Space Flight Center, Huntsville, Alabama, October 24, 1983.

5. Y. Soucy and F. Vigneron, "Modelling and Identification of the Structural Properties of an Astromast," Communications Research Center, CRC Report No. 1374, Ottawa, Canada, Nov. 1983.

6. L.E. Young and H.C. Pack, Jr., "Solar Array Flight Experiment/Dynamic Augmentation Experiment," NASA Technical Paper 2690, Marshall Space Flight Center, Huntsville, Alabama, 1987. ■

Sunspots
Computer Graphics, *Honorable Mention*
Lisa McCorkle

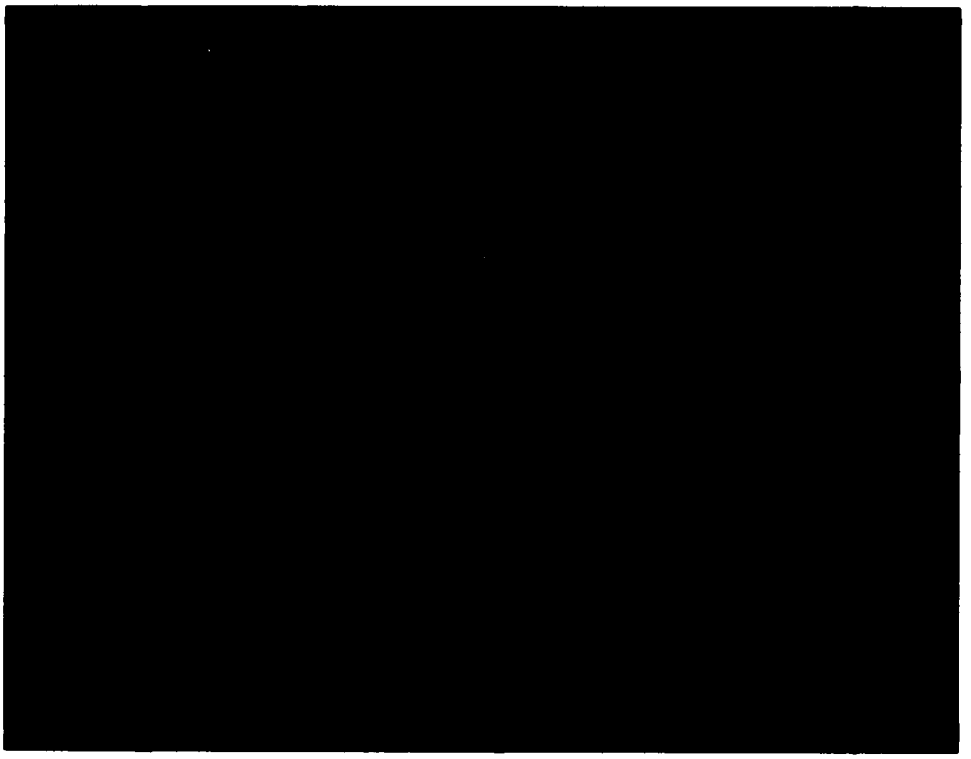

Sunspots
Computer Graphics, *Honorable Mention*
Lisa McCorkle
Material Science and Technology Division

A numerical simulation of continuous media often requires a large number of finite elements and nodes for accurate representation. The model shows a plate containing randomly generated holes, which was subdivided into 410 finite elements. The contours displayed are of element identification numbers optimized with regard to element connectivity for wavefront solution of the resulting matrix equations.

AWARDS AND RECOGNITION

245 **Special Awards and Recognition**

253 **Individual Honors**

267 **Alan Berman Research Publication and Edison Patent Awards**

271 **Awards for *NRL Review* Articles**

SPECIAL AWARDS AND RECOGNITION

NRL is proud of its many distinguished scientists and engineers. A few of these have received exceptional honors for their achievements.

Dr. Timothy Coffey
Director of Research

DELMAR S. FAHRNEY MEDAL FROM THE FRANKLIN INSTITUTE

Dr. Coffey was cited "for his leadership in scientific research and technology, both in acquiring the facts and describing their implications relative to a wide range of phenomena of current and future importance in Naval and Space applications, and for assembling, organizing and supporting teams of scientists who will explore for many consecutive years the frontiers of our knowledge of nature."

DoD DISTINGUISHED CIVILIAN SERVICE AWARD

"...for his outstanding contributions in managing the **premier DoD research laboratory**, and for his examination of the important priority issues associated with the DoD laboratories. ...he has provided top-level DoD management insight associated with the critically important parameters for improving laboratory productivity."

Dr. John Montgomery
Tactical Electronic
Warfare Division

SENIOR EXECUTIVE SERVICE DISTINGUISHED RANK AWARD

Dr. Montgomery's research in electronic warfare (EW) has fundamentally altered Navy EW as an essential warfare area. He pioneered offboard countermeasures—virtually all our ships and aircraft are equipped with systems he has developed. He has been especially successful in the development of new EW technologies and in their rapid reduction to practice in the form of deployed and nomenclatured operational systems....Particular success has been achieved in applying advanced technologies to remedy severe operational deficiencies resulting from crisis conditions in the Persian Gulf. These successes have had a major impact on the Navy's ability to perform its mission and have contributed to the formulation of National goals by demonstrating their achievability.

Dr. Homer Carhart
Navy Technology Center for
Safety and Survivability

CAPTAIN ROBERT DEXTER CONRAD AWARD FOR SCIENTIFIC ACHIEVEMENT

In recognition of his "pioneering research accomplishments, spanning nearly five decades." These accomplishments encompass a wide range of research areas, from the chemistry and physics of combustion, to fire safety and chemical warfare defense.

Dr. Uri Feldman
Space Science Division

E.O. HULBURT ANNUAL SCIENCE AND ENGINEERING AWARD

Dr. Feldman was cited for "his creative and imaginative insights into the structure of the solar transition region, the role of energetic particles in solar flare production, and element abundance variations in different regions of the solar atmosphere, which have produced major improvements in our understanding of the structure and dynamics of the solar atmosphere."

John H. Ablard
Contracting Division

NAVY MERITORIOUS CIVILIAN SERVICE AWARD

Mr. Ablard was recognized for his dedicated leadership and personal commitment to customer service resulting in NRL's achieving "one of the lowest procurement administrative leadtimes in the Department of the Navy and reputation for executing sound business decisions."

Martin B. Ferguson
Command Support Division

NAVY MERITORIOUS CIVILIAN SERVICE AWARD

Mr. Ferguson was recognized for his determination and leadership and creating an environment "where 'excellence' and 'flexibility' are standard. ...security and safety at NRL are without equal, due to Mr. Ferguson's unparalleled performance."

Dr. Martin Nisenoff
Electronics Science and
Technology Division

NAVY MERITORIOUS CIVILIAN SERVICE AWARD

Mr. Nisenoff was recognized for "his distinguished contributions and extreme dedication in the planning, organizing, coordinating, and managing of government programs in the fields of high-temperature superconductivity and cryogenics. Dr. Nisenoff is a technical consultant to NRL...and other DoD and government agencies in these areas, and in addition, was a primary contributor to the establishment of U.S. policy in the export controls of superconducting materials, devices, and systems."

Carol M. Veronda
Radar Division

OFFICE OF THE CHIEF OF NAVAL RESEARCH EQUAL EMPLOYMENT OPPORTUNITY AWARD (SUPERVISORY CATEGORY)

Mr. Veronda has been "continually in the forefront of using innovative recruitment techniques and methods to achieve NRL's affirmative action goals. He has participated extensively in various community outreach programs, and as a supervisor, has been exemplary in passing EEO goals and attritudes down to his employees....His efforts represent the true spirit of EEO....He has been exceptionally effective in motivating, encouraging, and assisting his employees to develop their full potential, regardless of their background."

Stephanie S. Everett
Information Technology Division

NRL COMMANDING OFFICER'S AWARD FOR ACHIEVEMENT IN THE FIELD OF EQUAL EMPLOYMENT OPPORTUNITY (Non-Supervisory Category)

Ms. Everett has been instrumental in coordinating child care efforts for NRL employees. She instituted discount plans with commercial child-care providers in the D.C. area to help ease the financial burden of child care for NRL employees. She worked with the Parents' Coalition to establish a referral service to assist parents in locating child-care services. In addition, Ms. Everett has been active in NRL's Community Outreach Program. She tutors math at a nearby elementary school. Since 1982, she has participated in NRL's annual Children's Christmas Party. She learned basic American Sign Language. She has used that training to help ensure that hearing-impaired employees are kept abreast of developments in the child-care program.

Dr. James R. Griffith
Chemistry Division

NAVY AWARD FOR DISTINGUISHED ACHIEVEMENT IN SCIENCE

Dr. Griffith was cited for his distinguished contributions in the design, synthesis, and evaluation of long-lived tank lining materials now used in most shore-based Navy petroleum fuel storage tanks. Further, Dr. Griffith was recognized for personal research in the generation of new materials, team leadership in the evolution of linings for concrete, welded steel, and riveted steel storage tanks, and worldwide on-site evaluation on behalf of the Naval Facilities Engineering Command. Major cost savings to the Navy have resulted from Dr. Griffith's work.

Dr. Stuart A. Wolf
Materials Science and
Technology Division

SIGMA XI 1991 PURE SCIENCE AWARD

Dr. Wolf is cited for "fundamental research in superconductivity leading to the development of an improved theoretical understanding of the new class of high transition temperature cuprate superconductors."

Dr. Christen Rauscher
Electronics Science and
Technology Division

SIGMA XI 1991 APPLIED SCIENCE AWARD

Dr. Rauscher is cited for "pioneering research in predicting the high-frequency nonlinear behavior of microwave field-effect transistors, and application of this research to key microwave components, including large-signal amplifiers, oscillators, frequency dividers, and optical receivers, as well as for invention and implementation of new classes of microwave active filters and frequency multiplexers."

Dr. Herbert Friedman
Chief Scientist Emeritus of NRL's
E.O. Hulburt Center for
Space Research

1991 INTERNATIONAL COOPERATION AWARD FROM THE AMERICAN INSTITUTE OF AERONAUTICS AND ASTRONAUTICS

The award recognized "individuals who have made significant contributions to the initiation, organization, and/or management of American programs that include extensive international cooperation activities in either space or aeronautics, or both." Dr. Friedman was honored "from the International Geophysical Year to the International Space Year—for 35 years of leadership in international cooperation in space science."

JANSSEN MEDAL FROM THE FRENCH ASTRONOMICAL SOCIETY

Dr. Friedman was honored for his "whole work and important contribution to the rise of spatial astronomy."

Dr. C. Michael Roland
Chemistry Division

1991 SPARKS-THOMAS AWARD OF THE RUBBER DIVISION, AMERICAN CHEMICAL SOCIETY

This award recognizes outstanding scientific contributions and innovations in the field of elastomers by younger scientists, technologists, and engineers.

Laurie E. Stackpole
Technical Information Division

1991 FEDERAL 100 AWARD

An "impact person" whose contributions went well beyond her job by establishing the Microcomputer Software Support Center within the Ruth H. Hooker Research Library and Technical Information Center.

Dr. Joel M. Schnur
Center for Bio/Molecular Science and Engineering

1991 FEDERAL LABORATORY CONSORTIUM AWARD FOR EXCELLENCE IN TECHNOLOGY TRANSFER

Dr. Schnur was recognized for spearheading the transfer of an advanced microelectronic photoresist system to the commercial sector. This technological process, developed at NRL, is a novel surface imaging process that uses optical lithography to achieve ultrahigh, submicron resolution. This process is a potentially low-cost, high-yield method to fabricate high-density microelectronic circuitry.

Dr. David J. Nagel
Condensed Matter and Radiation Sciences Division

1991 FEDERAL LABORATORY CONSORTIUM AWARD FOR EXCELLENCE IN TECHNOLOGY TRANSFER

Dr. Nagel received an award for transferring a plasma X-ray lithography process to a start-up company. X-ray lithography is a pattern transfer process that is expected to permit rapid, relatively inexpensive commercial production of integrated circuits later in this decade. Dr. Nagel performed spectroscopy of multimillion degree plasmas, which showed them to be excellent sources for X-ray lighography.

Frederick E. Betz
Space Systems Department

1991 AEROSPACE POWER SYSTEMS AWARD FROM THE AMERICAN INSTITUTE OF AERONAUTICS AND ASTRONAUTICS

Mr. Betz' award was given "for significant contributions in the broad field of aerospace power systems, specifically as related to the application of engineering sciences and system engineering to the production, storage, distribution, and processing of aerospace power."

Dr. Harold Hughes
Electronics Science and
Technology Division

1991 HARRY DIAMOND MEMORIAL AWARD

Mr. Hughes was cited for his "contributions and leadership in the field of radiation hardening of microelectronics devices."

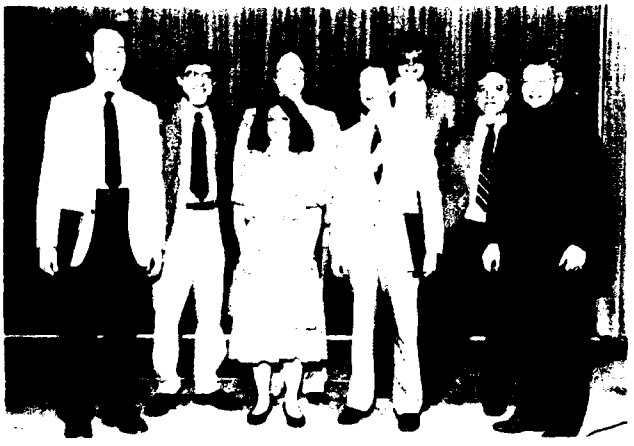

DEPARTMENT OF THE NAVY AWARD OF MERIT FOR GROUP ACHIEVEMENT

Scientists from the Plasma Physics Division were honored for their role in the successful launches of experiments on four separate space flight missions. "The team performed in an outstanding manner under intense pressure and worked well above normal levels of time and skill." From l to r: Paul Bernhardt, Paul Rodriquez, Linda Liston, Mark Baumback, Daniel Haas, Carl Siefring, John Stracka, and David Walker.

DEPARTMENT OF THE NAVY AWARD OF MERIT FOR GROUP ACHIEVEMENT

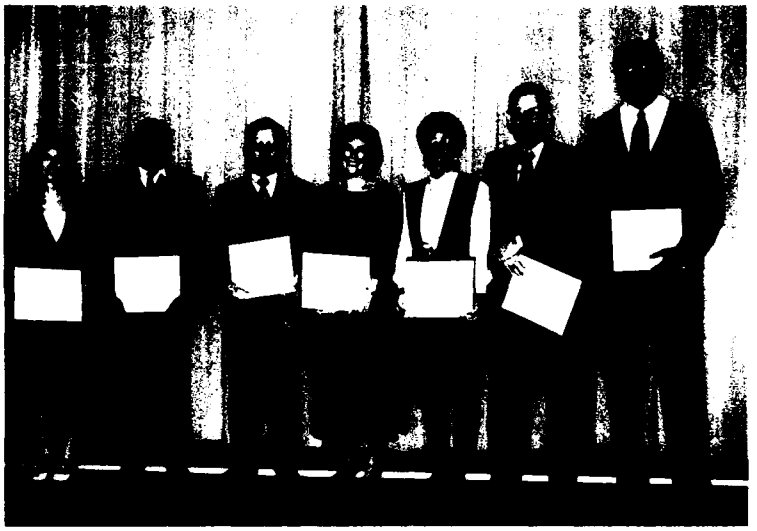

Employees from the Chemistry Division's Navy Technology Center for Safefy and Survivability were recognized for their significant contributions to safety through the prevention and control of fires in totally enclosed environments. From l to r: Jean Bailey, Walter Smith, Roger Brown, Carolyn Kaplan, Frederick Willams, and Harold Eaton.

TECHNICAL ACHIEVEMENTS LABORATORY AWARD FOR 1991 FROM THE AMERICAN DEFENSE PREPAREDNESS ASSOCIATION

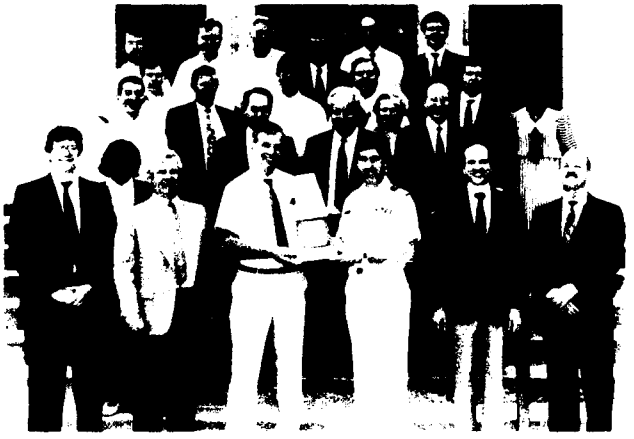

NRL's Low-power Atmospheric Compensation Experiment (LACE) satellite team received this award given annually to a government or industry laboratory for outstanding research and development. Pictured are the LACE team with Dr. Coffey, Director of Research, and CAPT Gaffney, Commanding Officer.

INDIVIDUAL HONORS

Laboratory employees received numerous scientific medals, military service awards, academic honors, and other forms of recognition, including election and appointment to offices in technical societies. The following is an alphabetical list of persons who received such recognition in fiscal year 1991.

Dr. Timothy Coffey, NRL's Director of Research (center), receives congratulations after receiving the Delmar S. Fahrney Medal awarded by the Franklin Institute. On the left is Dr. Larry Tice, Executive Director of the Benjamin Franklin National Memorial and on the right is Dr. Morton Malin, Head of the Fahrney Medal Committee for Sciences and the Arts.

Adams, J.H., Recipient of the Gagarin Medal awarded by the Presidium of the Academy of Astronautics of the USSR.

Aggarwal, I.D., Member, Organization Committee, Eighth Symposium on Halide Glasses.

Anderson, W.T., Technical Program Chairman of the GaAs Reliability Workshop; Member, Editorial Board of Quality and Reliability Engineering International; Member, the Steering Committee of the Export Evaluation and Control of Compound Semiconductor Materials and Technologies Workshop (EXMATEC); Member, Technical Program Committee of the International Reliability Physics Symposium; Member, Technical Program Committee of the Advanced Microelectronics Qualification Reliability and Logistics Workshop; and Member, Technical Program Committee of the European Symposium for Reliability of Electron Devices, Failure Physics, and Analysis (ESREF).

Andreadis, T.D., Organized and co-chaired 3rd Annual Laser Effects on Night Vision Goggles Conference; Member, Microwave Effects Panel (DoD); Member, Foreign Asset Assessment Team (DoD); and Member, System Effects Assessment Team (DoD).

Apruzese, J.P., Feature Editor of *Applied Optics* (special issue on ultrashort-wavelength lasers); Member, Program Committee, International Conference on Lasers '91; and Member, Program Committee, SPIE Technical Conference on Ultrashort Wavelength Lasers.

Armstrong, C.M., Member, Technical Program Subcommittee for the 1992 Microwave Power Tube Conference, Monterey, California.

Barone, F.R., Appointed Chairman of the Infrared Information Symposia Specialty Group on Infrared Countermeasures (a DoD-sponsored organization for the dissemination of classified information on Military Infrared Technology and its applications).

Bell, M.I., Session Chairman, American Physical Society Special Symposium on "Applications of Photon-In Photon-Out Spectroscopy with Third-Generation Synchrotron Radiation Sources," Washington, D.C., 25 Apr. 1991; and Invited Speaker, Workshop on Fundamental Experiments in Ferroelectrics, Williamsburg, Virginia, 3-5 Feb. 1991.

Bernhardt. P.A., Vice Chairman of Commission H of the U.S. National Committee of International Union of Radio Science; and Member, American Geophysical Union Books Board.

Betz, F.E., Recipient of the American Institute of Aeronautics and Astronautics 1991 Aerospace Power Systems Award and Medal.

Binari, S., Appointed to the 1991 GaAs IC Symposium Technical Program Committee.

Blue, J.E., Guest Editor for special issue of *U.S. Navy Journal of Underwater Acoustics* (Vol. 41, No. 1, Jan. 1991, "Special Feature—Underwater Acoustic Transducers.")

Dr. Timothy Coffey (right) (NRL's Director of Research) receives the highest DoD civilian honor, the Distinguished Civilian Service Award.

Bogar, F.B., Secretary, National Capital Section of the Electrochemical Society.

Boos, J.B., Appointed to the position of Conference Secretary for the 1992 International Conference on InP and Related Materials; appointed to serve on the Steering Committee of the International Conference on InP and Related Materials; and served as Area Chair of the Electron Devices Area for the 1991 International Conference on InP and Related Materials.

Bottka, N.B., Guest Editor of IEEE Proceedings on Chemical Vapor Deposition (special issue); Member, Program Committee 1991 International Symposium on GaAs and Related Compounds; and Member, Organizing Committee of the 6th International Conference on Organometal Vapor Phase Epitaxy, June 1992.

Boyer, L.L., Guest Editor, Proceedings of the 1990 Williamsburg Workshop on First Principles Calculations for Ferroelectrics, published in *Ferroelectrics*, by Gordon and Breach.

Brady, R.F., Visiting Scientist, Materials Research Laboratories, Melbourne, Australia, July 1990-July 1991; President, University of Virginia Chemists; Vice Chairman, Publications Committee and Member, Editorial Advisory Board, Federation of Societies for

Coatings Technology; and Member, Membership Affairs Committee, American Chemical Society.

Brown, D., Session Chairman, 1991 Hardened Electronics and Radiation Technology Conference; and Short-Course Chairman, 1991 Nuclear and Space Radiation Effects Conference.

Brown, M.A., Reappointed as Member, AIAA Space Systems Technical Committee.

CAPT Gaffney, NRL's Commanding Officer, presents Dr. Martin Nisenoff with the certificate of the Navy Meritorious Civilian Service Award. With Dr. Nisenoff is his daughter, Ms. Jennifer Nisenoff.

Bultman, J.D., Member, Committee on Creosote and Creosote Solutions and Member, Committee for the Evaluation of Wood Preservatives of the American Wood-Preservers' Association; Associate Editor and Member of the Editorial Board of *El Guayulero* (published by the Association for the Advancement of Industrial Crops); Associate Editor, *Biotropica* (published by the Association for Tropical Biology); and Associate Science Editor (NRL) for *Naval Research Reviews* (published by the Office of Naval Research).

Buot, F.A., Appointed to the Editorial Board, *Transport Theory and Statistical Physics* (published by Marcel Dekker, Inc.); appointed Session Chairman, 1991 International Electron Devices Meeting, Washington, D.C., Dec. 1991; and Member, Technical Program Committee, 1991 International Electron Devices Meeting, Washington, D.C., Dec. 1991.

Butler, J.W., Member of Organizing Committee for the Twelfth International Conference for Application of Accelerators in Research and Industry, Denton, Texas, Nov. 1992.

Campbell, F.J., Fellow, Institute of Electrical and Electronics Engineers; Fellow, American Institute of Chemists; Member, Subcommittee on Electrical Tests, D-09 Electrical Insulating Materials, ASTM; Member, Naval Aerospace Vehicle Wiring Action Group; Member, Sigma Xi; and Listed in *Who's Who in America*, 47th Edition (1992).

Campbell, J.R., Promoted to rank of Adjunct Associate Professor at the Uniformed Services University of Health Sciences, Bethesda, Maryland; appointed to editorial board of the international journal *Biomimetics*; and granted Special Award by Chief of Naval Research for support of Operations Desert Shield and Desert Storm.

Campillo, A.J., Member, Subcommittee on Precision Optical Measurements for the LEOS91 Technical Meeting.

Carruthers, G.R., Editor, *National Technical Association Journal*.

Carter, W.H., One-year appointment as Visiting Scientist to the Johns Hopkins University Applied Physics Laboratory; Member, Fellows and Awards Committees for the SPIE-International Society for Optical Engineering; and invited to chair a technical session on "Instabilities and Chaos I" at the 1991 OSA Annual Meeting.

Cherkis, N.Z., Elected Scientific Advisor to 8th Meeting of the Guiding Committee of the General Bathymetric Chart of the Oceans (IOC/IHO);elected Consulting Bathymetrist to Coordinating Committee of Circum-Atlantic

Project (IUGS/USGS); appointed to Defense Hydrographic Initiative (DMA) working group for Master Seafloor Digital Data Base; and appointed to Defense Hydrographic Initiative (DMA) working group for Archiving and Formatting.

Coffey, T., Recipient of the Delmer S. Fahrney Medal, Franklin Institute and DoD Distinguished Civilian Service Award.

Colton, R.J., Program Chairman, 38th National Symposium, American Vacuum Society; and Co-editor, Proceedings of the Fourth International Conference on Scanning Tunneling Microscopy/Spectroscopy (STM '90) and First International Conference on Nanometer Scale Science and Technology (NANO I).

Cooperstein, G., Fellow, American Physical Society; Technical Program Committee Member, IEEE Pulsed Power Conference; and Co-chairman, 9th International Conference on High Power Particle Beams to be held in May 1992.

DeGiorgi, V.G., Elected Woman of the Year—1991 by Colonial Chapter American Business Woman's Association; Member, ASTM Committee E-24 Fracture Toughness and Testing; Member, ASTM Committee G-1 Corrosion Control; and Member, TTCP Panel P-1 Operating Assignment on Fracture Control Technology.

Dobisz, E.A., Appointed to program committee of the 1992 Conference on Electron-Beam, X-ray, and Ion-Beam Submicrometer Lithographies for Manufacturing, sponsored by SPIE; served as conference co-chair and on program committee for the 1991 Conference on Electron-Beam, X-ray, and Ion-Beam Submicrometer Lithographies for Manufacturing, San Jose, March 6-7, 1991, sponsored by SPIE; and served on program committee in Nanometer Science and Technology Division of the 1991 National Symposium of the American Vacuum Society.

Dr. Uri Feldman is joined by his wife as CAPT Paul Gaffney, Commanding Officer, presents him with the 1989 E.O. Hulburt Annual Science and Engineering Award

Dozier, C.M., Member, Program Committee and Session Chairperson, IEEE Nuclear and Space Radiation Conference.

Dubbelday, P.S., Fellow, Acoustical Society of America.

Eisele, J.A., Appointed Visiting Professor of Aerospace Engineering, U.S. Naval Academy, Annapolis, Maryland.

Feldman, B., Appointed Program Subcommittee Chairman on Gas and Short Wavelength Lasers for the LEOS 91 Technical Meeting; and serves on Laser and Electro-Optics Advisor Board for ONT.

Fisher, S., Honorary Superior Accomplishment Award from NASA, Langley Research Center, for "foresight and achievement in promoting and conducting on-orbit testing of the structural dynamics of the Low-power Atmospheric Compensation Experiment (LACE) Satellite."

Flippen-Anderson, J.L., President, American Crystallographic Association.

Friebele, E.J., Chairman, NATO Panel IV, Research Study Group 12, Nuclear Effects Task Group; Fellow, American Ceramic Society; and Member, Defense Advanced Projects Agency Eye and Sensor Protection Steering Committee.

Friedman, H., Received Janssen Medal, French Astronomical Society, 1990; received Medal for International Cooperation in Space

Science, 1991; appointed a member of the joint National Academy of Sciences, American Philosophical Society and the Smithsonian Institution Committee for the Joseph Henry Papers; Co-chairman of the International Program Committee for the World Space Congress; Chairman, Nominating Committee for the Magellanic Premium of the American Philosophical Society; and elected for a second term as vice-president of COSPAR.

Gaber, B.P., Editor (with K.B.K. Easwaran) of *Biomembrane Structure and Function—The State of the Art* (Adenine Press, NY, 1991); appointed to International Editorial Board, Journal of Molecular Graphics; and elected to Executive Board Molecular Graphics Society of the Americas.

Gaffney, P.G., CAPT., U.S.N., Awarded the Legion of Merit Medal (2nd award) for his duties while assigned to the Office of the Chief of Naval Research as Assistant Chief of Naval Research.

Giallorenzi, T.G., Chairman, Steering Committee IEEE/OSA Optical Fiber Conference (OFC); Elected Board of Governors, IEEE Laser and Electro-optics Society; Vice President for Publications, IEEE Laser and Electro-optics Society; Editorial Boards of Optical Society of America, *Optics and Photonics* and *Laser Focus Magazine*; Member, Technical Committees (International Integrated Optics and Optical Communications Conference and of *Laser Focus Magazine* Semiconductor Device Research Symposium); Associate Editor, *IEEE Proceedings* and for *IEEE Lightwave Communications System Journal*; Member, National IRIS Executive Committee; and Member, Advisory Board of Opto-electronics Technology Center.

Glembocki, O.J., Chosen as Chairman and Editor for the Society of Photo-optical Instrumentation Engineers Conference on Optical Characterization for Semiconductor Technology.

Gold, S.H., Second year as elected member, Executive Committee of the Plasma Science and Applications Committee, IEEE Nuclear and Plasma Sciences Society, and member, Membership Subcommittee; fourth year as Associate Editor of *IEEE Transactions on Plasma Science*; Session Chairman, "High-Power Microwaves II," at the Thirty-Second Annual Meeting of the Division of Plasma Physics, American Physical Society, 12-16 Nov. 1990, Cincinatti, Ohio; Session Chairman, "Gyrotron V" at the Fifteenth International Conference on Infrared and Millimeter Waves, 10-14 Dec. 1990, Lake Buena Vista, Florida; Session Organizer and Chairman, "Intense Beam Microwave Sources," at the Eighteenth IEEE International Conference on Plasma Science, 2-4 June 1991, Williamsburg, Virginia; and appointed Session Organizer, "Intense Beam Microwave Sources," for the Nineteenth IEEE International Conference on Plasma Science to be held 1-3 June 1992, Tampa, Florida.

CAPT Paul Gaffney, Commanding Officer, presents the Navy Award for Distinguished Achievement in Science to Dr. James Griffith. Mrs. Griffith looks on.

Grabowski, K.S., Selected as Chairman of Symposium on "Materials Modification by Energetic Atoms and Ions" to be held at Spring Materials Research Society Meeting, 1992.

Gray, H.F., Associate Editor, *Journal of Micromechanics and Microengineering* (for Vacuum Microelectronics Technology); Special Editor, *Transactions of Electron Devices* for a special issue of *Vacuum Microelectronics* published in Oct. 1991; and Member, International Steering Committee on Vacuum Microelectronics.

CAPT Paul Gaffney, Commanding Officer, presents Dr. Jill Dahlburg with a 1991 Alan Berman Research Publication Award

Griscom, D.L., Chairman, Glass and Optical Materials Division, American Ceramic Society; and Fellow, American Ceramic Society.

Haber, I., Co-chairman of 14th International Conference on Computer Simulations of Plasmas.

Hollinger, J.P., Guest Editor for the September 1990 issue of IEEE's *Transactions on Geoscience and Remote Sensing*, which was judged by the American Association of Publishers, Scholarly Publishing Division to be the "Best Single Issue of a Journal" for 1990.

Holst, R.W., Appointed Senior Field Officer, Naval Reserve Technology Mobilization Program.

Hubler, G.K., Member, International Committee, Conference on Surface Modification of Metals by Ion Beams; Co-chairman, 7th International Conference on Surface Modification of Metals by Ion Beam; and Co-editor, SMMIB Proceedings.

Hughes, H.L., Recipient of the 1991 IEEE Harry Diamond Memorial Award.

Jacobs, V., Fellow, American Physical Society.

Jensen, K.L., Panelist on International Vacuum Microelectronics Conference Panel Discussion, Tokyo, Japan, Aug. 26, 1991.

Jordan, A.K., Elected Fellow, Institute of Electrical & Electronics Engineers, for "Contributions to Electromagnetic Inverse Scattering Theory and its Applications;" appointed visiting scientist, Research Laboratory of Electronics, Massachusetts Institute of Technology; and Member, American Society of Engineering Education Review Panel for ONR Graduate Fellowship Program.

Joyce, G.R., Fellow, American Physical Society, continuing membership.

Kabler, M.N., Fellow, American Physical Society; and spokesperson for Participating Research Team, Beam Line X24C, at National Synchrotron Light Source, Brookhaven National Laboratory.

Kailasanath, K., Associate Fellow, AIAA; Chairman, Continuing Education Subcommittee, AIAA Propellants and Combustion Technical Committee; Member, Program Subcommittee, 24th International Symposium on Combustion; and Member, AIAA Propellants and Combustion Technical Committee.

Karle, I.L., Fourth Paul Ehrlich Award Lecture, presented March 6, 1991 at the National Institutes of Health; and Nominating Committee member, National Academy of Sciences, USA.

Karle, J., Received the degree of Doctor of Science, Honoris Causa, at the midyear commencement of the University of Michigan; completed a three-year tenure as Chairman of

the Chemistry Section, National Academy of Sciences; Castle Lecturer at the University of South Florida; H. Martin Friedman Lecturer at Brooklyn College; received Order of Francisco de Miranda, First Class, from President Carlos Andres Perez of Venezuela for scientific accomplishments; Co-president of Academic Senate and Member of Board of Presidents, International Council for Scientific Development, International Academy of Science; and Member, Human Rights Committee of National Academy of Sciences.

Kelner, G., Elected as a member of Commission D of International Union of Radio Science.

Killiany, J.M., Chairman, IRIS Detector Specialty Group, 1990 - 1993.

Klein, B.M., Chairman, Peer Review Board, Pittsburgh Superconductor Center and National Center for Supercomputer Applications; and Member, Pennsylvania State Materials Research Laboratory Advisory Committee.

Krebs, J.J., Fellow, American Physical Society.

Kuperman, W.A., Associate Editor, *Journal of the Acoustical Society of America*; Consulting Editor, *Encyclopedia of Applied Physics*.

Kurfess, J.D., Chairperson, Division of Astrophysics, American Physical Society.

Lau, Y.Y., Fellow, American Physical Society, continuing membership.

Lee, J.L., Chairman, IEEE Steering Committee for the Journal of Lightwave Technology; Member, IEEE-OSA Coordinating Committee for the Journal of Lightwave Technology; Program Committee member, IEEE-OSA Conference on Lasers and Electro-optics (CLEO) IEEE Ultrasonics Symposium; reviewer for *Applied Optics*, *Journal of Lightwave Technology*, *IEEE Spectrum*, *Microwave and Optical Technology Letters*; Senior Member of IEEE; Editor, special issue of *Journal of Lightwave Technology on Optical Interconnects for Information Processing*; and Editor, *Design Issues in Optical Processing*, to be published by Cambridge University Press.

Love, J.R., CAPT., U.S.N., Awarded the Meritorious Service Medal (Second Gold Star in lieu of third award) for duties as Head of the Total Force and Mobilization Branch of OPNAV Code 06.

Dr. Christos Kapetanakos receives a 1991 Alan Berman Research Publication Award from CAPT Paul Gaffney, Commanding Officer

Marks, C.J., Vice President for Compliance, Federally Employed Women.

Marrian, C.R.K., Vice-chair, Program Committee, 38th National Symposium of the American Vacuum Society, Nov. 11-17, 1991; and Co-chair of the S.P.I.E. Conference, "Electron Beam, X-ray, and Ion-Beam Lithographies for Submicrometer Manufacturing II," Mar. 8-13, 1992.

McCafferty, E., Member, Corrosion Monograph Committee of the Electrochemical Society; and Professorial Lecturer, The George Washington University.

Mehl, M.J., Member, American Geophysical Union since 1985; Member, American Physical Society since 1977; and Member, Sigma Xi since 1978.

Meier, R., Member, NASA's Inner Magnetospheric Imager Study Panel.

Metzbower, E.A., Served on the Board of Directors, Laser Institute of America; at-large member Joining Division Council, ASM International; and Chairman of the Laser Materials Processing Symposium,

International Congress on Applications of Lasers and Electro-optics (ICALEO) '91.

Michel, D.J., Fellow, ASM International; Member, Technical Program Committee, Fourth International Symposium on Environmental Degradation in Nuclear Power Systems—Water Reactors; Member, Nuclear Materials Committee, ASM International and TMS; and Professorial Lecturer, The George Washington University.

Mowery, R.L., Second year as Chairman, DoD Instrument Bearing Working Group.

Murday, J.S., President-elect American Vacuum Society; Board of Directors, American Institute of Physics; and Editorial Board, *Nanotechnology*.

Nagel, D.J., Member, Proposal Review Committee, X-ray Lithography Program, Defense Advanced Research Projects Agency (DARPA); Member, NRL Management Training Committee; and Excellence in Technology Transfer Award from Federal Laboratory Consortium, 1991.

Dr. Paul Bernhardt, one of eight scientists from NRL's Plasma Physics Division to share a Navy Group Achievement Award for his role in the successful launches of experiments on four separate space flight missions, accepts his certificate from CAPT R. Michaux, NRL's past Chief Staff Officer

Natishan, P.M., Member, Baltimore-Washington Section of the National Association of Corrosion Engineers and 1991 Member of the Year; Chairman, National Capital Section of the Electrochemical Society; and Trustee, Baltimore-Washington Section of the National Association of Corrosion Engineers.

O'Grady, W.E., Editor for the Physical Electrochemistry Division of the Electrochemical Society; Member, Tenure Proposal Review Committee for the National Synchrotron Light Source; and elected Vice Chairman of the Physical Electrochemistry Gordon Conference 1991.

Oran, E.S., Member, Publications Committee, American Institute of Aeronautics and Astronautics; Chair, Journals and Technical Information Committee, American Institute of Aeronautics and Astronautics; Chair, Topical Group on Computational Physics, American Physical Society; Member, Committee of the Status of Women in Physics, American Physical Society; Member, Board of Directors of the Combustion Institute; Secretary of the Board of Directors, Institute of the Dynamics of Energetic and Reactive Systems; Co-editor (with Jay Boris), *Numerical Approaches to Combustion Modeling*, book published by the American Institute of Aeronautics and Astronautics; and Member, Editorial Board, *Progress in Energy and Combustion Science*.

Ossakow, S.L., Fellow, American Physical Society, continuing membership; and ONR General Physics Subelement Monitor.

Pande, C.S., Elected Chairman of Physical Metallurgy Committee of The Minerals, Metals and Materials Society.

Parker, R.K., Associate Editor, *IEEE Transitions on Electron Devices*; Chairman, Vacuum Electronics Steering Group, ODDRE (R&AT) ET; Chairman, Vacuum Electronics Subpanel under Project Reliance; and Member, Technical Program Committee for Microwave Power Tube Conference.

Patel, V., Fellow, American Physical Society, continuing membership; Member, National Academy of Sciences Task Group for Geomagnetic Studies; Member, Steering Committee, International Topical Conference on Nonlinear Space Plasma Physics, La Jolla, California, Feb. 1991; Member, NSF Interagency Committee on Solar-Terrestrial Research; and Board Member, Institute for Advanced Physics Studies, La Jolla, California.

Petersen, E.L., Guest editor for Proceedings of HEART Conference published in *Journal of Radiation Effects Research and Engineering*; and Member at Large on IEEE Nuclear and Space Radiation Effects Conference Steering Committee.

Pickett, W.E., Editorial Board, *Journal of Superconductivity* (published by Plenum Publ. Co.); and Fellow, American Physical Society.

Piquette, J.C., Elected to *American Men & Women of Science*, Aug. 1991.

Priest, R.G., Member, Program Committee for Infrared Information Society (IRIS) Targets, Backgrounds and Discrimination Meeting.

Prinz, G.A., Appointed Advisory Editor of the *Journal of Magnetism and Magnetic Materials*; and inducted into Society of Scholars of the Johns Hopkins University.

Prokes, S.M., Appointed Member, Materials Research Society Bulletin Publications Board (1991); and continuing member of the MRS Publications Committee.

Ramaker, D.E., Received the Washington Academy of Sciences 1991 award for "Achievement in the Physical Sciences."

Rath, B.B., Member, Organizing Committee, Fundamental Aspects of Dislocations Interaction Conference, Switzerland; Member, Editorial Board, *International Materials Review*; Member, Public Affairs Council, American Association of Engineering Societies; Member, Committee on Materials for National Planning of the Office of Science and Technology Policy, 1991; Member, Technical Division Board, ASM-International, 1991-present; Program Organizer, Symposium on Structure and Properties of Intermetallic Materials, Vancouver, 1990; and Member, External Visiting Board, Colorado School of Mines.

Rauscher, C., Recipient of 1991 NRL-Sigma Xi Applied Science Award.

Dr. David J. Nagel, Superintendent of the Condensed Matter and Radiation Sciences Division, receives a technology transfer award from Mr. Richard T. Shearer, the acting technical director of the Naval Ocean Systems Command

Reintjes, J.F., Topical Editor, *Nonlinear Optics for Applied Optics*.

Ripin, B.H., Fellow, American Physical Society; appointed Chairman of APS Task Force on Journal Financing, Chairman, DPP Publication Committee, and member of the APS Fellowship Committee; appointed to the DoE Fusion Energy Advisory Committee (FEAC); elected Councilor-at-Large of the American Physical Society; and serves on Editorial Boards of *Physical Review*, *Laser* and *Particle Beam Journals*.

Ritter, J.C., Invited to present tutorial short course "Spacecraft Survivability" at Hardened Electronics and Radiation Technology Conference, Gaithersburg, Maryland, 25 Feb. - 1

Mar. 1991; invited to chair session and present tutorial paper "Radiation Effects on Spacecraft" to Spacecraft Guidance and Control Conference, Keystone, Colorado, Feb. 2-4 1991; invited to chair faster session and present paper "High Temperature Superconductivity Space Experiment" at Applied Superconducting Conference, Snowmass, Colorado, Sept. 24-28 1990; served on Nominating Committee for the IEEE Nuclear and Space Radiation Effects Conference, July 1990 - July 1991; invited to present paper "Survivability of Spacecraft Systems to Space Radiation" at American Nuclear Society, Nov. 10-14 1991; and invited by NATO/SHAPE Technology Center to present papers "Post Cold War NATO Spacecraft Survivability Options" and "Superconductivity—New Technology for Future Space Systems" at Concepts for the Post-NATO IV SATCOM System Conference, The Hague, Netherlands, 1-3 Apr. 1992.

Dr. Karl Gerlach is congratulated by CAPT Paul Gaffney, Commanding Officer, for winning a 1991 Alan Berman Research Publication Award

Rolison, D.R., Member, Editorial Advisory Board for the American Chemical Society Journal *Analytical Chemistry*, 1990-1992.

Rudgers, A.J., Fellow, Acoustical Society of America; and Member, Membership Committee, Acoustical Society of America.

Saks, N.S., Appointed technical program chairman of the 1992 Nuclear and Space Radiation Effects Conference, New Orleans, Louisiana, July 13-17, 1992.

Sandberg, W.C., Chairman, Research Priority Subgroup, Society of Naval Architects and Marine Engineers; Chairman, Hydrodynamics Committee, Society of Naval Architects and Marine Engineers; and Member, Technical and Research Steering Committee of the Society of Naval Architects and Marine Engineers.

Schnur, J.M., Listed in *Who's Who in Science: Who's Who in East and South East*; Chairman, IEEE Conference on Synthetic Microstructures in Medicine and Biology; appointed to National Academy of Sciences' National Research Council Committee to asses "Frontiers of Science and Technology in Biomolecular Self-Assembling Materials;" recipient of Federal Laboratory Consortium Award for Technology Transfer; and Chairman, Gordon Conference on Organic Thin Films, 1990.

Sherman, K.B., LT., U.S.N., Awarded the Navy Commendation Medal for duties while assigned to Fleet Air Reconnaissance Squadron One.

Shettle, E.P., Elected Second Vice President, National Capital Section of the Optical Society of America.

Simpson, C.G., Appointed to National Blue Ribbon Evaluation Team to Enhance Future Stealth Technology.

Singer, I.L., Director, NATO Advanced Study Institute on "Fundamentals of Friction," 29 July to 9 Aug. 1991, Braunlage, Germany.

Skelton, E.F., Invited speaker and chairperson at the XIIIth International Conference on High Pressure Science and Technology held in Bangalore, India, 7-11 Oct. 1991; spokesperson for High Pressure Insertion Device Team at National Synchrotron Light Source, Brookhaven National Laboratory; re-elected representative for Energy Dis-

persive Group (1991–1992) on Users Executive Committee, National Synchrotron Light Source Brookhaven National Laboratory; and invited to serve as chairperson at March Meeting of the American Physical Society held in Cincinnati, Ohio, Mar. 1991.

Sleger, K.J., Appointed Chairman, RF Components Subpanel of JDL Reliance Electronic Devices; and continuing as Navy Deputy Member of Advisory Group on Electron Devices (AGED) Working Group A.

Smidt, F.A., Co-chairman, Organizing Committee, International Conference on Surface Modification of Metals by Ion Beams; Member, U.S. Government-TTG-A, Sub-Group C (Technology Export Control Advisory Group on Coatings); Fellow, ASM International; and Elected member of Böhmische Physical Society (Honorary).

Sprangle, P.A., Awarded 1991 Free Electron Laser Prize for recognition of outstanding contribution in FEL Science and Technology, 29 Aug. 1991; Fellow, American Physical Society, continuing membership; Member of Sigma Xi, continuing membership; appointed to Editorial Board of *Physics of Fluids B*, Jan. 1991 to Jan. 1994; Member, International Executive Committee of the 13th International FEL Conference, 1991; and Member, DARHT Feasibility Assessment Independent Consultants (DFAIC) 1991, 1992.

Stackpole, L.E., President, Military Librarians Division, Special Library Association; elected to Federal Library and Information Center Committee, Library of Congress; and named by *Federal Computer Week* as one of its 1991 Federal 100 "impact people."

Swean, Jr., T.F., Appointed to Scientific Advisory Panel for ONR University Research Initiative Program, "Dynamics and Control of Turbulent Shear Flows," at University of Southern California; and appointed to ONR Selection Panel to award University Research Initiative Program, "Vorticity/Free Surface Phenomena."

Anne Kusterbeck receives her award and looks on as Paul Charles accepts a *1991 NRL Review* award for coauthor Dr. Frances Ligler from Dr. Timothy Coffey, Director of Research

Tait, G.B., Elected 1991–1992 Chairman, IEEE Microwave Theory and Techniques Society, Washington, D.C./Northern Virginia Chapter.

Tang, C.M., Elected Fellow, American Physical Society, 1991; and Member, 13th International Free Electron Laser Conference Program Committee and Free Electron Laser Prize Committees.

Timme, R.W., Guest editor for special issue of *U.S. Navy Journal of Underwater Acoustics* (Vol. 41, No. 1, Jan. 1991, "Special Feature—Underwater Acoustic Transducers").

Ting, R.Y., Guest editor for special issue of *U.S. Navy Journal of Underwater Acoustics* (Vol. 41, No. 1, Jan. 1991, "Special Feature—Underwater Acoustic Transducers").

Tolstoy, A., Named Distinguished Lecturer by Association of Women Geoscientists; gave Invited Seminar by the Association of Women Geoscientists at George Mason University; Journal Referee for ASA; chaired sessions at AIP/APS Symposium, IMACS Symposium, Oceans 91 Conference and Co-organizer of MFP Workshop '91; Member, ASA Technical Specialty Group on Acoustical Oceanography; and Member, National Tomography Committee.

Toot, P.L., Appointed to the AIAA Flight Test Technical Committee; and selected as

Chairman of the 1992 AIAA Flight Test Conference.

Trunk, G.V., Chairman of KTP-2, a technical exchange panel on radar data processing under the auspices of subgroup K (radar) within The Technical Cooperation Program (TTCP).

Trzaskoma, P.P., Member, Board of Directors, The Electrochemical Society; Past Chairman, Council of Local Sections, The Electrochemical Society; Councillor, National Capital Section of The Electrochemical Society; and Delegate, Pre-White House Conference on Library and Information Sciences.

Turner, N.H., Alternate Councillor, Chemical Society of Washington (Washington Section of the American Chemical Society); and Membership Secretary, Division of Colloid and Surface Chemistry of the American Chemical Society.

Van Buren, A.L., Fellow, Acoustical Society of America; appointed member of Acoustical Society of America Committee on Standards; Chairman of session at 1991 Undersea Defence Technology Conference in Paris, France; and Chairman of two sessions at 1991 IEEE Instrumentation and Measurement Technology Conference.

Vandermeer, R.A., Fellow of American Society of Materials International; Chairman, Recovery and Annealing Committee of ASM International; and Vice Chairman, Surfaces and Interfaces Committee of ASM International.

Venezky, D., Appointed a member of the American Chemical Society Committee on International Activities and served as Chair of the Subcommittee on International Liaisons.

Vogt, P.R., Appointed to National Science Foundation "Ridge" (Midocean Ridge) Steering Committee, Apr. 91; and third year as Associate Editor, Geological Society of America Bulletin.

Wagner, R.J., Member, Program Committee of the International Conference on Narrow Gap Semiconductors, University of Southampton, 19-23 July 1992; and Member, Program Committee of the 1991 IRIS Specialty Group on Infrared Materials.

Waterman, J.R., Continuing membership on Program Committee for the Workshop on the Physics and Chemistry of Mercury Cadmium Telluride.

Webb, D.C., Member, Technical Program Committee, 1991 International IEEE Microwave Theory and Techniques Symposium, and Member, JDL Reliance Sub-subpanel on RF Solid-State Devices.

Whitlock, R.R., Member, Technical Program Committee, 1991 American Physical Society Topical Conference on Shock Compression of Condensed Matter.

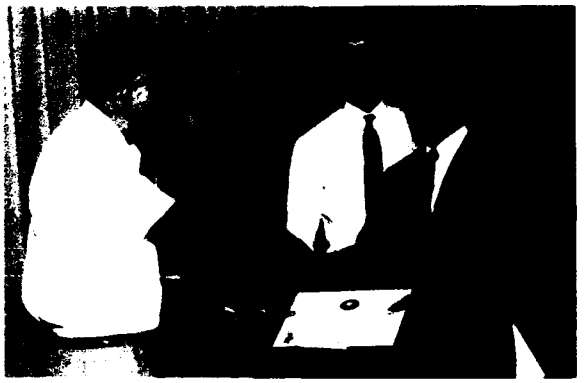

Dr. Timothy Coffey, Director of Research, congratulates Drs. Milton Kabler (center) and David Nagel (right) on receiving the *1991 NRL Review* featured article award

Wieting, T.J., Chairman, OUSD Microwave Effects Panel; Member, OUSD HPM Systems Effects Assessment Team (SEAT); Member, OUSD Team on Project Tiger Grip; Member, Review Group on AF Project Seek Needle; and Member, OUSD HPM Foreign Asset Assessment Team (FAAT).

Wilsey, N.D., Member, Editorial Board, *Journal of Materials Science: Materials in Electronics* (continuing position).

Wolf, S., Elected Divisional Councillor for Condensed Matter Division of the American Physical Society; and recipient of NRL Sigma Xi Pure Science Award.

Yang, T.C., Elected Fellow of the American Society of Acoustics.

Young, F.C., Elected Chairman of the Executive Committee of the IEEE Plasma Science and Applications Committee.

Young, R.V., CDR., U.S.N., Awarded the Meritorious Service Medal for service while assigned to the Staff of the Commander 6th Fleet.

Zedd, M.F., Member, American Institute of Aeronautics and Astronautics Atmospheric Flight Mechanics Working Group.

ALAN BERMAN RESEARCH PUBLICATION AND EDISON PATENT AWARDS

The Annual Research Publications Awards Program was established in 1968 to recognize the authors of the best NRL publications each year. These awards not only honor individuals for superior scientific accomplishments in the field of naval research, but also seek to promote continued excellence in research and in its documentation. In 1982, the name of this award was changed to the Alan Berman Research Publications Award in honor of its founder.

There were 260 separate publications published in 1991 that were considered for recognition. Of those considered, 33 were selected. These selected publications represent 116 authors, each of whom received a publication awards certificate, a bronze paperweight, and a booklet listing the publications that received special recognition. In addition, NRL authors share in their respective division's monetary award.

The winning papers and their respective authors are listed below by their research units. Non-Laboratory coauthors are indicated by an asterisk.

NRL also recognizes patents as part of its annual publication awards program. The NRL Edison (Patent) Awards were established in January 1991 to recognize NRL employees for outstanding patents issued to NRL by the U.S. Patent and Trademark Office during the preceding calendar year. The award recognizes significant NRL contributions to science and engineering as demonstrated by the patent process that are preceived to have the greatest potential benefit to the country. Of the 60 patents considered for 1991, two were selected, representing five inventors. They are listed under the Edison Patent Awards.

Space Science Division

Explosive Events and Magnetic Reconnection in the Solar Atmosphere
Kenneth P. Dere, John-David F. Bartoe,* Guenter E. Brueckner, John A. Ewing,* and Paul A. Lund*

Ultraviolet Spectroscopy and Remote Sensing of the Upper Atmosphere
Robert R. Meier

Center for Advanced Space Sensing

The Generation and Evolution of Mushroom-Like Vortices
Richard P. Mied, James C. McWilliams, and Gloria J. Lindemann

Marine Aerosols: A Review
James W. Fitzgerald

Laboratory for Computational Physics and Fluid Dynamics

Dynamics of Solar Coronal Magnetic Fields
Russell B. Dahlburg, Spiro K. Antiochos, and Thomas A. Zang

Condensed Matter and Radiation Sciences Division

Observation of ^{7}Be on the Surface of LDEF Spacecraft
Gerald J. Fishman, B. Alan Harmon, John C. Gregory, Thomas A. Parnell, Palmer N. Peters, Gary W. Phillips, Steven E. King, Robert A. August, James C. Ritter, Joseph H. Cutchin, Penelope S. Haskins, John E. McKisson, Donald W. Ely, Andrew G. Weisenberger, Rodney B. Piercey, and Tomas Dybler

Synchrotron X-Ray Diffraction from a Microscopic Single Crystal Under Pressure
Earl F. Skelton, Jack D. Ayers, Syed B. Qadri, Norman E. Moulton, Khershed P. Cooper, Larry W. Finger, Ho-kwang Mao, and Jingzhu Hu

Plasma Physics Division

Instability of Taylor-Sedov Blast Waves Propagating Through a Uniform Gas
Jacob Grun, John A. Stamper, Charles H. Manka, Joshua H. Resnick, H. Rayvon Burris, Jr., James R. Crawford, and Barrett H. Ripin

Measurement of Plasma Opacity from Laser-Produced Optically Thin Strongly Coupled Plasmas
Andrew N. Mostovych, Kevin J. Kearney, John A. Stamper, and Andrew Schmitt

Acoustics Division

Higher-order Padé Approximations for Accurate and Stable Elastic Parabolic Equations with Application to Interface Wave Propagation
Michael D. Collins

Radar Division

Scattering by an Infinite Wedge with Tensor Impedance Boundary Conditions—A Moment Method/Physical Optics Solution for the Currents
Henry J. Bilow

Point Defense Radar System for the Detection of Low-Altitude Low-Observable Targets
Gerard V. Trunk, Paul K. Hughes II, Steven M. Brockett, Jon D. Wilson, and Michael J. Siegert

Information Technology Division

Analysis of Two-Way Ground-Wave Communication Links for Arctic Naval Applications
Edward J. Kennedy and Michael A. Rupar

High Quality 800-b/s Voice Processing Algorithm
George S. Kang and Lawrence J. Fransen

Tactical Electronic Warfare Division

High-Frequency Over-the-Horizon Radar ECM
James G. Constantine, Dean D. Howard, Michael N. Asbery, and David B. Mann

Nonlinear Modeling of Gated Range Tracker Dynamics with Application to Radar Range Resolution
Eyad H. Abed, Allen J. Goldberg, and Robert E. Gover

Underwater Sound Reference Detachment

Free-field Acoustic Calibration of Long Underwater Acoustic Arrays in a Closed Chamber
L. Dwight Luker and Joseph F. Zalesak

Center for Bio/Molecular Science and Engineering

Deep UV Photochemistry of Chemisorbed Monolayers: Fabrication of Patterned Coplanar Molecular Assemblies
Charles S. Dulcey, Jacque H. Georger, Jr., Victor Krauthamer, Thomas L. Fare, David A. Stenger, and Jeffrey M. Calvert

Center for the Structure of Matter

The Structural Investigation of Energetic Materials
Richard D. Gilardi and Jerome Karle

Chemistry Division

Simulations of C_{60} Collisions with a Hydrogen-Terminated Diamond {111} Surface
Richard C. Mowrey, Donald W. Brenner, Brett I. Dunlap, John W. Mintmire, and Carter T. White

Thermal Marking of Amorphous Poly(ethylene terephthalate)
C. M. Roland, James P. Armistead, and Mark F. Sonnenschein

Materials Science and Technology Division

Determination of Elastic Constants of Anisotropic Materials from Oblique Angle Ultrasonic Measurements Part I: Analysis and Part II: Experimental
Richard B. Mignogna, Narendra K. Batra, and Kirth E. Simmonds

Spin Separation in Diluted Magnetic Semiconductor Quantum Well Systems
Berend T. Jonker, James J. Krebs, Gary A. Prinz, Athos Petrou, Xichun Liu, Wu-Ching Chou, and James Warnock

Optical Sciences Division

Cavity Quantum Electrodynamic Enhancement of Stimulated Emission in Microdroplets
Anthony J. Campillo, Jay D. Eversole,* and Horn-Bond Lin

Universal Noise Rise in a Parametric Magnetostrictive Amplifier
Sandeep T. Vohra, Frank Bucholtz, Kee P. Koo,* and Dominique Dagenais*

Electronics Science and Technology Division

Optoelectronic Approach to On-Chip Device and Circuit Characterization at Microwave and Millimeter-Wave Frequencies
Christen Rauscher

Excitons, Phonons, and Interfaces in GaAs/AlAs Quantum-Well Structures
Daniel Gammon, Benjamin V. Shanabrook, and Scott Katzer

Space Systems Development Department

On Metrics of "Super Performance"
Y.S. Wu

A Kalman Filter for a Gravity Gradient Satellite
Peter J. Melvin

Spacecraft Engineering Department

Kinematic and Dynamic Properties of an Elbow Manipulator Mounted on a Satellite
Michael F. Zedd, Robert E. Lindberg, and Richard W. Longman

Paint by Number: Uncovering Phase Flows of an Integrable Dynamical System
Liam Healy and Etienne Deprit

Space Systems Technology Department

Frequency Stability of GPS NAVSTAR Block I and Block II on-Orbit Clocks
Thomas B. McCaskill, Wilson G. Reid, James A. Buisson III, and Hugh E. Warren*

Polynomial Neural Nets for Signal and Image Processing in Chaotic Backgrounds
Sheldon B. Gardner

NRL Edison (Patent) Awards

Chemistry Division

Amino Phenyl Containing Curing Agent for High Performance Phthalonitrile Resin
Teddy M. Keller and Barry A. Edelberg

Center for Bio/Molecular Science and Engineering

Immobilization of Active Agents on Substrates with a Silane and Heterobifunctional Crosslinking Agent
Frances S. Ligler, Jeffrey M. Calvert, and Lisa C. Shriver-Lake

AWARDS FOR *NRL REVIEW* ARTICLES

Awards for *NRL Review* articles were established during 1990 to recognize authors who submit outstanding research articles for this scientific publication. The articles are judged on the relevance of the work to the Navy and the DoD, readability to the college-graduate level, and the use of graphics that are interesting and informative. The following awards were presented for articles that appeared in the *1991 NRL Review*.

FEATURED RESEARCH ARTICLE

Synchrotron X-Radiation Research
Milton N. Kabler, David J. Nagel, and Earl F. Skelton
Condensed Matter and Radiation Sciences Divison

DIRECTORATE AWARDS FOR SCIENTIFIC ARTICLES

General Science and Technology Directorate

Multidimensional Flame Instabilities
Kazhikathra Kailasanath
Laboratory for Computational Physics and Fluid Dynamics

Warfare Systems and Sensors Directorate

A New Approach to Acoustic Tomography
Alexandra Tolstoy and Orest I. Diachok
Acoustic Division

Materials Science and Component Technology Directorate

Drug Detection by Using an Antibody-based Sensor: The Flow Immunosensor
Anne W. Kusterbeck and Frances S. Ligler
Center for Bio/Molecular Science and Engineering

Naval Center for Space Technology

Along Track Formationkeeping for Satellites with Low Eccentricity
Jay W. Middour
Space Systems Development Department

Star Tracking with Laser at Air Force Maui Optical Station, Hawaii
Facilities/Project Photos, *Honorable Mention*
Mark S. Johnson

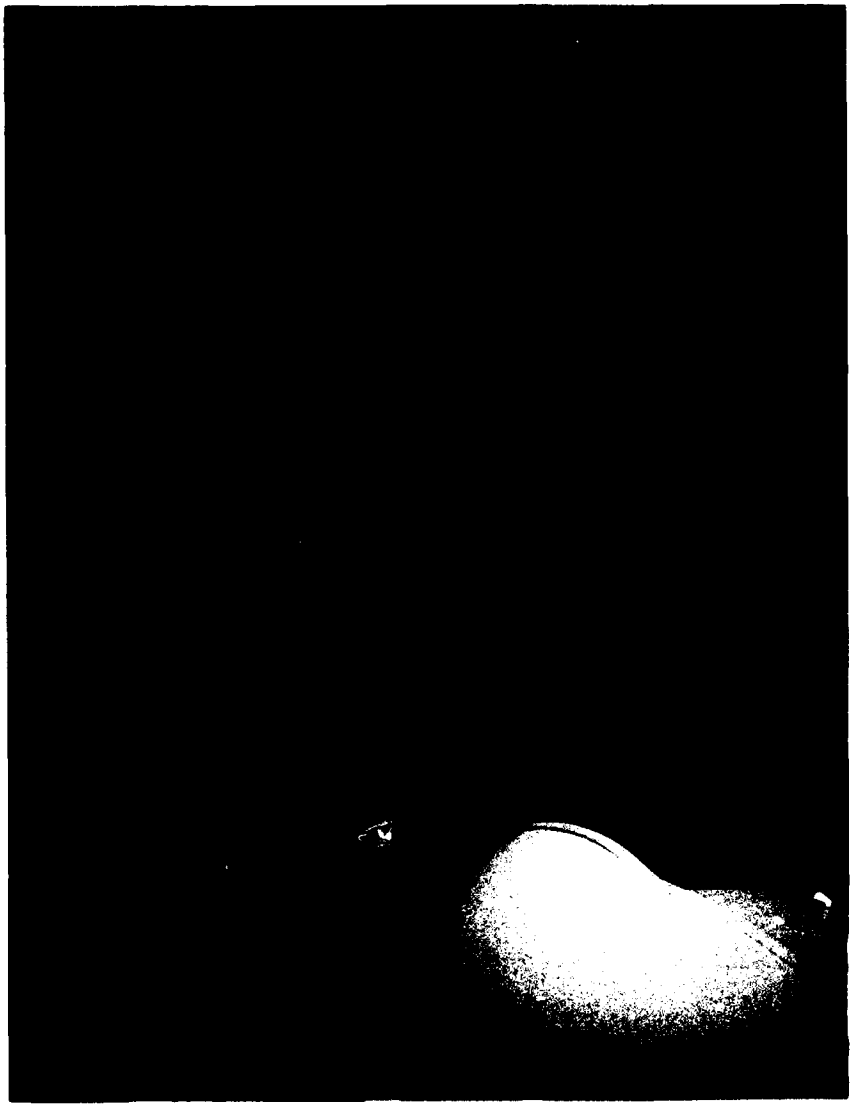

Star Tracking with Laser at Air Force Maui Optical Station, Hawaii
Facilities/Project Photos, *Honorable Mention*
Mark S. Johnson
Space Systems Development Department

The Air Force Maui Optical Station demonstrates its tracking ability with a star. The station was used in tests with NRL's Low-power Atmospheric Compensation Experiment (LACE).

PROFESSIONAL DEVELOPMENT

275 **Programs for NRL Employees—University education and scholarships, continuing education, professional development, and other activities**

282 **Programs for Non-NRL Employees—Fellowships, exchange programs, and cooperative employment**

PROGRAMS FOR NRL EMPLOYEES

During 1991, under the auspices of the Employee Development Branch, NRL employees participated in about 5000 individual training events. Many of these were presented as either videotaped or on-site instructed courses on diverse technical subjects, management techniques, and enhancement of such personal skills as efficient use of time, speed reading, memory improvement, and interpersonal communications. Courses are also available by means of computer-based training (CBT) and live television courses for monitoring nationwide.

One common study procedure is for employees to work full time at the Laboratory while taking job-related scientific courses at universities and schools in the Washington area. The training ranges from a single course to full graduate and postgraduate programs. Tuition for training is paid by NRL. The formal programs offered by NRL are described here.

GRADUATE PROGRAMS

• The **Advanced Graduate Research Program** (formerly the Sabbatical Study Program, which began in 1964) enables selected professional employees to devote full time to research or pursue work in their own or a related field for one academic year at an institution of their choice without the loss of regular salary, leave, or fringe benefits. NRL pays all educational costs, travel, and moving expenses for the employee and dependents. Criteria for eligibility include professional stature consistent with the applicant's opportunities and experience, a satisfactory program of study, and acceptance by the institution selected by the applicant. The program is open to paraprofessional (and above) employees who have completed 6 years of Federal Service, 4 of which are required at NRL.

Dr. Warren Pickett, of the Condensed Matter and Radiation Sciences Division, participated in the Advanced Graduate Research Program. He recently spent a year at Cavendish Laboratory in Cambridge, England.

• The **Edison Memorial Graduate Training Program** enables employees to pursue advanced studies in their fields at local universities. Participants in this program work 24 hours each workweek and pursue their studies during the other 16 hours. The criteria for eligibility include a minimum of 1 year of service at NRL, a bachelor's or master's degree in an appropriate field, and professional standing in keeping with the candidate's opportunities and experience.

• To be eligible for the **Select Graduate Training Program**, employees must have a college degree in an appropriate field and must have maintained at least a B average in undergraduate study. Students accepted in this program devote a full academic year to graduate study. While attending school, they receive one half of their salary, and NRL pays for tuition, books, and laboratory expenses. During the summer, they work at the Laboratory and receive normal pay and fringe benefits.

During FY 91, Todd Jessen, of the Materials Science and Technology Division, participated in the Select Graduate Training Program by spending a year at Rutgers University

Nick Divinic, of the Spacecraft Engineering Department, participated in the Naval Postgraduate School Program in FY 91

• The **Naval Postgraduate School** (NPS), located in Monterey, California, provides graduate programs to enhance the technical preparation of Naval officers and civilian employees who serve the Navy in the fields of science, engineering, operations analysis, and management. It awards a Master of Arts degree in National Security Affairs and a Master of Science degree in many technical disciplines. In addition, a Doctor of Philosophy degree may be earned in select fields of science and engineering.

NRL employees desiring to pursue graduate studies at NPS may apply for a maximum of six quarters away from NRL, with thesis work accomplished at NRL. Specific programs are described in the NPS Catalog. Participants will continue to receive full pay and benefits during the period of study.

• Under the **Foreign Liaison Scientist Program**, assistance is provided to the Chief of Naval Research (CNR), the Chief of Naval Operations (CNO), and the Commandant of the Marine Corps (CMC) in discharging their responsibilities on matters of general scientific and technical interest to the United States in the United Kingdom, Europe, and Far East in foreign liaison offices that are maintained in several areas of the world. Foreign liaison scientists serve in these offices to establish relationships with overseas scientists and scientific activities, to monitor contract and treaty agreements, and to promote the exchange of information and research results between foreign sources and the U.S. Navy R&D establishment. Each year NRL will make assignments to the Office of Naval Research European Office London, England, and the Office of Naval Research Liaison Office, Far East Tokyo, Japan. The purpose of such assignments is to acquaint a limited number of NRL's technical professionals with the functions of international operations, including such activities as developing productive liaison with foreign scientists and research activities, representing the interests of the U.S. Navy in multinational conferences and scientific meetings, and preparing technical reports and papers with editorial interpretation for appropriate audiences in the United States.

• In addition to NRL and university offerings, application may be made to a number of noteworthy programs and fellowships. Examples of such opportunities are the **Alfred P. Sloan Fellows Programs**, **Brookings Institute Advanced Study Program**, **The Fellowship in Congressional Operations**, and the **Women's Executive Leadership Program**. These and other programs are announced from time to time as schedules are published.

• Research conducted at NRL may be used as **thesis material for an advanced degree.** This original research is supervised by a qualified employee of NRL who is approved by the graduate school. The candidate should have completed the required course work and should have satisfied the language, residence, and other requirements of the graduate school from which the degree is sought. NRL provides space, research facilities, and supervision but leaves decisions on academic policy to the cooperating schools.

CONTINUING EDUCATION

• Local colleges and universities offer **undergraduate and graduate courses** at NRL for employees interested in improving their skills and keeping abreast of current developments in their fields. These courses are also available at many other DoD installations in the Washington, D.C. area.

• The Employee Development Branch at NRL offers to all employees **short courses** in a number of fields of interest including technical subjects, computer operation, supervisory and management techniques, and clerical/secretarial skills. Laboratory employees may attend these courses at nongovernment facilities as well. Interagency courses in management, personnel, finance, supervisory development, and clerical skills are also available.

For further information on any of the above programs, contact the Employee Development Branch (Code 3840), (202) 767-2956.

TECHNOLOGY TRANSFER

• The **Office of Research and Technology Applications Program** ensures the full use of the results of the Nation's federal investment in research and development by transferring federally owned or originated technology to state and local governments and the private sector.

• The **Navy Science Assistance Program** establishes an information loop between the Fleet and the R&D shore establishments to expedite technology transfer to the user. The program addresses operational problems, focuses resources to solve specific technical problems, and develops a nucleus of senior scientific personnel familiar with the impact of current research and system performance on military operations.

The Navy's Scientists-to-Sea Program offers Navy researchers and R&D managers the opportunity to learn firsthand about factors that affect shipboard system design and operations. The program includes personnel from NRL. The trips generally last from three to ten days. The Scientists-to-Sea Program is scheduled to continue indefinitely with new embarkations offered on a quarterly basis.

Inquiries concerning NRL's technology transfer programs should be made to Dr. Richard Rein or to Dr. George Abraham (Code 1003.1) at (202) 767-3521.

PROFESSIONAL DEVELOPMENT

NRL has several programs, professional society chapters, and informal clubs that enhance the professional growth of employees. Some of these are listed below.

• The **Counseling Referral Service** (C/RS) helps employees to achieve optimal job performance through counseling and resolution of problems such as family, stress and anxiety, behavioral, emotional, and alcohol- or drug-related problems that may adversely impact job performance.

C/RS provides confidential assessments and short-term counseling, as well as training workshops and referrals to additional resources in the community. Contact Robert Power, Code 9012, (202) 767-6857.

• A chartered chapter of **Women in Science and Engineering** (WISE) was established at NRL in 1983. Informal monthly luncheons and seminars are scheduled to inform scientists and engineers of women's research at NRL and to

These students from nearby Patterson Elementary School participated in the 10-week Youth Leadership Program sponsored by the Thomas Edison Toastmasters Club. With them are school and Toastmasters representatives and CAPT J. Love, NRL's Chief Staff Officer, who presented certificates recognizing those students who completed the program.

provide an informal environment for members to practice their presentations. WISE also sponsors a colloquium series to feature outstanding women scientists. (Contact Dr. Wendy Fuller at (202) 767-2793, Dr. Debra Rolison at (202) 767- 3617, or Dr. Cha-Mei Tang at (202) 767-4148.)

• **Sigma Xi**, the Scientific Research Society, encourages original investigation in pure and applied science. As an honor society for research scientists, individuals who have demonstrated the ability to perform original research are elected to membership in local chapters. The NRL chapter, comprised of approximately 400 members, encourages original research by presenting awards annually in pure and applied science to outstanding NRL staff members. The chapter also sponsors lectures at NRL on a wide range of scientific topics for the entire NRL community. The lectures are delivered by scientists from all over the nation and the world. The highlight of the lecture series is the Edison Memorial Lecture, usually featuring a Nobel laureate. (Contact Dr. Susan K. Numrich at (202) 404-7345.)

• Employees interested in developing effective self expression, listening, thinking, and leadership potential are invited to join either of two NRL chapters of **Toastmasters International**. Members of these clubs, who possess diverse career backgrounds and talents, meet three times a month in an effort to learn to communicate not by rules but by practice in an atmosphere of understanding and helpful fellowship. NRL's commanding officer endorses Toastmasters (see NRLINST 12410.11), and the Employee Development Branch pays for membership and educational materials for those employees whose supervisors see a need for their active training in public speaking or organizational communication skills. (Contact Mrs. Kathleen Parrish at (202) 767-2782.)

EQUAL EMPLOYMENT OPPORTUNITY (EEO) PROGRAMS

Equal employment opportunity is a fundamental NRL policy for all persons, regardless of race, color, sex, religion, national origin, age, or physical/mental handicap. The EEO Office's major functions include affirmative action in employment; discrimination complaint process; EEO training of supervisors, managers,

and EEO collateral duty personnel; advice and guidance to management on EEO policy; and the following special emphasis programs.

• The **Federal Women's Program (FWP)** supports and enhances employment and advancement opportunities for women and addresses issues that affect women in the workplace. It provides counseling and referral services and sponsors a chapter of Women in Science and Engineering to recognize outstanding female scientists and engineers. Distinguished women scientists are guest lecturers at quarterly presentations.

• The **Hispanic Employment Program (HEP)** focuses on working with supervisors, managers, and subcommittees to recruit and place qualified Hispanics. The program is involved with Hispanic community organizations and local schools and provides activities specifically designed to offer employment opportunities to Hispanics. "El Ingeniero" (The Engineer), which encourages Hispanic youth to pursue a career in engineering, is one such program.

• The **African American Employment Program (AAEP)** concentrates on recruiting, placing, developing, and advancing African Amerian employees throughout NRL. It also encourages them to achieve their maximum potential.

NRL sponsors an Art and Essay contest for neighboring schools during Black History Month. Shown are the 1991 winners from nearby Leckie Elementary School.

• The **Individuals with Handicaps Program (IHP)** assists management to improve employment and advancement opportunities for qualified handicapped and disabled-veteran employees. It also advises on accommodations necessary for handicapped persons. It recruits handicapped summer students from colleges and universities for technical positions in engineering and science and paraprofessional positions in accounting and administration; it also seeks Cooperative Education Program (Co-op) candidates who are pursuing degrees in engineering, computer sciences, or the physical sciences.

• The **Asian-American/Pacific Islander Program (API)** identifies areas of concern regarding the recruitment, selection, advancement, retention, and utilization of Asian-American/Pacific Islander employees throughout NRL. The program interacts with API professional/community organizations to address employment concerns.

The Korean Dance Troupe performed during NRL's National Asian/Pacific Heritage Month celebration

• The **American Indian/Alaskan Native Employment Program (AI/ANEP)** focuses on the employment concerns of AI/ANEP employees. The program provides counseling and referral services on recruitment, hiring, placement, promotion, retention, and other areas of employee interest.

An NRL Community Outreach volunteer demonstrates the optics of telescopes for the Young Astronauts' Club at the Harris Educational Center

During Career Day at neighboring Patterson Elementary School, Ms. Leona Jackson, of NRL's Technical Information Division, explains how the field of graphic arts is used in science and technology.

• The **Federal Employment Opportunity Recruitment Program (FEORP)** is designed to establish, maintain, and update targeted recruitment programs to reduce the conspicuous absence or manifest imbalance categories of NRL employment through innovative internal and external recruitment. In addition, it fosters relationships with minority and women's institutions and organizations.

Special programs are held during the year to promote an awareness of the contributions and capabilities of women and minorities. (Contact the EEO Office at (202) 767-2486 for all EEO programs.)

OTHER ACTIVITIES

• The **Community Outreach Program** traditionally has used its extensive resources to foster programs that provide benefits to students and other community citizens. Volunteer employees assist with and judge science fairs, give lectures, tutor, mentor, coach, and serve as classroom resource teachers. The program also sponsors Black History Month art and essay contests for local schools, student tours of NRL, a student Toastmasters Youth Leadership Program, an annual Christmas party for neighborhood children, and an annual collection for Children's Hospital. (Contact the Public Affairs Office at 767-2541.)

• Other programs that enhance the development of NRL employees include four computer user groups (**IBM PC, Mac, NeXT,** and **Sun**) and the **Amateur Radio Club**. The **Recreation Club** accommodates the varied interests of NRL's employees with its numerous facilities, such as a 25-yard, 6-lane indoor swimming pool; a gymnasium with basketball and volleyball; a weight room and exercise area; table tennis; meeting room; softball and basketball leagues; jacuzzi whirlpool; saunas; classes in five different martial arts groups, aerobics exercise, swimming, and water walking; and specialized

sports clubs (running, skiing, biking, golfing). The **Showboaters**, a nonprofit drama group that presents live theater for the enjoyment of NRL and the community, performs two major productions each year in addition to occasional performances at Laboratory functions and benefits for local charities. The most recent productions were "You Can't Take it With You" and "Little Shop of Horrors." Though based at NRL, membership in Showboaters is not limited to NRL employees.

NRL employees annually sponsor a Christmas Party for children from nearby schools. Shown here are some the 150 children as they await their visit with Santa and Mrs. Claus.

Members of NRL's Amateur Radio Club participated in the 55th Annual American Radio League Field Day emergency preparedness test held in June 1991

PROGRAMS FOR NON-NRL EMPLOYEES

Several programs have been established for non-NRL professionals. These programs encourage and support the participation of visiting scientists and engineers in research of interest to the Laboratory. Some of the programs may serve as stepping-stones to federal careers in science and technology. Their objective is to enhance the quality of the Laboratory's research activities through working associations and interchanges with highly capable scientists and engineers and to provide opportunities for outside scientists and engineers to work in the Navy laboratory environment. Along with enhancing the Laboratory's research, these programs acquaint participants with Navy capabilities and concerns.

RECENT Ph.D., FACULTY MEMBER, AND COLLEGE GRADUATE PROGRAMS

- The **National Research Council (NRC)/ NRL Cooperative Research Associateship Program** selects associates who conduct research at NRL in their chosen fields in collaboration with NRL scientists and engineers. The tenure period is 2 years. The Office of Naval Research offers the associate posttenure research grants tenable at an academic institution.

- The American Society for Engineering Education (ASEE) administers the **Office of Naval Technology (ONT) Postdoctoral Fellowship Program** that aims to increase the involvement of highly trained scientists and engineers in disciplines necessary to meet the evolving needs of naval technology. Appointments are for 1 year (renewable for a second and sometimes a third year). These competitive appointments are made jointly by ONT and ASEE.

- The American Society for Engineering Education also administers the Navy/ASEE **Summer Faculty Research Program** for university faculty members to work for 10 weeks with professional peers in participating Navy laboratories on research of mutual interest.

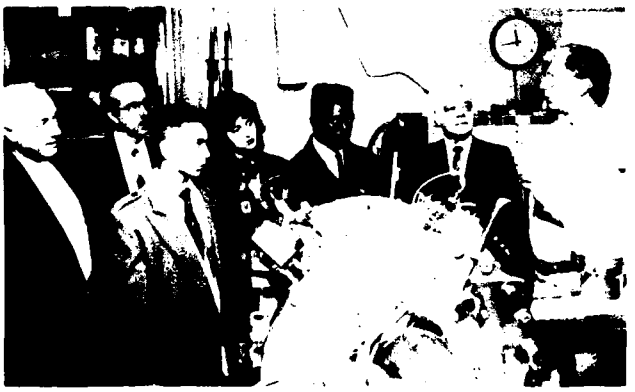

Dr. Jerome Karle, NRL's Nobel Laureate, leads students and science teachers from the Abraham Lincoln High School in New York City as they visited NRL's Superconducting Thin Film Facility of the Materials Science and Technology Division. Here a scientist explains the production process of high-temperature superconducting films.

• The **NRL/United States Naval Academy (USNA) Cooperative Program for Scientific Interchange** allows faculty members of the U.S. Naval Academy to participate in NRL research. This collaboration benefits the Academy by providing the opportunity for USNA faculty members to work on research of a more practical or applied nature. In turn, NRL's research program is strengthened by the available scientific and engineering expertise of the USNA faculty.

• The **Office of Naval Research Graduate Fellowship Program** helps U.S. citizens obtain advanced training in disciplines of science and engineering critical to the U.S. Navy. The 3-year program awards fellowships to recent outstanding graduates to support their study and research leading to doctoral degrees in specified disciplines such as electrical engineering, computer sciences, material sciences, applied physics, and ocean engineering. Award recipients are encouraged to continue their study and research in a Navy laboratory during the summer.

For further information about the above five programs, please contact Mrs. Jessica Hileman at (202) 767-3865.

• The **United States Naval Academy Ensign Program** assigns Naval Academy graduates to NRL to work in areas of their own choosing commensurate with their academic qualifications. These graduates provide a fruitful summer of research assistance, while gaining valuable experience in the Navy's R&D program. (Contact CDR Bob Young at (202) 767-2103.)

PROFESSIONAL APPOINTMENTS

• **Faculty Member Appointments** use the special skills and abilities of faculty members for short periods to fill positions of a scientific, engineering, professional, or analytical nature.

• **Consultants and experts** are employed because they are outstanding in their fields of specialization, or because they possess ability of a rare nature and could not normally be employed as regular civil servants.

• **Intergovernmental Personnel Act Appointments** temporarily assign personnel from the state or local government or educational institution to the Federal Government (or vice versa) to improve public services rendered by all levels of government.

UNDERGRADUATE COLLEGE STUDENT PROGRAMS

Several programs are tailored to the undergraduate that provide employment and work experience in naval research. These are designed to attract applicants for student and full professional employment in the laboratory's shortage category positions, such as engineers, physicists, mathematicians, and computer scientists. The student employment programs build an understanding of NRL job opportunities among students and educational personnel, so that educators can provide students who will meet NRL's occupational needs. The employment programs for college students include the following:

• The **Cooperative Education Program** alternates periods of work and study for students pursuing bachelor degrees in engineering, computer science, or the physical sciences. Several universities participate in this program.

• The **Clerical Cooperative Eduation Program** employs students interested in pursuing careers in the clerical occupation. Students work part time during the school year and full time during school breaks.

• The **Federal Junior Fellowship Program** hires needy students entering college to be assistants to scientific, professional, or technical employees.

Dr. James Butler, of NRL's Chemistry Division, shows a thin diamond membrane to high school students who visited the Lab during National Science and Technology Week.

• The **Summer Employment Program** employs students for the summer in paraprofessional and technician positions in engineering, physical sciences, and computer sciences.

• The **Student Volunteer Program** helps students gain valuable experience by allowing them to voluntarily perform educationally related work at NRL.

• The **1040-Hour Appointment** employs students on a half-time basis to assist in scientific work related to their academic program.

• The **Gifted and Talented Internship Program** provides a meaningful part-time employment experience for high school students who plan to pursue a bachelor's degree in engineering, computer science, or the physical sciences.

For additional information, contact Mrs. Cathy Downing at (202) 767-3030.

HIGH SCHOOL PROGRAMS

• The **DoD Science & Engineering Apprentice Program** employs high school juniors and seniors to serve for 8 weeks as junior research associates. Under the direction of a mentor, students gain a better understanding of research, its challenges, and its opportunities through participation in scientific programs. Criteria for eligibility are based on science and mathematics courses completed and grades achieved; scientific motivation, curiosity, and capacity for sustained hard work; a desire for a technical career; teacher recommendations; and achievement test scores. The Naval Research Laboratory program is the lead program and the largest in DoD.

For additional information on these programs, please contact the Employee Development Branch, Code 3840, at (202) 767-2956.

From 1979 to the present, the Science and Engineering Apprentice Program at NRL has given Washington-area high school students opportunities to learn and gain experience in science and technology. Shown here are some of the 70 apprentices and their mentors who participated in the 1991 program.

A Vortex in an Unconventional Superconductor
Computer Graphics, *Honorable Mention*
Daryl W. Hess

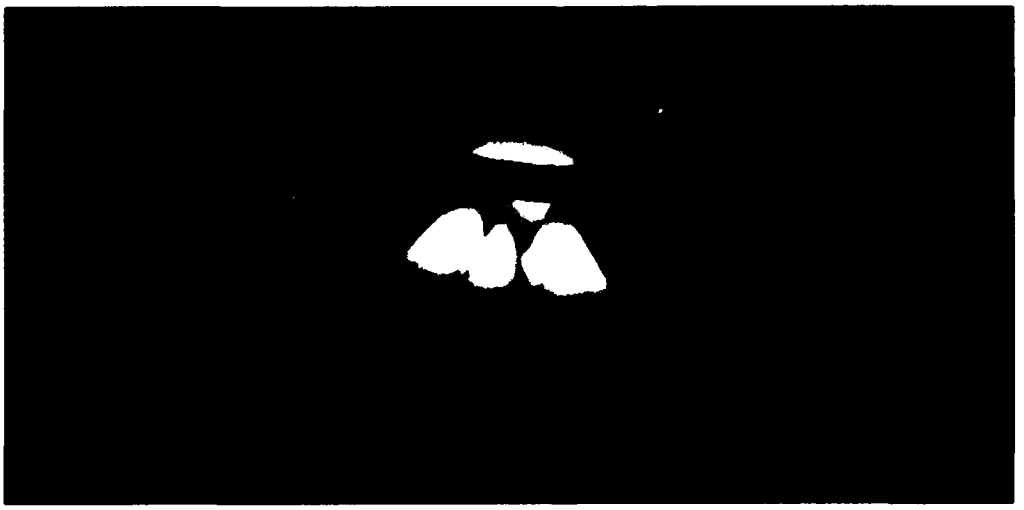

A Vortex in an Unconventional Superconductor
Computer Graphics, *Honorable Mention*
Daryl W. Hess
Condensed Matter and Radiation Sciences Division

A vortex in the Cooper-pair wave function of the unconventional superconductor UPt_3 near its superconducting phase transition in a magnetic field, from a calculation performed on the NRL Connection Machine and rendered on a Stardent GS 2000. The homogeneous bulk phase (depicted by the red plane) vanishes at the center of the vortex, where the magnetic field (not shown) is a maximum. The second component of the wave function, which is everywhere zero in the absence of the field (blue plane), forms four peaks in a pattern resembling a four-leaf clover in contour.

GENERAL INFORMATION

287 **Technical Output**

288 **Key Personnel**

289 **Organizational Charts**

293 **Contributions by Divisions, Laboratories, and Departments**

295 **Employment Opportunities**

297 **Location of NRL in the Capital Area**

298 **Index**

Inside back cover ***NRL Review* Staff**

TECHNICAL OUTPUT

The Navy continues to be a pioneer in initiating new developments and a leader in applying these advancements to military requirements. The primary means of informing the scientific and engineering community of the advances made at NRL is through its technical output—reports, articles in scientific journals and books, papers presented to scientific societies, and topical conferences, patents, and inventions.

This section lists a portion of NRL's output for FY 1991. The omitted parts are oral presentations (about 2000), reports that carry a military security classification, and letter reports to sponsors.

Type of Contribution	Unclass.	Class.	Total
Papers in periodicals, books, and proceedings of meetings	948	3	951
NRL Reports	38	15	53
NRL Memorandum Reports	111	22	133
Books	1	0	1
Patents granted			60
Statutory Invention Registrations (SIRs)			8

A complete listing of the publications by NRL authors, including reports, articles in scientific journals and books, patents, and SIRs appears in the *Bibliography of NRL Publications* as a separate publication.

Key Personnel

Code	Office		Direct-in-Dialing (202)76; Autovon 29- Extension
	EXECUTIVE DIRECTORATE		
1000	Commanding Officer	CAPT P.G. Gaffney II, USN	73403
1001	Director of Research	Dr. T. Coffey	73301
1002	Chief of Staff Officer Inspector General	CAPT J.R. Love, USN	73621
1003	Associate Director of Research for Strategic Planning	Dr. W.M. Tolles	73584
1004	Scientific Consultant to Director of Research	Dr. P. Mange	73724
1005	Head, Office of Management and Administration	Ms. M. Oliver	73086
1006	Head, Exploratory Development Program Office	Dr. S. Sacks	73666
1200	Head, Command Support Division	CAPT J.R. Love, USN	73621
1240	Head, Safety Branch	Mr. K. King*	72232
1270	Officer in Charge, Cheasapeake Bay Detachment	LCDR B. Jones, USN	301-257-4002
1280	Officer in Charge, Flight Support Detachment	CDR S.S. Smith, USN	301-863-3751
3008	Legal Counsel	Ms. H. Halper*	72244
3803	Deputy EEO Officer	Ms. D. Erwin*	72486
4810	Public Affairs Officer	Mr. J.W. Gately, Jr.*	72541
	BUSINESS OPERATIONS DIRECTORATE		
3000	Associate Director of Research	Mr. R.E. Doak	72371
3200	Head, Contracting Division	Mr. J. Ely	75227
3300	Comptroller	Mr. D.T. Green	73405
3400	Supply Officer	Mr. W.E. Ralls, Jr.	73446
3500	Public Works Officer	Mr. D.K. Woodington	73371
3800	Head, Civilian Personnel Division	Mrs. B.A. Duffield	73421
	GENERAL SCIENCE AND TECHNOLOGY DIRECTORATE		
4000	Associate Director of Research	Dr. R.A. LeFande	73324
4100	Supt., Space Science Division	Dr. H. Gursky	76343
4200	Center for Advanced Space Sensing	Dr. K. Johnston	72351
4400	Dir., Lab. for Computational Physics and Fluid Dynamics	Dr. J.P. Boris	73055
4600	Supt., Condensed Matter & Radiation Sciences Division	Dr. D.J. Nagel	72931
4700	Supt., Plasma Physics Division	Dr. S. Ossakow	72723
4800	Head, Technical Information Division	Mr. P.H. Imhof	73388
	WARFARE SYSTEMS AND SENSORS RESEARCH DIRECTORATE		
5000	Associate Director of Research	Mr. R.R. Rojas	73294
5100	Supt., Acoustics Division	Dr. D.L. Bradley	73482
5300	Supt., Radar Division	Dr. M.I. Skolnik	72936
5500	Supt., Inforamtion Technology Division	Dr. R.P. Shumaker	72903
5700	Supt., Tactical Electronic Warfare Division	Dr. J.A. Montgomery	76278
5800	Head, Research Computation Division	Mr. R.F. Saenger	72751
5900	Supt. Underwater Sound Reference Detachment	Dr. J.E. Blue	407-856-5230
	MATERIALS SCIENCE AND COMPONENT TECHNOLOGY DIRECTORATE		
6000	Associate Director of Research	Dr. B.B. Rath	73566
6030	Head, Laboratory for Structure of Matter	Dr. J. Karle	72665
6090	Center for Biomolecular Science and Engineering	Dr. J. Schnur	73344
6100	Supt., Chemistry Division	Dr. J.S. Murday	73026
6300	Supt., Materials Science & Technology Division	Dr. D.U. Gubser	72926
6500	Supt., Optical Sciences Division	Dr. T.G. Giallorenzi	73171
6800	Supt., Electronics Science and Technology Division	Dr. G.M. Borsuk	73525
	NAVAL CENTER FOR SPACE TECHNOLOGY		
8000	Director	Mr. P.G. Wilhelm	76547
8100	Supt., Space Systems Development Department	Mr. R.E. Eisenhauer	70410
8200	Supt., Spacecraft Engineering Department	Mr. R.T. Beal	76407
8300	Supt., Space Systems Technology Department	Mr. G.W. Hoskins†	73920
	NRL STENNIS SPACE CENTER/MONTEREY		
	Officer in Charge	CDR L.R. Elliott, USN	601 688-4011
	Technical Director	Dr. W.B. Moseley	601 688 4670
	Director, Ocean Acoustics & Technology Directorate	Dr. E.R. Franchi	601 688-5978
	Director, Ocean Science Directorate	Dr. H.C. Eppert, Jr.	601 688 4650
	Director, Atmospheric Directorate	Dr. J.B. Hovermale	Autovon 878 4721

*Additional duty
†Acting

ORGANIZATIONAL CHART
RESEARCH ADVISORY COMMITTEE

COMMANDING OFFICER
Code 1000
CAPT P.G. Gaffney II,
USN

DIRECTOR OF RESEARCH
Code 1001
Dr. T. Coffey

ASSOCIATE DIRECTORS OF RESEARCH

OFFICE OF
STRATEGIC
PLANNING
Code 1003
Dr. W.M. Tolles

BUSINESS
OPERATIONS
DIRECTORATE
Code 3000
R.E. Doak

GENERAL SCIENCE
AND TECHNOLOGY
DIRECTORATE
Code 4000
Dr. R.A. LeFande

WARFARE SYSTEMS
AND SENSORS
RESEARCH
DIRECTORATE
Code 5000
R.R. Rojas

MATERIALS SCIENCE
AND COMPONENT
DIRECTORATE
Code 6000
Dr. B.B. Rath

NAVAL CENTER
FOR SPACE
TECHNOLOGY
Code 8000
P.G. Wilhelm

ORGANIZATIONAL CHART (Continued)
EXECUTIVE DIRECTORATE

EXECUTIVE COUNCIL (DIVISION DIRECTORS)

COMMANDING OFFICER
Code 1000
CAPT P.G. Gaffney II, USN

RESEARCH ADVISORY COMMITTEE

DIRECTOR OF RESEARCH
Code 1001
Dr. T. Coffey

CHIEF STAFF OFFICER INSPECTOR GENERAL INTERNAL REVIEW
Code 1002
CAPT J.R. Love, USN

SAFETY OFFICER
Code 1240
K. King

LEGAL COUNSEL
Code 3008
H. Halper

DEPUTY EQUAL EMPLOYMENT OPPORTUNITY OFFICER
Code 3803
D. Erwin

PUBLIC AFFAIRS OFFICER
Code 4610
J.W. Gately, Jr.

OFFICE OF STRATEGIC PLANNING
Code 1003
Dr. W.M. Tolles

SCIENTIFIC CONSULTANT TO THE DIRECTOR OF RESEARCH
Code 1004
Dr. P. Mange

OFFICE OF MANAGEMENT AND ADMINISTRATION
Code 1005
M. Oliver

EXPLORATORY DEVELOPMENT MANAGER
Code 1006
Dr. S. Sacks

COMMAND SUPPORT DIVISION
Code 1200
CAPT J.R. Love, USN

CHESAPEAKE BAY DETACHMENT
Code 1270
LCDR B. Jones, USN

FLIGHT SUPPORT DETACHMENT
Code 1280
CDR S.S. Smith, USN

BUSINESS OPERATIONS DIRECTORATE
Code 3000
R.E. Doak

CONTRACTING DIVISION
Code 3200
J. Ely*
- Contract Negotiations
- Acquisition Strategies/Training
- Advance Acquisition Planning
- Contractual Execution
- Contract Administraion
- Acquisition Policy Interpretations and Implementation

FINANCIAL MANAGEMENT DIVISION
Code 3300
D. Green
- Budget
- Accounting
- Disbursing
- Asset Management
- Systems Operations

SUPPLY DIVISION
Code 3400
W.E. Ralls, Jr.
- Small Purchasing
- Technical Screening
- Receipt Control
- Material Distribution
- Shop Stores
- Disposal and Storage

PUBLIC WORKS DIVISION
Code 3500
D.K. Woodington
- Engineering
- Maintenance and Utilities
- Contracts
- Maintenance Control
- Administrative
- Programming
- Project Management
- Facilities Support

CIVILIAN PERSONNEL DIVISION
Code 3800
B. Duffield
- Staffing and Classification
- Employee Development
- Employee Relations
- Special Recruitment Programs

GENERAL SCIENCE AND TECHNOLOGY DIRECTORATE
Code 4000
Dr. R.A. LeFande

SPACE SCIENCE DIVISION
Code 4100
Dr. H. Gursky
- X-Ray Astronomy
- Upper Atmospheric Physics
- Gamma & Cosmic Ray Astrophysics
- Solar Physics
- Solar Terrestrial Relationships
- Ionospheric Effects
- E.O. Hulburt Center for Space Research
- Engineering Management
- Ultraviolet Measurement
- Solar Spectroscopy

CENTER FOR ADVANCED SPACE SENSING
Code 4200
Dr. K. Johnston
- Radio/IR/Optical Sensors
- Atmospheric.Ocean Sensing
- Imaging Systems and Research

LABORATORY FOR COMPUTATIONAL PHYSICS AND FLUID DYNAMICS CODE 4400
Dr. J.P. Boris
- Reactive Flow and Dynamical Systems
- Fluid/Structure Interactions
- Fluid Dynamics Developments
- Computational Physics Developments
- Mathematical Physics

CONDENSED MATTER AND RADIATION SCIENCES DIVISION
Code 4600
Dr. D.J. Nagel
- Radiation Effects
- Directed Energy Effects
- Surface Modification
- Dynamics of Solids
- Complex Systems Theory

PLASMA PHYSICS DIVISION
Code 4700
Dr. S. Ossakow
- Radiation Hydrodynamics
- Laser Plasma
- Charged Particle Physics
- Pulsed Power Physics
- Space Plasma Physics
- Beam Physics

TECHNICAL INFORMATION DIVISION
Code 4800
P. Imhof
- Information Services
- Technical Library Software Support
- Publications
- Graphic Design Services
- Systems Photographic
- Historian

ORGANIZATIONAL CHART (Continued)

GENERAL SCIENCE AND TECHNOLOGY DIRECTORATE
Code 4000
Dr. R.A. LeFande

SPACE SCIENCE DIVISION
Code 4100
Dr. H. Gursky
- X-Ray Astronomy
- Upper Atmospheric Physics
- Gamma & Cosmic Ray Astrophysics
- Solar Physics
- Solar Terrestrial Relationships
- Ionospheric Effects
- E.O. Hulburt Center for Space Research
- Engineering Management
- Ultraviolet Measurement
- Solar Spectroscopy

CENTER FOR ADVANCED SPACE SENSING
Code 4200
Dr. K. Johnston
- Radio/IR/Optical Sensors
- Atmospheric/Ocean Sensing
- Imaging Systems and Research

LABORATORY FOR COMPUTATIONAL PHYSICS AND FLUID DYNAMICS
CODE 4400
Dr. J.P. Boris
- Reactive Flow and Dynamical Systems
- Fluid/Structure Interactions
- Fluid Dynamics Developments
- Computational Physics Developments
- Mathematical Physics

CONDENSED MATTER AND RADIATION SCIENCES DIVISION
Code 4600
Dr. D.J. Nagel
- Radiation Effects
- Directed Energy Effects
- Surface Modification
- Dynamics of Solids
- Complex Systems Theory

PLASMA PHYSICS DIVISION
Code 4700
Dr. S. Ossakow
- Radiation Hydrodynamics
- Laser Plasma
- Charged Particle Physics
- Pulsed Power Physics
- Space Plasma Physics
- Beam Physics

TECHNICAL INFORMATION DIVISION
Code 4800
P. Imhof
- Information Services
- Technical Library/Software Support
- Publications
- Graphic Design Services
- Systems/Photographic
- Historian

WARFARE SYSTEMS AND SENSORS RESEARCH DIRECTORATE
Code 5000
R.R. Rojas

ACOUSTICS DIVISION
Code 5100
Dr. D. Bradley
- Acoustics Media Characterization
- Applied Ocean Acoustics
- Physical Acoustics
- Signal Processing
- Acoustic Systems

RADAR DIVISION
Code 5300
Dr. M.I. Skolnik
- Radar Analysis
- Radar Techniques
- Search Radar
- Target Characteristics
- Identification Systems
- Airborne Radar

INFORMATION TECHNOLOGY DIVISION
Code 5500
Dr. R.P. Shumaker
- Navy Center for Applied Research in Artificial Intelligence
- Communication Systems
- Transmission Technology
- Battle Management Technology
- Human-Computer Interaction
- Secure Information Technology

TACTICAL ELECTRONIC WARFARE DIVISION
Code 5700
Dr. J.A. Montgomery
- Offboard Countermeasures
- EW Support Measures
- Airborne EW Systems
- Ships EW Systems
- Advanced Techniques

RESEARCH COMPUTATION DIVISION
Code 5800
R.F. Saenger
- Software
- User Services
- Computer Operations and Communications

UNDERWATER SOUND REFERENCE DETACHMENT
Code 5900
Dr. J.E. Blue
- Acoustic Materials
- Technical Services
- Electronics
- Transducer Measurements
- Computer

MATERIALS SCIENCE AND COMPONENT TECHNOLOGY DIRECTORATE
Code 6000
Dr. B.B. Rath

LABORATORY FOR STRUCTURE OF MATTER
Code 6030
Dr. J. Karle
- Energetic Materials
- Analytical Theory
- Physiologically Active Materials
- Macromolecular Structure and Function
- Nanodiffraction and Nanoscopy
- Crystal Growth

CENTER FOR BIOMOLECULAR SCIENCE AND ENGINEERING
Code 6090
Dr. J. Schnur
- Biosystems
- Biosensors
- Advanced Materials

CHEMISTRY DIVISION
Code 6100
Dr. J.S. Murday
- Chemical Dynamics and Diagnostics
- Polymeric Materials
- Surface Chemistry
- Navy Technology Center for Safety and Survivability

MATERIALS SCIENCE AND TECHNOLOGY DIVISION
Code 6300
Dr. D. Gubser
- Physical Metallurgy
- Composites and Ceramics
- Mechanics of Materials
- Material Physics

OPTICAL SCIENCES DIVISION
Code 6500
Dr. T.G. Giallorenzi
- Advanced Concepts
- Applied Optics
- Laser Physics
- Electro-optical Technology
- Optical Techniques
- Fiber Optics Technology

ELECTRONICS SCIENCE AND TECHNOLOGY DIVISION
Code 6800
Dr. G.M. Borsuk
- Solid State Devices
- Electronic Materials
- Surface and Interface Sciences
- Microwave Technology
- Vacuum Electronics

RT (Continued)

MATERIALS SCIENCE AND COMPONENT TECHNOLOGY DIRECTORATE
Code 6000
Dr. B.B. Rath

LABORATORY FOR STRUCTURE OF MATTER
Code 6030
Dr. J. Karle
- Energetic Materials
- Analytical Theory
- Physiologically Active Materials
- Macromolecular Structure and Function
- Nanodiffraction and Nanoscopy
- Crystal Growth

CENTER FOR BIOMOLECULAR SCIENCE AND ENGINEERING
Code 6090
Dr. J. Schnur
- Biosystems
- Biosensors
- Advanced Materials

CHEMISTRY DIVISION
Code 6100
Dr. J.S. Murday
- Chemical Dynamics and Diagnostics
- Polymeric Materials
- Surface Chemistry
- Navy Technology Center for Safety and Survivability

MATERIALS SCIENCE AND TECHNOLOGY DIVISION
Code 6300
Dr. D Gubser
- Physical Metallurgy
- Composites and Ceramics
- Mechanics of Materials
- Material Physics

OPTICAL SCIENCES DIVISION
Code 6500
Dr T G Giallorenzi
- Advanced Concepts
- Applied Optics
- Laser Physics
- Electro-optical Technology
- Optical Techniques
- Fiber Optics Technology

ELECTRONICS SCIENCE AND TECHNOLOGY DIVISION
Code 6800
Dr G M Borsuk
- Solid State Devices
- Electronic Materials
- Surface and Interface Sciences
- Microwave Technology
- Vacuum Electronics

NAVAL CENTER FOR SPACE TECHNOLOGY
Code 8000
P.G. Wilhelm

SPACE SYSTEMS DEVELOPMENT DEPARTMENT
Code 8100
R.E. Eisenhauer
- Spacecraft Engineering
- Advanced Systems Development
- Communication Systems Technology
- Terrestrial Systems
- SDI Office

SPACECRAFT ENGINEERING DEPARTMENT
Code 8200
R.T. Beal
- Design, Manufacturing and Processing
- Systems Analysis and Test
- Control Systems
- Concept Development

SPACE SYSTEMS TECHNOLOGY DEPARTMENT
Code 8300
G.W. Hoskins*
- Space Applications
- Systems Engineering and Analysis
- Advanced Concepts and Processing

NRL STENNIS SPACE CENTER/MONTEREY

OFFICER IN CHARGE
CDR L.R. Elliott, USN

TECHNICAL DIRECTOR
DR. W.B. Moseley

OCEAN ACOUSTICS AND TECHNOLOGY DIRECTORATE
DR E R Franchi
- Very Low/Very High Frequency Acoustics
- Advanced Acoustic Data Acquisition Buoy System
- Array Design, Fabrication and Testing
- Expert Systems
- Acoustic Model Configuration Management

OCEAN SCIENCE DIRECTORATE
DR H C Eppert, Jr
- Tactical Oceanography
- Airborne Bathymetric Systems
- Wave Research and Forecasting
- Optical Oceanography
- Bottom, Subbottom Geoacoustics
- Magnetics

ATMOSPHERIC DIRECTORATE
DR J B Hovermale
- Meteorological Nowcasting Forecasting
- Computational Numerical Atmospheric Models
- Tactical Decision Aids

*ACTING

- - - - - - - - - - - ADDITIONAL DUTY

CONTRIBUTIONS BY DIVISIONS, LABORATORIES, AND DEPARTMENTS

Space Science Division (4100)

Science and Art: A Contest and a Celebration
by Herbert Gursky
From the Challenges of World War II to
the Frontiers of Space
by Herbert Friedman
Anomalous Cosmic Rays
by James H. Adams, Jr. and Allan J. Tylka
Far Ultraviolet Cameras Experiment on STS-39:
Observations of the Far UV Space Environment
by George R. Carruthers

Center for Advanced Space Sensing (4200)

High Resolution Remote Sensing
by Richard P. Mied, Farid Askari,
George O. Marmorino, Gaspar R. Valenzuela,
and Dennis B. Trizna
Atmospheric Aerosol Size Distributions in
the Marine Boundary Layer
by James W. Fitzgerald and William A. Hoppel

Laboratory for Computational Physics and Fluid Dynamics (4400)

Chemical Reaction Rates from First Principles
by Maribel R. Soto

Condensed Matter and Radiation Sciences Division (4600)

Ion-beam-assisted Deposition Provides Control
over Thin Film Properties
by Fred A. Smidt
Brightest X Rays Used to Probe Smallest Crystals
by Earl F. Skelton, Syed B. Quadri, and
Jack D. Ayers
Buckminsterfullerene: Building Blocks for
New Materials
by Mark M. Ross, John H. Callahan,
Steven W. McElvany, Mark R. Pederson,
Larry L. Boyer, and Warren E. Pickett
Single Event Upsets in Space
by Arthur B. Campbell

Plasma Physics Division (4700)

Probing the Magnetosphere by Using Chemical
Releases from the Combined Release and
Radiation Effects Satellite (CRRES)
by Paul A. Bernhardt, Joseph D. Huba, and
Paul Rodriguez
Atomic Physics in Ultrastrong Fields
by Jack Davis, Robert W. Clark, and
John L. Giuliani, Jr.

Acoustics Division (5100)

Acoustic Backscattering from the Sea Surface
by Peter M. Ogden and Fred T. Erskine
A Pictorial Analysis of Vibrating Shell Physics
by Earl G. Williams

Radar Division (5300)

Monolithic GaAs Antenna/Detector Array for
94 GHz Imaging
by William M. Waters
Skywave Over-the-horizon Radar Performance Model
by Benjamin T. Root
Ultrawideband Radar
by Grealie A. Andrews, J. Peter Hansen, and
Karl Gerlach
High Resolution Remote Sensing
by Richard P. Mied, Farid Askari,
George O. Marmorino, Gaspar R. Valenzuela,
and Dennis B. Trizna

Information Technology Division (5500)

A Graphical User Interface Design for Shipboard
Damage Control
by David L. Tate
A Networking Technology Demonstration for
Naval Tactial Communications
by Dennis N. McGregor, Dennis J. Baker,
and James P. Hauser
Decision Support for Operational Logistics
by James B. Hofmann

Tactical Electronic Warfare Division (5700)

Low Reynolds Number Aerodynamics for Electronic Warfare
by Richard J. Foch and Peggy L. Toot

A Programmable Antiship Infrared Guidance System
by Elmer F. Williams, Robert H. Evans, and Paul L. Alles

Scale Model Analysis Facility
by Stanley A. Moroz and Ernest S. Mak

Visualization Tools for Development of Electronic Warfare Techniques
by Tiziano Ricci and Robert Normoyle (QuesTech Inc.)

Underwater Sound Reference Detachment (5900)

Piezoelectric Composites for Transducer Applications
by Kurt M. Rittenmyer

Transducer Calibration in Multipath Environments
by Phillip L. Ainsleigh

Center for Bio/Molecular Science and Engineering (6090)

Fiber-optic-based Biosensor
by George P. Anderson, Lisa C. Shriver-Lake, Robert A. Ogert, Joel P. Golden, and Frances S. Ligler

Chemistry Division (6100)

Atomistic Processes in Surface Mechanics and Adhesion
by Richard J. Colton, Donald W. Brenner, Judith A. Harrison, and Nancy A. Burnham

Buckminsterfullerene: Building Blocks for New Materials
by Mark M. Ross, John H. Callahan, Steven W. McElvany, Mark R. Pederson, Larry L. Boyer, and Warren E. Pickett

High Temperature Phthalonitrile Resins for Structural Applications
by Teddy M. Keller

Structural Mapping of Ultrathin Films
by Yves U. Idzerda, Gary A. Prinz, and David E. Ramaker

Materials Science and Technology Division (6300)

A Process to Make Ultrafine Metal Powders
by Khershed P. Cooper and Jack D. Ayers

Brightest X Rays Used to Probe Smallest Crystals
by Earl F. Skelton, Syed B. Qadri, and Jack D. Ayers

Structural Mapping of Ultrathin Films
by Yves U. Idzerda, Gary A. Prinz, and David E. Ramaker

Understanding Superconductivity in the Cuprates: Theory and Experiment
by Stuart A. Wolf, Mark E. Reeves, Johsua L. Cohn, and Vladimir Z. Kresin (Lawrence Berkeley Laboratory)

Vertex Simulation of Two-dimensional Grain Growth
by Steven P. Marsh, Robert A. Masumura, and Chandra S. Pande

Optical Sciences Division (6500)

Subpicosecond All-fiber Laser
by Irl N. Duling III

1.06 μm All-fiber Optic Gyroscope
by William K. Burns and Robert P. Moeller

Heavy Metal Fluoride (HMF) Glass Windows
by Ishwar D. Aggarwal and John M. Jewell

Electronics Science and Technology Division (6800)

Advances in the State-of-the-art Growth of InSb by Using Molecular Beam Epitaxy and Organometallic Vapor Phase Epitaxy
by D. Kurt Gaskill, Phillip E. Thompson, John L. Davis, and Gregory T. Stauf

Interfaces in Semiconductor Nanostructures
by Daniel G. Gammon, D. Scott Katzer, and Benjamin V. Shanabrook

Space Systems Development Department (8100)

Battery Impedance Effects on Spacecraft Electrical Power System Stability
by Daniel J. Shortt and William E. Baker, Jr.

Spacecraft Engineering Department (8200)

Ground-based Laser Measurements of Vibration of the LACE Satellite
by Shalom Fisher, Donald Augenstein, and Kenneth I. Schultz

Space Systems Technology Department (8300)

Nonlinear Signal Processing for Detection in Chaotic Backgrounds
by Sheldon B. Gardner

EMPLOYMENT OPPORTUNITIES FOR ENTRY-LEVEL AND EXPERIENCED PERSONNEL

This *NRL Review* illustrates some of the exciting science and engineering carried out at NRL as well as the potential for new personnel.

The Naval Research Laboratory offers a wide variety of challenging positions that involve the full range of work from basic and applied research to equipment development. The nature of the research and development conducted at NRL requires professionals with experience. Typically, there is a continuing need for electronics, mechanical, aerospace, ceramic, and materials engineers; metallurgists with bachelor's and/or advanced degrees; and physical and computer scientists with Ph.D. degrees. Opportunities exist in the areas described below.

Ceramic and Materials Scientists/Engineers. These employees work on the mechanical properties, coating and materials processing, and materials research.

Electronics Engineers. These engineers work in the following areas: communications satellite design, analog and digital signal processing, information processing, strategic and tactical communication systems design, instrumentation, microcomputer design, satellite attitude-control systems, image processing, IR sensors, focal plane arrays, radar, inverse scattering phenomena, statistical communication theory, electro-optics, hardware/software interfacing, artificial intelligence, electromagnetic (EM) scattering, digital electronics, fiber optics, optical information processing, semiconductor device processing, microwave tubes, threat systems analysis, electroacoustic optics, RF measurement design, EM propagation, EM theory, HF radar propagation analysis, electronic warfare simulation, pulsed power technology, vacuum electronics, microwave technologies, networking techniques, speech processing, Navy C^3I, electronic countermeasure systems design, spacecraft attitude controls, and orbitology.

Mechanical and Aerospace Engineers. These employees may be assigned to satellite thermal design, structural design, propulsion, experimental fluid mechanics, experimental structural mechanics, solid mechanics, elastic/plastic fracture mechanics, materials characterization of composites, finite element methods, nondestructive elevation, characterization of fracture resistance of structural alloys, and combustion.

Computer Science Graduates. Employees in this field are involved with artificial intelligence, software engineering, software systems specifications, computer design/architecture, systems analysis, and command information systems.

Chemists. Chemists are recruited to work in the areas of inorganic and organometallic synthesis, solution kinetics and mechanisms, surface analysis, organic chemistry, combustion, colloid/surface chemistry, fire suppression, and nuclear decay.

Physicists. Physics graduates may concentrate on such fields as electromagnetics, image processing, inverse scattering phenomena, acoustics, inversion theory, mathematical modeling of scattering

processors, radar system development, electro-optics, focal plane arrays, signal processing, plasma physics, astrophysics, semiconductor technology, relativistic electronics, beam/wave interactions, low-temperature physics, superconductivity, physical/chemical vapor disposition of thin and thick coatings, wave propagation, ionospheric physics, computational hydrodynamics, computational atomic physics, and supersonic, gas-dynamic numerical modeling.

FOR FOREIGN NATIONALS

U.S. citizenship is required for employment at NRL.

APPLICATION AND INFORMATION

Interested applicants should submit a resume or an Application for Federal Employment (SF-171), which can be obtained from local offices of the Office of Personnel Management and Personnel Offices of Federal agencies, to the address below.

Direct inquiries to:

Naval Research Laboratory
Civilian Personnel Division, Code 3830 RV 92
Washington, DC 20375-5000
202-767-3030

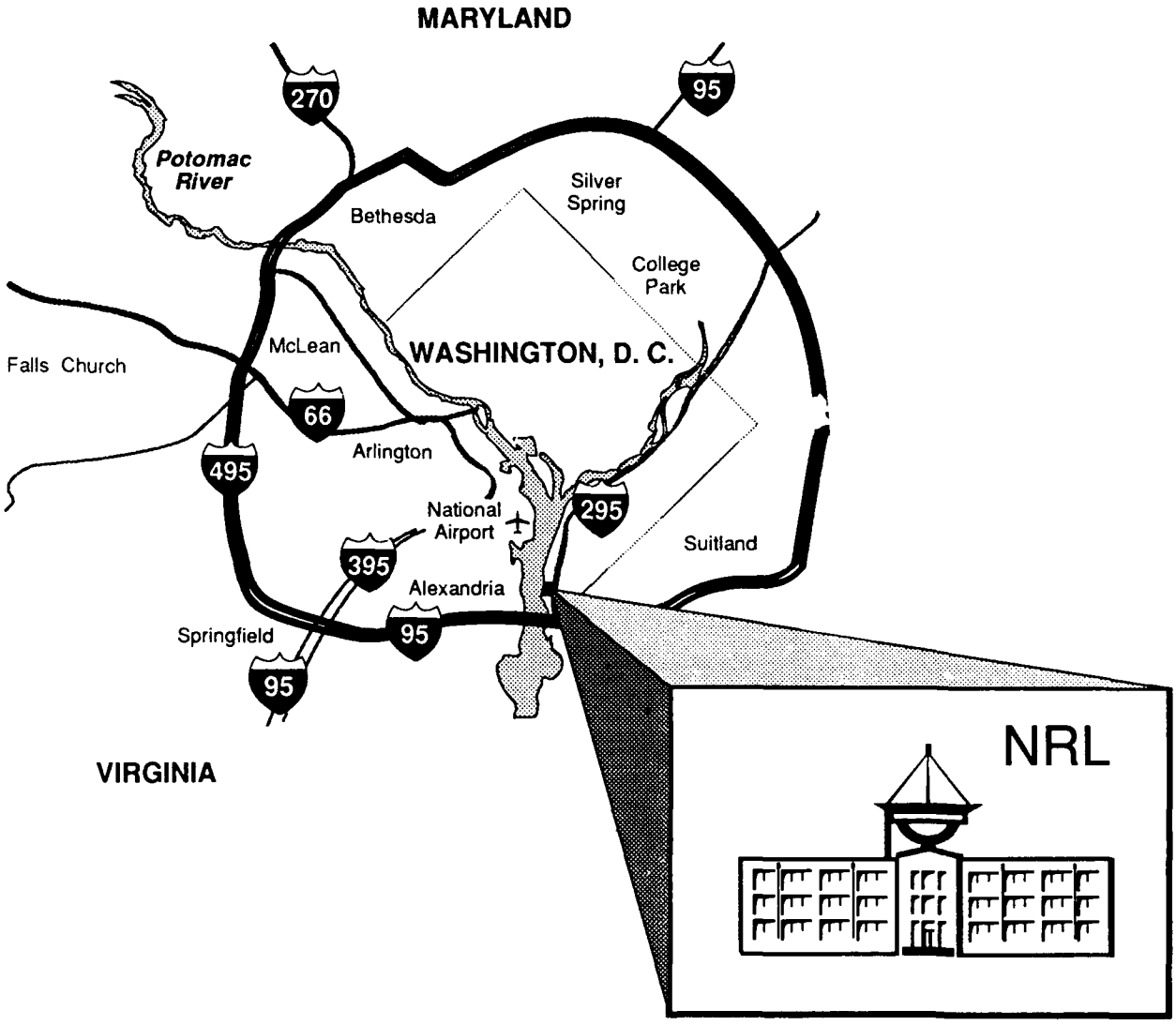

LOCATION OF NRL IN THE CAPITAL AREA

INDEX FOR THE 1992 *NRL REVIEW*

Acoustics, 47
  Target Research Tank, 60
Active experiments, 231
Advanced Graduate Research Program, 275
Advanced Spacing Sensing, 45, 57
Aerosol size distributions, 183
African American Employment Program, 279
Airglow, 226
Alan Berman Research Publication and Edison Patent Awards, 267
Alfred P. Sloan Fellows Program, 276
Amateur Radio Club, 280
American Indian/Alaskan *Native Employment* Program, 279
Asian-American/Pacific Islander Program, 279
Atomic force microscopy, 132
Atomic physics, 159
Attoliter volume, 157
Battery, 234
Bio/Molecular Science and Engineering, 49
Biosensor, 127
Bismuth, 157
Brookings Institute Advanced Study Program, 276
Center for Advanced Space Sensing, 45, 57
Center for Bio/Molecular Science and Engineering, 57
Center for Materials Research, 58
Central Computing Facility, 54
Chaos, 174
Chemical kinetics, 125
Chemistry, 51
Chesapeake Bay Detachment (CBD), 55
Clerical Cooperative Education Program, 283
Community Outreach Program, 280
Composites, 130
Computational Physics and Fluid Dynamics, 46
Computer Clubs, 280
Condensed Matter and Radiation Sciences, 46
Consultant and Expert Appointments, 283
Contributions by Divisions Laboratories, and Departments, 293
Controls-structures interaction, 236
Cooperative Education *Program*, 283
Cosmic rays, 233
Counseling Referral Service, 277
Credit Union, 44
Crystal structure determination, 157
Damage control, 172
Digital Processing Facility, 52
DoD Science and Engineering Apprentice Program, 284
Dynamics, 193
ECM, 144
Edison Memorial Graduate Training Program, 275
Electron forward scattering, 195
Electronic Warfare, 49
Electronics Science and Technology, 53, 58, 60
Emittance Measurements Facility, 52
Employment Opportunities, 295
Energetic fluids, 196
Equal Employment Opportunity Programs, 278
Evanescence, 127
Executive Directorate, 290
Faculty Member Appointments, 283
Far ultraviolet, 226
Federal Employment Opportunity Recruitment Programs, 280
Federal Junior Fellowship Program, 283
Federal Women's Program, 279
Fellowship in Congressional Operations, 276
Fiber
  gyroscope, 216
  laser, 215
  optic, 127
  sensors, 52, 162
  sources, 216
Flight Support Detachment (NRL FSD), 56, 60
Fluid dynamical interactions, 196
Fluoride glass, 218
Focal plane arrays, 162
Focal Plane Evaluation Facility, 52
Foreign Liaison Scientist Program, 276
Gas-to-particle conversion, 183
Gifted and Talented Internship Program, 284
Grain growth, 193
Graphical user interface, 172
High-energy pulsed deuterium fluoride laser, 162
High frequency, 169
High resolution, 164
High temperature phthalonitrile resins, 130
Hispanic Employment Program, 279
Homodyne, 147
Hypervelocity Impact Facilities, 47
Imaging, 226

Immunoassay, 127
Impulse, 164
Individual Honors, 253
Individuals with Handicaps Program, 279
Information Technology, 48, 59
Infrared seeker, 149
InSb, 200
Intergovernmental Personnel Act Appointments, 283
Interface roughness, 151
Ion Implantation Facility, 46
Junior Fellowship Program, 282
Key Personnel, 288
Laboratory for the Structure of Matter, 49
Large space structures, 236
Laser Doppler, 115
Laser window, 218
Lasers, 159
Location of NRL in the Capital Area, 297
Low-power Atmospheric Compensation Experiment, 236
Marine Corrosion Facility, 56
Materials Science and Technology, 60
Meet the Researchers, 70
Meteorology, 181
Microlayer physics, 181
Midway Research Center, 58
Molecular beam epitaxy, 200
Multiple processor, 149
Nanomechanics, 132
National Research Council/NRL Cooperative Research Program, 282
Naval Center for Space Technology, 53
Naval Postgraduate School, 276
Navy Science Assistance Program, 277
Nebulae, 226
Networking, 169
Neural networks, 174
NRL Review Article Awards, 271
NRL Review Staff, Inside back cover
Oceanography, 181
Office of Naval Research Graduate Fellowship Program, 283
Office of Naval Technology Postdoctoral Fellowship Program, 282
Office of Research and Technology Applications Programs, 277
Optical
  probing, 2
  Sciences, 58
Optics, 51, 159
Organometallic vapor phase epitaxy, 200
Over-the-horizon radar, 207
Parameter estimation, 113
Performance model, 207
Piezoelectric
  ceramics, 115
  composite, 115
Plasma Physics
  Facilities, 58, 59
Plasma waves, 231
Quantum chemistry, 125
Radar, 48, 59
Rapidly spinning cup atomization, 196
Reaction rates, 125
Recreation Club, 280
Remote sensing, 181
Research Advisory Committee, 289
Research platforms, 57
Reverberation, 113, 187
RCS, 147
Scientists-to-Sea Program, 277
Select Graduate Student Program, 275
Semiconductor heterostructure, 151
Ship identification, 149
Shock Test Facility, 59
Showboaters, 281
Sigma Xi, 278
Signal
  modeling, 113
  processing, 174
Simulation, 193
Single event upset, 143, 223
60-MeV Electron Linear Accelerator (LINAC), 46
SMAF, 50, 147
Space
  radiation, 143
  Science, 44
  Technology, 53
Spacecraft power system, 234
Special Awards and Recognition, 245
Stability, 234
Stars, 226
Structural applications, 130
Structural dynamics, 236
Structure characterization, 195
Structure of Matter, 49
Student Volunteer Program, 284
Submillimeter, 147
Subpicosecond, 215
Summer Employment Program, 284
Summer Faculty Research Program, 282
Surface scattering, 187
Synchrotron radiation, 157
Technical Information Services, 53
Technical Output, 287
1040-Hour Appointment, 284
Thermosetting polymers, 130
3-MeV Tandem Van De Graaff, 46
Time-temperature superposition, 115
Toastmasters International, 278
Trapped particles, 223
Ultrafine metal powders, 196
Ultrastrong fields, 159
Ultrawideband, 164
Underwater
  acoustics, 187
  Sound Reference Detachment (USRD), 50, 60
U.S. Naval Academy Cooperative Program for Scientific Interchange, 283
  Ensign Program, 283
Vacuum Ultraviolet Space Instrument Test Facility, 58
Velocimetry, 115

Viscoelastic, 115
Visualization, 144
Wideband, 164
Women in Science and
Engineering, 277
Women's Executive Leadership
Program, 276